Intercellular mitochondrial transfer in the bone marrow microenvironment of acute myeloid leukaemia and multiple myeloma

By

Christopher Richard Marlein

A thesis submitted for the Degree of Doctor of Philosophy

Norwich Medical School
Department of Molecular Haematology
The University of East Anglia, Norwich, UK

Date of submission: 1st October 2018

Declaration

I declare that the contents of my thesis entitled “Intercellular mitochondrial transfer in the bone marrow microenvironment of acute myeloid leukaemia and multiple myeloma” was carried out and completed by myself, unless otherwise acknowledged and has not been submitted in support of an application for another degree or qualification in this or any other university of institution.

This thesis is approximately 53,500 words in length.

Parts of this research have been published prior to submission and is referenced in the List of Publications.

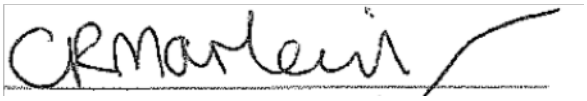

Christopher Richard Marlein

Acknowledgement

The journey to achieving a PhD is a long and sometimes frustrating process requiring large amounts of support and encouragement to succeed. I have been very fortunate to have both of these from family, friends and colleagues, which have now become friends. The main and most important thesis acknowledgement I will make is to the AML/MM patients who have generously donated research samples. I imagine the decision must have been difficult after their life changing cancer diagnosis, hand-on-heart this research could not have been carried out without them. On the same note, I would like to thank the staff at the NNUH whose tireless devotion caring for cancer patients is a real credit to them. Also thank you to the Rosetrees Trust who very kindly funded my PhD.

To my PhD supervisors Stuart and Kris, thank you so much for taking a chance on me. Your support and guidance throughout this process has been second to none, our trip to Atlanta with our visit to “Fat Matts” will live long in the memory. I have also had fantastic colleagues who I have had the pleasure to share the lab with throughout my PhD; thank you to Rachel, Manar, Amina, Yve, Genevra, Charlotte, Jayna, Becky and Adam. A special mention to my “Best Friend” Rachel, thank you for being there for me and keeping me sane in those long days in the DMU. Hopefully we can continue our friendship during our Post-Docs in New York City!

Finally, I would like to thank my family (Richard, Ruth and Emma), who have supported me both emotionally and financially. A special mention to my mum Ruth who single handily supplied the lab with fantastic cakes (which would not be out of place on the Great British Bake Off!!!). Scientific research definitely runs on its belly!

I sadly lost my Grandad, Jim, during the course of my PhD. I would like to dedicate my thesis to his memory, hopefully I have done you proud Grandad.

Abstract

Acute Myeloid Leukaemia (AML) and Multiple Myeloma (MM) are currently incurable malignancies which have devastating effects on patients who develop them. Chemotherapeutic regimens have remained largely unchanged over recent decades, it is therefore apparent that there is a need for novel therapeutic interventions. It is thought that these new treatments will come to fruition through a better understanding of the biological processes which underpin these diseases. Cancer cells have classically been thought to generate ATP through the non-mitochondrial based Warburg hypothesis, however it is becoming apparent that malignant cells are equally reliant on mitochondrial oxidative phosphorylation to fuel their rapid proliferation. Mitochondria were thought to remain in their somatic cell for their lifetime; however, ground-breaking research from the Gerdes laboratory has shown that mitochondria can move between somatic cells. In my thesis, I aimed to examine whether mitochondria were transferred between non-malignant bone marrow stromal cells (BMSC) and AML/MM cells.

Mitochondria were shown to move from BMSC to AML blasts and MM cells, this process enhanced the proliferation of these malignancies. AML-derived NOX2 superoxide was shown to stimulate mitochondrial biogenesis in BMSC, allowing mitochondria to move to AML blasts through tunnelling nanotubes. In the MM, it was found that CD38 expression on MM cells was able to form tunnelling nanotubes which facilitated the trafficking of mitochondria. Inhibition of NOX2 and CD38, in AML and MM respectively, reduced disease progression *in vivo* in part by reducing the quantity of mitochondria which move to the malignant cell. Furthermore, it was shown that AML/MM hijack this process from normal haematopoiesis as mitochondria move *in vivo* to haematopoietic stem cells in response to bacterial infection. Taken together I have presented a novel biological process in haematopoietic malignancies, which may be exploited to treat AML and MM.

Table of Contents

List of publications and conference papers

First author publications

Marlein CR, Piddock RE, Zaitseva L, Hellmich C, Horton RH, et al. CD38 drives mitochondrial trafficking promoting bioenergetic plasticity in multiple myeloma. **Cancer Research.** 2019.

Marlein CR, Zaitseva L, Piddock RE, Raso-Barnett L, Scott MA, Ingham CJ, et al. PGC-1alpha driven mitochondrial biogenesis in stromal cells underpins mitochondrial trafficking to leukemic blasts. ***Leukemia***. 2018.

Marlein CR, Zaitseva L, Piddock RE, Robinson S, Edwards D, Shafat MS, et al. NADPH oxidase-2 derived superoxide drives mitochondrial transfer from bone marrow stromal cells to leukemic blasts. ***Blood***. 2017; 130: 1649-60.

Marlein CR, Zaitseva L and Rushworth SA. Pulling the plug – halting cancer's theft of mitochondria. ***Oncoscience.*** 2017; 4:173-174

Conference papers

Mitochondrial trafficking in the bone marrow microenvironment promotes bioenergetic flexibility in multiple myeloma. **Oral presentation. American Association for Cancer Research Annual Meeting 2018, Chicago IL, USA.**

Mitochondria are transferred from non-malignant stroma cells to malignant plasma cells, via tunnelling nanotubes in a CD38 dependent mechanism, a process that promotes myeloma proliferation. **Oral presentation. American Society of Hematology Annual Meeting 2017, Atlanta GA, USA.**

PGC1α driven mitochondrial biogenesis within the bone marrow stromal cells of the acute myeloid leukemia micro-environment is a pre-requisite for mitochondrial transfer to leukemic blasts. **Poster presentation. American Society of Hematology Annual Meeting 2017, Atlanta GA, USA.**

Bone marrow mesenchymal stromal cells transfer their mitochondria to acute myeloid leukaemia blasts to support their proliferation and survival. **Oral presentation. American Society of Hematology Annual Meeting 2016, San Diego CA, USA.**

AML orchestrates mitochondrial metabolism in bone marrow stromal cells through an increase in PGC-1α. **Poster presentation. European Hematology Association Congress 2016, Copenhagen, Denmark.**

Other relevant publications

Piddock RE, **Marlein CR**, Abdul-Aziz A, Shafat MS, Auger MJ, et al. Myeloma derived macrophage inhibitory factor regulates bone marrow stromal cell derived IL-6 via c-MYC. ***Journal of Hematology and Oncology***. 2018

Abdul-Aziz A, Shafat MS, **Marlein CR**, Piddock RE, Robinson SD, et al. HIF1α drives chemokine factor pro-tumoral signaling pathways in acute myeloid leukemia. ***Oncogene***. 2018.

Shafat MS, Oellerich T, Mohr S, Robinson SD, Edwards DR, **Marlein CR**, et al. Leukemic blasts program bone marrow adipocytes to generate a protumoral microenvironment. ***Blood***. 2017;129(10):1320-32.

Piddock RE, Loughran N, **Marlein CR** et al. PI3Kdelta and PI3Kgamma isoforms have distinct functions in regulating pro-tumoural signalling in the multiple myeloma microenvironment. ***Blood Cancer J***. 2017;7(3):e539.

List of figures

List of tables

List of abbreviations

ADPR - Adenosine diphosphate-ribose
ALL - Acute lymphoblastic leukaemia
AML - Acute myeloid leukaemia
APRIL - A proliferation-inducing ligand
ASCT - Autologous stem cell transplant
ASXL1 - Additional sex comb-like 1
ATCC - American type culture collection
ATP - Adenosine triphosphate
ATRA - All-trans retinoic acid
BAFF – B-cell-Activating Factor
BCR - B cell receptor
BM-MSC - Bone marrow mesenchymal stem cell
BMM - Bone marrow microenvironment
BMSC - Bone marrow stromal cell
BSA - Bovine serum albumin
C/EBPα - CCAAT/enhancer-binding protein
CAR - CXCL12-abundant reticular
CBPα - CCAT enhancer binding protein α
CD - Cluster of Differentiation
CLL - Chronic lymphoblastic leukaemia
CLP - Common lymphoid progenitor
CML - Chronic myeloid leukaemia
CMP - Common myeloid progenitor
CN - Cytogenetically normal
CRAB - Calcium, Renal insufficiency, Anaemia and/or Bone lesions
Ct - Cycle threshold
CytoB - Cytochalasin B
DCA - Dichloroacetate
DCF - 2', 7' –dichlorofluorescin
DMEM - Dulbecco's Modified Eagle's Medium
DMU - Disease modelling unit
DNA - Deoxyribose Nucleic Acid
DNMT3A - DNA methyltransferase
DPI - Diphenyleneiodium chloride
EBF - Early B cell factor
ECAR - Extracellular acidification rate
ECL - Enhanced chemiluminscence
ECM - Extracellular matrix
EGFR - Epidermal growth factor receptor
EMMPRIN - Extracellular metalloproteinase inducer
FAB - French American British
FACS - Fluorescence activated cell sorting
FAD - Flavin adenine dinucleotide
FAM - 6-Carboxyfluorescein
FAO - Fatty acid oxidation
FCCP - Carbonyl cyanide-4-(trifluoromethoxy)phenylhydrazone
FCS - Foetal calf serum
FDG-PET - Fluorodeoxyglucose positron emission tomography
FFA - Free fatt acids
FLT3 - Fms-Like Tyrosine Kinase

FMO - Fluorescence minus one
Fo – Follicular
GAPDH - Glyceraldehyde 3-phosphate dehydrogenase
gDNA - Genomic DNA
GFP - Green fluorescent protein
GMP - Granulocyte-erythroid progenitor
GOI - Gene of interest
GSH -Glutathione
GSK3 - glycogen synthase kinase-3
GVHD - Graft v host disease
H_2O_2 - Hydrogen peroxide
HLA - Human leukocyte antigen
HRP - Horseradish peroxidase
HSC - Haematopoietic stem cell
HSCT - Haematopoietic stem cell transplant
IDH - Isocitrate dehydrogenase
IFN - Interferon
Ig - Immunoglobulin
IgH - Immunoglobulin heavy chain
IL - Interleukin
IP - Intraperitoneal
IV - Intravenous
JAK/STAT - Janus associated kinase-signal transducer and activator of transcription
KD - Knockdown
LB - Luria Bertani
Lin - Lineage
LPS - Lipopolysaccharide
LSK - Lin-Sca+c-Kit+
LT-HSC - Long Term haematopoietic stem cell
MACS - Magnetic activated cell sorting
MAPK - Mitogen-activated protein kinase
MAT - Marrow Adipose Tissue
MDS - Myelodysplastic syndrome
MEP - Megakaryocyte-erythroid progenitor
MFI - Mean fluorescence intensity
MGUS - Monoclonal gammopathy of unknown significance
MIF - Macrophage inhibitory factor
Miro1 - Mitochondrial Rho-GTPase
MM - Multiple myeloma
MMP-2 - Metalloproteinase-2
MOI - Multiplicity of infection
MPP - Multipotent progenitor
MSC - Mesenchymal stem cells
mtDNA - Mitochondrial DNA
MYH - Myosin heavy chain gene
NAC - N-Acetyl Cysteine
NAD+ - Nicotinamide adenine dinucleotide
NFκB - Nuclear factor-κB
NGS - Next generation sequencing
NK Cell - Natural killer cell
NKP - Natural killer cell progenitor
NNUH - Norfolk and Norwich University Hospital
NOX2 - NADPH oxidase 2

NPM1 - Nucleophosmin 1
NSG - NOD SCID Gamma
OCR - Oxygen consumption rate
OXPHOS - Oxidative phosphorylation
PBS - Phosphate buffered saline
PCL - Plasma cell leukaemia
pCMV - Cytomegalovirus promoter
PDK1 - Phosphoinositide-dependent kinase 1
PGC-1α - Peroxisome proliferator-activated receptor gamma coactivator 1-alpha
PIP3 - Phosphatidylinositol-3,4,5-triphosphate
PPR - PTH/PTH-related receptor
PVDF - Polyvinyladine fluoride
qRT -PCR - Quantitative real time polymerase chain reaction
RANK - Receptor activator of nuclear factor κ-B
RANKL -Receptor activator of nuclear factor κ-B ligand
RIPA - Radioimmunoprecipitation assay
RISC - RNA-induced silencing complex
RNA - Ribose Nucleic Acid
ROS - Reactive oxygen species
RT- Room temperature
RTK - Receptor tyrosine kinase
SCF - Stem cell factor
SCID - Severe combined immunodeficient
shRNA - short hairpin RNA
SMM - Smoldering MM
SNP - Single nucleotide polymorphism
ST-HSC - Short Term haematopoietic stem cell
TAE - Tris acetate EDTA
TAP - TNT-anchor point
TCA cycle – Tricarboxylic acid cycle
TCR - T cell receptor
TET2 - Ten-eleven translocation oncogene family member 2
TNT - Tunneling nanotube
TSP - Thymus-seeding progenitor
VCAM-1 - Vascular cell adhesion molecule 1
VEGF - Vascular endothelial growth factor
VIC - 2′-chloro-7′phenyl-1,4-dichloro-6-carboxy-fluorescein
VSV-G - Vesicular stomatitis virus glycoprotein
WHO - World Health Organisation
5hmC – 5-hydroxymethylcytosine
5mc - 5-methylcytosine

1 Introduction

1.1 Haematopoiesis

To understand haematopoietic malignancies such as Acute Myeloid Leukaemia (AML) and Multiple Myeloma (MM), it is of paramount importance to explore the development of normal blood cells. Haematopoiesis is a complex process which generates blood cells within the bone marrow (1). The blood is a highly regenerative tissue with approximately 1 x 10^6 mature blood cells generated every second (2). Haematopoiesis initiates from a pluripotent stem cell, the haematopoietic stem cell (HSC) (3). Despite its complexity, extensive animal experimentation means that haematopoiesis is the one of the best understood and described processes within the human body (4). Pioneering work by Till, McCulloch and colleagues in the 1960s paved the way for the discovery of the HSC (5). Mice treated with a lethal dose of irradiation, were rescued from death via the transplantation of bone marrow cells from a non-radiated mouse. Interestingly, small splenic lumps were observed in the irradiated mice following transplantation (6). Extensive analysis determined these colonies were formed from a single cell, capable of multi-lineage differentiation (7). The specific isolation of HSCs and other blood progenitor cells, using specific surface markers, allowed the complex hierarchical structure of haematopoiesis to be elucidated (8). In this system, mature blood cells are generated from a specific lineage multipotent progenitor cell which, in turn, have been derived from HSCs (9). Figure 1.1 highlights the hierarchical structure of haematopoiesis which is further described below.

1.1.1 Haematopoietic Stem Cell (HSCs)

The work by Till and McCulloch demonstrated a single cell type had the ability to differentiate into and re-constitute all cells within the bone marrow (5, 7, 10). This cell was termed the HSC, a pluripotent stem cell with the ability to self-renew (9). Under basal conditions the number of HSCs remains relatively constant with the majority of cells residing in the G0 phase of the cell cycle (11). The HSC is a very

rare cell type - early studies that purified HSCs from mice found that only 0.05% of the total BM cells were HSCs (12, 13). These HSCs were isolated by the then relatively new technology fluorescence-activated cell sorting (FACS) using monoclonal antibodies, which revolutionised the field. Early HSCs were sorted using two surface markers; Thy-1^{low} lineage marker (Lin) and Sca-1, with HSCs being Lin^- and $Sca\text{-}1^+$ (12, 13). These $Lin^-Sca\text{-}1^+$ HSCs were the only cells found to re-populate the entire haematopoietic system of irradiated mice (13), with $Lin^+Sca\text{-}1^+$ and $Lin^-Sca\text{-}1^-$ cells unable to re-populate the bone marrow (14). More extensive purification, using additional surface markers CD117/c-Kit and CD34, highlighted that the HSC population isolated by Spangrude and colleagues (13) contained at least 3 multipotent populations; long term HSCs (LT-HSCs), short term HSCs (ST-HSCs) and multipotent progenitors (MPPs) (15). Through the use of additional surface markers, CD150 and CD48, these populations are now well defined (16).

LT-HSCs are pluripotent and can undergo asymmetric cell division, differentiating into ST-HSCs in addition to self-renewing and maintaining the pool of HSC (17). ST-HSCs are multipotent and can differentiate into MPPs, which produce the common myeloid and lymphoid progenitors (see section 1.1.2 and 1.1.3). LT-HSCs are able to sustain haematopoiesis for more than 11 months, compared to the relatively short time of 6-10 weeks of ST-HSCs (18).

Mouse models have been critical in the evolution of our understanding of the human haematopoietic system. The development of mice lacking mature T and B cells has allowed the creation of xenograft models that incorporate human haematopoietic cells, which can specifically analyse human haematopoiesis *in vivo* (19). Using this model, it was found that human peripheral blood leukocytes were able to generate human T and B cells (20). More recently the specific transplantation of HSCs isolated from umbilical cord blood, into a modified SCID NOD-SCID-Gamma (NSG) mouse, has been used for the analysis of human haematopoiesis (21). Engraftment of human $CD45^+$ cells was found in the bone marrow and spleen, along with mature human blood cells in the peripheral blood

(22). These experiments have resulted in the well understood hierarchical system of haematopoiesis (Figure 1.1).

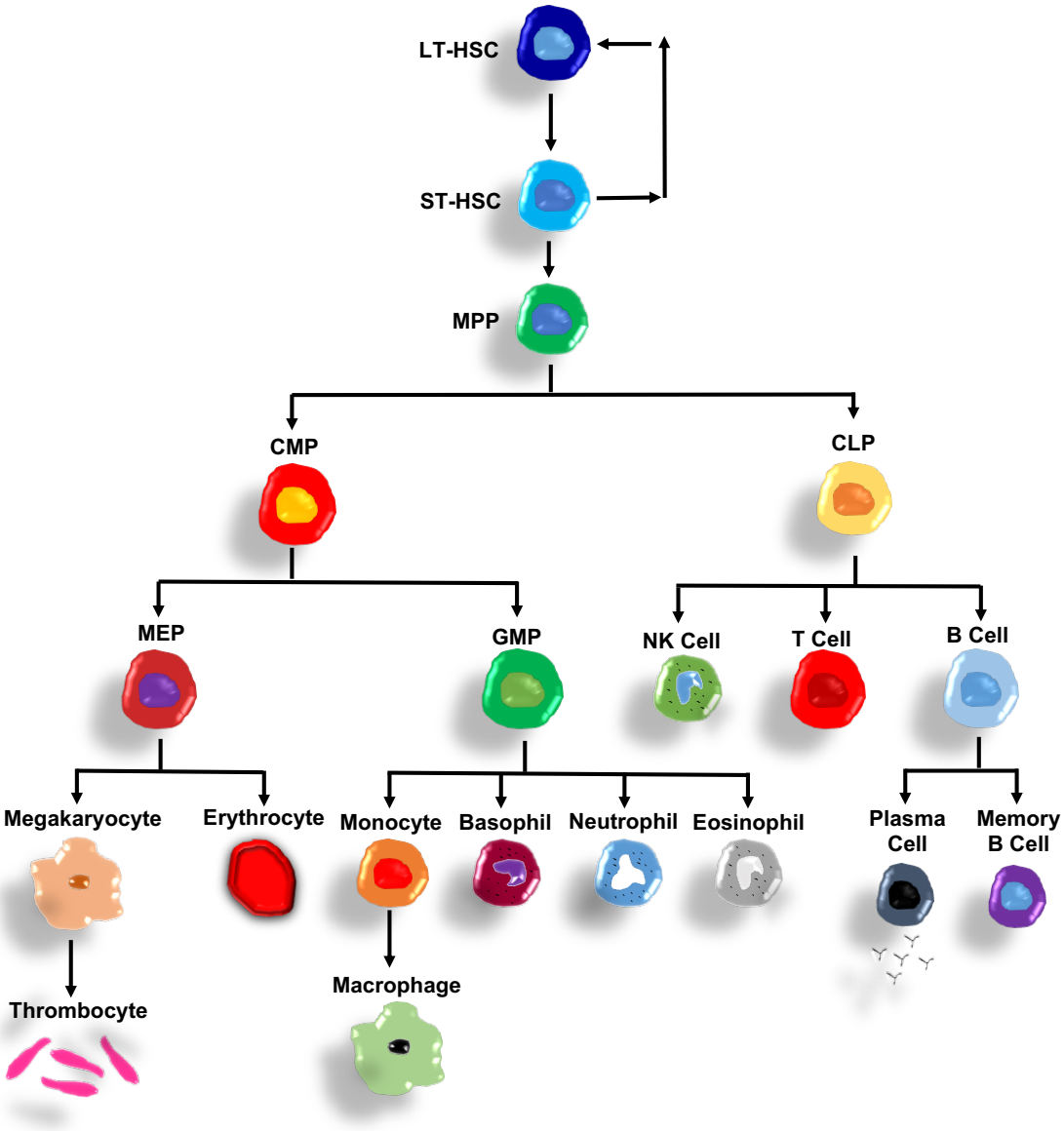

Figure 1.1. A schematic overview of the hierarchical system of haematopoiesis.

The process of haematopoiesis starts with the pluripotent LT-HSC which differentiates into the ST-HSC whilst self-renewing to maintain the HSC pool. The ST-HSC then differentiates into the MPP, which gives rise to the CMP and CLP starting the myeloid and lymphoid lineages. Through a number of intermediate progenitors, the wide range of mature blood cells are generated. This figure is modified from Marlein and Rushworth 2017 (18).

1.1.2 Myeloid Lineage

Haematopoiesis diverges into two distinct cell lineages; the myeloid and lymphoid lineages (23). The MPP has the ability to differentiate into either the common lymphoid progenitor (CLP) or the common myeloid progenitor (CMP), which is the first cell of the myeloid lineage and is capable to generating all of the cells that make up this lineage (24). The immediate differentiation step of the CMP is to create either the megakaryocyte-erythroid progenitor (MEP) or the granulocyte-erythroid progenitor (GMP) (25). Through a range of intermediates, the GMP can generate basophils, neutrophils, eosinophils and macrophages via monocytes whereas the MEP can generate erythrocytes (red blood cells) and thrombocytes (platelets) (25). There has also been recent evidence suggesting there is a progenitor, separate to the CMP/CLP lineage, which lacks the ability to generate cells of the MEP lineage (26).

There are a number of different transcriptional regulators which cause the commitment to either the GMP or MEP lineage. For commitment to the GMP fate, the transcription factor CCAAT/enhancer-binding protein (C/EBPα) is crucial (27). HSCs express low levels of C/EBPα but levels increase upon differentiation of CMPs to GMPs (27). Artificially expressing C/EBPα in B cells of the lymphoid lineage causes them to differentiate into monocytes of the myeloid lineage (28), highlighting that this transcription factor is crucial for generation of cells downstream of the GMP. In addition, when C/EBPα is conditionally removed from mice, these mice lack the ability to generate GMPs from CMPs (29).

There is also a key transcription factor involved in commitment of the CMP to the MEP lineage, this transcriptional factor is GATA-1 (30). Again GATA-1 expression levels are low in HSCs, with higher expression found in MEP and erythroid precursors. The importance of this transcription factor has been shown in mice lacking GATA-1, where these mice are unable to generate mature red blood cells (31).

1.1.3 Lymphoid Lineage

As well differentiating into the CMP, MPPs also have the ability to generate the CLP. The CLP can then differentiate into the T cell, B cell and natural killer (NK) progenitor cells, which in turn creates mature T cells, B cells and NK cells (32). Mature T and B cells form the adaptive immune response (33, 34) whilst NK cells contribute to the innate immune system (35). T and B cells acquire a single antigen specific receptor through somatic DNA re-arrangements of T Cell Receptor (TCR) and Ig genes, creating a vast repertoire capability of recognising a wide range of antigens (36). Expression of the IL-7 receptor is critical for the commitment to the lymphoid lineage (37).

The majority of B cell maturation takes place within the bone marrow, originating from the B cell progenitor which is irreversibly committed to the B cell lineage (38). Initiation of B-cell development requires two key transcription factors; E2A and early B cell factor (EBF). In the absence of either of these transcription factors, B cell development is arrested at the first stage of development (39, 40). On their surface, mature B cells have a specific B cell receptor (BCR) which is comprised of two heavy chains and two light chains (41). This receptor is capable of binding to specific antigens generating an immune response. The key step in creating this receptor is the re-arrangement of the heavy chain upon the activation of recombination-activating genes, which occurs between the pre-pro B cell and pro-B cell stage (42). Upon the generation of the late pre-B cell the light chain of the BCR is rearranged (V to J), if the resulting joints are in a continuous open reading frame the rearrangement is classed as “productive” (43).

A fully functional follicular B cell (FoB) is made after a negative selection process, to remove autoreactive B cells (44). These cells can then migrate from the bone marrow to join the pool of circulating B cells. Upon activation by a foreign antigen, the FoB cell differentiates into an effector plasma cell which secretes specific antibodies to eliminate pathogens. Memory B cells are also created upon FoB cell activation, for use in subsequent exposure to the same antigen (45).

Contrary to B cell maturation, only a limited part of the T cell maturation occurs within the bone marrow with T cell progenitors migrating to the thymus for maturation (46). Bone marrow-derived thymus-seeding progenitors (TSPs), which include MPPs and CLPs (47), migrate to the thymus to differentiate into mature $CD4^+$ (helper) and $CD8^+$ (cytotoxic) T cells capable of mounting an immune response to pathogens. The number of TSPs in the peripheral blood is relatively small, with less than a total of 1000 found in the peripheral blood of mice (48).

TSPs enter the thymus and differentiate into double negative cells ($CD4^-CD8^-$), which in turn generate double positive ($CD4^+CD8^+$) cells (49). After the re-arrangement of the α and β chains of the TCR the double positive cells become single positive cells (either $CD4^+$ or $CD8^+$), which enter the cortex of the thymus for positive selection (50). Here single positive cells are selected on their ability to engage host MHC complexes (51). Upon the successful completion of positive selection, the single positive cells move to the medulla of thymus to undergo negative selection - here cells that recognise self-antigens are eliminated (52). A critical signalling pathway in the development of T cells is the Notch1 signalling pathway, activated by ligands of the Jagged family (53). Ectopic expression of the intracellular domain of the Notch1 receptor in haematopoetic progenitors resulted in T cell maturation in the bone marrow, which completely blocked B cell development (54).

Unlike B and T cell development, NK cell development does not include the somatic rearrangement of genes encoding for antigen specific receptors. This is mainly due to their role in the innate immune whereby they secrete IFNγ and TNFα, rather than adaptive antigen sensing (55). The pre-NKP (natural killer progenitor) is the first committed cell to this lineage and IL-15 is crucial in the formation of this cell from the CLP (56). A key process in the maturation of the NK cell is the acquisition of CD56 and CD16 (57) along with the S1P5 receptor, which allows egress of the mature NK cell from the bone marrow (58).

1.2 Bone Marrow

The bone marrow is the site of the majority of steps in haematopoiesis, whilst also being the location where malignant haematopoietic cells proliferate and accumulate. Therefore, it is important to discuss the anatomy and the complex microenvironment within the bone marrow.

1.2.1 Bone Marrow Anatomy

Human bone is composed of trabecular bone surrounded by a layer of cortical bone and a range of connective tissues (59), as shown in Figure 1.2. The trabecular bone is made up of four regions (endosteal, subendosteal, central and perisinusoidal) and is made up of a lattice filled with blood vessels, along with red and yellow bone marrow (60). In haematopoiesis, the most important region of trabecular bone region is the endosteal as it forms the point of contact between the bone marrow and bone (61). This region contains a range of non-haematopoietic cells that are involved in the maintenance and regulation of both normal and malignant blood cell development (62). In addition, within the endosteal there are thin-walled blood vessels called sinusoids whose role is to aid blood cell migration away from the bone marrow (63).

The bone marrow is made up of both haematopoietic red marrow and the fatty non-haematopoietic yellow marrow (64). All bone marrow at birth is composed of red marrow and is converted slowly to yellow marrow as we age. However, yellow marrow has been shown to be able to revert back to red marrow under certain stress stimuli such as severe blood loss (65). Red marrow contains the parenchyma, the location of haematopoietic stem cells and resultant progenitors, and the vascular component which comprises of supporting stromal cells (59). The yellow marrow is made up of fat cells, which serve as the energy reserve and can be used in times of severe starvation (66).

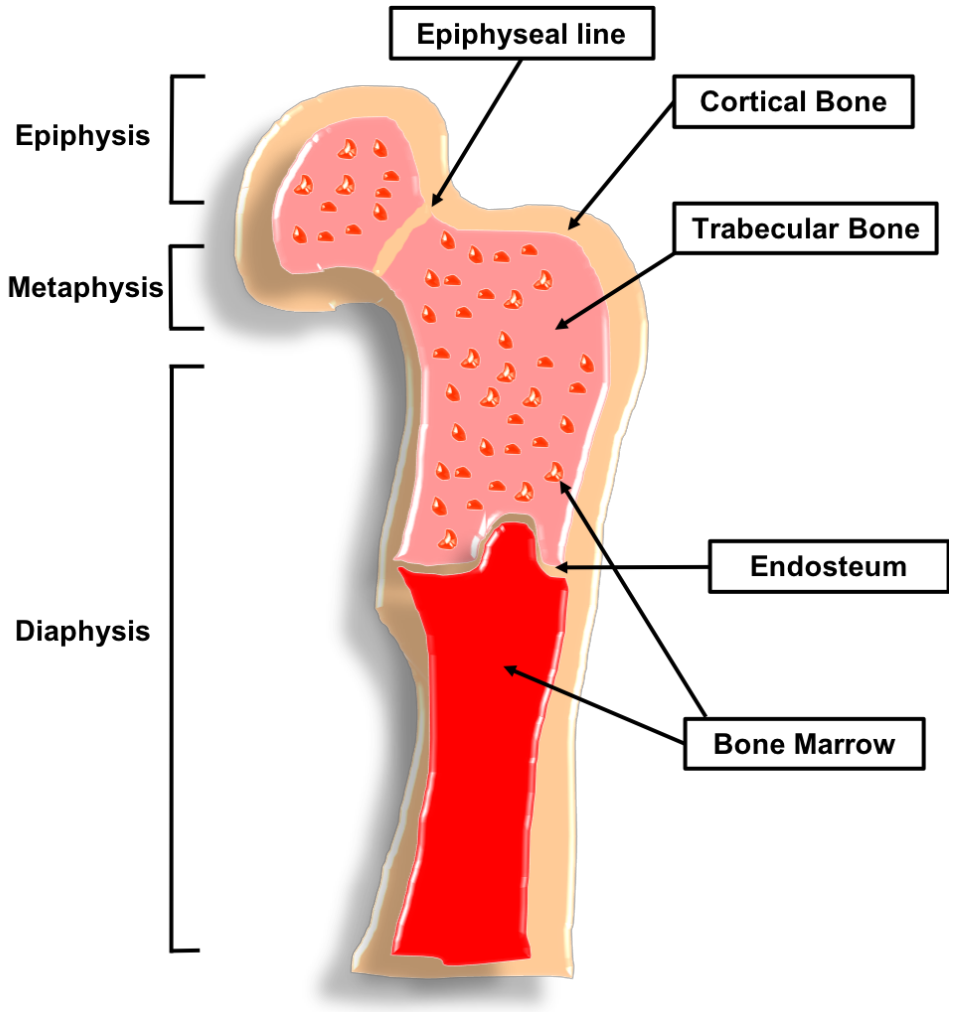

Figure 1.2. Schematic representation of the structure of the human bone.

Human bone is made up of three regions; the epiphysis, metaphysis and diaphysis. Each region contains trabecular bone surrounded by cortical bone. The bone marrow is located within hollow regions of the trabecular bone, with the endosteum forming the divide between bone and bone marrow. Adapted from Marlein and Rushworth (18).

1.2.2 Bone Marrow Microenvironment

The expansion and differentiation of the HSC population occurs within a well-controlled environment containing a number of different cell types and secretory molecules (62). Through the 3D imaging of mouse bone marrow, it was seen that there were high concentrations of HSCs in specific micro-domains or “niches” (67). The vascular component of the red bone marrow contains a vast array of stromal cells, which are present in HSC niches. These stromal cells arise from a multipotent stem cell, the bone marrow mesenchymal stem cell (BM-MSC), which

has the ability to differentiate into adipocytes, chondrocytes, osteoblasts, endothelial cells and myocytes (68, 69). The differentiation hierarchy of the BM-MSC is schematically represented in Figure 1.3.

There is still great debate as to the actual identity of BM-MSCs within the bone marrow. In 2006, the Mesenchymal and Tissue Stem Cell Committee of the International Society for Cellular Therapy introduced a minimum criteria for the identification of BM-MSCs using cell surface marker expression. Under these guidelines, BM-MSCs must be positive for CD73, CD90 and CD105 whilst being negative for CD31, CD34 and CD45 (70). These criteria are not perfect in defining BM-MSCs (due to the difficulty in reliably characterizing the stemness of populations expressing the above surface markers (71)), however these parameters are utilized in my thesis to define the BM-MSC stromal population. The aim was to isolate the BM-MSC population from human bone marrow aspirates, however during *in vitro* culture the BM-MSC may differentiate into early multipotent progenitors. Therefore, I define the heterogeneous "stromal" population used in this study as bone marrow stromal cells (BMSC) (Figure 1.3).

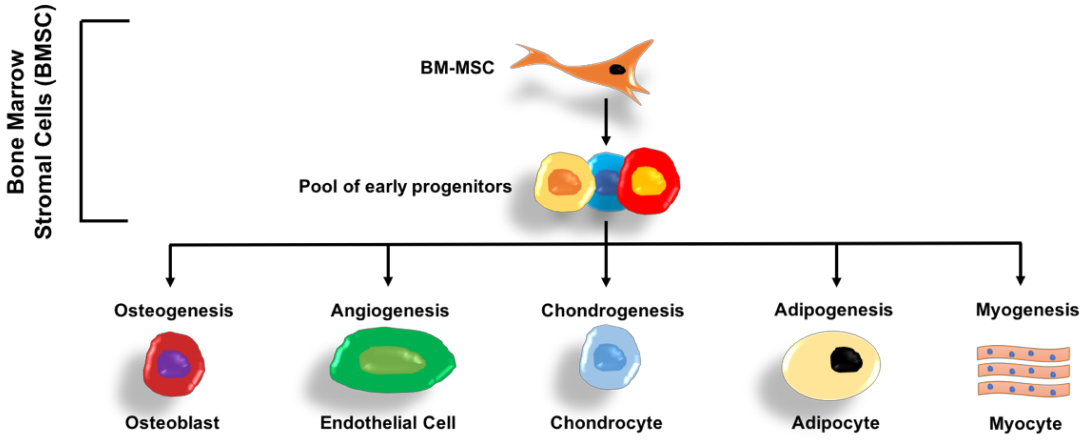

Figure 1.3. The vascular (stromal) component of the red bone marrow.

BM-MSC have the ability to differentiate into osteoblasts, endothelial cells, chondrocytes, adipocytes and myocytes via intermediate mesenchymal stromal cells. BM-MSC were isolated from human bone marrow aspirates for this study, however during culture it is likely that this cell will differentiate. Therefore, the heterogeneous "stromal" cell population used in my thesis are defined as bone marrow stromal cells (BMSC).

1.2.3 Bone Marrow Stromal Cells (BMSC)

Bone marrow stromal cells (BMSC) encompass the BM-MSC and early multipotent progenitors prior to mature differentiation. BMSC line the sinusoids within the endosteal region of the trabecular bone (72) and provide cytokines and chemokines that are required for the maintenance of the HSC pool (62). One such chemokine, CXCL12 (or SDF-1), stimulates the attraction and retention of HSCs within the niche via its CXCR4 receptor (73). Deletion of CXCL12 in BMSC (74), or CXCR4 on HSCs (75), can result in a drastic loss of HSC numbers within bone marrow niches - highlighting the crucial role of this chemokine in HSC maintenance. Recently, it has been found that circadian oscillations can control the secretion of CXCL12 by BMSC (76). In this study, noradrenaline was released by sympathetic nerve fibres, causing BMSC to downregulate their CXCL12 secretion and results in HSC egress from the bone marrow.

Another key cytokine in the regulation of the HSC niche is stem cell factor (SCF), which again is produced by BMSC (77). SCF has both membrane-bound and soluble forms which bind to the receptor tyrosine kinase c-KIT (CD117) on HSCs, regulating maintenance and proliferation (78, 79). The membrane-bound form is crucial in maintaining haematopoiesis, as mice which only express the soluble form (Sl/Sl^d mutant mice) are completely devoid of HSCs and resultant downstream haematopoietic cells (80).

Recently, three distinct populations of highly CXCL12-expressing perivascular BMSC have been identified; CXCL12-abundant reticular (CAR) cells, nestin-GFP^+ stromal cells and leptin $receptor^+$ stromal cells (77). These populations were identified by transgene expression using stromal promoters; GFP was knocked into the CXCL12 locus and the Nestin promoter to identify CAR cells and nestin-GFP+ stromal cells respectively (81, 82). The Leptin $receptor^+$ stromal cells were identified using lineage mapping using Cre-recombinase expressed under the control of leptin receptor elements (83). CAR cells are mesenchymal progenitors which have the ability to differentiate into adipocytes and osteoblasts, removal of these cells results in depleted HSC numbers associated with a

reduction of CXCL12 and SCF levels (84). Nestin-GFP$^+$ cells express CXCL12 and SCF at comparable levels, however, a reduction in these cells only caused a modest loss of HSC numbers (77). Finally, leptin receptor$^+$ stromal cells also express CXCL12 and SCF whilst having the ability to differentiate into adipocytes, but lack the ability of osteoblastic differentiation (84). It is apparent that these 3 distinct stromal cells types have commonalities, especially in SCF and CXCL12 expression, therefore it is still widely accepted to class these distinct populations as BMSC.

1.2.4 Osteoblasts

BMSC have the ability to differentiate into bone forming osteoblasts (85). This differentiation process is controlled by the transcription factor Runx2 and is achieved through a pro-osteoblast intermediate (86). Heterozygous and homozygous Runx2 knockout mice have severely disrupted osteogenesis, with homozygous knockout animals dying at birth (87). Mature osteoblasts undergo a three-step process; proliferation, matrix maturation and mineralisation which results in the formation of bone (88).

Like BMSC, there is evidence that osteoblasts contribute to the regulation of proliferation of HSCs. This was initially proposed after analysing the proximity of HSCs and mature haematopoietic progenitors to osteoblasts - HSCs were found close to osteoblasts with mature progenitors positioned further away (89). Conditional knockout of osteoblasts within the bone marrow resulted in the inability of the bone marrow to support normal haematopoiesis (90, 91). In a later study, the number of osteoblasts was increased through genetic manipulation of the PTH/PTH-related receptor (PPR) which is located on osteoblasts themselves (92). It was found that the increase in osteoblast number resulted in secretion of high levels of Notch ligand jagged 1. This caused an expansion of the HSC population within the bone marrow and this process can be reversed with the

administration of a γ-secretase inhibitor. Osteoblasts can also secrete CXCL12, albeit 1000-fold less than BMSC, but they lack the ability to secrete SCF (93).

1.2.5 Bone Marrow Endothelial cells

BMSC can differentiate into bone marrow endothelial cells, which also regulate the trafficking and homing of HSCs (94). Early studies using a conditional deletion of the gp130 receptor on endothelial cells resulted in a reduction of HSC numbers in bone marrow HSC niches (95). Like BMSC and osteoblasts, endothelial cells secrete CXCL12 – however this is at a level 100-fold less than BMSC and 10-fold greater than osteoblasts (96). Stimulation of endothelial cells with IL-1 or TNFα results in the production of cytokines (including G-CSF, GM-CSF and IL-6) that are crucial in the maintenance of the HSC pool (97). Endothelial cells also express the vascular cell adhesion molecule 1 (VCAM-1) (98) which binds to VLA-4 on HSC, enabling HSC retention within preferable bone marrow niches. Furthermore, endothelial cells synthesise soluble and membrane bound forms of SCF - knockout of this factor results a depletion of HSC numbers (83).

1.2.6 Adipocytes

Adipocytes present within the bone marrow also originate from BMSC and form marrow adipose tissue (MAT) (99). These cells make up approximately 15% of the bone marrow and are shown to increase in number during aging, reaching up to 60% by the age of 65 (100). Differentiation of adipocytes from BMSC is an intricate process controlled mainly by the PPARγ transcription factor (101) - PPARγ knockout mice were shown to lack terminally differentiated adipose tissue (102). In addition, the C/EBPα transcription factor is crucial in forming adipocytes with C/EBPα knockout mice lacking the ability to generate MAT (103). Adipocytes have been shown to produce and secrete SCF (104) whilst having the ability to produce CXCL12, IL-8 and IL-3 (105); which contributes significantly to the maintenance of the HSC niche.

1.2.7 Chondrocytes and Myocytes

Another cell type which is formed from the differentiation of BMSC are chondrocytes, which in turn forms cartilage (106). Chondrocytes are metabolically active and can generate large quantities of extra cellular matrix (ECM) components including collagen, proteoglycans and glycoproteins. A major transcription factor involved in the generation of chondrocytes is Sox9, inactivation results in failure of chondrocyte differentiation (107). There is very little evidence to suggest that chondrocytes are involved in the maintenance of the HSC pool within the bone marrow, however downstream ECM components generated by chondrocytes make up key parts of the HSC niche.

Myocytes form muscle tissue and are also formed by differentiation of BMSC - under the control of the transcription factor MyoD (108). As with chondrocytes, myocytes do not readily contribute to the maintenance of the HSC niche.

1.2.8 Osteoclasts

Although not part of the BMSC differentiation cascade, osteoclasts are a very important component of the bone marrow microenvironment. The process of bone formation is a highly dynamic remodeling process involving bone forming osteoblasts (see 1.2.4) and bone resorbing osteoclasts (109). Osteoclasts are generated in the haematopoietic component of the bone marrow from the GMP in the myeloid lineage (110). Two haematopoietic factors are required for the formation of osteoclasts, the cytokine RANKL and CSF-1 (111). Osteoclasts are crucial in generating the HSC niche; functional niches are not present in oc/oc mice (which lack osteoclasts) due to defects in HSC homing (112). Reduced osteoblasts are present in oc/oc mice, therefore the role of osteoclasts in HSC maintenance is likely to be indirectly through osteoblasts. Soluble and membrane forms of SCF are not synthesised by osteoclasts and only small quantities of CXCL12 are secreted.

1.2.9 Non-malignant Bone Marrow Disorders

As with any other organ in the body errors can occur in the bone marrow which lead to disorders with varying degrees of severity. As haematopoiesis is the major process which occurs within the bone marrow, it is not surprising that the majority of non-malignant and malignant disorders arise from defects in this process.

The most common non-malignant disorder of the bone marrow in which medical treatment is sought is anaemia. Anaemia is characterised by the reduction of functional erythrocytes in the bone marrow and peripheral blood, or by a decrease in the amount of haemoglobin in the erythrocyte (113). Errors in erythrocyte production or reduced functionality of haemoglobin synthesis can ultimately impact the ability of the blood to transport oxygen - the major symptom of anemia. Iron deficiency anaemia is a very common subtype which, as the name suggests, is caused by a lack of intake of iron in the diet (114). A more severe type of anaemia is aplastic anaemia where the bone marrow is unable to produce both functional red and white blood cells in addition to platelets (115). Here mature immune cells attack HSCs which inhibits haematopoiesis and increases the number of fat cells.

Another non-malignant disorder of the bone marrow that affects cellular homeostasis is myelodysplastic syndrome (MDS) - however in this case MDS causes an increase in the number of cells. This disorder results in the overproduction of myeloid cells resulting in cytopenia lowering the number and production of normal blood cells. This disorder can manifest into a far more severe malignant disorder, acute myeloid leukemia (AML), if not managed properly (116).

1.2.10 Malignant Bone Marrow Disorders

Although non-malignant disorders of the bone marrow have profound effects on individuals who suffer from them, they are very manageable in the clinic. However, malignant disorders of the bone marrow are by far more severe and are very difficult to treat by clinicians. There are multiple malignant disorders that

can arise in the bone marrow, whereby blood cells generated at various points can become cancerous and proliferate without control.

Haematological cancers are classed into three groups; Leukaemia, Myeloma and Lymphoma (although lymphoma is not present in the bone marrow) (117). The incidence of these cancers can be seen in Figure 1.4. The term leukaemia can be further split into four sub-types; acute myeloid leukaemia (AML), chronic myeloid leukaemia (CML), acute lymphoblastic leukaemia (ALL) and chronic lymphoblastic leukaemia (CLL). As the names suggest AML and CML effect cells of the myeloid lineage and ALL and CLL effect the lymphoid lineage, with the fast progressing acute conditions being more severe than the slower chronic conditions. Leukaemia of the lymphoid lineage has a favourable survival outcome compared to leukaemia of myeloid lineage (118).

Myeloma is a clonal chronic malignancy that specifically effects the plasma cell of the lymphoid lineage (119). Leukaemia and myeloma are liquid malignancies that are present within the bone marrow and peripheral blood, whereas lymphoma is a solid tumour which resides within the lymphatic system and comprises of lymphocytes. This malignancy can be split into Hodgkin and Non-Hodgkin lymphoma; Hodgkin lymphoma is characterised by the cancerous Reed-Sternburg cells whilst Non-Hodgkin encompasses the remainder of lymphomas (120). My thesis is focused on AML and multiple myeloma and these malignancies will be discussed further in sections 1.3 and 1.4.

A

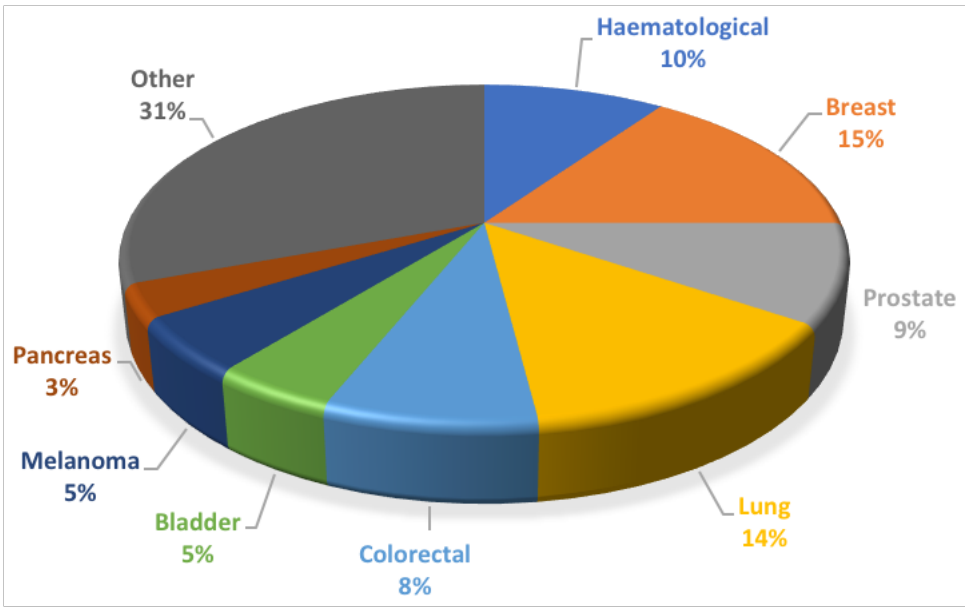

B

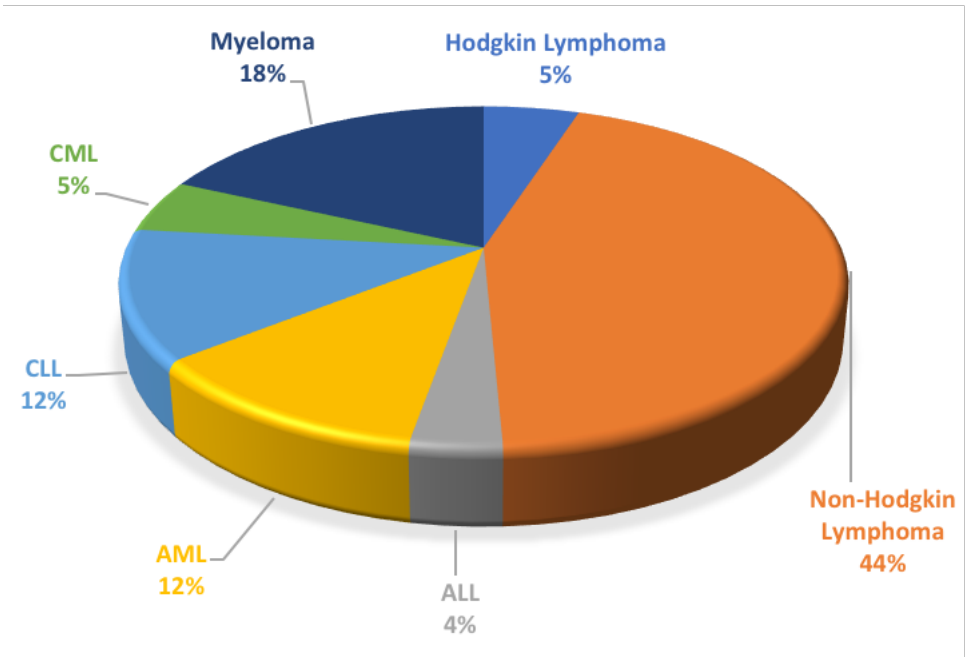

Figure 1.4. National Cancer Institute Incidence Statistics 2018.

The estimated incidence of specific cancers in 2018 is presented as a percentage of total cancers diagnosed. (A) Shows an overview of all types of cancers diagnosed, of note haematological malignancies make up 10% of total cancers diagnosed. (B) Shows a breakdown of the specific haematological subtypes. In relation to my thesis the most important values are that AML and Myeloma make up 12 and 18% of the haematological malignancies diagnosed in 2018. This data was accessed on August 2018 from the Surveillance, Epidemiology, and End Results Program statistics generated by the National Cancer Institute; https://seer.cancer.gov/statfacts/.

1.3 Acute Myeloid Leukaemia (AML)

1.3.1 Overview of AML

AML is an aggressive neoplasm characterised by the accumulation of immature haematopoietic myeloid progenitor cells (blasts) in the bone marrow (121). These blasts increase their proliferative rate whilst halting their differentiation capacity. AML disease is maintained by a small pool of leukaemic stem cells (LSCs), which have the ability to survive chemotherapy and cause disease relapse (minimal residual disease) (122). AML is a very heterogeneous disease due to the fact that there are multiple differentiation points down the myeloid lineage (from CMP to mature myeloid cells) where the blast can arrest differentiation and start to proliferate. In addition, there are various chromosomal translocations present in AML (123). Therefore, specific subtypes of AML have been classified to aid diagnosis and treatment, these will be discussed in section 1.3.3.

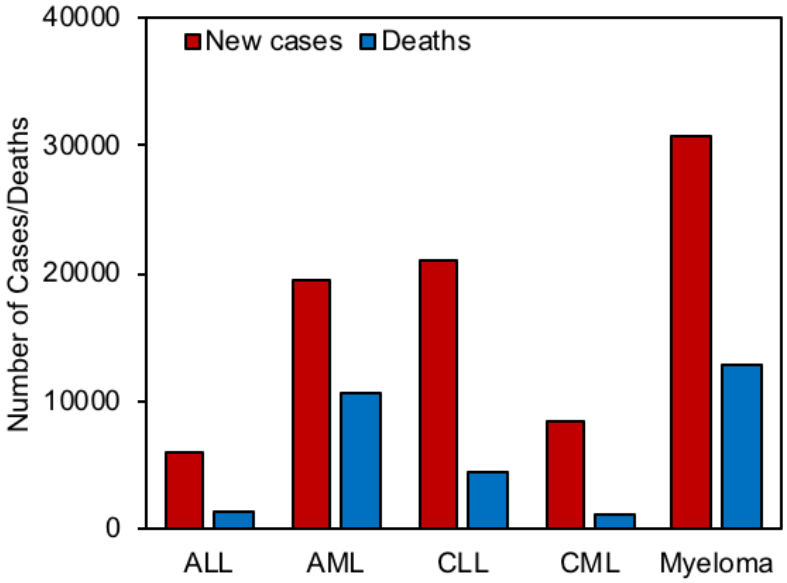

Figure 1.5. Comparison of new cases to deaths in Leukaemia and Myeloma.

This figure shows the number of new US cases of leukaemia and myeloma compared to the number of deaths, highlighting the less treatable diseases. The lowest case/death ratio, which highlights poor prognosis, is AML followed by myeloma. The highest case/death ratio, showing good survival, is CML. This graph was generated from data from the Surveillance, Epidemiology, and End Results Program statistics, accessed August 2018; https://seer.cancer.gov/statfacts/.

AML is a disease of the elderly with the median age of patients at diagnosis being 71 - it is very uncommon to be diagnosed in patients less than 45 years of age (124). The survival rate of patients with AML is poor, with only 27.4% of patients surviving 5 years post diagnosis (125). In addition, the number of US deaths expected in 2018 (10670) compared to number of new cases (19520) is elevated compared to other leukaemias, this is shown graphically in Figure 1.5. The incidence of AML is higher in males, with 5.2 cases per 100,000 in men compared to 3.6 cases per 100,000 in women (125). It has also been reported that AML is more common in Caucasian populations compared to populations of African descent. The incidence of AML is lower in Asian populations followed by Hispanic and American Indian populations. The frequency of AML is increasing in developed countries such as the Canada and Australia (126), in addition to the UK where the number of AML cases has increased by 8% over the last decade (127). However, this increase is most likely due to a combination of an aging demographic and the development of more sophisticated detection techniques. Within the UK, AML incidence is more common in males living in deprived areas whereas there is no link in females (127).

1.3.2 Symptoms, Diagnosis and Treatment

Like any other disease, the symptoms of AML vary from patient to patient. A recent study compared a cohort of AML patients to determine the frequency of known AML symptoms. It was found that the most common symptom was fatigue followed by bruising, weakness, dizziness, shortness of breath and bleeding (128). Due to the un-specific nature of these symptoms there is a need for a diagnostic procedure to confirm the presence of AML.

The initial procedure for diagnosing leukaemia used by clinicians is a blood test - where a high abnormal white blood cell count or very low blood count could indicate the presence of leukaemia (129). A bone marrow aspirate is then conducted where a small sample of bone marrow is taken from the patient and analysed for the presence and sub-type of leukaemia (130). Flow cytometry and Wright-Giesma staining are used to diagnose AML (131). AML blasts are myeloid

cells therefore they express the myeloid markers CD13 and CD33; secondly AML blasts have large nuclei with very little cytoplasm in addition to containing azurophilic granules, which can be determined using Wright-Giesma staining. To fully diagnose AML, greater than 20% of the total cells in the bone marrow must be AML blasts (132). Non-malignant MDS may be diagnosed if there are less than 20% blasts in the bone marrow.

The treatment of AML has not changed in over 40 years and involves an intense regime of chemotherapy, the primary goal is to induce remission where blast levels are reduced to less than 5% (133). This chemotherapy regimen is called 7+3 and involves a continuous infusion of cytarabine (Ara-C) for 7 days, with an anthracycline such as daunorubicin given on days 1, 2 and 3 (134). There are variations in this procedure; at the Norfolk and Norwich University Hospital (NNUH) 10+3 is used, where Ara-C is given for 10 days with daunorubicin given at days 1, 3 and 5 (Information provided by Dr Charlotte Hellmich, NNUH Haematology Registrar). While over 70% of patients treated with intense chemotherapy enter remission, a number enter disease relapse (131). Therefore, there is a need for consolidation/curative therapy, which is most commonly an allogenic haematopoietic stem cell transplant (HSCT). In this process donor HSCs with the same human leukocyte antigen (HLA) are administered to AML patients after myeloablative conditioning of the bone marrow usually with cyclophosphamide (135). In this process, the patient's bone marrow is ablated and replaced with the donors haematopoietic system, thereby reducing the chance of relapse. A side effect of this process is graft vs host disease (GVHD), whereby T cells differentiated from donor HSCs can attack non-haematopoietic host cells within the bone marrow. This can be managed using immunosuppressant medication such as cyclosporine (136), therefore HSCTs remain a common treatment regime in the treatment of AML. Autologous transplants are also used if an appropriate donor is not found, although this is rare.

The current treatments of AML are highly aggressive and consequently they are not well tolerated by the elderly patients that generally develop AML and results

in the poor 5-year survival rate. Therefore, new research into the biology of the disease is needed to develop new treatments which are tolerable to the demographic of the disease, which may increase patient survival duration.

1.3.3 Classification of AML

As AML is a very heterogeneous disorder, the French-American-British (FAB) classification was developed in 1976 based on the type of cell which the leukaemia developed and the degree of maturity, with AML initially split into six subtypes (M0-M6) (137). Updates to this system were introduced in 1985 and 1987, which added two more classifications the M7 and M0 respectively (138, 139). Acute basophilic leukaemia was proposed as M9 in 1999, however this has not been widely accepted (140). Table 1.1 presents the FAB AML classification system.

Table 1.1. FAB classification of AML.

Data from (141).

Type	Name	Cytogenetics	% Adults with AML
M0	Acute myeloblastic leukaemia, minimally differentiated	-	5%
M1	Acute myeloblastic leukaemia, without maturation	-	15%
M2	Acute myeloblastic leukaemia, with granulocytic maturation	t(8;21)(q22;q22), t(6;9)	25%
M3	Promyelocytic, or acute promyelocytic leukaemia (APL)	t(15;17)	10%
M4	Acute myelomonocytic leukaemia	inv(16)(p13q22), del(16q)	20%
M4eo	Myelomonocytic together with bone marrow eosinophilia	inv(16), t(16;16)	5%
M5	Acute monoblastic leukaemia (M5a) or acute monocytic leukaemia (M5b)	del(11q), t(9;11), t(11;19)	10%
M6	Acute erythroid leukaemia, including erythroleukaemia (M6a) and very rare pure erythroid leukaemia (M6b)	-	5%
M7	Acute megakaryoblastic leukaemia	t(1;22)	5%

More recently (2002) the World Health Organization (WHO) proposed an alternate classification system, which could be more clinically useful and produce more meaningful prognostic information that the FAB system (142). This included 4 major classifications of AML with specific subtypes located within these major classifications. An updated version of this classification was published in 2008

(143) and currently the WHO classifications are used interchangeably with FAB classifications. The current WHO classification of AML is presented in Table 1.2.

Table 1.2. World Health Classification of AML.

Major Classification	Minor Classifications
Acute myeloid leukaemia with recurrent genetic abnormalities	• Acute myeloid leukaemia with t(8;21)(q22;q22), (AML1/ETO) • Acute myeloid leukaemia with abnormal bone marrow eosinophils and inv(16)(p13q22) or t(16;16)(p13;q22) • Acute promyelocytic leukaemia with t(15;17)(q22;q12), (PML/RARα) and variants • Acute myeloid leukaemia with 11q23 abnormalities
Acute myeloid leukaemia with multilineage dysplasia	• Following myelodysplastic syndrome (MDS) • Without antecedent MDS but with dysplasia in at least 50% of cells in 2 or more myeloid lineages
Acute myeloid leukaemia and myelodysplastic syndromes, therapy related	• Alkylating agent/radiation-related type • Topoisomerase II inhibitor-related type (some may be lymphoid)
Acute myeloid leukaemia, not otherwise categorised	• Acute myeloid leukaemia, minimally differentiated • Acute myeloid leukaemia without maturation • Acute myeloid leukaemia with maturation • Acute myelomonocytic leukaemia • Acute monoblastic/acute monocytic leukaemia • Acute erythroid leukaemia (erythroid/myeloid and pure erythroleukemia) • Acute megakaryoblastic leukaemia • Acute basophilic leukaemia • Acute panmyelosis with myelofibrosis • Myeloid Sarcoma

1.3.4 Molecular basis of AML

Nonrandom cytogenetic chromosomal translocations have been identified in roughly 52% of total cases of AML and have long been considered the genetic events that drive the formation of the disease (144). The first chromosomal translocation identified was the t(8;21)(q22;q22), which fuses AML1 (RUNX1) on chromosome 8q22 with ETO (MTG8) on chromosome 21q22 (145). This alteration is one of the most frequent, found in approximately 6% of patients with AML (144), and forms the AML1-ETO protein which interferes with the tumour repressor p14(ARF) (146). Another common translocation that occurs in AML is the inv(16)(p13;q22) which fuses the myosin heavy chain (MYH) gene at 16p13 with the core binding protein β (CBPβ) gene at 16q22 (147) - this fusion protein has been shown to impair neutrophil development (148). These two translocations have a good prognostic outcome, whereas translocations which involve the 11q23 (MLL) gene have poor prognosis (149). A specific example is

the t(9;11)(p22;q23), which produces the MLL-AF9 fusion protein resulting in aberrant transcription of MLL target genes (150).

40-50% of diagnosed AML cases are deemed cytogenetically normal (CN) when assessed using conventional band analysis (151); therefore it is important to analyse the effect of alternate molecular events. With the advent of next generation sequencing (NGS) the genetic landscape of CN AML patients has been more clearly defined, leading to the discovery of mutations which contribute to AML disease progression. Each CN AML case is seen to have an average of 13 mutations - 5 of which are driver mutations and 8 being random passenger mutations (152). Key driver mutations found in AML patients will be discussed in more detail below.

The most common mutation in AML are mutations of Nucleophosmin 1 (NPM1), which occurs in between 25 and 30% of patients diagnosed with AML (153). These mutations result in the aberrant expression of the NPM1 protein in the cytoplasm (which usually resides in the nucleus) promoting myeloid proliferation and the development of AML (154). Patients with NPM1 mutations have a favourable prognosis due to the sensitivity of the AML blasts to intense chemotherapy (155). NPM1 mutations are often associated with other key mutations that are involved in the development and progression of AML, including DNA Methyltransferase 3A (DNMT3A), Fms-Like Tyrosine Kinase 3 (FLT3) and Isocitrate Dehydrogenase (IDH) mutations (156).

Missense mutations affecting the arginine codon 882 of the DNMT3A gene are present in approximately 18 to 22% of AML cases and result in a defect in normal haematopoiesis and proper methylation (157). These mutations have recently been identified as pre-leukaemic mutations and are persistent at times of remission, therefore the prognostic outcome of these mutations is adverse (158). FLT3 was found in 1993 to be strongly expressed in haematopoietic cells and important for cell survival and proliferation (159). Internal tandem duplications (ITD) in the juxtamembrane domain of FLT3 are present within 20% of all AML cases and results in the constitutive activation FLT3 signaling promoting blast

proliferation (160). FLT3-ITD mutations have been associated with increased chance of relapse (161). Gain-of-function mutations of the IDH1/2 genes are oncogenic and result in the loss of normal enzyme function, creating a new ability of the enzyme to convert α-ketoglutarate into 2-hydroxyglutarate. Mutations of the highly conserved arginine residue at codon 132 in IDH1 and codon 140 of IDH2 have been identified in around 15-20% of AML patients (162). IDH1/2 mutations are found more frequently in older patients and confer a poor overall survival (163).

In addition to the most frequent mutations described, there are other mutations that are present in AML patients which contribute to disease progression. One of these is a mutation of the ten-eleven translocation oncogene family member 2 (TET2), which is found to be mutated in around 9-13% of AML cases (164). TET2 is an enzyme involved in DNA methylation where it converts 5-methylcytosine (5mC) to 5-hydroxymethylcytosine (5hmC) in DNA; the role of loss of function mutations (in regard to overall AML patient survival) are not clear and still debated (165). The runt-related transcription factor (RUNX1 or AML1) is crucial in normal haematopoiesis and is frequently involved in the AML1-ETO chromosomal translocation leading to AML disease progression (166). In addition to chromosomal translocations, mutations of RUNX1 are present and are found in 5-13% of AML cases and are found to be resistant to conventional induction chemotherapy regimens (167). Other mutations involving the CCAT enhancer binding protein α (CBPα), additional sex comb-like 1 (ASXL1) and p53 have also been described as driver mutations within AML cases (165).

1.3.5 Key Signaling Pathways in AML

Chromosomal translocations and genetic mutations (described in 1.3.4) can lead to the aberrant activation of key intracellular signaling pathways – resulting in leukaemogenesis. In addition, the overexpression of key secretory cytokines within the bone marrow microenvironment (BMM) can have a similar effect on signaling cascades. The majority of intracellular signaling cascades that are aberrantly activated in AML originate from a receptor tyrosine kinase (RTKs),

which are significant components in the pathogenesis of this malignancy (168). The most commonly affected RTK in AML is FLT3, which as discussed previously, is mutated in approximately 20% of cases and causes constitutive activation of this specific RTK (169). Other members of this class of receptor exist (c-kit, c-fms, vascular endothelial growth factor (VEGF) receptor and Brutons tyrosine kinase (BTK)) and all are implicated in AML progression, where mutations again cause the aberrant constitutive expression of the receptor (170-172).

The MAPK/ERK pathway is a key process in cellular homeostasis that links extracellular stimuli with proliferation, differentiation and survival of the cell (173). In this process, the receptor tyrosine kinase activity of the epidermal growth factor receptor (EGFR) is activated by external stimuli promoting Ras to bind to GTP causing activation. Ras then activates RAF kinase, which phosphorylates and activates MEK which in turn phosphorylates and activates mitogen-activated protein kinase (MAPK). MAPK can then activate transcription factors (such as c-myc and c-Jun) which promote protein synthesis and cell cycle progression. This signaling process is constitutively activated in AML blasts, resulting in disease progression (174). FLT3-ITD mutations have also been shown to activate MAPK in AML blasts (175). In addition, AML blasts have been shown to be susceptible to small molecule MAPK inhibitors (176).

Another key intracellular signaling pathway that is abnormally activated in AML is the PI3K/AKT/mTOR pathway, this pathway is crucial to many aspects of cell growth and survival (177). Activation of growth factor receptor protein kinases results in the auto-phosphorylation and recruitment and activation of phosphatidyl-inositol-3-kinases (PI3Ks) (178). Activation of PI3K causes the production of the second messenger phosphatidylinositol-3,4,5-triphosphate (PIP_3) which in turn activates phosphoinositide-dependent kinase 1 (PDK1) and Akt/protein kinase B (PKB) (179). Akt has the ability, through mTOR and glycogen synthase kinase-3 (GSK3), to regulate several cell processes which result in cell survival and cell cycle progression. This pathway is over-activated in over 50% of patients with AML and AML blasts have been shown to be susceptible to PI3K pathway inhibitors (180).

The JAK/STAT (Janus associated kinase-signal transducer and activator of transcription) signaling pathway has also been implicated in AML disease progression. This pathway includes four tyrosine kinases (JAK1-3 and Tyk2) (181) and upon the binding of its ligand, the receptor activates through dimerization and phosphorylation of its cytoplasmic domain (182). Activated JAK-cytokine receptor complexes recruit specific cytoplasmic transcription factors called STAT proteins (183). STAT proteins dimerize and translocate to the nucleus, where they regulate the transcription of a wide range of genes controlling cell division and cell cycle progression. A strong expression of JAK/STAT proteins is observed in AML blasts along with constitutive expression of this signaling pathway (184). Inhibitors of the JAK/STAT pathway have been shown to decrease the proliferation of AML blasts (185).

The three major signaling pathways implicated in AML disease progression have been discussed. Other pathways are also aberrantly expressed in AML, including the Wnt/ β-catenin (186) and NF- κB pathways (187). The combination of all these pathways result in the aberrant expression of genes that increase protein synthesis, cell cycle progression and cellular survival - subsequently this could simulate the formation and progression of AML.

Although these pathways may provide a novel therapeutic window for disease intervention, it is also important to note that there is a vast amount of cross-talk between the pathways. Therapies targeting a single cellular pathway in AML may be ineffective, as other compensatory pathways may still generate the same pro-tumoral aberrant activation of key genes.

1.3.6 Current clinical trials

As discussed earlier the treatment of AML has not changed in over 40 years, therefore new therapies are required as the overall survival of patients with AML is poor. There are current clinical trials ongoing which are analysing the effectiveness of therapies that target some of the ideas discussed in this section, along with other novel therapeutic targets. An overview of the current clinical trials

occurring in AML is presented in Table 1.3. In my opinion, one of the most promising new therapeutics in clinical trials for AML is Venetoclax (ABT-199), which targets the anti-apoptotic Bcl-2 protein within the mitochondria (188). Venetoclax has achieved a durable response in elderly AML patients ineligible for induction therapy, with 73% reaching complete remission (189).

Table 1.3. An overview of current clinical trials ongoing for the treatment of AML.

Data in the table is from a combination of (190) and from https://clinicaltrials.gov/ct2/home

Trial Number	Target Effect	Agent	Suggested AML population	Single/Combination therapy	Phase
NCT01696084	Liposomal formulation of 7+3	CPX-351	>60 years, fit for induction therapy	Single	3
NCT01191801	Topoisomerase II inhibitor	Vosaroxin	>60 years, relapsed/refractory	With cytarabine	3
NCT02920008	DNMT Inhibitor	Guadecitabine	Unfit for induction therapy or relapsed/refractory	Single	3
NCT02074839	IDH1 Inhibitor	AG-120	IDH1 Mutated AML	Single	1
NCT02577406	IDH2 Inhibitor	AG-221	IDH2 Mutated AML	With low dose/medium dose cytarabine	3
NCT00946647	HDAC Inhibitor	Panobinostat	Ongoing investigation	With Azacytidine	1
NCT02668653	FLT3 Inhibitor	Quizartinib	FLT ITD, relapsed/refractory	Single	3
NCT01713582	BET Inhibitor	OTX015	Ongoing investigation	Single	1
NCT01721876	Polo-like kinase Inhibitor	Volasertib	Unfit for induction therapy	With low dose cytarabine	3
NCT02203773	Bcl-2 Inhibitor	Venetoclax (ABT-199)	Unfit for induction therapy, >60 years	With Azacytidine	2
NCT03286530	JAK2 Inhibitor	Ruxolitinib	AML patients in remission or after stem cell transplant	Single	2
NCT03390296	Immunotherapy, targeting CD134 on T cells	PF-04518600	No specifications	Combinations with PD-1 inhibitors (example: Avelumab)	2
NCT02953561	PD-1 Inhibitor (Immunotherapy)	Avelumab	Relapsed and refractory	With Azacytidine	1
NCT01822015	mTOR Inhibitor	Sirolimus	Newly diagnosed	With Idarubicin/Daunorubicin	1
NCT02089230	MEK Inhibitor	MEK162	Unfit for induction therapy	Single	2

1.4 Multiple Myeloma (MM)

1.4.1 Overview of MM

The second haematological malignancy my thesis will focus on is Multiple Myeloma (MM) which is a neoplastic disorder of plasma cells, the terminal differentiation stage of a B cell. This disease is characterised by the accumulation and proliferation of monoclonal plasma cells within the bone marrow and

accounts for approximately 10% of all diagnosed haematological disorders (191, 192). In addition, MM is the second most commonly diagnosed haematological malignancy behind lymphoma (see Figure 1.4). In MM malignant plasma cells are unable to produce functional antibodies, instead producing monoclonal or light chain only (Bence Jones protein) immunoglobulins (193). There are numerous clinical stages of this disease, which will be discussed in 1.4.3.

Looking back at Figure 1.5, it can be seen that MM has the second worst prognostic outcome behind AML. The number of US MM deaths predicted in 2018 (12770) compared to number of new cases (30770) is elevated compared to other haematological malignancies (125). Like AML, this disease affects primarily the older demographic with the average age at diagnosis being 66 (194) and only 50.7% of patients survive 5 years (125). When analysing the likelihood of developing MM in various geographic locations, it appears that the frequency of MM cases is far greater in the western world (such as North America and Europe) compared to traditionally weaker economic countries (such as Africa) (195). However, it is important to consider the predicted life expectancies in these countries - on average people are only expected to live to about 50-year-old in weaker economic countries. Therefore, as MM patients are generally diagnosed at around 66, the chance of developing MM is lower in these younger populations in developing countries. When analysing the prevalence of MM in those of African descent compared to Caucasians, MM is twice as common in those of African descent compared to Caucasians (196). When these results were normalized with economic factors the difference is still observed, implying there is a biological difference for the observed results (197). In addition, MM is 40-50% more commonly diagnosed in males compared with females (198).

1.4.2 Clinical Stages of MM

Plasma cell disorders cover a plethora of disease states ranging from the asymptomatic premalignant proliferation of plasma cells (monoclonal gammopathy of unknown significance (MGUS)) and asymptomatic MM (smoldering MM (SMM)) to symptomatic malignant disease (MM and plasma cell

leukaemia) (199). Research has determined that almost all cases of MM evolve from MGUS (200), however only around 1% of MGUS cases progress to malignant disease (201).

Abnormal immunoglobulin protein (paraproteins) are found in the blood of MGUS patients, first noted by Waldenström in 1960 when abnormal gamma-globulin bands were found when carrying out protein electrophoresis on the serum from healthy patients (202). There are three distinct clinical subtypes of MGUS depending on the abnormal monoclonal protein secreted; non-IgM, IgM and light-chain MGUS (203). In 2003, the International Myeloma Working Group (IMWG) developed a diagnosis classification for known monoclonal gammopathies (204). For MGUS to be diagnosed there must be <30g/L monoclonal immunoglobulin in the patient's serum, with fewer than 10% monoclonal plasma cells in the bone marrow. An update of these criteria in 2010 added the absence of end stage organ damage to the classification of MGUS (205). There are vast variations in the speed of progression from MGUS to malignant MM, with some progressing swiftly and others not at all. The risk of progression is effected by a number of factors including type of monoclonal Ig that is secreted (206). Patients with MGUS are monitored yearly and there are currently no therapeutic interventions for this stage of the disease.

The progression of MGUS disease can lead to SMM, which is the intermediate stage to malignant MM. SMM is also a disease with elevated monoclonal plasma cells which produce paraproteins. It is diagnosed when the number of monoclonal plasma cells in the bone marrow increases to over 10%, paraprotein concentration in patient serum exceeds 30g/L and there is no sign of end organ damage (207). The risk of developing malignant MM from SMM is far greater compared with MGUS, 10% of patients diagnosed with SMM will develop MM within 5 years (208). SMM is biologically heterogeneous as it contains a subset of late MGUS patients and early MM patients who have not developed end organ damage (209). As this is the case, treating patients in the SMM stage provides an opportunity to decrease the cases of MM - although currently there are no treatment regimens for this condition. A recent study showed that treating SMM

patients with approved MM therapeutics (Lenalidomide and Dexamethasone) increased the 5-year MM progression free time from 30 to 77% compared to no treatment (210).

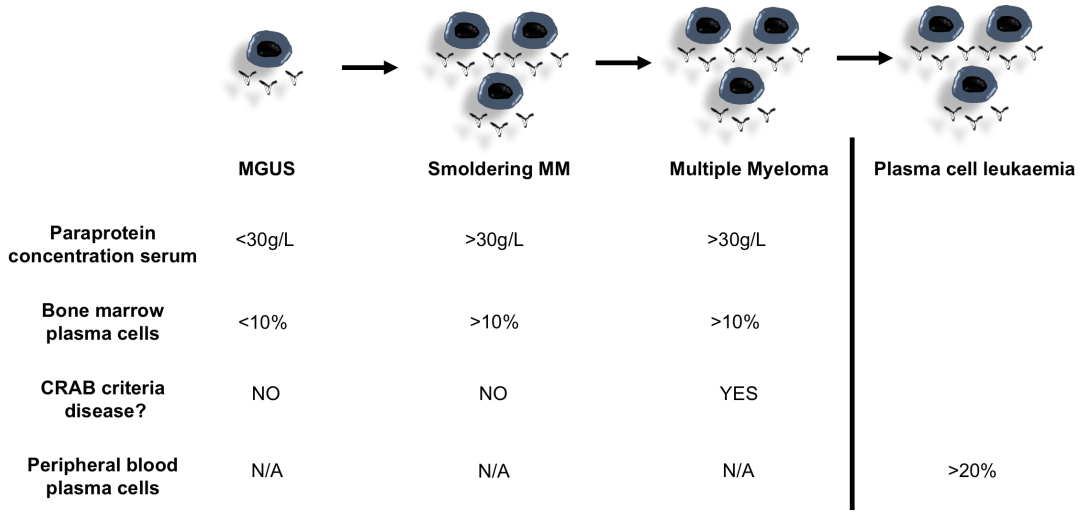

Figure 1.6. The clinical stages of Multiple Myeloma disease progression.

SMM can lead to symptomatic MM upon the detection of tissue damage using the CRAB criteria; Calcium, Renal insufficiency, Anaemia and/or Bone lesions (211). The symptoms, diagnosis and treatments of symptomatic MM will be described in section 1.4.3. The rare disorder of plasma cell leukaemia (PCL) can arise from Symptomatic MM (212). This condition is very aggressive and is characterised by the presence of circulating monoclonal plasma cells in the peripheral blood. PCL is diagnosed when there are more than 20% monoclonal plasma cells in the peripheral blood and an absolute plasma cell count of greater than $2x10^9$/L (213). There are two types of PCL (primary and secondary) where primary PCL is diagnosed in patients with no history of MM, whereas secondary PCL is observed as a leukaemic transformation of relapsed or refractory MM disease in MM patients (204). The incidence of primary PCL is greater than secondary PCL - 60-70% compared to 30-40% respectively.

1.4.3 Symptoms, Diagnosis and Treatment

Symptomatic MM is diagnosed when CRAB criteria have been reached, as mentioned above. Of the CRAB criteria, the most common symptoms in MM are fatigue (often caused by anaemia) and bone pain (119). 90% of MM patients present with bone disease at some point during the MM progression (214), ultimately due to an imbalance of osteoblast and osteoclast production (215). The bone damage can often lead to hypercalcemia resulting in renal failure in around 50% of all MM patients (216).

To diagnose MM numerous clinical procedures are carried out - one of these is a test to detect paraprotein levels in serum/urine. To achieve this either a serum protein electrophoresis assay, serum immune-fixation assay or serum FLC assay is carried out in parallel to a 24-hour urinary protein electrophoresis (217). The Ig type of the paraproteins can be detected using these methods: 50% of MM patients are IgG, 20% are IgA, 20% are light chain only, 2% are IgD and 0.5% are IgM (194). In rare cases (2-3% of patients) no detectable paraprotein is detected and these patients are deemed non-secretory MM (218). Bone marrow biopsies are also carried out in patients suspected of having MM, this test will determine the number of monoclonal plasma cells in the bone marrow. Additional tests, such as FDG-PET (fluorodeoxyglucose positron emission tomography) and CT scans of the entire skeleton, are utilised to diagnose bone lesions. MRI scans are sometimes carried out when it is difficult to distinguish between SMM and MM (219).

The first case of MM was first described in 1844 (220), however the first working treatment was not discovered until 100 years later. The nitrogen mustard alkylating agent melphalan was the first drug shown to have beneficial effect on MM patient survival - 50% of patients treated showed improved survival (221). Melphalan was then combined the corticosteroid prednisone, which increased MM patient survival by 6 months compared to patients treated with melphalan alone (222). This treatment was used as a MM core therapy for decades until a study presented the idea that thalidomide, used very famously for morning

sickness in the 1950s, had anti-MM properties reducing bone marrow plasma cell number along with reducing levels of paraproteins (223). Thalidomide was approved for use in MM, commonly in combination with melphalan and prednisone, along with the thalidomide derivative lenalidomide. The proteasome degradation pathway is very important for MM survival (see section 1.4.6), therefore the anti-MM effect of proteasome inhibitors such as bortezomib and carfilzomib was studied. 35% of patients treated with bortezomib had complete or partial response to bortezomib (224), and when combined with melphalan and thalidomide the median patient survival increased from 16 months to 24 months (225).

The most important phases of MM therapy are the initial therapy, stem cell transplant and consolidation/maintenance therapy. Initial therapy depends on the risk factor of the patient, but all contain a regimen of three drugs: a proteasome inhibitor, a thalidomide derivative and a corticosteroid (119). Patients with low or medium risk are given 4 cycles of bortezomib, lenalidomide and dexamethasone - followed by an autologous stem cell transplant (ASCT). Patients at high risk are given a slightly modified 4 cycles of carfilzomib, lenalidomide and dexamethasone - followed by an ASCT. Maintenance therapy for low, medium and high-risk patients is lenalidomide, bortezomib or carfilzomib respectively. Only around 50% of MM patients survive 5 years after diagnosis as they become refractory and resistant to treatments - there is therefore a need for alternate therapeutic interventions. It is envisaged that these will arise from a better understanding of the biology of MM pathogenesis.

1.4.4 Plasma Cell Immunoglobulins

The most important function of a non-malignant plasma cell is to its ability to produce immunoglobulins in response to encountering foreign pathogens (226). These immunoglobulins can be secreted or bound to the cell membrane and are composed of two heavy (α, γ, δ, ε or μ) and two light chain (κ or λ) peptides that form a tetrameric complex (Figure 1.7) (227). Based on the specific peptide sequence in the heavy chain, the immunoglobulin can be sub-divided into 5

different classes; IgA, IgG, IgD, IgE and IgM. Monoclonal plasma cells in MM secrete large quantities of one specific type of immunoglobulin and, as discussed in 1.4.3, there is variation in the percentage of patients with each type of Ig heavy chain. Each type of heavy chain Ig confers a different prognostic outcome; with the rare IgD having a poor prognosis (21 months) and IgG patients having a more favourable prognosis (61.8 months) (194, 228).

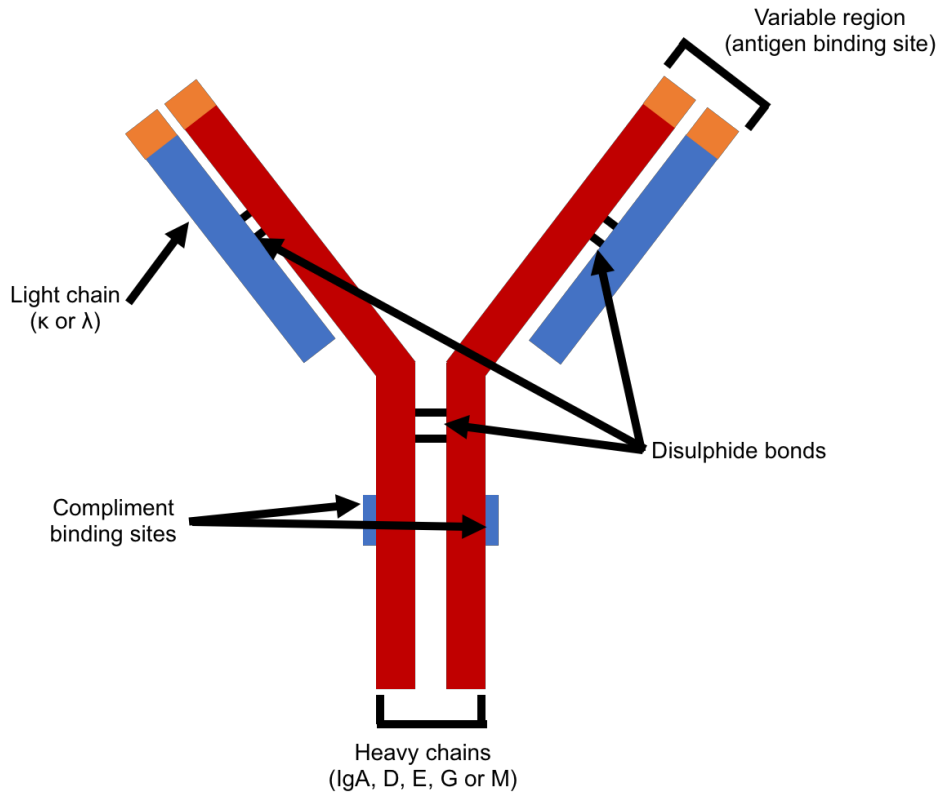

Figure 1.7. Schematic representation of an immunoglobulin (Ig).

The structure of an immunoglobulin is presented that is either secreted or present on the cell surface of a normal or malignant plasma cell. MM cells secrete large quantities of monoclonal immunoglobulins with a specific heavy chain peptide sequence, these are defined as paraproteins.

1.4.5 Molecular Basis of MM

Multiple myeloma is classified as a single disease, however within this disease there are various different cytogenetically distinct plasma cell neoplasms (229). Using fluorescence in situ hybridization studies, 40% of all MM cases were shown to have the presence of trisomies in the malignant cell (230). In the majority of the

remaining cases, chromosomal translocations were found involving the immunoglobulin heavy chain (IgH) on chromosome 14q32 (231). In a small number of cases both trisomies and chromosomal translocations were found, along with a minimal number of cases having no genetic abnormalities. These trisomies and chromosomal translocations (highlighted in Table 1.4) are considered primary cytogenetic abnormalities' and are present from the development of MGUS (119). Other cytogenetic abnormalities can occur throughout the progression of MM are defined secondary cytogenetic abnormalities. A number of key MM driver mutations have also been found in key proto-oncogenes and tumour suppressors, including KRAS, NRAS, BRAF and TP53, which promote MM cell proliferation and survival (232).

Table 1.4. Genetic abnormalities present in MM and their associated prognostic outcome.

Table modified from (119).

Cytogenetic abnormality	Effected Gene	%MM cases	Prognostic Outcome
Trisomy	One or more odd numbered chromosomes	42	Good
t(11;14)(q13;q32)	CCND1 (Cyclin D1)	15	Good
t(4;14)(p16;q32)	FGFR3 and MMSET	6	Intermediate
t(14;16)(q32;q23)	C-MAF	4	High
t(14;20)(q32;q11)	MAFB	<1	High
Other IgH translocations	CCND3 (Cyclin D3) in t(6;14) MM	5	Varying
Combined IgH translocation and trisomy	Trisomies plus one IgG translocation	15	High
Isolated monosomy 14	-	4.5	Not Clear
Other	-	5.5	Varying
Normal	-	3	Good

1.4.6 Key Signaling Cascades in MM

There is much overlap in key signaling cascades that are promoted in AML and MM disease progression. Pathways include the PI3K/AKT/mTOR, MAPK/ERK and JAK/STAT (described in 1.3.5), whose aberrant activation also leads to an increased proliferative drive and survival of MM (233). These pathways are also able to stimulate osteoclast production and suppress osteoblasts, leading to the bone lesions observed in MM pathogenesis (234). Inhibitors of the PI3K, MAPK

and JAK/STAT pathways have been shown to reduce MM disease progression (235-237); however, like AML these have not translated to the clinic as there are multiple compensatory mechanisms which can recover the observed phenotype.

One current therapy used in the treatment of MM, however, does target a key signaling pathway that is aberrantly activated in MM disease pathogenesis - the nuclear factor-κB (NFκB) pathway. This pathway is a major regulator of immune and inflammatory responses within the cell and it's activation leads to the expression of genes such as IL-6 and TNFα (238). The NFκB pathway is activated by external signals including VEGF (which is in some cases secreted by supporting cells in the BMM), but more importantly by A proliferation-inducing ligand (APRIL) and B-Cell-Activating Factor (BAFF) which are two of the most crucial survival factors for healthy plasma cells and MM cell alike (239, 240). TACI and BCMA are the common receptors that these factors bind to activating the NFκB pathway, however BAFF can also activate an alternate pathway through the BAFF-R receptor.

The NFκB transcription family composes of a number of transcription factors including NFKB1 (p50 and p105), NFKB2 (p52 and p100), RelA (p65), RelB and c-Rel (241). The transcription factors are held in their inactive form by their inhibitory protein IκBα and after stimulation of TNFR-associated factors, IκBα is activated by phosphorylation leading to its degradation by the proteasome (242). This results in the accumulation of homodimers and heterodimers of NFκB transcription factors within the nucleus, leading to the expression of genes including those involved in cell survival and cell cycle progression. Inactivation of the NFκB pathway, via the inhibition of IκBα degradation, can cause dividing cells to be more susceptible to apoptosis (243). Proteasome inhibitors (such as bortezomib and carfilzomib) can exploit this mechanism and have shown to be successful in treating MM. Proteasome inhibitors were approved by the FDA in 2003.

Another key molecule in the pathogenesis of multiple myeloma is CD38, also known as cyclic ADP ribose hydrolase, which is found uniformly of the surface of

MM cells (244). CD38 is a multi-functional 48 kDa type II glycoprotein discovered by Reinhertz and colleagues in 1980 (245), and it plays a role in the activation and proliferation of mature lymphocytes as well as malignant plasma cells (246). CD38 is presently known to have two main functions, firstly as an ectoenzyme catalysing the conversion of nicotinamide adenine dinucleotide (NAD+) to cyclic adenosine diphosphate-ribose (ADPR) - which is a potent intracellular calcium releaser (247). Secondly, CD38 functions as a receptor which mediates leukocyte migration through the endothelium via its co-receptor CD31 (248). Preclinical studies of CD38 inhibition shows that it mediates MM cytotoxicity in the presence of the protective bone marrow (249). More recently early phase clinical trials of Daratumumab (a CD38 targeting antibody) in MM patients has demonstrated a favourable safety profile and encouraging efficacy in patients with heavily pre-treated and refractory disease (250, 251). Daratumumab has now been FDA approved for the treatment of relapse refractory myeloma in combination with bortezomib or lenalidomide (252). Although highly promising in the treatment of MM, the actual mechanism of MM cytotoxicity through inhibition of CD38 is relatively unknown.

1.4.7 Current Clinical Trials in MM

The treatment of multiple myeloma has progressed over the last 20 years, however due to the still relatively poor 5-year survival rate other novel therapies are required. It is envisaged that survival rates will improve due to the FDA approval of the CD38 monoclonal antibody Daratumumab, however this is only used in relapse MM patients and is not currently a front-line treatment. Having said this there is always a need for new therapeutics and there are a number of clinical trials ongoing in the treatment of MM. In my opinion, the most promising novel therapeutic for the treatment of MM is Daratumumab. Although already approved for the treatment of relapsed/refractory patients, I believe this drug will become a front-line therapy in the years to come.

Table 1.5 summarises the current clinical trials ongoing in MM. It can be seen that the majority of clinical trials ongoing are focusing on the relapsed/refractory

patients, most probably due to the high rates of relapse within MM patients after successful front-line treatments described in 1.4.3.

Table 1.5. An overview of current clinical trials occurring in Multiple Myeloma.

Clinical trial data was collected from https://clinicaltrials.gov/ct2/home accessed August 2018.

Trial Number	Target Effect	Agent	Suggested MM population	Single/Combination therapy	Phase
NCT01549431	HDAC Inhibitor	Panobinostat	Relapsed/Refractory	With Carfilzomib	1
NCT01038388	HDAC Inhibitor	Vorinostat	Newly diagnosed	With Bortezomib, Lenalidomide and Dexamethasone	1
NCT01638936	CD138 monoclonal antibody (coupled to cytotoxic DM4)	BT-062	Relapsed/Refractory	With Lenalidomide	1/2
NCT01456689	Pan-PIM kinase inhibitor	LGH447	Relapsed/Refractory	Single	1
NCT02186834	Selective Inhibitor of Nuclear Export (XPO1 inhibitor)	Selinexor (KPT-330)	Relapsed/Refractory	With Liposomal Doxorubicin	1/2
NCT02384083	Kinase Spindle Protein Inhibitor	Filanesib	Newly diagnosed and Relapsed/Refractory	With Pomalidomide and Dexamethasone	1/2
NCT01478581	BTK Inhibitor	Ibrutinib	Relapsed/Refractory	Dexamethasone	2
NCT02954796	Anti-CD352 antibody	SGN-CD325A	Relapsed/Refractory	Single	1
NCT01832727	Second generation proteasome inhibitor	Oprozomib	Relapsed/Refractory	Dexamethasone	1/2
NCT01484275	Anti-IL-6 antibody	Siltuximab	High-risk smoldering MM	Single	2
NCT02265731	Bcl-2 Inhibitor	Venetoclax (ABT-199)	Ongoing study	With Azacytidine	1/2

1.5 Malignant Bone Marrow Microenvironment

It is envisaged that novel therapeutics in the treatment of AML and MM will arise from a better understanding of the biology that underpins disease pathogenesis and proliferation. A key factor that requires further investigation is the interaction the malignant haematopoietic cell has with its microenvironment and how this interaction promotes the survival and proliferation of the disease. The “seed and soil” hypothesis was first postulated in 1889 (253) and describes how metastatic tumours only grow in a distant organ if that organ offers the correct “soil” or microenvironment. This theory was largely forgotten until the last couple of decades (254), and due to revised interest we now know that the “seed and soil” hypothesis may be true for tumour initiation and proliferation itself (255). Not only does the microenvironment play a role in disease initiation and proliferation, it is also a key player in the development of chemo-resistance and disease relapse (256) - two major concerns in haematopoietic malignancies. The vast majority of

chemotherapeutics used today to treat a plethora of cancers target the malignant cell itself, rather than the microenvironment in which the malignancy resides. The BMM is a highly specialised niche that comprises of a variety of cell types including BMSC, osteoblasts and endothelial cells which are comprehensively reviewed in section 1.2. Finely elucidating the complex interactions between tumour "seed" and microenvironment "soil" will hopefully give rise to novel therapeutic interventions and increase the survival of patient with AML and MM.

1.5.1 AML

Isolated AML blasts undergo high levels of apoptosis when cultured ex vivo, signifying the important role that the bone marrow microenvironment has on the survival of AML (257). AML patients have high levels of relapse caused by minimal residual disease, where small numbers of AML blasts are sequestered within the bone marrow. Compared with the understanding of the genetic abnormalities that contribute to AML disease progression (see section 1.3.4), little is understood about the complex interactions between the AML blasts and its BMM. The role of the microenvironment first came to the forefront when the level of apoptosis within AML blasts was shown to reduce when cultured with a layer of BMSC *ex vivo* (258). This was followed by a study that showed culturing the AML blasts with the BMSC cell line HS-5, provided protection against chemotherapy treatments (259).

Our understanding of how the BMM confers chemo-resistance and protects against apoptosis is increasing as we elucidate the complex mechanisms involved. It has been found that AML blasts can shape their own microenvironment to favour their survival and proliferation (260, 261), which involves direct contact or stimulating cells of the BMM to secrete key soluble factors.

As discussed in section 1.2.3, BMSC secrete high levels of CXCL12. AML blasts express CXCR4 and hijack the CXCR4/CXCL12 axis – allowing homing to favourable niches within the BMM (262). After the migration of AML blasts to

these niches, they are able to manipulate cells of the BMM to their advantage. BMSC continue to secrete CXCL12 in the BMM and this chemokine has been shown to activate the PI3K/Akt signaling pathway, promoting the survival and proliferation of AML blasts (263). The direct co-culture of AML blasts with BMSC was shown to up-regulate the master transcription factor c-Myc in BMSC, which contributed to chemo-resistance via the downregulation of apoptosis related genes (264). Furthermore, this chemo-resistance was overcome upon the addition of a small molecule inhibitor of c-Myc. BMSC have increased levels of IL-6 secretion in the presence of AML blasts which has been shown to protect AML blasts through activation of the JAK/STAT pathway, through the IL-6 receptor (265). In another example of AML manipulating the BMM; AML blasts have been shown to secrete the macrophage inhibitory factor (MIF), which in turn stimulates BMSC to secrete IL-8 (266). IL-8 can activate the PI3K/Akt and MAPK signaling pathways to promote survival and proliferation (267).

Other cells within the BMM can contribute to the survival and proliferation of AML blasts. Endothelial cells express VCAM-1, which binds to the VLA-4 on AML cells and maintains their retention within favourable niches (268). The matrix metalloproteinase-2 (MMP-2) is an endopeptidase-like enzyme which remodels the ECM and has been shown to contribute to tumour progression (269). Endothelial cells and fibroblasts express MMP2 and are activated by the extracellular metalloproteinase inducer (EMMPRIN), also known as CD147, located on AML blasts (270). The interaction of receptor activator of nuclear factor κ-B ligand (RANKL) and receptor activator of nuclear factor κ-B (RANK) is important in osteoblast regulation of osteoclasts (271). AML blasts express RANK and utilise RANKL (secreted by osteoblasts) to activate the NFκB pathway and impair NK cell anti-leukaemic immunosurveillance (272). Finally, adipocytes have been shown to transfer free fatty acids (FFA) to AML blasts (273), through CD36 (274) - increasing fatty acid oxidation (FAO). As a result, AML blasts have been shown to be susceptible to the FAO inhibitor Avocatin B (275).

Comparable with the non-malignant HSC niche, AML resides in a microenvironment with low oxygen (<1%) levels defined as hypoxic (276).

Residing in hypoxic environments minimises the exposure to chemotherapeutic drugs as well as activating key signaling cascades such as the PI3K/Akt/mTOR pathway (277). AML blasts generate high levels of reactive oxygen species (ROS), which contribute to the hypoxic niche, through the overexpression of NADPH oxidase 2 (NOX2) (278). NOX2 is an enzyme present on the surface of myeloid cells and catalyses the conversion of molecular oxygen to superoxide - used by phagocytic cells to neutralise pathogens (279). In the context of AML, the overexpression of NOX2 has been shown to increase AML disease progression through the activation of the MAPK pathway (278).

Taken together, the BMM plays a significant role in the progression of the AML and may provide favourable places of therapeutic intervention. The BMM protection of AML is summarised schematically in Figure 1.8.

1.5.2 MM

Multiple myeloma is also a disease heavily reliant on its bone marrow microenvironment for migration, survival, proliferation and drug resistance. Many of the aspects of the AML BMM are also apparent in the microenvironment of MM. Direct contact between BMSC and MM cells, or through BMSC derived soluble factors, has been shown to aid MM cells evade chemotherapeutic drugs (280). MM cells migrate to favourable niches very similarly to AML blasts, whereby they exploit the CXCR4/CXCL12 axis (281) and remain in these niches due to the VLA-4/VCAM-1 interaction (282). The adhesion of MM cells to BMSC stimulates the Notch signaling pathway in both cell types, subsequently stimulating the production of IL-6 and VEGF (283). VEGF promotes angiogenesis which has been shown to be crucial for MM disease progression (284). This interaction also promotes the NFκ-B pathway in BMSC and again leads to the production of IL-6, which stimulates MM cells to produce VEGF (284). Recently, BMSC have been shown to release exosomes containing miRNA which can be sequestered by MM cells, promoting disease progression (285).

Of the factors released by BMSC, IL-6 is most arguably the most crucial for MM cell proliferation and survival. Also produced by osteoblasts, IL-6 paracrine production by BMSC has been shown to be reliant on MM stimulation. The cytokine IL-1β, released by MM cells, has been shown to stimulate the production of IL-6 within BMSC (286). In addition, the secretion of MIF by MM cells results in the same increase in BMSC IL-6 secretion (287). Upon IL-6 binding to the IL-6 receptor, many key signaling pathways (such as PI3K/Akt, MAPK, and JAK/STAT) are activated - leading to MM proliferation and survival (288). Increased IL-6 levels in the serum of patients with MM has been shown to confer a poor overall prognosis (289).

Other cells within the BMM are also crucial in MM disease progression. The increased number of osteoclasts in MM patients leads to characteristic bone lesions found in the disease. Activation of osteoclasts occurs through the RANK ligand which is produced upon MM cells binding to BMSC; blocking of the RANK receptor on osteoclasts can result in reduced tumour burden (290). In addition, osteoclasts can constitutively release proangiogenic factors, such as VEGF (291). MM cells express the MMP-2 inducer EMMPRIN which causes endothelial cells and fibroblasts to remodel the ECM to the advantage of MM cells (292). More recently, MM cells have also been shown to release microvesicles which contain high levels of EMMPRIN (293). Osteoblasts have the ability to secrete IL-6 (294), however the suppression of osteoblast function is found in MM patients. This is achieved through the Wnt signaling antagonist DKK-1 secreted by MM cells, which inhibits osteoblast differentiation promoting osteoclast generation (295). The interactions the MM cell has with its BMM, described in this section, are summarised schematically in Figure 1.8.

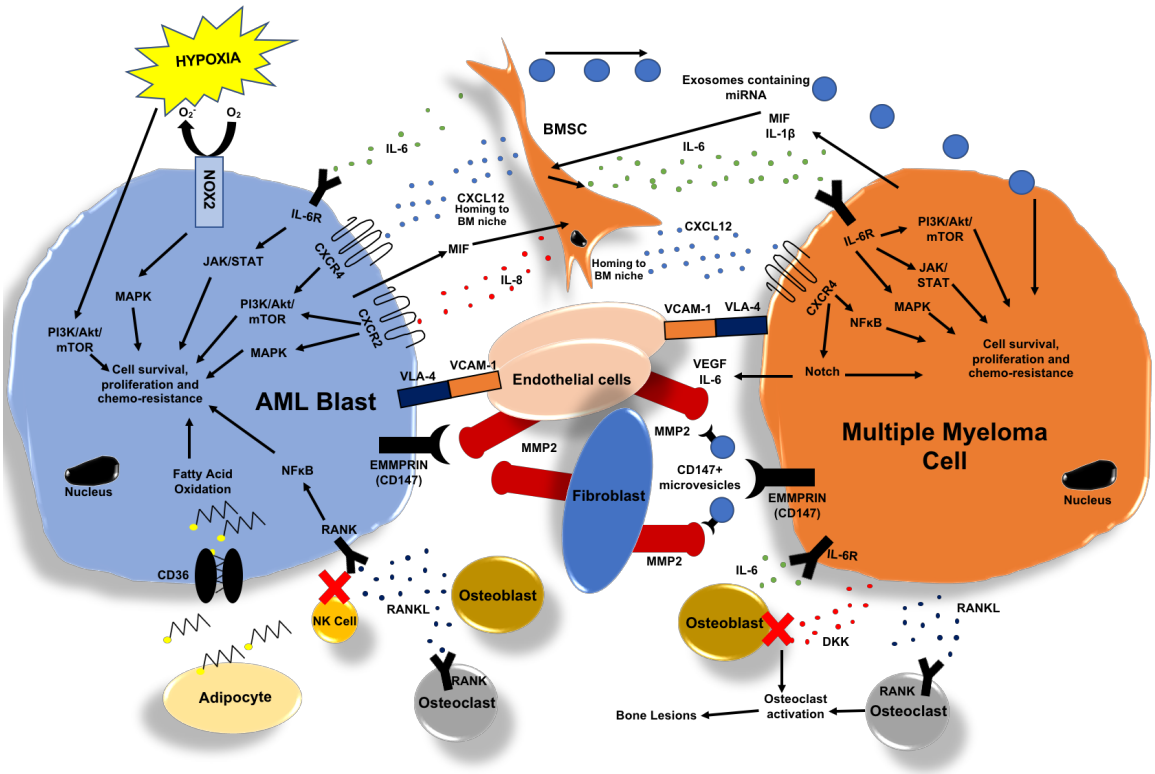

Figure 1.8. The bone marrow microenvironment of AML and MM.

A schematic representation of how the BMM provides protection from chemotherapeutics and promotes proliferation of survival of AML and MM cells. AML blasts are shown in blue and MM cells in orange, with cells of the BMM in the centre of the schematic.

1.6 Metabolism

1.6.1 Metabolism Overview

Metabolism is defined as the sum of the biochemical processes (more than 8,700 reactions and 16,000 metabolites) which transduce or consume ATP (296). Core metabolism involves the utilisation of nutrients such as carbohydrates, fatty acids and amino acids through numerous biochemical processes defined in the “Golden Age of Biochemistry” (1920s to 1960s). Cells require energy in the currency of ATP to function and maintain cellular homeostasis. The vast majority of this ATP is generated through aerobic respiration, using glucose as the energy source (297). The first stage in this process is glycolysis, whereby glucose is converted into two molecules of pyruvate - which yields two molecules of ATP. Pyruvate is then fed into the tricarboxylic acid cycle (TCA) cycle within mitochondria (after

conversion to acetyl-coA) which reduces nicotinamide adenine dinucleotide (NAD+) to NADH and flavin adenine nucleotide (FAD) to $FADH_2$ (298). Only one ATP molecule is generated in the TCA cycle, however 3 molecules of NADH and one molecule of $FADH_2$ are produced - which provide electrons for the next stage of the process. As the TCA cycle occurs twice per glucose molecule, these values can be doubled.

The final stage of glucose metabolism is oxidative phosphorylation which involves the transfer of electrons (from NADH and $FADH_2$) along four protein complexes (I, II, III and IV) located on the inner membrane of mitochondria (297). Electrons are passed from Complex I (NADH/ubiquinone oxidoreductase), which removes electrons from NADH, to Complex II (Succinate dehydrogenase), which removes electrons from $FADH_2$, to ubiquinone. This reduces ubiquinone to ubiquinol, which in turn transfers electrons to cytochrome C via Complex III (ubiquinone/cytochrome c oxidoreductase). The final complex electrons are transferred to is cytochrome c oxidase - here electrons are passed to oxygen reducing it to water. As the electrons are moved through the four protein complexes, protons are transported into the inner membrane space of mitochondria - generating a difference in electrical potential (299). This creates a proton motive force which drives protons across the mitochondrial inner membrane through the ATP synthase, triggering a rotation of the F_0 subunit to produce ATP (300).

The 1978 and 1997 Nobel Prize in Chemistry were awarded for the elucidation of chemiosmosis and the underlying enzymatic mechanisms of ATP synthase respectively. The number of protons required to generate one molecule of ATP is highly debated, one study suggested four protons are required (301). This study however did not examine the mammalian ATP synthase, this is an important point as there are likely to be species variations in regard to the number of protons required to produce ATP molecules. One NADH molecule has the ability of releasing 10 protons to the inner membrane space; four by Complex I, four by Complex III and two by Complex IV (297). $FADH_2$ only releases 6 protons as it

skips Complex I. Therefore, a large number of ATP molecules can be generated from the metabolism of each glucose molecule.

1.6.2 Mitochondria

During aerobic respiration, the TCA cycle and electron transport chain both occur in a specialised organelle - the mitochondrion. Mitochondria evolved as the result of a symbiotic relationship between aerobic bacteria and eukaryotic cells, where ancient bacterial symbionts were acquired by eukaryotic cells enabling the utilisation of aerobic respiration (302). Mitochondria are double membraned organelles, which are capable of highly efficient ATP production. The inner membrane forms cristae, which enhance the surface area of the electron transport chain allowing enhanced ATP production. The structure of the mitochondrion is presented in Figure 1.9, with an overview of the process of aerobic respiration.

As mitochondria originated from bacteria they contain a unique genome (mitochondrial DNA (mtDNA)) that is distinct from nuclear genomic DNA (gDNA) and inherited on the maternal line (303). The mitochondrial genome is made up of a 16 kilobase circular mtDNA which contains 37 genes, 12 of which encode protein subunits of the electron transport chain proteins (304). The remaining proteins encoded are made up of mitochondrial tRNAs and rRNAs; in addition, there are still 900 proteins encoded on gDNA. The biogenesis of new mitochondria is a tightly controlled process, facilitated by the master transcription factor peroxisome proliferator-activated receptor gamma coactivator 1-alpha (PGC-1α) (305).

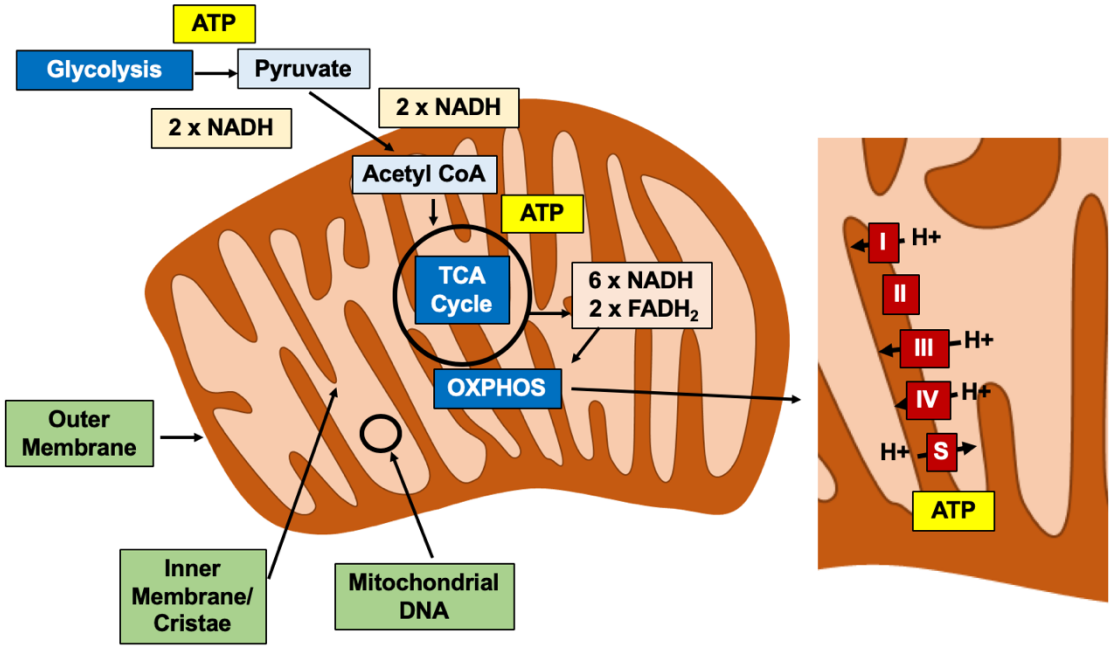

Figure 1.9. The structure of the mitochondrial organelle.

A schematic representation of the structure of the mitochondrial organelle with key biochemical pathways involved in aerobic glycolysis highlighted. These include glycolysis, the TCA cycle and OXPHOS. The electron transport chain is also highlighted (enlarged image) showing the movement of protons across complex I, III and IV into the intermembrane space, followed by the generation of ATP through ATP synthase (shown in the schematic as S).

1.6.3 Cancer Metabolism

Cancer cells have been shown to have atypical respiration whereby they utilise the non-mitochondrial based process of aerobic glycolysis to generate ATP. This mechanism was first discovered by Otto Warburg and is deemed the Warburg effect (306). In this process cancer cells generate pyruvate from glucose (as with aerobic respiration), however they use fermentation to generate lactate from pyruvate rather than generate acetyl-CoA. This effect results in the increased consumption of glucose, as glycolysis is far less efficient than oxidative phosphorylation (OXPHOS) at generating ATP. The increased glucose consumption has proved a valuable tool in cancer diagnosis; FDG-PET scans can detect the increased glucose consumption of a cancer cell (307).

The reason why cancer cells utilise aerobic glycolysis is highly debated. Initially it was thought that mitochondria within cancer cells are defective and this resulted

in an impairment of OXPHOS, therefore non-mitochondrial ATP generation methods were employed. However, it was later found that the OXPHOS capacity of cancer mitochondria is intact (308). The reason for the switch to aerobic glycolysis is therefore more likely to be due to a number of other factors including the tumour microenvironment and activation of oncogenes. As the tumour increases in size, the tumour microenvironment becomes hypoxic - leading to the stabilization of hypoxia inducible factor (HIF). As the dependence on aerobic respiration becomes less, there is a switch in metabolism towards glycolysis (309). In addition, the activation of certain oncogenes including Ras drive a change in tumour metabolism; Ras activates mTOR, which in turn induces HIF which promotes glycolysis (310).

Not all tumours, however, are dependent on the Warburg hypothesis: for example, AML blasts require OXPHOS for survival. The THP-1 AML cell line has been shown to be more sensitive to OXPHOS inhibitors compared to glycolysis inhibitors (311). Also, there are AML blasts which have a high OXPHOS gene signature and these cells are less sensitive to the chemotherapeutic Ara-C when compared to low OXPHOS AML cells (312). In another study, AML blasts were shown to utilise OXPHOS to generate an antioxidant response (313). Furthermore, AML blasts have been shown to have increased mitochondrial levels compared to HSCs (314), which makes them more susceptible to the mitochondrial translation inhibitor tigecycline (315).

Multiple myeloma appears to be a “Warburg cancer” relying predominantly on glycolysis. MM is susceptible to glycolysis inhibitors such as dichloroacetate (DCA) (316) and has an elevated glycolysis gene profile (317). However, these studies were conducted solely on MM cells and did not take into account the effect of the protective microenvironment. MM cells do however have the ability to utilise OXPHOS under ritonavir treatment (318) and HIF-1α suppression (319).

1.6.4 The Transfer of Mitochondria between Somatic Cells

The mitochondrion organelle was classically thought to reside in its somatic cell for its lifetime, where they undergo fission and fusion to generate mitochondrial networks and are ultimately turned over by the specific type of autophagy - mitophagy (320). However, recently it was found that this was not the case - mitochondria were found to move between cells. In a landmark paper by the Gerdes Lab in 2004, intercellular mitochondrial transfer was first shown to occur between PC12 rat pheochromocytoma cells, normal rat kidney cells and HEK239 human embroyonic kidney cells (321). This study opened up the idea that intercellular mitochondrial transfer could occur in a range of non-malignant and malignant settings, an overview of which is shown in Table 1.6.

Table 1.6. Overview of intercellular mitochondrial systems described in literature.

Donor Cell	Recipient Cell	Species	Method	Consequence	Reference
PC12	PC12	Rat	Tunneling nanotubes	Rescues PC12 from apoptosis	321
MSC	A549 rho0 cells	Human	Tunneling nanotubes	Restoration of aerobic respiration	323
MSC	Osteosarcoma (143B)	Human	Tunneling nanotubes	Restoration of mitochondrial function	324
MSC/Endothelial cells	Ovarian Cancer (SKOV3)	Human	Tunneling nanotubes	Chemo-resistance	326
MSC/Endothelial cells	Breast Cancer MCF7	Human	Tunneling nanotubes	Chemo-resistance	326
Murine cells	Melanoma (B16 rho0 cells)	Mouse	Unknown	Restoration of tumourigenic potential	325
Murine cells	Breast Cancer (4T1 rho0 cells)	Mouse	Unknown	Restoration of tumourigenic potential	325
Laryngeal carcinoma	Laryngeal carcinoma	Human	Tunneling nanotubes	Cell-cell communication	328
Mesothelioma	Mesothelioma	Human	Tunneling nanotubes	Cancer Progression	327
Bladder Cancer (T24)	Bladder Cancer (RT4)	Human	Tunneling nanotubes	Increased invasiveness	329
BMSC	Lung Epithelial Cells	Mouse and Human	GAP junctions / Microvesicles	Protection against acute lung injury	330
Astrocytes	Neurons	Mouse	Microvesicles	Repairs neurons after stroke	331

The use of cells devoid of mtDNA (rho0 cells) has been a useful tool in studying intercellular mitochondrial transfer, as restoration of mtDNA within the rho0 cell highlights the acquisition of external mitochondria. These cells can be generated in cell lines using long term culture with ethidium bromide (322). Ethidium bromide

specifically intercalates with mtDNA (over genomic DNA) causing shearing and degradation. Using these cells, mitochondrial transfer was seen to occur from mesenchymal stem cells (MSC) to a number of difference malignancies both *in vitro* and *in vivo*. Mitochondria have been seen to move to both A549 (lung adenocarcinoma) (323) and 143B (osteosarcoma) (324) rho0 cells *in vitro* from MSCs. *In vivo*, B16 (melanoma) and 4T1 (breast cancer) rho0 cells were shown to acquire mitochondria from MSCs (325). The latter study used single nucleotide polymorphisms (SNP) in mtDNA to determine the host origin of mitochondria acquired by the malignant cells.

The intercellular transfer of mitochondria has been shown to occur from MSC to other cancer cells, including SKOV3 cells (ovarian cancer) and MCF7 (breast cancer); however, in this study the authors found increased mitochondrial transfer occurred from endothelial cells over MSCs (326). Mitochondria have also been shown to be transferred within cancer cell populations and not from a specific mitochondrial donor such as MSCs. This was seen to occur between human mesothelioma cells populations (327) and between human laryngeal squamous cell carcinoma populations (328). Mitochondria were also found to move between T24 and RT4 bladder cancer cells (329). To date there has been no literature describing intercellular mitochondrial transfer within a haematological setting.

This biological phenomenon is not unique to malignancies - intercellular mitochondrial transfer has also been shown to occur in non-malignant settings. A study by Islam and colleagues in 2012 described the transfer of mitochondria from airway instilled BMSC to lung epithelial cells under lipopolysaccharide (LPS) treatment (330). In a separate study mitochondria were observed to move from astrocytes to injured neurons in a CD38 dependent mechanism (331).

Mitochondria have been shown to move between cells in various independent ways. Firstly, and most commonly, mitochondria have been shown to move between cells via tunneling nanotubes (TNT). TNTs are continuous cellular projections of the cytoskeleton, which are actin based and also contain microtubules (332). Mitochondria have been shown to move via TNTs from MSCs

to lung adenocarcinoma (323), ovarian and breast cancer cells (326); in addition to between pheochromocytoma PC12 cell (321, 333), bladder cancer cells (329) and mesothelioma cell populations (327). The mitochondrial Rho-GTPase (Miro1) aids in the coupling of mitochondria to the actin cytoskeleton and overexpression results in increased mitochondrial transfer. Mitochondria have also been shown to move through connexin43 gap junctions (330) and extracellular vesicles (331). Apart from the methods of mitochondrial movement, little is known about the underlying mechanisms that control this biological process.

There have been numerous biological consequences of intercellular mitochondrial transfer described. Firstly, the transfer of mitochondria has been shown to rescue cells from stress induced apoptosis (333). Furthermore, chemo-resistance has been shown to occur in malignant cells that have acquired mitochondria (326). Restoration of tumourigenic potential has also been shown in cancer cell lines that lack mtDNA (rho0 cells) in which mitochondrial transfer has occurred. This was mainly through reinstatement of the ability to utilise aerobic respiration to generate ATP (323, 334) - which is evidence to suggest that the Warburg effect may not occur in all cancers. In addition, intercellular mitochondrial transfer between bladder cancer cell populations increases invasiveness of the recipient cell (329). Finally, mitochondrial transfer occurs in non-malignant settings to protect against disease; mitochondria moved to lung epithelial cells from BMSC to protect against lipopolysaccharide induced acute lung injury (330), whereas mitochondria moved from astrocytes to recover injured neurons after stroke (331). Overall it can be seen that there are many biological consequences of mitochondrial transfer, all of which benefit the recipient cell and ultimately lead to cell survival.

1.7 Research Rationale and Objectives/Aims

1.7.1 Rationale

AML and MM are incurable diseases with the two poorest survival rates within haematological malignancies. Treatment of these cancers has hardly changed over recent decades, accounting for the lack of improvement in patient survival compared to other malignancies. Therefore, novel therapeutic interventions are required to improve overall survival of patients. It is envisaged that these new therapies will evolve from a better understanding of the biological processes that underpin the malignancies. AML and MM have been shown to rely heavily on their BMM to develop, proliferate and evade current chemotherapy regimens - this may be therapeutically targetable in combination with low-dose chemotherapy.

This study aims to further dissect underlying mechanisms within the BMM that contribute to the protection of AML and MM. Research will focus on whether intercellular mitochondrial transfer occurs within AML and MM – aiming to elucidate mechanisms which may control this biological phenomenon.

1.7.2 Objectives/Aims

1. Investigate intercellular mitochondrial transfer within AML. Establish the underlying mechanisms that stimulate and facilitate the transfer.

2. Determine the metabolic state of MM within the BMM, analyse intercellular mitochondrial transfer and determine control mechanisms.

3. Determine whether intercellular mitochondrial transfer is tumour specific or a process hijacked by cancer to fuel its metabolic requirements.

2 Materials and methods

2.1 Materials

Materials and reagents used in my thesis will be highlighted in the experimental procedures described in the methods below and in Table 2.1. All reagents were sourced from Sigma Aldrich (St Louis, MO, USA), unless otherwise stated.

Table 2.1. Reagents used in my thesis, with the manufacturer and catalogue number.

Agilent (Santa Clara, CA, USA), BioLegend (San Diego, CA, USA), Cell Signaling Technologies (Danvers, MA, USA), Clontech Takara Bio, Saint-Germain-en-Laye, France), Detroit R&D (Detroit, MI, USA), Fisher Scientific (Hampton, New Hampshire, USA), GE Healthcare (Little Chalfont, UK), Machery-Nagel, Duren, Germany), Merck Millipore (Burlington, MA, USA), Miltenyi Biotec (Bergisch Gladbach, Germany), New England BioLabs (Ipswich, MA, USA), PCR Biosystems (London, UK), Promega (Madison, WI, USA), Qiagen (Hilden, Germany), Santa Cruz Biotechnology (Dallas, TX, USA), Sigma Aldrich (St Louis, MO, USA) and ThermoFisher (Waltham, MA, USA).

Product	Manufacturer	Catalogue Number
100 Base Pair DNA Ladder	New England BioLabs	N3231S
10X RBC Lysis Buffer	ThermoFisher	00-4300-54
26G Butterfly Needles	Fisher Scientific	12349169
26G Needles	Fisher Scientific	12349189
30% Polyacrylamide/Bis Solution	Bio-Rad	1610154
4% Paraformaldehyde solution	Sigma Aldrich	1004968350
All-transretinoic acid (ATRA)	Sigma Aldrich	R2625-50MG
Amicon® Ultra-15 centrifugal filters	Merck Millipore	UFC900324
Ammonium Persulfate	Sigma Aldrich	A3678
Amplex Red Assay	ThermoFisher	A22188
AnnexinV Apoptosis Detection Kit	ThermoFisher	88-8005-72
Bovine Serum Albumin	Fisher Scientific	BP1600-100
COX2 Primer	Sigma Aldrich	8020816442 0060
CD38 Antibody	Santa Cruz Biotechnology	sc-374650
CD38 Primer	Sigma Aldrich	8023507096
CellTire-Glo Assay	Promega	G7570
D-Luciferin	Fisher Scientific	8829
DMEM Medium	ThermoFisher	10566016
DMSO	Fisher Scientific	BP231-100
dNTP Solution Mix	New England BioLabs	N0447S

Product	Manufacturer	Catalogue Number
EDTA	Sigma Aldrich	E9884
Ethidum Bromide Solution	Sigma Aldrich	E1510
FluoroBrite DMEM	ThermoFisher	A1896701
Fetal Calf Serum	ThermoFisher	10500056
FuGENE 6	Promega	E2691
GeneElute Mammalian Genomic DNA Miniprep	Sigma Aldrich	G1N70
Glycine	Fisher Scientific	BP381-5
Goat anti-mouse IgG HRP	Dako (Agilent)	P044701-2
Goat anti-rabbit IgG HRP	Dako (Agilent)	P044801-2
H2DCFDA	ThermoFisher	D399
Histopaque-1077	Sigma Aldrich	10771
Human CD105-FITC Antibody	Miltenyi Biotec	130-098-774
Human CD138 Microbead Kit	Miltenyi Biotec	130-051-301
Human CD138-FITC Antibody	Miltenyi Biotec	130-098-772
Human CD13-FITC Antibody	Miltenyi Biotec	170-078-011
Human CD33-APC Antibody	BioLegend	303407
Human CD33-FITC Antibody	Miltenyi Biotec	130-113-910
Human CD34 Microbead Kit	Miltenyi Biotec	130-046-702
Human CD34-FITC Antibody	Miltenyi Biotec	130-113-740
Human CD34-VioBlue Antibody	Miltenyi Biotec	130-113-744
Human CD38-Alexa Fluor 647 Antibody	BioLegend	303514
Human CD38-APC Antibody	Miltenyi Biotec	130-110-345
Human CD38-FITC Antibody	Miltenyi Biotec	130-113-988
Human CD45-FITC Antibody	Miltenyi Biotec	130-080-202
Human CD45-FITC Antibody	Miltenyi Biotec	130-080-202
Human CD45-PE Antibody	Miltenyi Biotec	130-110-770
Human CD45RA-PERCP Antibody	Miltenyi Biotec	130-113-920
Human CD49f-PE-Cy7 Antibody	Miltenyi Biotec	130-107-832
Human CD73-FITC Antibody	Miltenyi Biotec	130-100-463
Human CD90-APC-Cy7 Antibody	Miltenyi Biotec	130-114-863
Human CD90-FITC Antibody	Miltenyi Biotec	130-114-859
Human FLT3 ligand cytokine	Miltenyi Biotec	130-093-854
Human IL-3 cytokine	Miltenyi Biotec	130-093-908
Human IL-6 cytokine	Miltenyi Biotec	130-093-929
Human Mitochondrial DNA Monitoring Primer Set	Clontech	7246

Product	Manufacturer	Catalogue Number
Human TPO cytokine	Miltenyi Biotec	130-094-011
IL-6 Primer	Sigma Aldrich	8018577158
Immuno-Blot PVDF Membrane	Bio-Rad	1620177
Lenti-X qRT-PCR titration kit	Clontech	631235
L-Glutamine	Sigma Aldrich	G7513
Lipopolysaccharide	Sigma Aldrich	L2630
Magnesium Chloride Solution	New England BioLabs	B9021S
Miro1 Primer	Sigma Aldrich	8021455084
MISSION® shRNA Bacterial Glycerol Stock: CD38	Sigma Aldrich	SHCLNG-NM_001775
MISSION® shRNA Bacterial Glycerol Stock: NOX2	Sigma Aldrich	SHCLNG-NM_000397
MISSION® shRNA Bacterial Glycerol Stock: PGC-1α	Sigma Aldrich	SHCLNG-NM_013261
Mitochondrial D-loop primer	Sigma Aldrich	8020816442 0080
MitoTracker Green FM	ThermoFisher	M7514
MitoTracker Red CMXRos	ThermoFisher	M7512
Monosodium Citrate	Sigma Aldrich	71497
Mouse Anti-Biotin VioBlue Antibody	Miltenyi Biotec	130-098-800
Mouse CD117-PE-Cy7 Antibody	Miltenyi Biotec	130-108-355
Mouse CD150-BV510 Antibody	BioLegend	115929
Mouse CD34-PE-Cy5 Antibody	BioLegend	103131
Mouse CD45-APC Antibody	Miltenyi Biotec	130-110-660
Mouse CD45-BV510 Antibody	BioLegend	103137
Mouse CD48-APC-Cy7 Antibody	BioLegend	103431
Mouse Lineage Cell Depletion Kit	Miltenyi Biotec	130-110-470
Mouse Mitochondrial DNA Copy Number Kit	Detroit R&D	MCN1
Mouse Sca-1-APC Antibody	Miltenyi Biotec	130-102-343
ND1 TaqMan Gene Expression Assay, Human	ThermoFisher	4331182_Hs02596873
ND1 TaqMan Gene Expression Assay, Mouse	ThermoFisher	4331182_Mm04225274
NE-PER Nuclear and Cytoplasmic Extraction Reagents	ThermoFisher	78833
NOX2 Primer	Sigma Aldrich	8022588756
NucleoSpin® Dx Virus kit	Macherey-Nagel	740895.5
NucleoSpin® Plasmid kit	Macherey-Nagel	740588.5
Opti-MEM Reduced Serum Medium	ThermoFisher	31985062
OrangeG Gel Loading Dye	New England BioLabs	B7022S
Penicillin-Streptomycin	GE-Healthcare	SV30010
PGC-1α Antibody	Santa Cruz Biotechnology	sc-517380

Product	Manufacturer	Catalogue Number
PGC-1α Primer	Qiagen	QT00095578
Pierce ECL Western Blotting Substrate	ThermoFisher	32106
Polybrene Infection/Transfection Reagent	Sigma Aldrich	TR-1003
Poly-D-Lysine Solution	Sigma Aldrich	A-003-E
Precision Plus Protein standard ladder	Bio-Rad	1610373
ProLong Gold Mountant	ThermoFisher	P36941
qPCRBIO cDNA Synthesis Kit	PCR Biosystems	PB30.11-10
qPCRBIO SyGreen Mix	PCR Biosystems	PB20.12-51
ReliaPrep RNA Cell Miniprep system	Promega	Z6012
RIPA Buffer	ThermoFisher	89900
rLV.EF1.AcGFP1-Mem-9 Lentivirus	Clontech	0019VCT
rLV.EF1.mCherry-Mito-9 Lentivirus	Clontech	0024VCT
RPMI Medium	Thermofisher	11875093
SAM68 Antibody	Cell Signalling Technologies	12538S
Seahorse Mito Stress Test Kit	Agilent	103010-100
Seahorse XFp Base Medium	Agilent	103335-100
Seahorse XFp FluxPak	Agilent	103022-100
Sodium Dodecyl Sulfate	Sigma Aldrich	L3771
Sodium Pyruvate Solution	Fisher Scientific	11501871
StemMACS HSC Expansion Medium	Miltenyi Biotec	130-101-526
SYBR Safe DNA Gel Stain	ThermoFisher	S33102
Taq DNA Polymerase with Standard Taq Buffer	New England BioLabs	M0273S
TaqMan Copy Number Reference Assay, Human TERT	ThermoFisher	4403316
TaqMan Copy Number Reference Assay, Mouse TERT	ThermoFisher	4458368
TaqPath ProAmp Master Mix	ThermoFisher	A30865
TE Buffer	ThermoFisher	12090015
TEMED	Sigma Aldrich	T9281
Tris Base	Fisher Scientific	BP152-1
Trypan Blue Solution	Sigma Aldrich	T8154
Trypsin-EDTA	ThermoFisher	25200056
Tween-20	Fisher Scientific	BP337-100
UltraPure Agarose	ThermoFisher	16500500
Uridine	Sigma Aldrich	U3750
Vybrant DiI Stain	ThermoFisher	V22885
β- Actin Antibody	Sigma Aldrich	A2228

2.2 Cell culture

All cells described below were cultured in a humidified culture incubator (ThermoFisher, Waltham, MA, USA) at 5% CO_2 and 37 ˚C.

2.2.1 Cell lines

AML cell lines; OCI-AML3, MV4-11, THP-1 and U937 were obtained from the American Type Culture Collection (ATCC) and were maintained in RPMI-1640 medium, supplemented with 10% foetal calf serum (FCS), 2mM L-glutamine, 100U/ml penicillin and 10µg/ml streptomycin (pen-strep). Cells were cultured at a concentration of 0.5 $x10^6$ cells/ml and split accordingly on a weekly basis. The MM cell lines; MM1S, MM1R, U266, RPMI and H929 were obtained and cultured as per the AML cell lines (335).

293T cells were provided by Dr Ariberto Fassati (University College London, UK), which were derived from human embryonic kidney (HEK) 293 cells. These cells are a highly transducable cell line used in lentiviral production. 293T cells were cultured in 10mm tissue culture dishes at a 50-90% confluency, in Dulbecco's Modified Eagle's Medium (DMEM) supplemented with 10% FCS and without pen-strep as previously described (336). Cells were split 1:3 when they reached a 90% confluency. Briefly, 0.25% Trypsin was diluted 1:3 using PBS and 7.5ml was added to the 293T cells. The cells were incubated at room temperature for 2-3 minutes before gently swirling the dish to remove the cells. 5ml of DMEM was added to inactivate the trypsin and the cell suspension was transferred to a 50ml falcon tube, where a vigorous mixing step occurred to ensure no clumps of 293T cells remained. The suspension was topped up to 32ml and aliquoted into 3 fresh 10mm plates.

2.2.2 Primary cell isolation

Bone marrow aspirates from patients with AML and MM were obtained by haematology registrars at the NNUH, following informed consent under approval

from the UK NHS Health Research Authority (LCREref07/H0310/146) as previously described (273). Primary cell isolation was achieved using Histopaque density centrifugation. Briefly 10ml of Histopaque-1077 was added to a 50ml falcon tube and 15-20ml of bone marrow was layered on top. This was centrifuged at 1400rpm for 20 minutes with brakes and acceleration removed, which ensured successful separation of the different blood components. The mononuclear cells formed a "buffy coat" on top of the Histopaque layer and were isolated using a Pasteur pipette. A schematic overview of the density separation can be seen below in Figure 2.1.

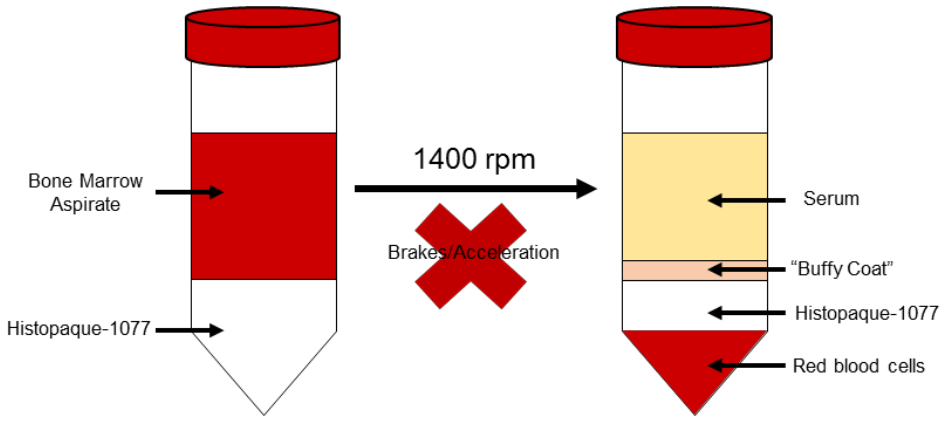

Figure 2.1. Schematic of the Histopaque density centrifugation of primary bone marrow.

Bone marrow aspirate was layered on Histopaque-1077 and centrifuged to produce the "buffy coat" containing AML/MM cells along with BMSC.

PBS was added to the isolated buffy coat to a final volume of 15ml and centrifuged at 1400rpm for 5 minutes, with the acceleration and brakes turned on. Any remaining red blood cells were removed by the addition of 1X red cell lysis buffer (1ml) (ThermoFisher, Waltham, MA, USA) to the cell pellet for 5 minutes, prior to the addition of 14ml of PBS. Pelleted mononuclear cells, after centrifugation, were cultured for 24 hours in DMEM supplemented with 10% FCS and penstrep. Suspension cells were removed at this time and fresh DMEM was added to the remaining adherent cells in the flask.

Malignant AML and MM cells were located in the suspension cell fraction after the 24-hour incubation. AML samples with <90% purity were purified using CD34 microbeads (Miltenyi Biotec, Bergisch Gladbach, Germany) and magnetic-

activated sorting (MACS). All MM samples were purified using CD138 microbeads (Miltenyi Biotec, Bergisch Gladbach, Germany) with MACS. Up to 200 million AML/MM cells were centrifuged at 1400rpm for 5 minutes and re-suspended in MACS buffer (PBS pH 7.4 supplemented with 0.5% BSA and 1mM EDTA). Magnetically labelled CD34/CD138 antibodies were added to the AML and MM cell suspension respectively and incubated at 4˚C for 30 minutes. After another centrifugation step, as above, the cells were re-suspended in MACS buffer and added to a MS column (Miltenyi Biotec, Bergisch Gladbach, Germany) attached to a magnet. Three column washes in MACS buffer were carried out before CD34/CD138+ cells were eluted by removal of the MS column from the magnet.

Non-malignant BMSC were located in the adherent fraction. Fresh DMEM medium was added to the flask twice weekly until patches of adherent BMSC were visible. At this point the BMSC were removed from tissue culture plastic using the serine protease trypsin. Briefly, medium was removed from the flask and cells were washed with 10ml of PBS followed by the addition of 3ml 0.25% Trypsin. After a short incubation in a humidified culture incubator, the flask was lightly tapped to remove the adherent cells followed by the addition of 5ml DMEM medium to inactivate the Trypsin. 20ml of DMEM was added to the cell suspension and was placed back in the incubator, allowing the cells to re-adhere to the tissue culture plastic. This formed of a uniform layer of BMSC which were expanded for around 2 weeks until 80% confluency then passaged again prior to use in experiments. BMSC were characterised by the expression of surface markers CD73, CD90 and CD105 whilst being negative for the myeloid marker CD45.

Non-malignant CD34+ HSCs were isolated from peripheral blood venesections from haemochromatosis patients at the NNUH. One pint of blood was initially centrifuged in multiple 15ml falcon tubes for 20 minutes at 1400rpm, with brakes and acceleration turned off. This allowed the separation of the red blood cells from the serum, shown in Figure 2.2. A small buffy coat of cells, including HSCs, formed on top of the red cells and was removed with a Pasteur pipette and pooled

together obtaining ~50ml per pint of blood. This cell solution was diluted 2-fold in PBS and 25ml was layered on top of 15ml of Histopaque-1770. A further buffy coat of cells was obtained using Histopaque density centrifugation, as described above, and these cells were washed in PBS twice before suspension in MACS buffer. CD34+ cells were then isolated using CD34 microbeads and MACS, as per AML primary samples. These cells were used in experimental procedures at the time of purification.

CD34+ HSC were also isolated from umbilical cord blood of babies born via caesarean section, using an adapted protocol by Hogan and collegues (337). Cord blood was isolated by Dr Charlotte Hellmich and Dr Genevra Pillinger at the NNUH. Roughly 50ml of cord blood was layered onto 2 x 15ml of Histopaque-1770 and density separated using centrifugation as described above. CD34+ cells were isolated using MACS as per the venesection blood. Purified cord blood CD34+ HSC were injected into NSG mice to create “humanised” NSG mice (22) to analyse *in vivo* non-malignant mitochondrial transfer.

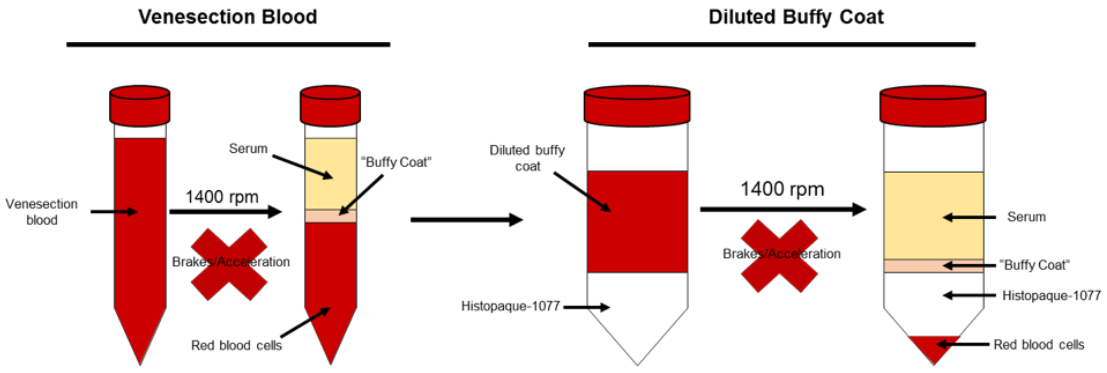

Figure 2.2. Schematic representation of CD34+ HSC isolation from venesection blood.

The buffy coat generated is then taken and purified by CD34+ MACS, resulting in a pure population of CD34+ HSCs.

2.2.3 Cryopreservation of primary cell and cell lines

Aliquots of primary AML and MM samples were frozen at the point of extraction prior to CD34/CD138 MACS purification. Total mononuclear cells (buffy coat) were frozen at a $5x10^6$ cells/ml concentration in FCS supplemented with 10% DMSO. Cells were slowly frozen in a cryo-freezing container (ThermoFisher,

Waltham, MA, USA) to a temperature of -80˚C. AML and MM cell lines were also frozen in this way.

To thaw the aliquots, the vial of cells was removed from the -80˚C freezer and placed in a 37˚C incubator to defrost. The cells were then transferred into a 15ml falcon tube and topped up to 15ml with fresh culture medium to dilute the DMSO concentration, which ensured maximum cell viability after thawing. Cells were centrifuged at 1400rpm for 5 minutes, supernatant was discarded and the cells were re-suspended in 15ml of fresh DMEM (primary samples) or RPMI-1640 (cell lines). Primary samples were then cultured as per fresh primary samples; removal of suspension cells and purification of the malignant cell along with expansion of the adherent BMSC. Cell lines were cultured for 1 week prior to splitting and maintenance at a 0.5 x10^6 cells/ml concentration.

2.2.4 Counting cells via Trypan Blue exclusion

Trypan Blue exclusion was used to determine cell concentrations. Briefly, 10µl of cell suspension was mixed with 10µl Trypan Blue and 10µl of this solution was pipetted onto a haemocytometer. Healthy living cells did not take up the Trypan Blue stain as their cell membrane was intact; however, dead or dying cells took up the stain as their cell membrane was fractured. The number of healthy cells in the four outer quadrants of the haematocytomer were counted and the cell concentration (cells/ml) was calculated, see Figure 2.3.

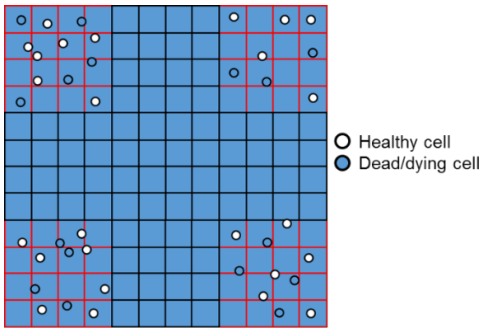

$$\text{Cell concentration} = \left(\frac{\text{Healthy cells in four outer quadrants}}{4}\right) \times \text{Dilution factor: } 2 \times 10{,}000$$

Figure 2.3. Determining cell concentrations using Trypan Blue exclusion.

The calculated cell concentration was used throughout my thesis to calculate the number of cells needed per experimental procedure. The equation below was used to determine this.

$$\left(\frac{\text{Number of cells required}}{\text{Cell concentration}}\right) = \text{Volume of cell suspension required (ml)}$$

2.2.5 Generation of a cell line depleted of mitochondria (rho0 cells)

To assess mitochondrial transfer to AML cells, I attempted to generate a cell line that was severely depleted of mitochondria, as per the protocol by Tan and colleagues (325). Here the OCI-AML3 cell line was cultured in RPMI-1640 medium (10% FCS and penstrep) supplemented with 50ng/ml ethidium bromide, 100µg/ml sodium pyruvate and 50µg/ml uridine. The ethidium bromide was used to specifically intercalate with and deplete mtDNA, the addition of pyruvate and uridine allowed the cell line to enhance glycolysis to generate the ATP required for cell survival. The medium was changed twice weekly by centrifuging the cells, discarding the supernatant and adding fresh medium. After a 40-day culture the mtDNA content in these cells was analysed by qPCR.

2.3 Cell culture assays

Primary and cell line AML and MM (along with BMSC) were cultured as above prior to use in the cell culture assays described below.

2.3.1 Co-cultures of AML/MM and BMSC

Co-culture systems were used to show that mitochondrial transfer occurred between BMSC and AML/MM cells. Primary BMSC were plated on 6, 12 and 24 well plates at a density of $2x10^5$, $5x10^4$ and $2x10^4$ respectively. The medium was replaced 24 hours after plating, BMSC were ready to use after 48 hours. At this point primary or cell line AML/MM cells were added to BMSC in a volume of 2, 1.5 and 1ml for 6, 12 and 24 well plates respectively. AML/MM were added to BMSC in a ratio of 5 malignant cells per BMSC. At various time points, the two

cell types were separated by gentle mixing (as BMSC are adherent cells and AML/MM are suspension cells) and analysed independently.

2.3.2 MitoTracker based mitochondrial transfer assay

Mitochondrial transfer was shown to occur between BMSC and AML/MM using three independent methods. Firstly, a MitoTracker based staining method was developed to show the specific movement of BMSC mitochondria to malignant AML/MM. The specific mitochondrial stain MitoTracker Green FM (ThermoFisher, Waltham, MA, USA) was utilised for this method. BMSC plated on 24 well plates were stained for 1 hour with 200nM MitoTracker, in 500μl FluoroBrite DMEM medium (ThermoFisher, Waltham, MA, USA) supplemented with 10% FCS. After the incubation, BMSC were washed 3 times with PBS to remove any un-bound probe. AML/MM were then added to the stained BMSC for 24 hours and levels of MitoTracker in AML/MM cells were then analysed by flow cytometry, compared with mono-cultured cells.

Naïve un-labelled AML/MM cells were initially added to stained BMSC, however results were un-convincing as very large increases in MitoTracker fluorescence were observed in AML/MM cells. I found this was due to MitoTracker dye leaking from BMSC and staining AML/MM mitochondria. To eliminate this, I additionally stained AML/MM cells with 200nM MitoTracker Green for 30 minutes before they were added to BMSC. This saturated AML/MM mitochondria with MitoTracker, therefore any dye leakage will have a negligible effect on the MitoTracker fluorescence within the malignant cell. This change achieved more believable increases in MitoTracker fluorescence in the AML/MM, which was attributed to BMSC derived mitochondria moving into AML/MM cells.

Table 2.2. Pharmacological agents used to assess mitochondrial transfer levels.

Pharmacological Agent	Target/effect	Concentration used
Carbenoxolone (CBX)	GAP junction block	50 μM
Chetomin (Chelo)	HIF-1α inhibitor	10 μM
$CoCl_2$	Mimics hypoxia (<1% O_2)	100 μM
Cytochalasin B	Actin (TNT formation) inhibitor	350 nM
Dansylcadaverine	Endocytosis inhibitor	50 μM
Daunorubicin (DNR)	Chemotherapeutic - increases ROS	50 nM
Diphenyleneiodonium (DPI)	NOX2 inhibitor	1 μM
Everolimus (Evero)	mTOR inhibitor	40 μM
EX527	SIRT-1 Inhibitor	1 μM
Glutathione (GSH)	ROS quencher	5 mM
Humira	TNFα inhibitor	5 μg/ml
Hydrogen peroxide	ROS inducer	50 μM
IL-1RA	IL-1 inhibitor	10 μM
JNKV	JNK inhibitor	10 μM
JQ1	c-myc inhibitor	10 μM
Lenalidomide (Len)	Chemotherapeutic	10 μM
LPS	Bacterial mimic	10 μg/ml
LY294002	PI3K inhibitor	25 μM
Metformin (Met)	Mitochondrial complex I inhibition	10 nM
MK2206	AKT inhibitor	1 μM
n-acetylcysteine (NAC)	ROS quencher	5 mM
Nutlin3	p53 activation	20 μM
PS1145	IKK inhibitor	2 μM
R406	Syk inhibitor	20 μM
Ro-32-8220	Protein kinase C inhibitor	2 μM
TNFα	Induces inflammation	30 ng/ml

This method was also used to quantify levels of mitochondrial transfer. Stained AML/MM in mono-culture were compared to when they were cultured with stained BMSC, this achieved a baseline level of transfer. The effect of pharmacological compounds (seen in Table 2.2) on mitochondrial transfer levels could then be determined by comparing mitochondrial transfer between drug treatment and baseline transfer.

2.3.3 rLV.EF1.mCherry mitochondrial transfer assay

For the second method, I used a stable lentiviral transfection of BMSC mitochondria with a red mCherry fluorescence in order to track BMSC mitochondria. A rLV.EF1.mCherry-Mito-9 lentivirus was purchased from Clontech and was used to transduce human BMSC. 0.5μl of the virus ($0.5x10^6$ virus

particles) was added to $5x10^5$ BMSC in 500µl of penstrep free 10% FCS DMEM medium. 1ml of DMEM medium was added after 24 hours, BMSC were then cultured for a further week. At this point, successful transduction was assessed by the detection of mCherry fluorescence in the BMSC using fluorescent microscopy. If successful transduction was observed, AML/MM cells were added to BMSC for 1 week. Mitochondrial transfer was observed by acquisition of the Mito-9 mCherry fluorescence in AML/MM cells using fluorescent microscopy. Microscopy with AML blasts was carried out with live cells, the protocol was however optimised with MM. The co-culture was carried on tissue culture coverslips, with the cells fixed in 4% Paraformaldehyde and mounted with ProLong™ Gold Antifade Mountant containing DAPI (ThermoFisher, Waltham, MA, USA).

2.3.4 Visualisation and quantification of tunnelling nanotubes

To visualise TNTs formed between BMSC and AML/MM cells, the 1,1'-Dioctadecyl-3,3,3',3'-Tetramethylindocarbocyanine Perchlorate (DiI) stain (ThermoFisher, Waltham, MA, USA) was utilised. DiI is a lipophilic membrane stain that diffuses laterally staining the whole cell. $1x10^6$ AML/MM cells in a volume of 1 ml were stained with a DiI concentration of 5µg/ml for 15 minutes. The cells were washed thrice in PBS and incubated for 30 minutes in culture medium. BMSC were also stained with MitoTracker Green FM (200nM) for 1 hour before washing thrice in PBS. The stained AML/MM were combined with the BMSC for 24 hours before fixing with 4% Paraformaldehyde. Cells were imaged by confocal microscopy.

A second method was utilised for the MM study, whereby MM cell plasma membranes were labelled with GFP using stable lentiviral transduction. The rLV.EF1.AcGFP1-Mem-9 lentivirus was purchased from Clontech. 0.5µl of the virus ($0.5x10^6$ virus particles) was added to $5x10^5$ MM1S/U266 MM cell lines in 500µl of penstrep free RPMI medium supplemented with 10% FCS. After confirmation of lentiviral transduction, these cells were added to BMSC stained

with 200nM MitoTracker Red CMXRos (ThermoFisher, Waltham, MA, USA) as above. TNT visualisation was carried out using confocal microscopy.

Only a very small number of TNTs were visualised as they form and dissociate very rapidly. To quantify TNTs formed between AML/MM cells and BMSC I utilised the TNT-anchor points (TAPs) formed on the BMSC. These TAPs were residual DiI stain remaining after AML/MM derived TNTs had dissociated. These TAPs were not present on BMSC when AML/MM cells were cultured in a 0.4μM trans-well system, they are therefore specific to the cell-cell contacts observed.

2.4 Cell viability assays

2.4.1 CellTitre-Glo

The viability of AML, MM and BMSC was assessed using the CellTite-Glo assay (Promega, Fitchburg, WI, USA), as previously described (338). Addition of the CellTitre-Glo substrate causes cell lysis and a luminescent signal proportional to the amount of ATP present, which is a representation of the number of metabolically active cells (summarised in Figure 2.4). For the reaction, $5x10^4$ cells were plated on a white 96 well plate in a 50μl volume. 50μl of CellTitre-Glo substrate was added, followed by a 10-minute incubation in the dark. Luminescence at an emission wavelength of 560nm was detected using the LUMIstar Omega microplate reader (BMG LABTECH, Ortenberg, Germany). This assay was also used to determine the levels of ATP produced by AML/MM after co-culture with BMSC.

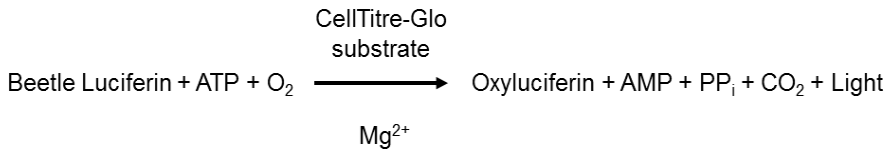

Figure 2.4. An equation showing the CellTitre-Glo reaction.

In the presence of ATP, the CellTitre-Glo substrate is converted to Oxyluciferin. This reaction produces light which can be detected by luminescence at a wavelength of 560nm.

2.4.2 Annexin V/PI

Cell viability was also assessed using the eBioscience™ Annexin V/PI detection kit (ThermoFisher, Waltham, MA, USA), as previously described (339). The annexin V FITC antibody binds to phosphatidylserine externalised on apoptotic cells. Propidium iodide (PI) stains DNA of necrotic and apoptotic cells, healthy cells are not stained as PI cannot cross their membrane. To perform the assay, $2x10^4$ AML/MM cells were centrifuged and re-suspended in 800µl of 1X annexin/PI binding buffer containing 2µl of annexin V FITC antibody and 4µl of PI. The cells were incubated in the dark for 15 minutes before washing in ice-cold PBS. The cells were then run on the Sysmex Cube 6 flow cytometer and results analysed using FCS Express 5 software (De Novo Software, Glendale, CA, USA). An example of a flow cytometry plot generated from this assay is shown in Figure 2.5.

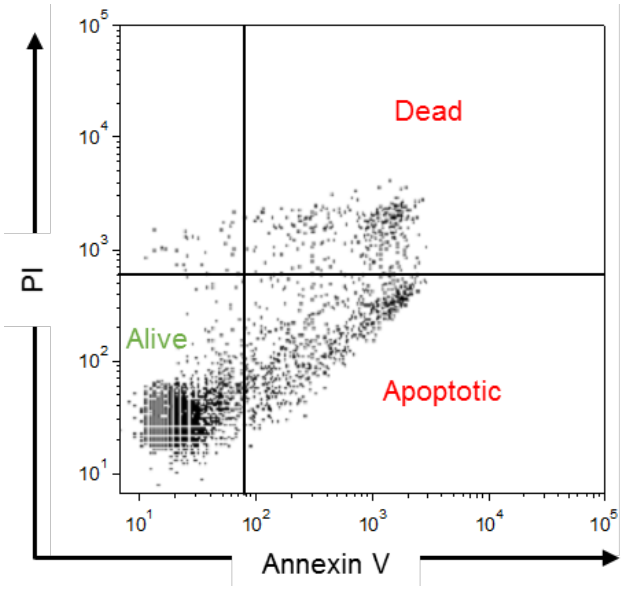

Figure 2.5. Representative flow cytometry plot of an Annexin V/PI viability assay.

Cells were stained with PI and Annexin V and analysed by flow cytometry. Live cells (PI^- Annexin V^-), Apoptotic (PI^- Annexin V^+) and Dead (PI^+ Annexin V^+) cells can be determined.

2.5 Detection of reactive oxygen species

2.5.1 DCFDA / H2DCFDA (DCF) assay

To determine ROS levels in BMSC the DCF assay (ThermoFisher, Waltham, MA, USA) was utilised as per the manufacturers protocol. For this assay H_2DCFDA was added to the cell of interest which is taken up and deacetylated by cellular esterases to a non-fluorescent compound H_2DCF. This compound is oxidised in the presence of ROS to the highly fluorescent compound 2', 7' –dichlorofluorescin (DCF). This compound has an emission wavelength of 529 nm and can be detected by flow cytometry in the FITC channel. A schematic overview of this reaction is shown in Figure 2.6.

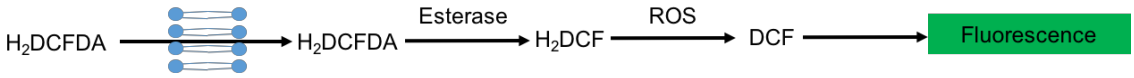

Figure 2.6. Overview of the DCF assay to detect ROS.

The H_2DCFDA reagent is taken up by cells and converted to H_2DCF by cellular esterases. In the presence of ROS H_2DCF is oxidised to form the fluorescent DCF.

To perform the reaction $1x10^5$ BMSC were stained with 10μM H_2DCFDA in 500μl FluoroBrite DMEM medium (ThermoFisher, Waltham, MA, USA) - supplemented with 10% FCS for 15 minutes at 37 °C. BMSC were removed from tissue culture plastic with trypsin prior to staining. The cells were washed three times in PBS after staining, the cells were then run through the Sysmex Cube 6 flow cytometer. Results were analysed using FCS Express 5 software.

2.5.2 Amplex™ Red superoxide detection assay

The DCF assay described above has the capability of measuring total ROS in cells – which includes superoxide, peroxide, hydroxyl radicals and hydroxyl ions. In the AML study superoxides were of interest as NOX2 on the surface of the AML blasts generates large amounts of superoxide. The Amplex™ Red superoxide detection assay (ThermoFisher, Waltham, MA, USA) was used to specifically measure superoxide levels generated (as per the manufacturers

protocol). This assay is a one-step reaction where (in the presence of horseradish peroxidase (HRP)) the Amplex Red reagent (10-acetyl-3,7-dihydroxyphenoxazine) reacts with superoxide forming Resurfin. This product fluoresces at an emission wavelength of 585nm and is designed to be detected in a 96 well plate format. This reaction was carried as per the manufacturer's specifications.

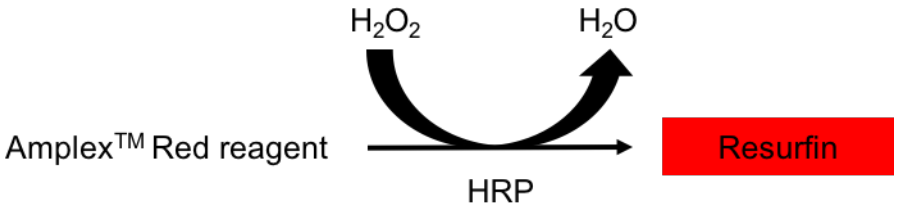

Figure 2.7. Overview of the Amplex™ Red reaction used to detect superoxides.

In the presence of superoxides the Amplex Red Reagent to converted to the fluorescent compound Resurfin.

To perform the reaction $2x10^5$ AML blasts were plated on a black 96 well plate with a transparent base in a volume of 50μl FluoroBrite DMEM medium supplemented with 10% FCS. A master mix was created by mixing 0.5μl Amplex Red reagent, 1μl HRP and 48.5μl 1X reaction buffer per sample. 50μl of this master mix was added to the cell suspension and fluorescence was measured using the FLUOstar Omega microplate reader (BMG LABTECH, Ortenberg, Germany). A hydrogen peroxide standard curve was performed on each 96 well plate measured to determine an accurate superoxide concentration in the samples tested.

2.6 Microscopy

2.6.1 Confocal Microscopy

To visualise TNT formations between BMSC and AML/MM cells (along with TAPs on BMSC) confocal microscopy was carried out using a Zeiss LSM 800 Axio Observer.Z1 confocal microscope with 40X and 63X water objectives (Carl Zeiss, Oberkochen, Germany). Cells were prepared as described in section 2.3.4. Fixed cells on 24 well black walled imaging plates (Ibidi, Munich, Germany) were placed

on the microscope using a plate holder. ZEN Blue imaging software (Carl Zeiss) smart setup was used to define fluorophore wavelength acquisition parameters of DiI stain and MitoTracker Green FM or GFP and MitoTracker CMXRos. TNT formations were infrequently observed, TAP formation on BMSC was therefore used to quantity the number of TNT formation per culture. Multiple images were taken for TAP quantification. ImageJ software was used to achieve accurate quantification and for image processing. Confocal microscopy was also used to detect CD38 expression on BMSC after MM co-culture, whether CD38 localised to TAPs and whether CD38 was found on TNTs. Cells were prepared as per section 2.3.4 with the addition of 2µl of anti CD38-Alexa Fluor 647 antibody prior to fixing (Miltenyi Biotec, Bergisch Gladbach, Germany). Another smart setup was carried out in ZEN Blue imaging software to incorporate the extra fluorophore. ImageJ was used for image processing.

2.6.2 Fluorescent microscopy

Fluorescent microscopy was carried out on a Zeiss Axio Vert.A1 microscope with 20X and 40X air objectives (Carl Zeiss, Oberkochen, Germany). This microscope was used to detect mCherry-Mito-9 in AML/MM cells after co-culture with rLV.EF1.mCherry-Mito-9 transduced BMSC. Cells were prepared on 24 well black walled imaging plates (or coverslips as described in 2.3.3) and placed on the plate/slide holder on the microscope. ZEN Blue imaging software was used to acquire fluorescent and light images. Image processing was achieved using ImageJ software.

2.7 Flow Cytometry

Flow cytometry was used in my thesis for a number of different applications:

- To analyse mitochondrial levels in AML/MM/BMSC in addition to mitochondrial transfer levels (using MitoTracker Green Fluorescence).
- To detect cell surface receptors with antibodies conjugated to a fluorophore.
- To sort a specific cell population based on its cell surface receptors.

To achieve the above applications a range of flow cytometers were used based on the number of fluorophores they can detect in a single sample and whether they had cell sorting capabilities. Table 2.3 shows a comparison of the flow cytometers capabilities. Table 2.4 shows all antibodies used in the analysis, purchased from Miltenyi Biotech (Bergisch Gladbach, Germany) and BioLegend (San Diego, CA, USA).

2.7.1 Sysmex Cube 6

The Cube 6 flow cytometer (Sysmex, Gorlitz, Germany) is a multi-channel flow cytometer with 2 lasers - the blue 488nm and red 633nm. This laser combination can detect the following fluorophores: FITC, PE, PERCP and APC. The Cube 6 flow cytometer was used in my thesis for single colour flow cytometry only, due to the lack of sophisticated colour compensations - cross-over of emission spectre therefore could not be controlled and accounted for. The MitoTracker based flow cytometry assay was performed on this cytometer as only the FITC channel (in which MitoTracker Green is detected) was required.

Prior to use an automated priming sequence was performed to ensure no blockages or air bubbles were present in the system. To run the samples, ~$1x10^5$ cells were re-suspended in 1ml of PBS and transferred into a flow cytometry analysis tube. The flow cytometry tube was attached to the cytometer and the analysis was started through the FCS software - $1x10^4$ cells were analysed in a pre-defined gated region. An automated cleaning cycle was carried out after all sample tubes had been analysed. Sample data was exported as an FCS file and analysed using FCS Express 5 software. For the MitoTracker based staining assay this analysis determined the mean fluorescence intensity (MFI) of MitoTracker Green in AML/MM cells.

2.7.2 Beckman Coulter CytoFLEX

The Beckman Coulter CytoFLEX flow cytometer (Brea, CA, USA) also is a two-laser flow cytometer (488 and 633nm) capable of detecting FITC, PE, PERCP and APC (as per the Cube 6 flow cytometer). This cytometer is however more sophisticated as bandpass filters allows the further detection of PE-cy5, PE-cy7 and APC-cy7. Colour compensation also allows the detection of up to four fluorophores within the same sample tube. In my thesis, this flow cytometer was used when multiple fluorophores were assessed (<4) in the same sample tube. An example of this is the confirmation of CD34+ HSC engraftment into NSG mice, whereby human CD45-FITC and mouse CD45-APC were used to detect human and mouse cells in the peripheral blood of mice.

Prior to use the automated daily clean process was carried out to ensure the flow cytometer was cleaned and primed. A compensation matrix was calculated by running single stained samples and a dual/tri/quad stained sample. This matrix determined the level of spectre cross over and created a compensation to account for the overlap in future samples tested. This compensation was applied prior to running the “real” test samples. $1x10^5$ cells were stained with the antibodies of interest (along with appropriate isotype controls) in 50µl PBS for 15 minutes before the addition of a further 300µl of PBS. These stained samples were transferred to a flow cytometry tube and placed in the CytoFLEX for analysis. $1x10^4$ cells were analysed in a pre-defined region. Data analysis was performed using the CytExpert 1.2 software.

2.7.3 BD FACSCanto II

The FACSCanto II flow cytometer (BD, Franklin Lakes, NJ, USA) is a three-laser flow cytometer (405, 488 and 633nm) capable of assessing up to 7 different fluorophores within the same sample. These fluorophores included FITC, PE-Cy5, PE-Cy7, APC, APC-Cy7, BV421 and BV510. A colour compensation (for each antibody panel used) was carried out using single stained samples to calculate fluorophore emission cross-over. This compensation was applied to

each experiment prior to running the samples. In addition, fluorescence minus one (FMO) controls for each fluorophore were carried out to determine the positive and negative gates for each marker. This flow cytometer was used to detect mitochondrial levels in various cell populations within mouse bone marrow - antibodies panels used can be seen in Table 2.5. This flow cytometer was located in the Pathology Laboratory at the NNUH and was maintained by Dr Allyson Tyler and Dr Ian Thirkettle.

To perform the analysis $5x10^6$ mouse bone marrow cells were stained for 15 minutes with 200nM MitoTracker in 500µl Flurobrite DMEM - with 10µl Lineage depletion cocktail bound to biotin (Miltenyi Biotec, Bergisch Gladbach, Germany). The cells were centrifuged at 1400rpm for 5 minutes and re-suspended in 50µl of PBS. A master mix of antibodies was made (where a 1X mix contained 2µl of each antibody) and was added to the cells. After a subsequent 15-minute incubation, 300µl of PBS was added and the cells were transferred to a flow cytometry tube. The samples were run on the FACSCanto II using the automated carousel function. Sample data was analysed using a combination of FCS Express 5 and FlowJo software.

2.7.4 BD FACSAria II

The FACSAria II (BD, Franklin Lakes, NJ, USA) has the same flow cytometry abilities as the FACSCanto II with the additional capability of cell sorting. This flow cytometer was used to sort a pure population of OCI-AML3, MV4-11, MM1S, and U266 luciferase cells used for *in vivo* studies. Cell sorting was carried out by Dr Zhigang Zhou.

2.7.5 BD FACSMelody

The FACSMelody (BD, Franklin Lakes, NJ, USA) also has the same capabilities as the FACSCanto II and has the sorting capabilities of the FACSAria II. This flow cytometer was located at the Earlham Institute and was used to sort human HSCs

from the bone marrow of “humanised” NSG mice. This sorting was carried out by Dr Iain Macaulay and Dr Laura Mincarelli.

Table 2.3. Capability comparison of the flow cytometers used.

	Cube 6	CytoFlex	FACSCanto II	FACSAria II	FACSMelody
Number of lasers	2	2	3	3	3
Fluorophore capability (same sample)	1	4	7	7	7
Colour compensation	No	Yes	Yes	Yes	Yes
Automated	No	No	Yes	No	No
Cell sorting	No	No	No	Yes	Yes

Table 2.4. Antibodies used in flow cytometry assays.

Cell Marker	Species	Fluorophore
CD13	Human	PE
CD33	Human	FITC/APC
CD34	Human	FITC/BV421
CD34	Mouse	PE-Cy5
CD38	Human	FITC/APC
CD45	Human	FITC/PE
CD45	Mouse	APC/BV510
CD45RA	Human	PERCP

Cell Marker	Species	Fluorophore
CD48	Mouse	APC-Cy7
CD49f	Human	PE-Cy7
CD90	Human	APC-Cy7
CD105	Human	FITC
CD117	Mouse	PE-Cy7
CD138	Human	FITC
CD150	Mouse	BV510
Sca-1	Mouse	APC

Table 2.5. Antibody panels used to detect human and mouse HSCs.

Fluorophore	Antibody Panel	
	Mouse HSC	**Human HSC**
FITC	MitoTracker Green FM	
PE-Cy5	CD34	CD45RA
PE-Cy7	CD117	CD49f
APC	Sca-1	CD38
APC-Cy7	CD48	CD90
BV421	Anti-Biotin	CD34
BV510	CD150	Mouse CD45

2.8 Seahorse Extracellular Flux Assay

To analyse the metabolic activity of AML and MM cells the Seahorse XFp Analyzer (Agilent Technologies, Santa Clara, CA, USA) was used with the Seahorse XFp Cell Mito Stress Test Kit (as per the manufacturers protocol). Levels of OXPHOS (mitochondrial respiration) and glycolysis (non-mitochondrial respiration) in a cell of interest can be determined using this method, through the analysis of oxygen consumption rates (OCR) and extracellular acidification rates (ECAR) respectively. In my thesis, this method was used primarily to observe the changes in mitochondrial respiration between mono and co-cultured AML and MM cells, along with respiration dynamics in BMSC post culture with malignant cells. Not only can this assay determine basal mitochondrial respiration rates it can also determine the maximum respiration, spare capacity of a cell, proton leak and ATP production (Figure 2.8). This was achieved using periodic injections of Oligomycin (inhibiting ATP synthase reducing OCR), FCCP (increases H^+ ion permeability of the lipid bilayer facilitating H^+ transport across the hydrophobic mitochondrial inner membrane independently of ATP synthase - increasing OCR) and Rotenone/Antimycin A (targeting complex 1 and 3 reducing OCR).

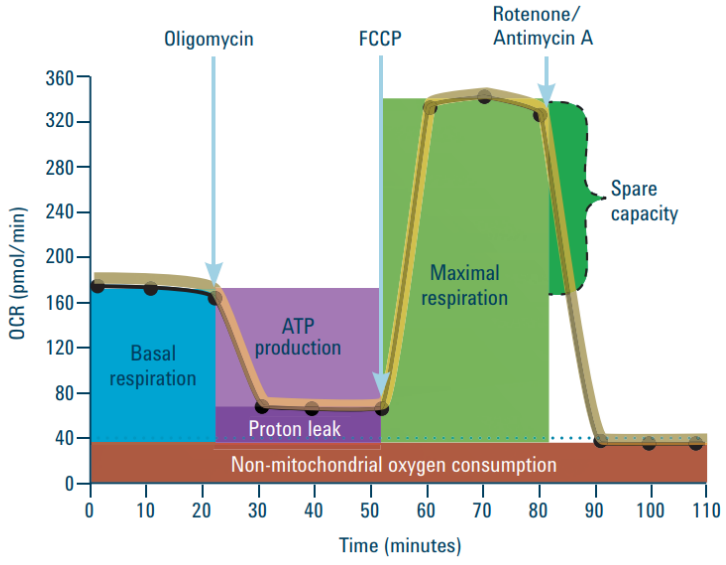

Figure 2.8. The Mito Stress test experimental profile.

Periodic injections of Oligomycin, FCCP and Rotenone/Antimycin A allowed basal and maximum respiration to be determined using oxygen consumption rate (OCR). ATP production, spare capacity and proton leak were also able to be analysed. Source: Agilent Technologies, https://www.agilent.com/cs/library/flyers/public/5991-7118EN.pdf, accessed May 2018.

To run the assay AML and MM cells were first cultured for 72 hours with or without BMSC. Specific numbers of cells were then plated on Seahorse XFp cell culture plates (coated with Poly-D-Lysine) in Seahorse XFp Base Medium supplemented with 2.5mM Glucose, 2mM Glutamine and 1mM Pyruvate. To analyse BMSC, these cells were plated on coated seahorse plates prior to AML co-culture. $1x10^5$ AML/MM cells were plated in triplicate in 50µl volumes, followed by centrifugation at 1400rpm for 5 minutes to ensure a confluent mono-layer of cells is achieved. 24 hours prior to the assay the Seahorse Extracellular Flux analyser was switched on to allow it to equilibrate at 37˚C. Seahorse XFp sensor cartridges were also hydrated in XFp Calibrant overnight at 37˚C. To run the assay Oligomycin, FCCP and Rotenone/Antimycin A were loaded into the pre-calibrated sensor cartridge in 1µM, 1µM and 0.5µM concentrations respectively. The sensor was loaded into the extracellular flux analyser and the pre-defined MitoStress protocol was run. After a 20-minute sensor equilibration the cell plate (with wells topped up to 180µl of Seahorse Base Medium) was loaded into the analyser. Results obtained were analysed using Graphpad and Microsoft Excel.

2.9 Genetic knockdown of AML, MM and BMSC

To analyse the effect of NOX2, PGC-1α and CD38 on mitochondrial transfer genetic knockdown was carried out with short hairpin RNA (shRNA) targeted to a gene of interest (GOI) using a lentiviral system. The cell type of interest is transduced with a lentivirus containing RNA which encodes shRNA targeting a GOI. This RNA is incorporated into the genome of the cell resulting in shRNA being transcribed by RNA polymerase III machinery. This shRNA mimics pri-miRNA and is modified by Drosha and Dicer enzymes to produce double stranded RNA, removing the short hairpin. This is then loaded into the RNA-induced silencing complex (RISC) where the sense strand (passenger) is degraded by Argonaute-2. The remaining anti-sense strand leads the RISC to mRNA complementary to itself, resulting in mRNA cleavage by RISC - silencing the GOI. The process of lentiviral preparation is explained below. The protocol was designed by Dr Lyubov Zaitseva, as previously described (340).

2.9.1 Lentiviral production

2.9.1.1 Plasmid preparation

Escherichia coli (*E. coli*) glycerol stocks (containing pLKO.1-amp vectors encoding shRNA specific for a GOI) were purchased from Sigma Aldrich's MISSION® shRNA library (see Table 2.6 for details).

Table 2.6. pLKO.1-amp vectors containing shRNA targeting a GOI

Gene of interest	TRC number	shRNA sequence
NOX2	TRCN0000064588	CCGGGCCCGAGTCAATAATTCTGATCTCGAGATCAGAATTATTGACTCGGGCTTTTTG
PGC-1α	TRCN0000001168	CCGGCGACTTGGATACAGACAGCTTCTCGAGAAGCTGTCTGTATCCAAGTCGTTTTT
CD38	TRCN0000050869	CCGGCCAGAGAAGGTTCAGACACTACTCGAGTAGTGTCTGAACCTTCTCTGGTTTTTG

The initial step in the preparation of a lentivirus is the generation of pLKO.1-amp plasmids from *E. coli* stocks. Luria Bertani (LB) agar plates, containing 50µg/ml ampicillin, were made and left to set at room temperature. Using a stringent aseptic technique, the MISSION® glycerol stocks were streaked on these plates and incubated upside down at 37˚C for 16 hours. Single *E. coli* colonies were then picked with a sterile pipette tip and transferred into a 10ml tube containing 5ml of sterile LB broth supplemented with 50µg/ml ampicillin. This tube was then incubated at 37˚C on shaking platform set at 240rpm.

After incubation, bacterial growth caused the LB broth to turn cloudy and plasmid purification could now take place. The bacterial culture was centrifuged at a high speed for 10 minutes to pellet the bacterial cells - the supernatant was discarded. Plasmid DNA was then purified from the E. coli cells using the NucleoSpin® Plasmid kit (Macherey-Nagel, Duren, Germany), as per manufacturer's instructions. Briefly, E. coli cells were lysed and neutralised prior to loading onto a plasmid DNA binding spin column. Plasmid DNA was washed and eluted from the column. Purified plasmid DNA was quantified using a Nanodrop spectrophotometer (ThermoFisher, Waltham, MA, USA) - with purity confirmed using A260/230 and A260/280 ratios.

2.9.1.2 Plasmid precipitation

A total plasmid concentration of 180ng/µl or greater was required to proceed with lentiviral production. If a lower concentration was generated a precipitation step was carried out to increase the plasmid concentration. Here 3M sodium acetate was added at a ratio of 1:10 to the total plasmid volume, followed by the addition of ice cold absolute ethanol (greater than two times the total plasmid volume). The solution was then frozen at -80˚C for several hours, then centrifuged at a high speed for 5 minutes at 4˚C. The supernatant was discarded and 1ml of ice cold 70% ethanol was added and another centrifugation step was carried out as above. As much of the ethanol was removed as possible and the plasmid pellet was dried out in a tissue culture hood. The plasmid pellet was finally re-suspended in water to achieve the desired plasmid concentration of >180ng/µl.

2.9.1.3 Transfection of packaging cells

293T packaging cells were cultured as described in 2.2.1 and split 1:2 prior to transfection. To create a functional lentivirus encoding shRNA targeted to a GOI, three different plasmids were required along with a transfection reagent. The pLKO.1-amp plasmid generated in 2.9.1.1 was the first plasmid used. In addition, Vesicular stomatitis virus glycoprotein (VSV-G) and cytomegalovirus promoter (pCMV) were also required as envelope proteins and packaging protein promoter respectively. The latter two plasmids were made from glycerol stocks as per the pLKO.1-amp plasmid. The transfection reagent used was FuGENE® 6 (Promega, Fitchburg, WI, USA).

For each 10mm tissue culture dish of 293T cells a master mix of plasmids and transfection reagent was made as follows: 1µg of VSVG and pCMV plasmids were mixed with 1.5µg of pLKO.1-amp plasmid in a total volume of 15µl TE buffer. This DNA mixture was added to 200µl of Opti-MEM medium (ThermoFisher, Waltham, MA, USA) along with 18µl of FuGENE® 6. The medium was removed from the plate of 293T cells and replaced with 7.5ml of fresh 293T DMEM medium before the addition (in a dropwise manner) of the Opti-MEM medium containing

plasmid and transfection reagent. After a 24-hour incubation, the medium was removed and discarded from the 293T cells and replaced with fresh medium. This was repeated at 48, 72 and 96-hour time points, however at these times the medium removed was collected and stored at -80˚C - as it contained the lentivirus.

2.9.1.4 Lentivirus titre

Small 70µl aliquots from each virus collection time point were kept aside from the bulk collection - these were used to determine the lentivirus titre. Viral RNA was isolated from the 3-pooled lentiviral time point collections using the Nucleospin® Dx Virus kit (Machery-Nagel, Duren, Germany). 150µl of the 210µl total pooled volume was taken aside, 600µl of RAV1 buffer was added and vortexed thoroughly. After a 5-minute incubation, 600µl of absolute ethanol was added and vortexed for 30 seconds. The solution was then loaded into a Nucleospin® Dx Virus column and centrifuged at 8000 x g for 1 minute discarding the waste. The column was placed in a new collection tube, before the addition of 500µl of RAW buffer and a further centrifugation step using the above parameters. The column was then washed with RAV3 buffer twice (600 and 200µl respectively) using 1 minute centrifugation steps at 8000 and 11000 x g. RNA was then eluted into clean and sterile Eppendorfs using 50µl of nuclease free water (warmed to 70˚C). Any remaining contaminating DNA was removed using a DNase step - 12.5µl of viral RNA was added to 10µl of DNase and 2.5µl DNase1 buffer. The solution was incubated in a thermocycler for 30 minutes at 30˚C followed by a 5-minute incubation at 70˚C.

The RNA genome copy number was then calculated using the Lenti-X qRT-PCR titration kit (Clontech Takara Bio Europe, Saint-Germain-en-Laye, France). Briefly, a master mix was generated (detailed in Table 2.7) on ice, with 10% extra volume to account for pipetting errors. The RT enzyme mix was added last. A standard curve was made in 8-well PCR strips using a known concentration of $5x10^7$ copies/µl as the top concentration, which was diluted down to $5x10^3$ in EASY dilution buffer. Viral RNA samples were also diluted using a 10-fold serial dilution method resulting in 4 concentrations. 2µl of the control template, viral

RNA and negative control were added in duplicate to a 96 well Lightcycler PCR plate (Roche, Basel, Switzerland) - containing 18µl of the master mix detailed in Table 2.7 The plate was sealed and run on a Lightcycler LC480 (Roche, Basel, Switzerland) using the following program:

- **RT Reaction** – 5 minutes at 42˚C, 10 seconds at 95˚C (1 cycle)
- **Amplification** – 5 seconds at 95˚C, 30 seconds at 60˚C (40 cycles)
- **Melting Curve** – 15 seconds at 95˚C, 30 seconds at 60˚C (1 cycle)

Table 2.7. Master mix for Lenti-X lentiviral titration qPCR

Reagent	µl per reaction
RNAse-free water	6.0
Quant-X Buffer	10.0
Lenti-X forward primer (10 µM)	0.4
Lenti-X reverse primer (10 µM)	0.4
ROX Reference Dye	0.4
Quant-X enzyme	0.4
RT enzyme mix	0.4

A standard curve was generated using cycle threshold (Ct) values of the known copy number dilutions - enabled by the Roche Lightcycler software. This was used to determine the raw copy number of the viral RNA. Actual copy numbers per ml was determined using the equation below:

$$\text{Copies per ml} = \frac{\text{Raw copy number} \times 1000\ \mu\text{l/ml} \times \text{DNAse dilution factor} \times \text{Viral RNA elution volume}}{\textit{Initial sample volume (pre viral RNA extraction)} \times \textit{Sample volume added to PCR}}$$

For example, a raw copy number of 2 x 10^7 would give the following copy numbers per ml:

$$\text{Copies per ml} = \frac{20000000 \times 1000 \times 2 \times 50}{150 \times 2}$$
$$= 6.66 \text{ x } 10^9$$

If a concentration of above 1 x 10^8 copies per ml was obtained the process was continued, if not the 293T packaging cells were transfected once again as per Section 2.9.1.3.

Next, the copies per ml was translated into transducing units per ml (TU/ml) using the following equation:

$$\frac{\text{TU}}{\text{ml}} = \frac{\text{Copies per ml}}{100000}$$

The qPCR based lentiviral titration method was compared to a traditional fluorescent microscopy method for titrating lentiviral vectors, which obtained the above division factor of 100,000. This experiment was performed by Dr Lyubov Zaitseva.

The volume of prepared virus needed to infect a given cell number with a particular number of viral particles (multiplicity of infection (MOI)) was generated using the equation below:

$$\text{Volume of prepared virus} = \frac{\text{Number of cells to be infected}}{\text{TU/ml}} \times \text{desired MOI}$$

The volume of prepared virus was concentrated (30-40 fold) using Amicon® Ultra-15 centrifugal filters (Merck Millipore, Burlington, MA, USA). During this process, lentivirus from the 3-time point collections was pooled on ice, and centrifuged at 15,000rpm for 15 minutes at 4˚C. This was continued until the full volume was added to the centrifugal filter and concentrated to approximately 1ml. Upon completion of the concentration step a new TU/ml was generated and used for MOI calculations. The lentivirus was stored at -80˚C until use.

2.9.2 Lentiviral knockdown

AML/MM/BMSC were infected with the lentivirus prepared in 2.9.1. 5 x 10^5 cells were seeded on 24 well plates in 500µl of pen-strep free medium. 0.5µl of

hexadimethrine bromide (Polybrene) was added to aid the uptake of lentivirus into cells. The volume of virus calculated to give the required MOI was added to the cells. Empty construct virus (ShE) was also added to other wells of cells as controls - to rule out any non-specific viral effects. 24 hours after infection, 1ml of fresh medium was added and the cells were cultured for a further 48 hours. Knockdown (KD) was tested using qPCR after 72 hours (detailed in section 2.10.4). If knockdown was successful the control and GOI KD cells were used in mitochondrial transfer based experiments.

MM and BMSC were transduced with a lentivirus purchased from Clonetech (rLV.EF1.mCherry-Mito-9 and rLV.EF1.AcGFP1-Mem-9) and were used as per the above method - with the exception of no ShE control used.

2.10 Molecular biology techniques

2.10.1 RNA extraction

Gene expression levels in AML/MM/ BMSC were analysed using RT-qPCR. The first step in this process was the extraction of RNA from these cells. RNA was extracted using the ReliaPrep™ RNA Cell Miniprep Kit (Promega, Fitchburg, WI, USA) as per manufacturer's instructions. Briefly, cells were collected and washed in PBS and 250µl of BL+TG buffer was added and mixed thoroughly - followed by the addition of 85µl Isopropanol. The lysate was vortexed thoroughly before it was loaded into a ReliaPrep™ minicolumn - the column was then centrifuged at 13000 x g for 30 seconds. 24µl of Yellow Core Buffer was mixed with 3µl of 0.09M $MgCl_2$ and 3µl of DNase I enzyme (in that order) and was added to the column. The column was incubated for 15 minutes at RT before the addition of 200µl of column wash solution and a further centrifugation step using the above parameters. 500µl of RNA wash solution was added to the column and was centrifuged again at 13000 x g for 30 seconds - the minicolumn was then placed in a fresh collection tube. A further 300µl of RNA wash solution was added and the column was centrifuged for 3 minutes at 16000 x g. The minicolumn was then placed in an elution tube, 20µl of nuclease free water was added and the tube

was centrifuged for 1 minute at 13000 x g to elute the RNA. RNA was stored at -20˚C until further use.

2.10.2 DNA extraction

To detect inter-species mitochondrial transfer DNA was isolated from human AML and MM cells - mouse mitochondrial DNA was then detected using qPCR. DNA was extracted using the GenElute Mammalian Genomic DNA Miniprep Kit (Sigma Aldrich, St Louis, MO, USA) using the manufacturer's instructions. Briefly, cells were harvested and washed in PBS and the suspended in 200µl of Resuspension solution. To lyse the cells 20µl of Proteinase K was added followed by 200µl of Lysis Solution C. This lysate was vortexed and incubated at 70˚C for 10 minutes. After incubation 200µl of absolute ethanol was added to the lysate, followed by loading the lysate onto the column. The column was centrifuged at 12000 x g for 1 minute - discarding the waste. 500µl of Wash Solution was added to the column and a further centrifugation step was carried out as above. A further 500µl of Wash Solution was then added to the column, this time however the centrifugation time and speed were increased to 3 minutes and 16000 x g respectively. Finally, 100µl of Elution Solution was added directly to the column and centrifuged for 1 minute at 12000 x g, which eluted the DNA from the column. DNA was stored at -20˚C until further use.

2.10.3 Quantification of extracted RNA/DNA

Once extracted, RNA and DNA was quantified using the NanoDrop spectrophotometer (ThermoFisher, Waltham, MA, USA). The apparatus was blanked using 1µl of elution buffer (water for RNA and Elution Solution for DNA). 1µl of sample was then loaded onto the NanoDrop and RNA/DNA concentration (ng/µl) was determined. Sample purity was determined using the A260/230 ratio - a sample was deemed pure between 1.7 and 2.3.

2.10.4 cDNA synthesis

In order to analyse the gene expression levels in AML/MM/BMSC, cDNA was synthesised from RNA extracted in 2.10.3. This was achieved using reverse transcription with the qPCRBIO cDNA synthesis kit (PCR Biosystems, London, UK), as per the manufacturers protocol. For a 10µl reaction, 2µl of 5X cDNA Synthesis Mix was mixed with 0.5µl of 20X RTase and 300ng of RNA. The remaining volume was made up to 10µl with nuclease free water. PCR tubes were placed in a Thermocycler (Bio-Rad, Watford, UK) and a pre-defined program involving a 42˚C incubation for 30 minutes and an 85˚C incubation for 10 minutes was run. The cDNA samples were then held at 4˚C for up to 3 hours before a 5-fold dilution in nuclease free water. The samples were stored at -20˚C until further use.

2.10.5 Real time qPCR

The Roche Lightcycler 480 (Roche, Basel, Switzerland) was used to carry out real time quantitative PCR (qPCR). This method was used for gene expression analysis along with human and murine mtDNA analysis.

2.10.5.1 Gene Expression

cDNA synthesised in section 2.10.4 was used to perform qPCR to determine gene expression levels. The qPCRBIO SyGreen Mix (PCR Biosystems, London, UK) was used to carry out qPCR on 96 and 384 well Roche Lightcycler reaction plates (287). Briefly, a master mix was created containing 4µl of SyGreen Mix, 1µl of 10µM forward and reverse primer mix (see Table 2.8 and 2.9) and 1µl nuclease free water. 4µl of the diluted cDNA was added to the PCR wells along with 6µl of the appropriate master mix. PCR plates were then sealed and centrifuged briefly before loading into the light cycler. qPCR was run using a pre-programmed method described below. Upon amplification, SybrGreen was incorporated into newly synthesised DNA which could be detected by fluorescence.

- **Pre-amplification** (95˚C for 2 minutes).
- **Amplification** over 45 cycles (95˚C 15 seconds, 60˚C for 10 seconds and 72˚C for 10 seconds).
- **Melting curve analysis** to confirm PCR product specificity (95˚C for 5 seconds, 65˚C for 1 minute and 97˚C continuous).
- **Cooling** (40˚C for 30 seconds).

Cycle threshold (Ct) values were determined for each GOI, along with a housekeeping gene (Glyceraldehyde 3-phosphate dehydrogenase (GAPDH) or β-actin) as their expression does not change with the treatment or genetic alteration of cells. ΔCt values for GOIs were determined (Ct GOI – Ct housekeeping gene) and ΔΔCt was determined (ΔCt control – ΔCt test). The change in expression was expressed as a fold change of treated cells compared to untreated control cells ($2^{-\Delta\Delta Ct}$).

Table 2.8. KiCqStart® SybrGreen Primers (Sigma Aldrich) used in qPCR analysis.

Gene	Forward Primer 5' – 3'	Reverse Primer 5' – 3'
GAPDH	CTTTTGCGTCGCCAG	TTGATGGCAACAATATCCAC
β-actin	GATCAAGATCATTGCTCCTC	TTGTCAAGAAAGGGTGTCCA
NOX2	AGATGTTGTAGCTGAGGAAG	AATTAATATGAGGCACAGCG
CD38	CAGACCTGACAAGTTTCTTC	GATGACATAAACCACAAGGAG

Table 2.9. QuantiTect Primers (Qiagen) used in qPCR analysis.

Primer sequences were not disclosed by the manufacturer.

Gene	Assay Name	Catalogue Number
PGC-1α	Hs_PPARG1A_1_SG	QT00095578

2.10.5.2 SybrGreen based mtDNA analysis

To detect cross species mitochondrial transfer SybrGreen based qPCR using human and mouse specific primers was utilised. Two kits were purchased, the

human mitochondrial DNA (mtDNA) monitoring primer set (Clontech, Clontech Takara Bio Europe, Saint-Germain-en-Laye, France) and the mouse mitochondrial DNA copy number kit (Detroit R&D, Detroit, MI, USA). The human kit contained a human mtDNA primer (ND1) and a human genomic DNA (gDNA) primer (SLCO2B1) whilst the mouse kit contained mouse mtDNA and gDNA primers (specific genes not disclosed). DNA (extracted in 2.10.2) was diluted to 2ng/µl in water and 4µl was loaded onto a Lightcycler PCR plate. Human and mouse mtDNA and gDNA master mixes were created as follows: 4µl SybrGreen, 1µl of 10µM forward/reverse primer mix and 1µl water. 6µl of the appropriate master mix was added to the 4µl of DNA and the plate was sealed and centrifuged briefly. The mouse and human qPCR were run using different methods which are highlighted below:

Human mitochondrial kit:

- **Pre-amplification** (98˚C for 2 minutes).
- **Amplification** over 30 cycles (98˚C for 10 seconds, 61˚C for 15 seconds and 68˚C for 30 seconds).
- **Melting curve analysis** (95˚C for 5 seconds, 65˚C for 1 minute and 97˚C continuous).
- **Cooling** (40˚C for 30 seconds).

Mouse mitochondrial kit:

- **Pre-amplification** (95˚C for 10 minutes).
- **Amplification** over 30 cycles (95˚C for 15 seconds and 60˚C for 60 seconds).
- **Melting curve analysis** (95˚C for 5 seconds, 65˚C for 1 minute and 97˚C continuous).
- **Cooling** (40˚C for 30 seconds).

PCR products obtained were ran on agarose gel electrophoresis gels, explained in section 2.10.6.

2.10.5.3 Taqman® based mtDNA analysis

To show the cross-species mitochondrial transfer from BMSC to HSCs (under lipopolysaccharide (LPS) treatment *in vivo),* a qPCR was carried out using Taqman® chemistry compared to SybrGreen chemistry. In this method, a sequence specific probe containing both a 2′-chloro-7′phenyl-1,4-dichloro-6-carboxy-fluorescein (VIC)/ 6-Carboxyfluorescein (FAM) fluorophore and a TAMRA® quencher binds to the GOI. Upon amplification of the DNA the probe is cleaved releasing both the fluorophore and quencher allowing for the detection of the fluorophore.

Pre-designed Taqman® assays were obtained from ThermoFisher (see Table 2.10), encompassing both human and mouse mtDNA and gDNA. Cell lysate was loaded onto a PCR plate (2µl). The human and mouse mtDNA Taqman® assays were run in duplex reactions due to the difference in fluorophore (VIC and FAM). Human and mouse gDNA Taqman® assays were run in simplex reactions. Simplex and duplex master mixes were generated. For the simplex master mix 0.5µl of Taqman® assay (containing primers and probe) was mixed with 5µl of TaqPath ProAmp enzyme (ThermoFisher, Waltham, MA, USA) and 2.5µl water. For the duplex master mix 0.5µl of each Taqman® assay (total 1µl) was mixed with 5µl of TaqPath ProAmp enzyme and 2µl water. This master mix (8µl) was then added to the cell lysate on the PCR plate. The PCR plate was sealed and centrifuged at 1000rpm for 1 minute before it was loaded into the Lightcycler - qPCR was run using the following pre-programmed method:

- **Pre-amplification** (60˚C for 30 seconds and 95˚C for 5 minutes).
- **Amplification** over 50 cycles (95˚C for 15 seconds and 60˚C for 1 minute).
- **Cooling** (40˚C for 30 seconds).

From the Ct values obtained, human and mouse mitochondrial copy numbers in human HSCs were generated. Human and mouse mtDNA Ct values were normalised against the human gDNA Ct to obtain the ΔCt (Ct human/mouse mtDNA – Ct human gDNA). The ΔCt value was used to generate the

mitochondrial copy number ($2^{-\Delta Ct}$). This method was adapted from the Takara Clontech human mitochondrial DNA (mtDNA) monitoring primer set protocol (http://www.clontech.com/GB/Products/Stem_Cell_Research/Pluripotency_and_Differentiation/qPCR_Primer_Sets/ibcGetAttachment.jsp?cItemId=90270&fileId=7220863&sitex=10030:22372:US. Accessed June 2018). The mouse mtDNA assay was used to ensure no mouse cell contamination. Mitochondrial copy numbers were used to determine the percentage of mouse mitochondria in human HSCs after isolation from "humanised" NSG mice - using the equation below.

$$\%\ \text{Mouse mitochondria} = \frac{\text{Mouse mtDNA copy number}}{\text{Mouse mtDNA copy number} + \text{Human mtDNA copy number}} \times 100$$

Table 2.10. Taqman® assays used for mouse and human copy number assessment.

Taqman® Assay	Target Gene	Fluorophore	Assay Specifics
Human mtDNA	ND1	FAM	Hs02596873_S1 ND1
Mouse mtDNA	ND1	VIC	Mm04225274_S1 ND1
Human gDNA	Telomerase reverse transcriptase (TERT)	VIC	Taqman® copy number reference assay human
Mouse gDNA	Telomerase reverse transcriptase (TERT)	VIC	Taqman® copy number reference assay mouse

2.10.6 Agarose gel electrophoresis

Agarose gel electrophoresis was used to analyse qPCR products - 1.25% agarose gels were cast containing SYBR Safe (ThermoFisher, Waltham, MA, USA). For 60ml of agarose gel, 0.75g of agarose was diluted in 60ml of 1X Tris Acetate EDTA (TAE) buffer with 6µl of SYBR Safe. The solution was microwaved on full power for 60 seconds to dissolve all agarose and was cooled slightly before pouring into gel casts. A lane dividing well comb was added to allow the loading of samples. After the gel had set it was loaded into a DNA gel running tank with the comb removed - 1X TAE was added to the gel tank to submerge the gel. PCR products (10µl) were prepared by adding 2µl of 6X Orange G loading dye- 10µl of the sample was loaded into appropriate wells on the gel along with 5µl of 100 base pair DNA ladder (New England Biolabs, Ipswich, MA, USA) to determine

PCR product size. The gel was run for 1 hour at 100V and was imaged using the UV function (filter 1) of the Chemdoc-It2 Imager (UVP, LLC, Upland, CA, USA). Images were edited using ImageJ software.

2.10.7 Protein extraction

To analyse protein levels within BMSC, protein was extracted and Western blotting analysis was carried out - as per (266). The first step in this process was protein extraction - both whole cell protein along with cytoplasmic and nuclear components. To extract whole cell protein radioimmunoprecipitation assay (RIPA) buffer supplemented with protease and phosphatase inhibitors was used. This buffer lyses the cells allowing the isolation of total protein. 50µl of RIPA buffer was added to cell pellets (~$1x10^6$ cells) and incubated on ice for 15 minutes. After the incubation, the cell lysate was centrifuged at maximum speed for 15 minutes at 4ºC. The supernatant was collected and stored at -20ºC until use - the cell pellet was discarded.

To extract nuclear and cytoplasmic protein fractions the NE-PER Nuclear and Cytoplasmic Extraction Reagents kit (ThermoFisher, Waltham, MA, USA) was utilised. Cell pellets were re-suspended in 100µl of CER I buffer, vortexed for 30 seconds and incubated on ice for 10 minutes. 5.5µl of CER II buffer was subsequently added and vortexed once again for 30 seconds and incubated on ice for 1 minute. The cell lysate was then centrifuged at maximum speed for 5 minutes and the supernatant was collected as it contained the cytoplasmic component. The pellet (containing nuclei) was re-suspended in 50µl of NER buffer and vortexed for 30 seconds. The nuclei containing lysate was incubated on ice for 50 minutes with a brief vortex carried out every 10 minutes. Finally, the lysate was centrifuged on the highest setting for 10 minutes - the nuclear containing supernatant was collected. Both fractions were stored at -20˚C until use.

2.10.8 Western Blotting

12.5% polyacrylamide gels were made using 30% Polyacrylamide/Bis Solution (BioRad, Hercules, CA, USA). The gel mixture contained 10% SDS, 1.5M Tris pH 8.8, 10% ammonium persulphate and TEMED (detailed volumes are seen in Table 2.11). Protein samples were prepared (from 2.10.7) by adding 4X sample loading buffer (containing β-mercaptaethanol and bromophenol blue) and denatured at 100˚C for 5 minutes.

Table 2.11. Recipe for making 12ml of 12% polyacrylamide gel mix (enough for 1 gel).

Reagent	Volume (ml)
Water	3.96
30% Polyacrylamide	4.8
1.5M Tris	3
10% SDS	0.12
10% Ammonium persulphate	0.12
TEMED	0.005

After the polyacrylamide gels were set protein samples (10µl) were loaded into the wells on the gel. 5µl of Precision Plus Protein All Blue Prestained Protein standard ladder (BioRad, Hercules, CA, USA) was also added to determine protein size. The gels were run at 200V for 45 minutes in running buffer containing 10% SDS, 20µM glycine and 157µM Tris-Base. After completion of the run, the protein was transferred from the gel onto polyvinyladine fluoride (PVDF) membranes pre-treated with methanol. The gel and PVDF membrane were placed in transfer casts and added to a transfer tank containing transfer buffer (20µM Glycine and 157µM Tris-Base) - with an ice pack to lower the temperature generated by the electric current. The transfer took place at 100V for 1 hour, after which the membranes were blocked at RT in 5% bovine serum albumin (BSA) for 1 hour.

To detect the protein of interest the blocked membrane was added to a tube containing primary antibody and was incubated overnight at 4˚C. Antibodies used in this study can be found in Table 2.12. Following an extensive washing step in TBST buffer (1X PBS and 0.01% Tween) the membranes were incubated for 1 hour at RT with horseradish peroxidase (HRP) conjugated secondary antibodies. The same membrane was also probed for β-actin (total and cytosolic fractions) and SAM-68 (nuclear fractions) as above for loading controls.

Table 2.12. Antibodies used in Western Blot analysis.

Antibody	Isotype	MW (kDa)	Supplier
PGC-1α	Rabbit	91	Santa Cruz Biotechnology
CD38	Mouse	45	Santa Cruz Biotechnology
β-actin	Mouse	45	Sigma Aldrich
SAM-68	Rabbit	68	Cell Signalling Technology
Goat anti-Mouse IgG HRP	-	-	Dako (Agilent)
Goat anti-Rabbit IgG HRP	-	-	Dako (Agilent)

The membranes were imaged using enhanced chemiluminscence (ECL) reagent (GE healthcare, Little Chalfont, UK). A 1:1 ratio of solutions A and B were mixed and 500µl was added to the membrane for 30 seconds. Excess solution was removed and the membrane was imaged using the Chemdoc-It2 Imager (UVP, LLC, Upland, CA, USA) - with the filter set to position 3. Images were edited and densitometry was determined using ImageJ software.

2.11 Animal procedures

All animal experiments used in this study were carried out in accordance with the UK Home Office regulations - under project license 70/8814 (Prof. Kristian Bowles) and 70/8722 (Dr Stephen Robinson). All work was carried out by myself (under UK Home Office personal license IBB43C002) with the assistance of Dr Rachel Piddock (ICC440663) and Dr Stuart Rushworth (ICD3874DB). Before carrying out the techniques outlined below, full training was conducted by Mr Richard Croft (IGEBEFB87) and Mrs Anja Croft (L8A2ACED). All animals were

housed in a containment level 3 laboratory (pathogen free) in the Disease Modelling Unit (DMU) at the University of East Anglia.

2.11.1 Maintenance of animal colonies

Two mouse strains were used in this study the non-obese diabetic (NOD) severe combined immunodeficiency (SCID) Il2rg knockout (NOD.Cg.Prkd^{scid}IL2rg^{tm1Wji}/SzJ or NSG) mice and the C57BL/6J mice. Colonies of NSG (originally purchased from the Jackson Laboratory, Bar Harbour, ME, USA) and C57BL/6J (originally purchased from stock at the DMU, UEA, UK) were maintained and bred in the "barn" area of the DMU. Breeding trios (1 Male and 2 Females) were housed together for 6 months before separation. All offspring were weaned from their parents 3 weeks after birth and used in experiments at 4-12 weeks of age.

2.11.2 Xenograft Models

The NSG mouse model was used in xenograft experiments whereby human AML/MM cell lines and primary AML blasts were transplanted. Human cells can engraft in the bone marrow of these mice as they are severely immunocompromised - lacking mature T, B and Natural Killer cells. The mice were not irradiated prior to transplantation, the animals were therefore in good health.

AML and MM cell lines injected into the NSG were lentivirally modified with a pCDH-luciferase-T2A-mCherry construct (kindly gifted by Prof. Irmela Jeremias, Helmholtz Zentrum München, Germany). The luciferase construct allowed for the detection of human AML and MM cells *in vivo* using bioluminescence. Luciferase AML/MM cells were sorted prior to injection by Dr Zhigang Zhou using a FACSAria II cell sorter.

To analyse mitochondrial transfer to normal CD34+ HSCs, a humanized mouse was created. Briefly, 3-4-week-old NSG mice were treated with 25mg/kg Busulfan

twice over a 48-hour time period. $2x10^5$ primary human cord blood CD34+ HSCs were then injected into the tail vein. Engraftment of HSCs was determined through the analysis of human and mouse CD45+ cells in the peripheral blood. These animals were then treated with 1mg/kg LPS or PBS control for 2 hours to analyse mitochondrial transfer.

2.11.3 Wild type C57BL/6J Models

The C57BL/6J mice were used in this study to analyse the levels of mitochondria in LT and ST-HSC. 1mg/kg LPS or PBS control were injected by intraperitoneal (IP) injection (341) and after a 2-hour incubation the mice were sacrificed and bone marrow was isolated for flow cytometry analysis. These mice were also administered with live salmonella by oral gavage injection.

2.11.4 Intravenous injections

AML, MM and HSCs were administered into NSG mice through intravenous (IV) tail vein injection. To dilate the tail vein, mice were placed in a 37˚C hot box for 10 minutes prior to injection. The mice were then placed in a benchtop restrainer and injected with a 26G needle into the lateral tail vein. After a short recovery time they were returned to their home cage. Cells were suspended and injected in a total volume of 200µl PBS - containing $0.5x10^6$ and $2x10^5$ cells for malignant and non-malignant cells respectively.

2.11.5 Intraperitoneal injections

Drug compounds and D-luciferin were administered to mice using an IP injection. Mice were manually restrained in a “scruff” and injected (with a 26G needle) into the peritoneum with a volume of 200µl. In cases where daily IP injection was required, alternate flanks of the animal were injected.

2.11.6 Subcutaneous injections

Combinations of AML and BMSC were administered to mice using a subcutaneous injection. The mice were manually restrained and 200µl of cells were injected (using a 26G needle) under the skin on the hind flank. To compare the effect of PGC-1α knockdown in BMSC on the progression of AML, both flanks of the animal were utilised (see Figure 2.9).

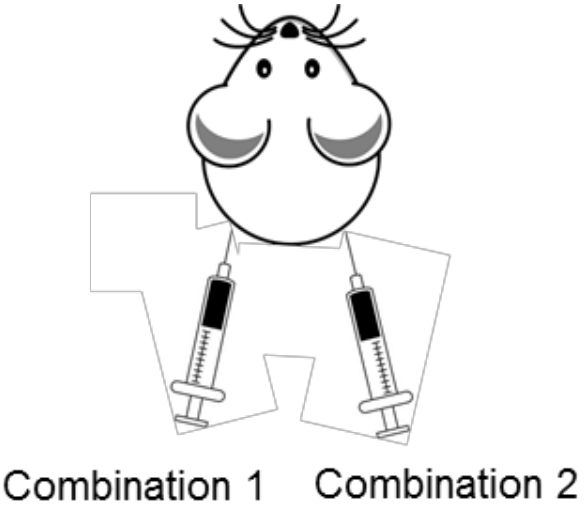

Figure 2.9. Schematic overview of the experimental set up for the subcutaneous model.

Combinations 1 and 2 contained a mix of AML cells and BMSC. BMSC were modified lentivirally to analyse AML disease progression compared to a control viral modification.

2.11.7 Blood Sampling

Blood was taken from the tail vein of mice for flow cytometry analysis. Animals were placed in the 37˚C hot box for 10 minutes to dilate the vein. Mice were then placed in a benchtop restrainer and up to 200µl of blood was collected in a 1.5ml Eppendorf tube (using a 26G butterfly needle). 25µl of monosodium citrate was added to Eppendorf tubes prior to collection to ensure the blood did not clot. Antibodies of interest were then added to the blood for 15 minutes, the red cells were lysed using 1X red blood cells lysis buffer (ThermoFisher, Waltham, MA, USA) and then analysed using flow cytometry.

2.11.8 Live animal imaging using Bioluminescence

To analyse tumour burden and location, bioluminescent imaging of live mice was carried out (342). This was enabled as AML and MM cells expressed the luciferase construct described in 2.11.2. 150mg/kg D-luciferin was IP injected and the mice were incubated at RT for 15 minutes to allow for maximum luciferase signal to be detected. During the last 5 minutes of the incubation the mice were anaesthetised in a chamber of isoflurane using a flow rate of 3%. Mice were imaged by the Bruker In-Vivo Xtreme (Bruker, Coventry, UK) using a pre-defined method (30 seconds exposure bioluminescent image, x-ray and light image). Mice were recovered in their home cage after imaging. Tumour burden and location was visualised by the detection of light produced by the formation of Oxyluciferin from luciferin, which is catalysed by the luciferase in the modified AML/MM cells. Images obtained were edited using ImageJ - bioluminescent images were merged with X-Ray images. Densitometry was also carried out using ImageJ software.

2.11.9 Oral gavage

To administer live *Salmonella enterica* to C57BL/6J mice an oral gavage injection was utilised - this procedure was carried out by Dr Devina Divekar. 100µl of salmonella (containing $1x10^9$ bacteria) was loaded into an oral gavage needle. The mouse was restrained in a “scruff” and the salmonella was administered down the oesophagus directly into the stomach of the mouse.

2.11.10 Schedule 1

At the end point of the experiment (whether at a specific time point or during signs of animal disease) the mice were humanely sacrificed using schedule 1 killing. Signs of animal disease were piloerection, hunched posture and hind limb paralysis. Animals were sacrificed by exposure to a rising CO_2 gradient followed by dislocation of the neck.

2.11.11 Isolation of mouse bone marrow

The bone marrow was extracted from mice to allow for *ex vivo* analysis. The femur and tibia were isolated and stripped of soft tissue, the bone caps were removed and each individual bone was placed in a 0.5ml Eppendorf tube which was perforated to allow the removal of the bone marrow. This tube was placed in a 1.5ml Eppendorf and was centrifuged on full power for 20 seconds to remove the bone marrow. The 4 bone marrow portions from each mouse were pooled and washed in PBS. Engraftment of AML cells was determined by staining the bone marrow with human CD45 and CD33 antibodies. Engraftment of MM cells was determined using the human CD45 antibody only (see Figure 2.10). AML/MM were deemed to have engrafted if the engraftment percentage was greater than 1%. Human CD45 AML/MM cells were sorted from the mouse bone marrow using MACS with CD45 microbeads (as per 2.2.2). These cells were used to determine mitochondrial content using flow cytometry and metabolic capabilities using the Seahorse extracellular flux assay.

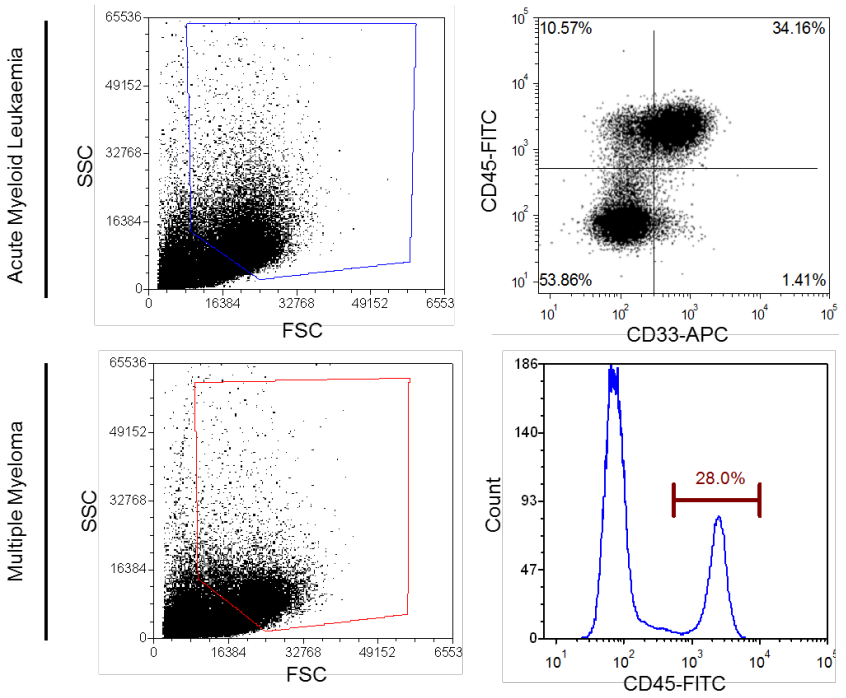

Figure 2.10. Gating strategy to determine AML/MM engraftment in mouse bone marrow.

Live cells were gated from the forward and side scatter plots. Human CD45 and CD33 expression is determined for the AML xenograft. Human CD45 expression is determined for the MM xenograft.

2.12 Statistical Analysis

All data produced in my thesis was analysed by Prism software (Version 7.0, GraphPad Software, San Diego, CA, USA). The Mann-Whitney U test was used to analyse non-paired test groups, whereas the Wilcoxon signed-rank test was used to analyse paired test groups. Correlation data was analysed using the Pearson's correlation co-efficient. Animal survival data was analysed by the Kaplan-Meier log-rank test. Results were considered significant where $P<0.05$ (*), $P<0.01$ (**) and $P<0.005$ (***). Results represent the mean ± standard deviation of 4 or more independent experiments.

3 AML derived NOX2 superoxide drives pro-tumoral mitochondrial transfer.

3.1 Introduction

Warburg stated in the 1920s that cancers utilise aerobic glycolysis (non-mitochondrial based) to generate ATP rather than OXPHOS (306). However, AML appears to contradict this hypothesis as the malignancy is susceptible to OXPHOS inhibitors (311). In addition, primary AML blasts which have an OXPHOS gene signature are less susceptible to Ara-C (312). AML blasts have also been shown to have increased mitochondrial levels compared to normal CD34+ cells (314). This chapter of my thesis will determine how and why AML blasts have extra mitochondria.

3.2 Results

3.2.1 Mitochondria are transferred from BMSC to AML blasts

Prior to determining how AML blasts acquire an increased mitochondrial mass, it's important to confirm that primary AML blasts obtained from patients at the NNUH also had increased mitochondrial levels compared to normal CD34+ cells. AML blasts were indeed found to have on average a 4-fold increase in mitochondrial levels compared to CD34+ cells (Figure 3.1A), which is comparable to previously published literature.

Taking this further, mitochondrial levels in primary AML blasts were assessed after they were cultured with BMSC. AML (suspension cells) and BMSC (adherent cells) were cultured in a 5:1 ratio for given time periods, followed by separation by gently mixing and mtDNA analysis. Mitochondrial levels in AML blasts were increased after a 72-hour (3-fold) and 1 week (6-fold) co-culture, compared with AML blasts cultured alone (Figure 3.1B). These results suggest that culture with BMSC caused an increase in mitochondrial levels within the AML blast.

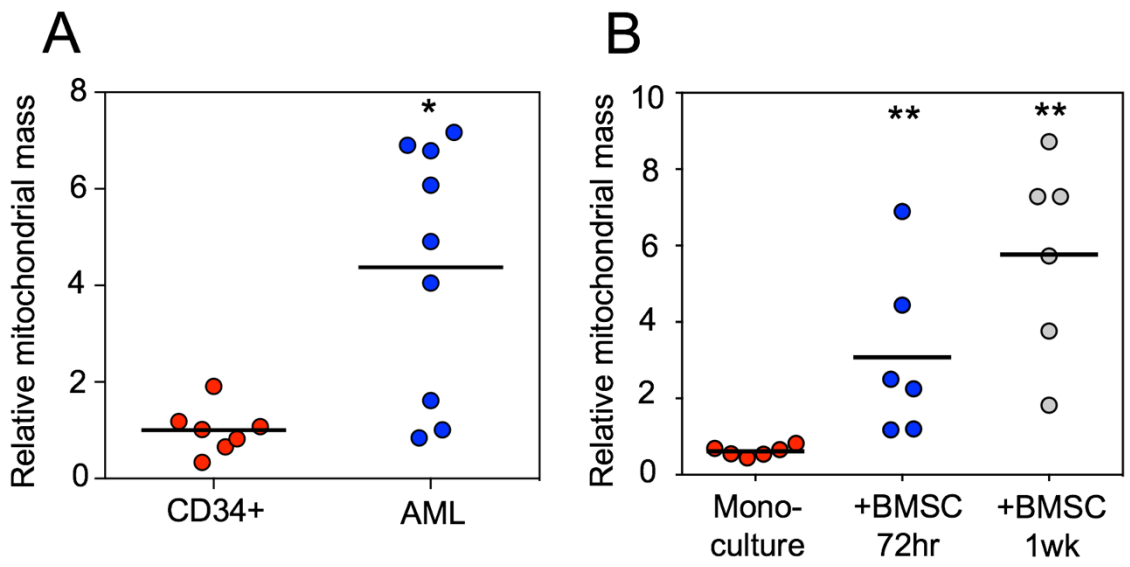

Figure 3.1. Mitochondrial levels are elevated in AML blasts compared to CD34+ cells, and after co-culture with BMSC.

Mitochondrial levels were calculated using qPCR with extracted DNA, ultilising a species specific mtDNA monitoring primer set. (A) Mitochondrial levels in "normal" CD34+ cells were compared to AML blasts. (B) The levels of mitochondria in AML blasts were determined after co-culture with BMSC over a 72-hour and 1 week time period. AML (suspension cells) and BMSC (adherent cells) were cultured in a 5:1 ratio for given time points, prior to separation by gentle mixing and independent mtDNA analysis. This experiment was performed by Dr Lyubov Zaitseva.

To determine if intercellular mitochondrial transfer occurred between BMSC and AML blasts, three experiments were designed to specifically analyse the movement of mitochondria. The first of these utilised a specific mitochondrial dye (MitoTracker Green FM) which allowed labelled mitochondria to be detected by flow cytometry. BMSC pre-stained with MitoTracker were cultured with primary AML blasts for 24-hours, resultant MitoTracker MFI in AML blasts was examined by flow cytometry. In this assay AML blasts were also pre-stained with MitoTracker to eliminate dye leakage. An increase in MitoTracker MFI was observed in AML blasts (n=11) co-cultured with BMSC compared to AML blasts cultured alone - highlighting the specific movement of MitoTracker labelled mitochondria from BMSC to AML blasts (Figure 3.2). No significant change in MitoTracker MFI was observed in CD34+ cells (n=7) when co-cultured with BMSC, therefore mitochondrial transfer does not occur between BMSC and CD34+ cells under normal conditions (Figure 3.2).

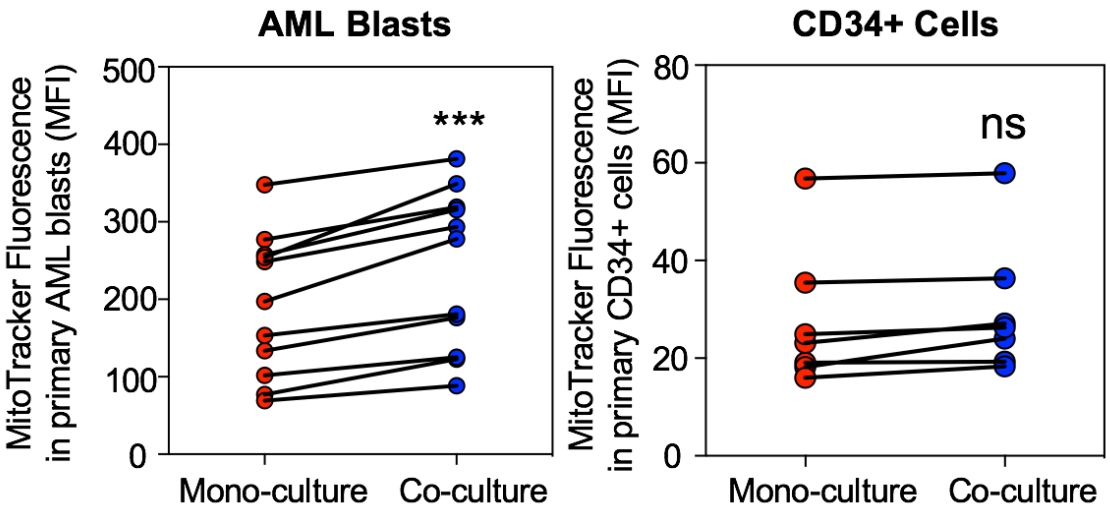

Figure 3.2. MitoTracker Green MFI is increased in AML blasts but not in CD34+ cells after co-culture with BMSC.

BMSC and AML blasts/CD34+ cells were pre-stained with 200nM MitoTracker Green FM. BMSC were then cultured with either AML blasts or CD34+ cells for 24-hours. MitoTracker MFI was measured by flow cytometry in AML blasts/CD34+ cells after co-culture with BMSC and in cells cultured alone.

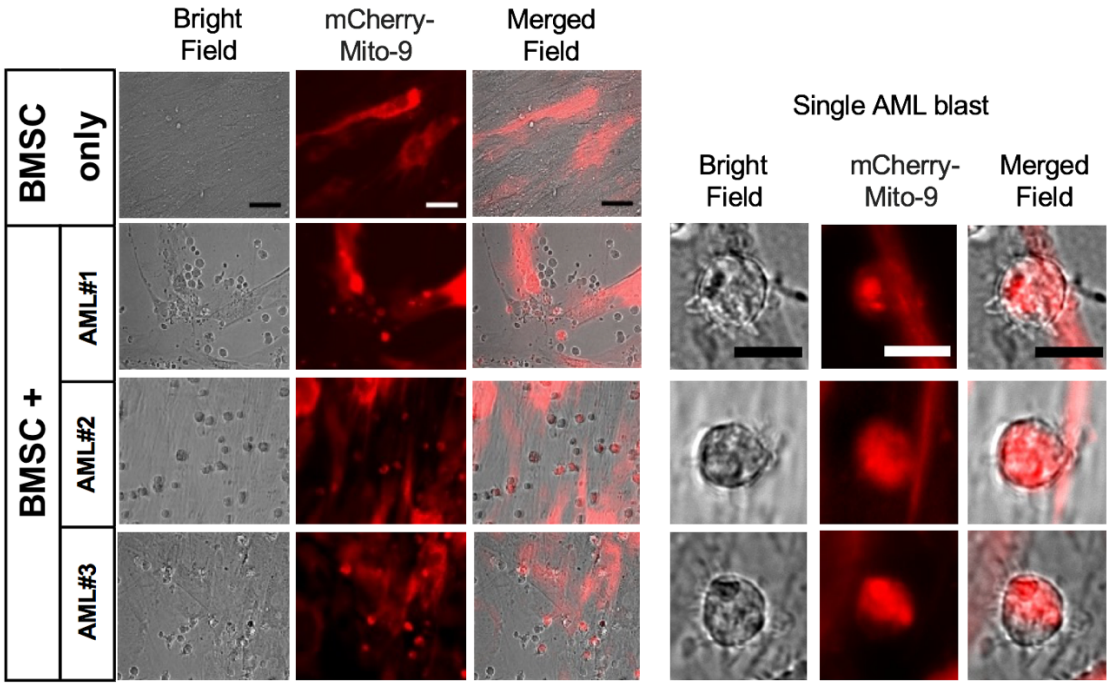

Figure 3.3. mCherry tagged BMSC mitochondria move to primary AML blasts.

BMSC mitochondria were tagged with a mCherry fluorophore using the rLV.EF1.mCherry-Mito-9 lentivirus. Un-labelled primary AML blasts (n=3) were cultured on these BMSC for 72-hours and imaged using fluorescence microscopy. Scale bar = 10μm. Experiment performed by Dr Lyubov Zaitseva.

In the second method, mitochondria in BMSC were specifically tagged with an mCherry fluorophore using the rLV.EF1.mCherry-Mito-9 lentivirus purchased from Clontech. Un-labelled primary AML blasts were cultured on these BMSC for 72 hours and live cell fluorescence microscopy was used to image the co-cultures. BMSC labelled mitochondria were seen to move to AML blasts, visualised by the acquisition of the mCherry fluorescence by AML blasts (Figure 3.3).

The third method I used was an *in vivo* xenograft model, enabled by sequence differences between human and murine mtDNA which can be detected by PCR. Four primary AML blast samples were injected into the tail vein of NSG mice, three weeks post administration the animals were sacrificed and bone marrow was extracted. Human AML blasts were seen to engraft into the bone marrow of NSG mice (using human CD45 and CD33 flow cytometry) at levels greater than 50% (Figure 3.4A). Human AML blasts were purified from the bone marrow using MACS with human CD45 microbeads - the purity of human AML blast sample was determined again using flow cytometry (Figure 3.4B). PCR was carried out on extracted DNA using species specific mtDNA and gDNA primers, PCR products were visualised using agarose gel electrophoresis. In AML blasts grown *in vitro* only human mtDNA was detected, whereas in AML blasts purified from mouse bone marrow, murine mtDNA was detected with no murine gDNA (Figure 3.5). Therefore, murine mitochondria moved from the BMM to human AML blasts *in vivo*.

One possible limitation of this experiment was the purity of AML blasts sorted from the mouse bone marrow. A purity of 98.96% human $CD45^{+}CD33^{+}$ was achieved, there was therefore a possibility of 1.04% mouse contamination. To examine the potential consequence of murine mtDNA in the assay I deliberately spiked human DNA (98.96%) with mouse DNA (1.04%) and repeated the PCR. The spiked sample did not create the same result as my mitochondrial transfer assay (Figure 3.6) and excluded contamination as the cause of murine mtDNA detection.

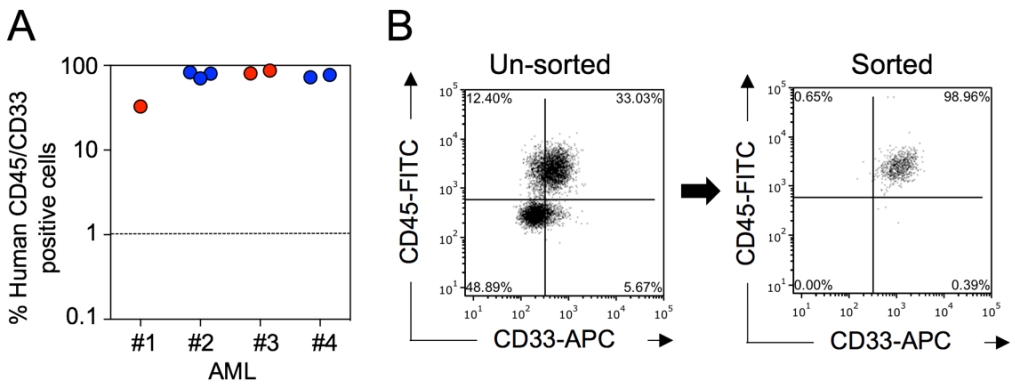

Figure 3.4. Engraftment and purification of primary AML blast xenografts.

Four primary AML blast samples were injected into NSG mice. After 3 weeks the animals were sacrificed and bone marrow was extracted. (A) shows the engraftment of AML blasts in the bone marrow using human CD45 and CD33 expression. (B) shows a representative flow cytometry plot of the purity of AML blast samples before and after MACS sorting.

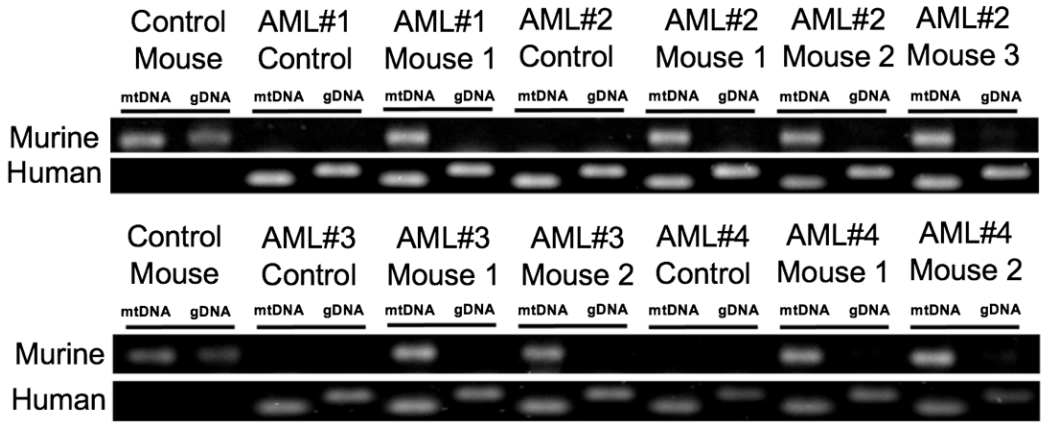

Figure 3.5. Murine mtDNA is detected in AML blast xenografts.

PCR was carried out with DNA extracted from purified AML blast xenografts, using species specific mtDNA and gDNA primers. The figure presents an agarose gel on which PCR products were run.

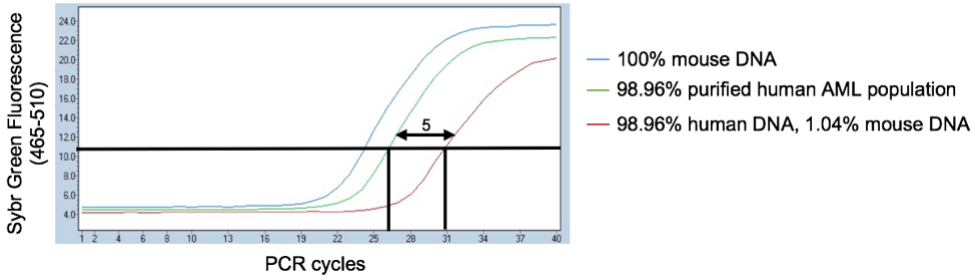

Figure 3.6. PCR trace of purified AML xenograft and a spiked DNA sample.

A qPCR was run using the murine mtDNA primer with 100% murine DNA, the purified AML xenograft (98.96% pure) and a spiked human DNA sample with 1.04% murine DNA. The figure presents the PCR trace showing cycle threshold (Ct) values of the samples with the difference between xenograft and spiked sample (containing the same murine DNA percentage) highlighted.

Taken together, these three methods show that mitochondria are transferred from BMSC to AML blasts. The observation that AML blasts have increased mitochondrial levels (after culture with BMSC and compared with normal CD34+ cells) may therefore in part be a result of intercellular mitochondrial transfer.

Previous studies analysing intercellular mitochondrial transfer utilised rho0 cells (devoid of mitochondria as described in Section 1.6.4), I therefore tried to generate AML rho0 cells to analyse mitochondrial transfer further. This was rather unsuccessful and took up a large amount of my PhD research time - due to the 40-day culture required to generate these cells. During culture (in ethidium bromide, pyruvate and uridine) the growth rate of the OCI-AML3 cells used was severely reduced and I constantly battled bacterial infections in my cultures. Through increasing the penstrep concentration 3-fold, I managed to generate one batch of OCI-AML3 rho0 cells which had severely reduced mitochondrial levels (Figure 3.7A). I cultured these cells on human BMSC for 24 hours and found only a small increase in mtDNA copy number from ~0 to 2 copies per cell (Figure 3.7B). I attempted to engraft the remaining cells from this batch into NSG mice, unfortunately they were not seen to engraft as NSG mice showed no sign of disease after 3 months - as a result no further rho0 cells were generated for use in this study.

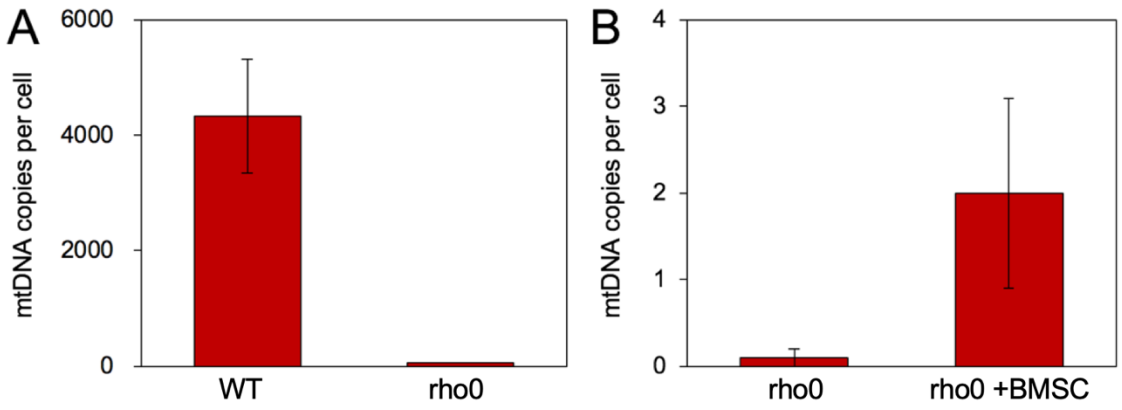

Figure 3.7. OCI-AML3 cells cultured in ethidium bromide have reduced mtDNA content.

OCI-AML3 cells were cultured in ethidium bromide, pyruvate and uridine for 40-days to generate rho0 cells (which are devoid of mtDNA). qPCR with a human mitochondrial monitoring kit was carried out to determine mtDNA content in WT and rho0 cells (A), and in rho0 cells after culture with human BMSC for 24 hours (B).

3.2.2 Mitochondria are transferred from BMSC to AML through TNTs

How the mitochondria move from BMSC to AML blasts was next examined. From previous literature describing mitochondrial transfer it can be seen the most prominent transfer mechanism is through TNTs - these were examined in the context of mitochondrial transfer to AML blasts. First, I assessed the levels of mitochondrial transfer when AML blasts were directly and indirectly cultured with BMSC. This was achieved using the MitoTracker based assay which can quantify levels of transfer. As per the previous experiment there was a significant increase in MitoTracker MFI in AML blasts (n=4) cultured directly with BMSC, however there was no increase when AML blasts were cultured in a 0.4µm transwell system (Figure 3.8A). This shows that direct cell culture is required to facilitate mitochondrial transfer from BMSC to AML blasts.

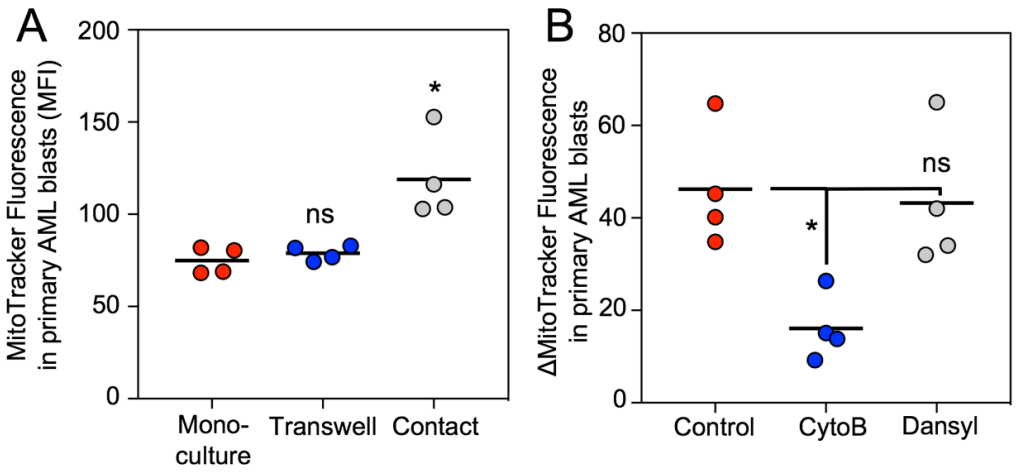

Figure 3.8. Mitochondrial transfer requires direct contact and is inhibited by CytoB.

The MitoTracker based assay was used to assess mitochondrial transfer levels when primary AML blasts (n=4) were cultured with BMSC in direct and indirect culture (A). (B) CytoB and Dansylcadavarine were added to the AML/BMSC co-culture and mitochondrial transfer levels were assessed (n=4). Mitochondrial transfer levels in (B) are presented as ΔMitoTracker Fluorescence (MFI) between mono-cultured and co-cultured AML blasts.

Furthermore, I analysed mitochondrial transfer levels upon the addition of Cytochalasin B (TNT inhibitor) and Dansylcadavarine (Endocytosis/Microvesicle inhibitor). Cytochalasin B (CytoB) was seen to inhibit mitochondrial transfer 3-fold, whereas there was no change upon the addition of Dansylcadavarine (Figure 3.8B). These results show that TNTs are the likely mechanism in which mitochondria move from BMSC to AML blasts.

CytoB is commonly used as a TNT inhibitor, however this compound is an actin inhibitor so therefore not specific to inhibiting TNT formations. Ergo, it was important to actually visualise TNTs that form between AML and BMSC to confirm that mitochondria move via this mechanism. TNTs are projections of the plasma membrane, therefore a plasma membrane dye (Vybrant DiI) was used to visualise AML plasma membrane projections. BMSC were stained with MitoTracker Green to label mitochondria and Vybrant DiI stained AML blasts were cultured with these for 24 hours. Confocal microscopy was used to visualise TNTs - however initially none were found. TNTs are highly dynamic which form and dissociate readily, therefore a fixation step was added to the protocol prior to visualisation. Using this method TNTs were visualised between AML blasts and BMSC (Figure 3.9), these TNTs were AML derived and contained mitochondria of BMSC origin.

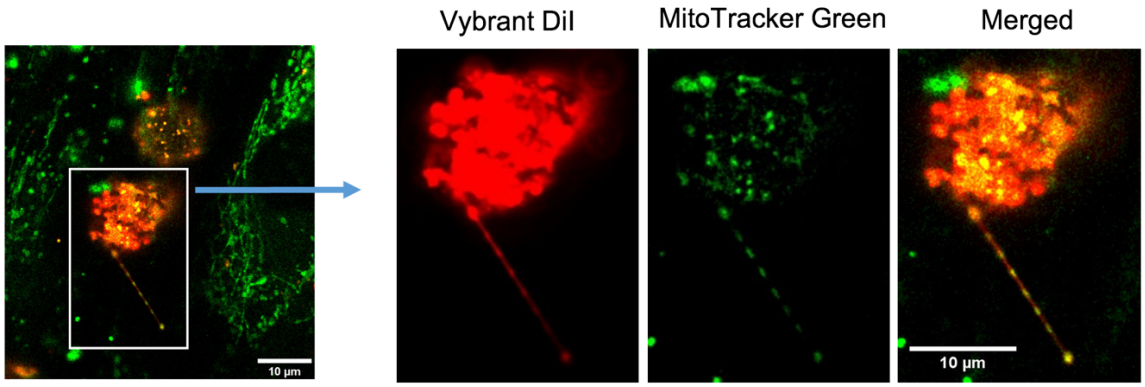

Figure 3.9. Visualisation of a TNT formed between AML blasts and BMSC.

Primary AML blasts were stained with Vybrant DiI and cultured with MitoTracker Green stained BMSC. Fixed cell confocal microcopy was used to visualise TNT formations. A TNT formed by AML blasts can be seen containing BMSC derived mitochondria. Image taken by Dr Lyubov Zaitseva.

I next aimed to quantify the number of TNTs which are formed during a co-culture between primary AML blasts and BMSC. During confocal microscopy, very few TNTs were observed however multiple Vybrant DiI dots were observed on BMSC - which remained after the dissociation of TNT formations (Figure 3.10A). These dots were called TNT-anchor points (TAPs) and were used to quantify the number of TNTs that formed between primary AML blasts and BMSC. TAPs were not found when AML blasts were cultured on BMSC in 0.4µm transwells (Figure 3.10B). Examining four primary AML blasts, on average 300 TAPs were formed

over the 24-hour time period - per confocal image (Figure 3.10C). CytoB was found to decrease the number of TAPs by around 3.5-fold (Figures 3.10D).

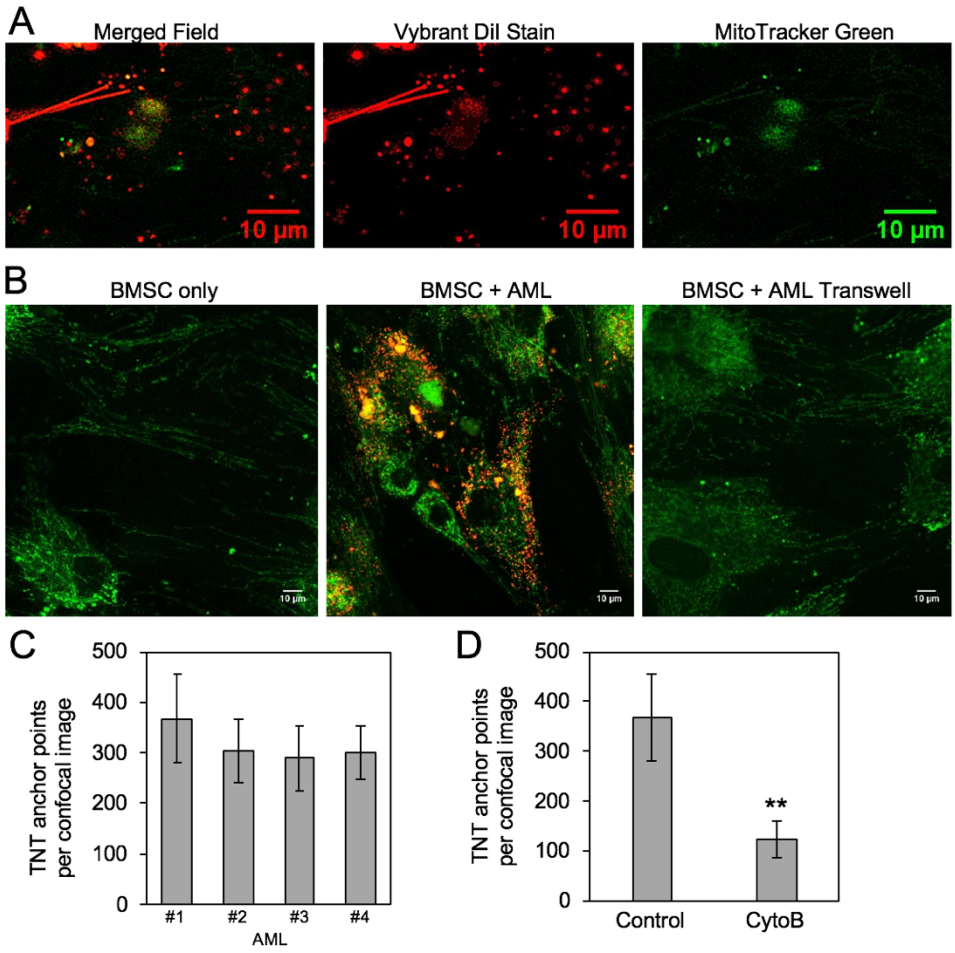

Figure 3.10. TAPs are formed by TNTs and can be used to quantify the TNT formations.

TAPs are residual Vybrant DiI points where TNTs have formed and dissociated, shown in (A). (B) TAPs are only formed upon direct contact of primary AML blasts and BMSC. (C) The number of TAPs was quantified (per confocal image) between co-cultures of BMSC and four primary AML blast populations. (D) TAP formations were assessed upon the addition of CytoB (n=4).

The results of these experiments have determined that one of the ways mitochondria move to AML blasts is through TNTs and the number of TNTs can be quantified using TAPs.

3.2.3 Mitochondrial transfer increases AML OCR and ATP production

Next, the functional consequence of mitochondrial transfer was examined. Using the Seahorse Extracellular Flux Analyser (which measures the oxygen consumption rate (OCR) of cells - comparable with mitochondrial respiration levels within cells) it was found that AML blasts have increased OCR after co-culture with BMSC (Figure 3.11). The maximum respiration and spare capacity was increased in AML blasts cultured with BMSC, with basal respiration and post oligomycin OCR increased in 1/2 AML blasts tested (Figure 3.12A). However, in this experiment oligomycin was not seen to have the expected effect on the respiration dynamics (should decrease OCR due to ATP synthase inhibition). This is likely due to the use of the wrong oligomycin concentration in the assay - the post Oligomycin result is therefore not reliable. In addition to the Seahorse data, the CellTitre-Glo assay revealed AML blasts cultured on BMSC had increased levels of ATP production (Figure 3.12B) – which suggested increased OCR in AML blasts results in increased ATP production.

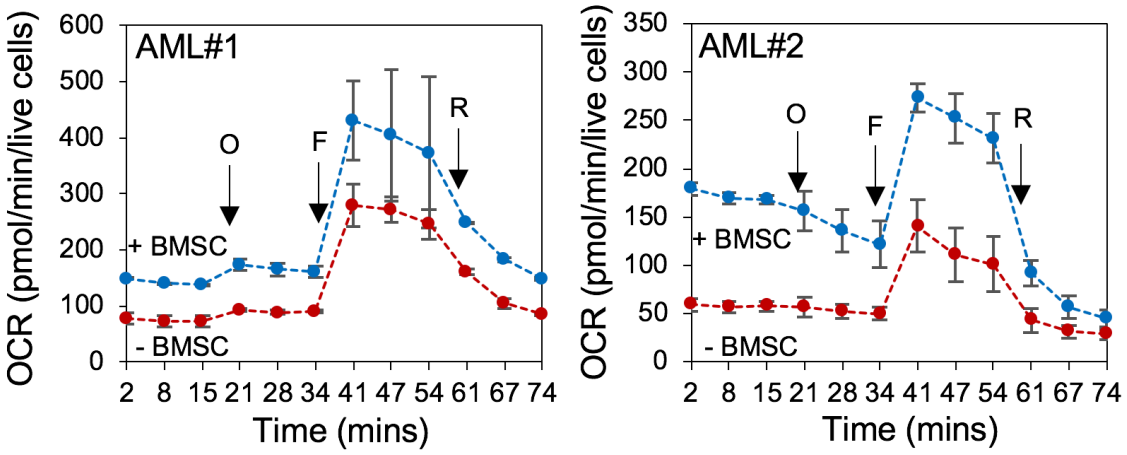

Figure 3.11. AML blasts have increased levels of OCR after co-culture with BMSC.

Primary AML blasts (n=2) were cultured with and without BMSC for 24 hours and then OCR was analysed in AML blasts - using the Seahorse XFp Analyzer with the Mito Stress Test Kit. Data is represented as mean +/- standard deviation. Sequential injections of oligomycin (O), carbonyl cyanide-4-(trifluoromethoxy)phenylhydrazone (FCCP) (F), and rotenone/antimycin A (R) were used to obtain respiration dynamics seen in Figure 3.12.

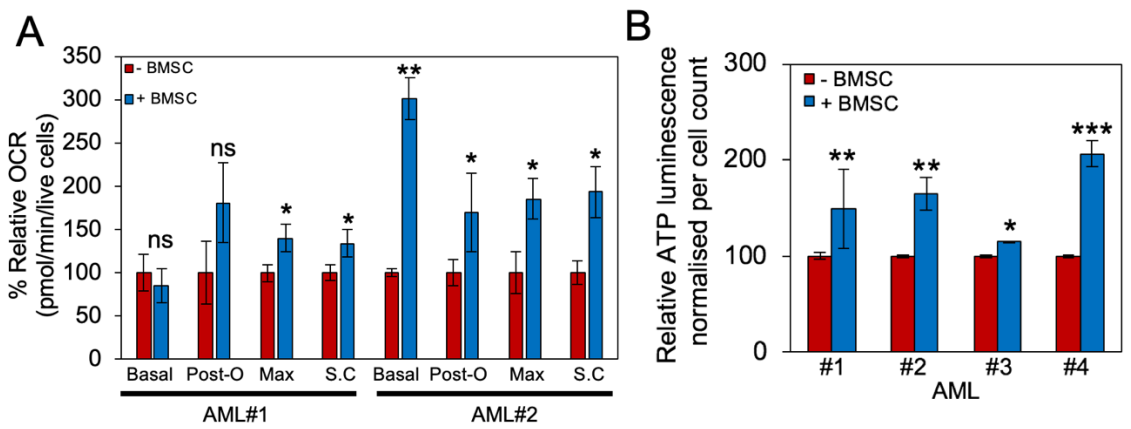

Figure 3.12. Elevated OCR in co-cultured AML cells results in enhanced ATP production.

(A) Basal and maximum OCR rates were determined in AML blasts (n=2) (in addition to the post oligomycin (Post-O) OCR and spare capacity (S.C)) with and without BMSC culture. These values were determined using the respiration dynamics presented in 3.11 and as per 2.8 – and presented as % relative OCR. In all cases non-mitochondrial respiration (post rotenone/antimycin A) was subtracted from OCR values. (B) ATP production in AML blasts (n=4) +/- BMSC culture was determined using the CellTitre-Glo ATP assay.

3.2.4 Induction of oxidative stress promotes mitochondrial transfer

In sections 3.2.1, 3.2.2 and 3.2.3 I have presented data which shows that mitochondria move from BMSC to AML blasts, that this transfer can occur through TNTs and that the transfer results in increased OCR and ATP production. This data is comparable with other published literature from other cancers where mitochondrial transfer has been described. Next, I aimed to take these results further by elucidating the stimulus mechanism of mitochondrial transfer in AML - which to date has not been described in any other cancer mitochondrial transfer system.

Initially, a pharmacological screen was carried out using the MitoTracker based mitochondrial transfer assay to determine what effect different compounds have on the levels of mitochondrial transfer. It was found that compounds which induce oxidative stress (H_2O_2, Daunorubicin, $CoCl_2$) increased mitochondrial transfer, whereas antioxidants (GSH and NAC) reduced the levels of mitochondrial transfer (Figure 3.13).

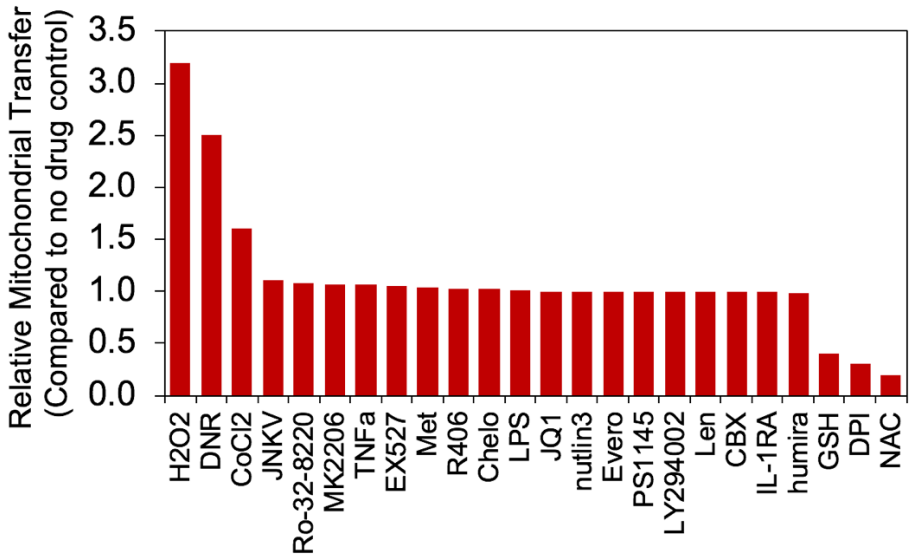

Figure 3.13. Pharmacological screen to assess mitochondrial transfer levels.

Mitochondrial transfer levels were assessed between BMSC and AML blasts (n=1) upon the addition of a range of compounds which enhance or inhibit various key cell signalling pathways and processes. Details of the compounds used can be found in the methods section in Table 2.2. The levels of mitochondrial transfer are presented relative to a no drug control. H_2O_2 – hydrogen peroxide. DNR – daunorubicin. $CoCl_2$ – cobalt chloride. JNKV – c-Jun N-terminal Kinase inhibitor. TNFa – tumour necrosis factor alpha. EX527 – selisistat. Met – metformin. Evero – everolimus. Len – lenalidomide. CBX – carbenoxolone. GSH – glutathione. DPI - diphenyleneiodonium. NAC – N-acetyl cysteine.

H_2O_2 was seen to increase mitochondrial transfer 3-fold whereas NAC was seen to reduce the process 4-fold. These results were replicated with an increased number of primary AML blast samples (n=8 for NAC and n=11 for H_2O_2) (Figure 3.14).

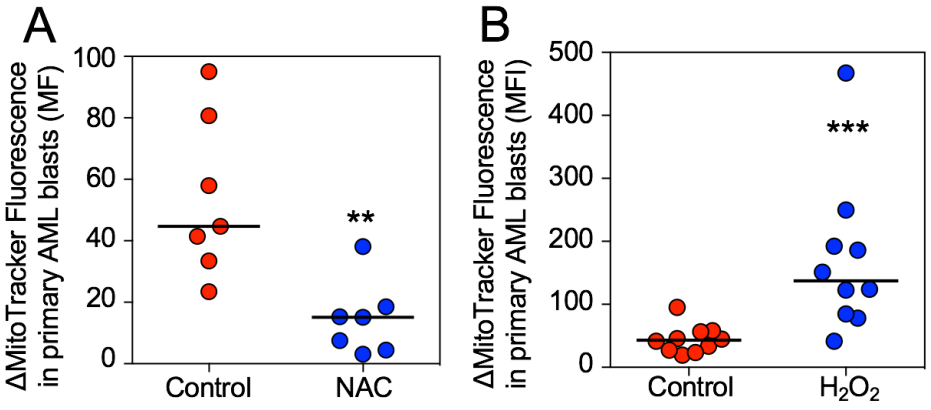

Figure 3.14. The effect of NAC and H_2O_2 on mitochondrial transfer levels.

The MitoTracker based mitochondrial transfer assay was used to analyse the effect of NAC (A) (n=7) and H_2O_2 (B) (n=11) on the levels of transfer. The results are presented as ΔMitoTracker Fluorescence (MFI) between co-cultured and mono-cultured AML blasts, which corresponds to the level of mitochondrial transfer.

Normal CD34+ cells were not seen to acquire mitochondria from BMSC (Figure 3.2). However, very interestingly the addition of H_2O_2 to the culture stimulated the transfer of mitochondria from BMSC to CD34+ cells (Figure 3.15).

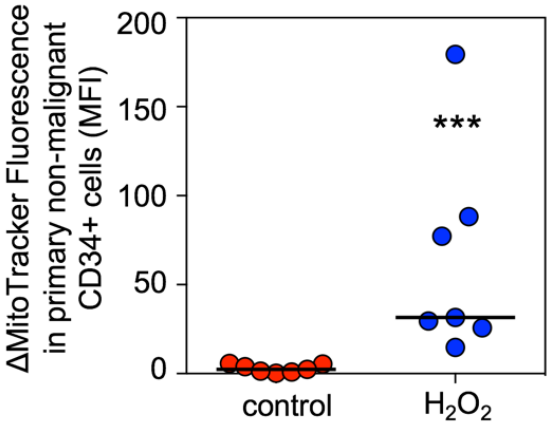

Figure 3.15. H_2O_2 promotes CD34+ cells to acquire mitochondria from BMSC.

The levels of mitochondrial transfer were assessed between CD34+ cells (n=7) and BMSC with and without the addition of 50μM H_2O_2.

Next, I examined whether NAC had an effect on AML disease progression *in vivo*. I injected the AML cell line OCI-AML3 (containing a luciferase construct) into NSG mice and administered NAC into their drinking water at a concentration of 2g/L, as per previous studies (343). However, no difference in disease progression was observed between NAC treated and control animals (Figure 3.16A). In addition, there was no difference in overall animal survival (Figure 3.16B).

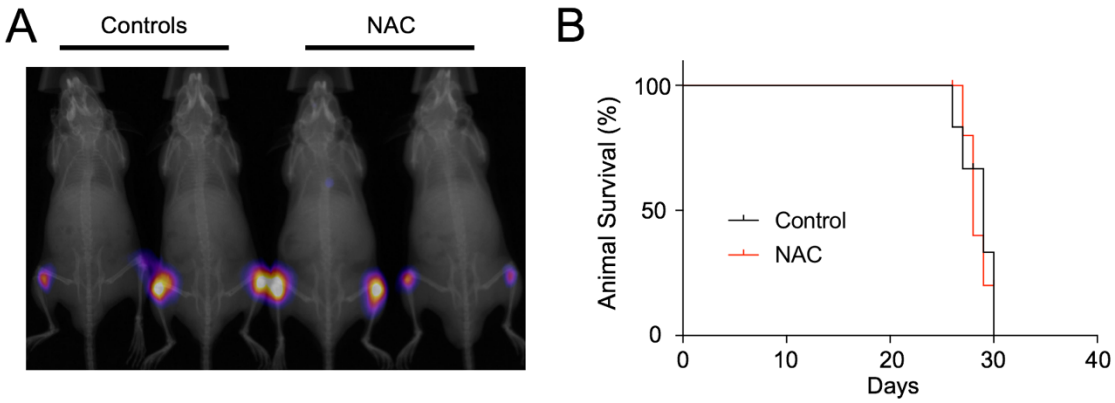

Figure 3.16. NAC has no effect on AML disease progression *in vivo*.

OCI-AML3 cells (with luciferase construct) were injected into the tail vein of NSG mice and AML disease progression was monitored by bioluminescence (A). At signs of disease animals were sacrificed and survival data is presented in (B).

3.2.5 AML derived NOX2 superoxide drives mitochondrial transfer

From the pharmacological screen, it was found that the NOX2 inhibitor Diphenyleneiodium chloride (DPI) had a similar effect on mitochondrial transfer as per NAC and GSH. NOX2 is elevated on AML blasts and converts molecular oxygen to superoxide, which increases oxidative stress. To examine the effect of DPI further the MitoTracker based mitochondrial transfer was repeated on an increased number of primary AML blast samples (n=11). Approximately a 2-fold reduction in mitochondrial transfer was observed (Figure 3.17).

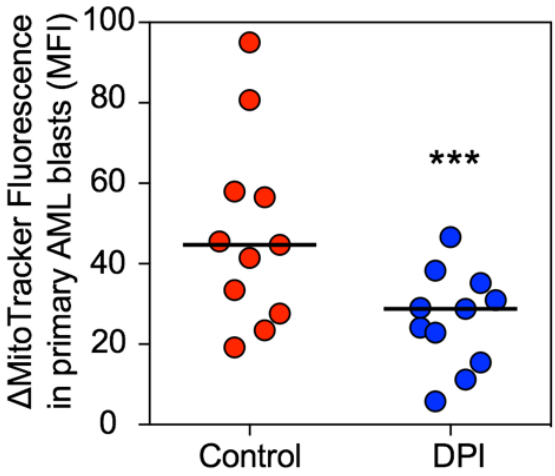

Figure 3.17. DPI inhibits the transfer of mitochondria from BMSC to AML.

Mitochondrial levels were assessed between AML blasts (n=11) and BMSC upon the addition of 1μM DPI, which inhibits NOX2 on AML.

The effect of DPI on AML blast survival was next tested, DPI was added to the co-culture between AML blasts and BMSC and levels of apoptosis were measured in AML blasts after co-culture. DPI was seen to increase the level of apoptosis from 20 to 80% in AML blasts (Figure 3.18A), whereas no change in apoptosis levels were found in CD34+ cells (Figure 3.18B). This highlights the possibility of a specific therapeutic window for targeting NOX2 on AML blasts.

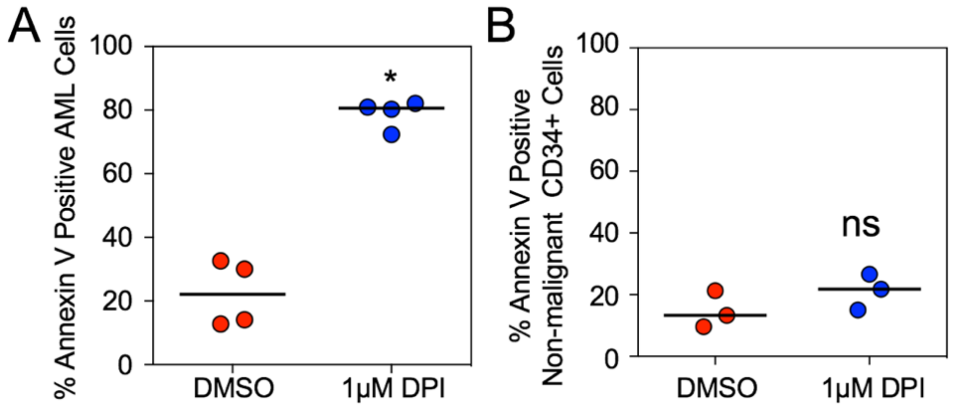

Figure 3.18. DPI induces apoptosis in AML blasts but not in CD34+ cells.

AML blasts (A) or CD34+ cells (B) were cultured with BMSC and treated with either DMSO or 1μM DPI. Levels of apoptosis were determined using Annexin/PI and flow cytometry.

Next, I made a lentivirus encoding shRNA specifically targeted to NOX2 mRNA. Four AML blast populations were transduced with this lentivirus (or lentivirus containing an empty construct) and mitochondrial transfer levels were assessed in these cells when cultured with BMSC. NOX2 was successfully knocked down in AML on average by 70% (Figure 3.19A) and this resulted in reduced mitochondrial transfer by approximately 2-fold (Figure 3.19B). In addition, NOX2 KD AML blasts had a significantly reduced OCR compared with control KD cells after culture with BMSC (Figure 3.20). There was no change in OCR between control KD and NOX2 KD AML blasts when cultured alone (Figure 3.20).

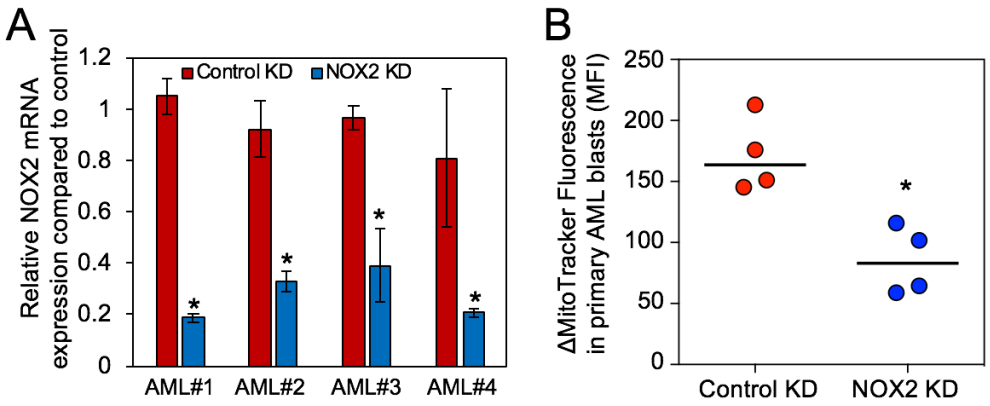

Figure 3.19. NOX2 KD in AML blasts reduces mitochondrial transfer.

Four AML blast populations were transduced with a lentivirus encoding shRNA specific to NOX2 or an empty construct. qPCR was used to confirm the level of knockdown presented in (A). These NOX2 KD and control KD cells were cultured with BMSC, levels of mitochondrial transfer were assessed using the MitoTracker based assay (B).

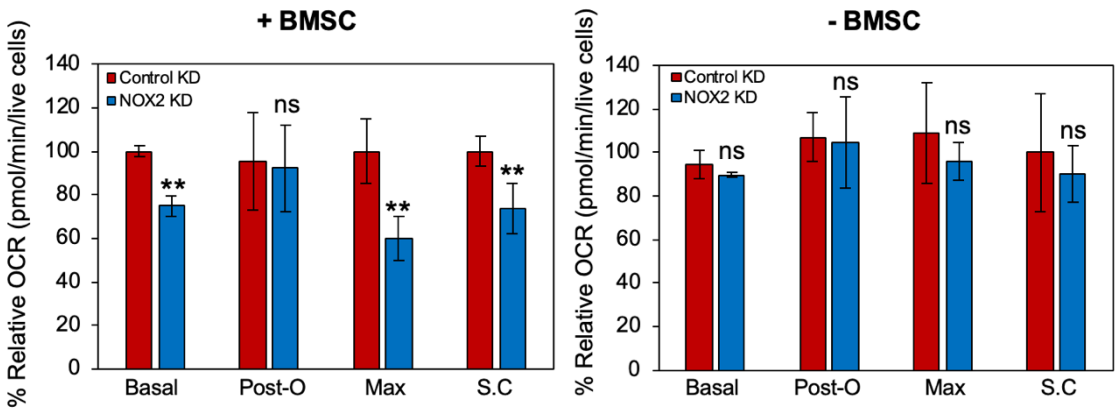

Figure 3.20. OCR levels are reduced in NOX2 KD AML blasts.

Basal and maximum OCRs were determined (along with OCR post oligomycin (Post-O) and spare capacity (S.C)) using the Seahorse extracellular flux assay. Control KD and NOX2 KD cells were analysed after co-culture with BMSC and when cultured alone. All OCRs are presented as % relative OCR and have had non-mitochondrial respiration (post rotenone/antimycin A treatment) subtracted.

As NOX2 is known to produce extracellular superoxide, the levels of these superoxides were next measured in control KD and NOX2 KD AML blasts. As expected there was a reduction in NOX2 derived superoxide from 700nM in control KD cells to 400nM in NOX2 KD cells (Figure 3.21).

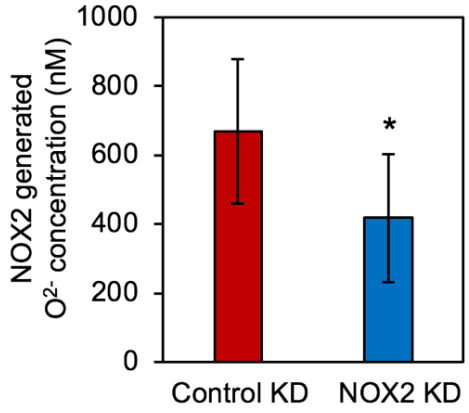

Figure 3.21. NOX2 KD AML blasts secrete lower levels of superoxide.

NOX2 production in control KD and NOX2 KD AML blasts (n=4) was measured using the Amplex Red superoxide detection assay. The level of superoxide is presented as a concentration in nM.

Next, I assessed whether the superoxide secreted by AML blasts caused a change in oxidative stress levels in BMSC. Primary AML blasts were cultured with BMSC (n=10) and ROS levels were analysed - using the DCF assay. ROS levels were significantly elevated in BMSC (n=10) cultured with AML blasts compared

to BMSC cultured alone (Figure 3.22A). This was specific to AML culture as when CD34+ cells were cultured with the BMSC (n=5) there was no change in ROS levels (Figure 3.22B).

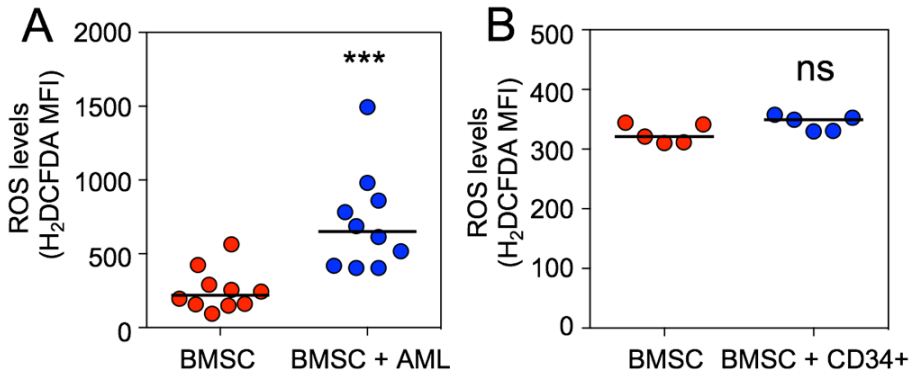

Figure 3.22. AML blasts, but not CD34+ cells, stimulate ROS in BMSC.

BMSC were cultured with AML blasts (A) or CD34+ cells (B). ROS levels in co-cultured BMSC were assessed using the DCF assay compared to BMSC cultured alone. ROS levels are presented as DCF MFI.

To assess whether increased ROS in BMSC was dependant on AML contact, I repeated the assay with AML blasts cultured in a transwell system. ROS levels remained elevated in BMSC when AML blasts were cultured in 0.4μM transwells (Figure 3.23A), therefore cell-cell contact is not necessary for this observation. To determine whether NOX2 derived superoxide caused the oxidative stress in BMSC I repeated the ROS detection assay in BMSC cultured with control KD and NOX2 KD AML blasts. ROS levels were reduced 2-fold in BMSC cultured with NOX2 KD cells compared with control KD cells (Figure 3.23B), which suggests that AML derived NOX2 superoxide contributes to the stimulation of oxidative stress in BMSC.

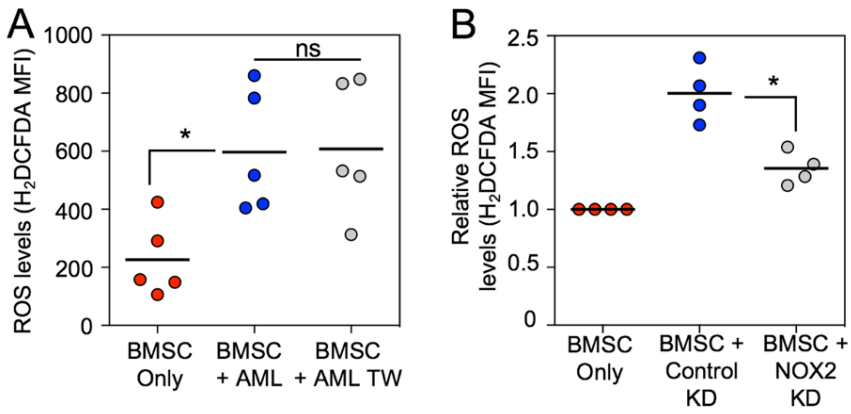

Figure 3.23. NOX2 derived superoxide is responsible for oxidative stress in BMSC.

ROS levels were assessed using the DCF assay in BMSC when AML blasts were cultured in direct contact and when cultured in 0.4μm transwells (A). ROS levels were also determined in BMSC when cultured with control KD and NOX2 KD AML blasts (B).

3.2.6 AML stimulates PGC-1α driven mitochondrial biogenesis in BMSC

Next, I examined the consequence of AML-induced oxidative stress in BMSC and how this resulted in enhanced mitochondrial transfer. BMSC appeared unaffected by the loss of mitochondria to AML blasts, therefore I first examined mitochondrial levels in BMSC (n=8) after culture with AML blasts. A 3-fold increase in mitochondrial mass was observed in BMSC after AML culture (Figure 3.24A), suggesting that AML promotes mitochondrial biogenesis in BMSC. In addition, this increase in mitochondria caused BMSC to have elevated OCR compared when BMSC were cultured alone (Figure 3.24B).

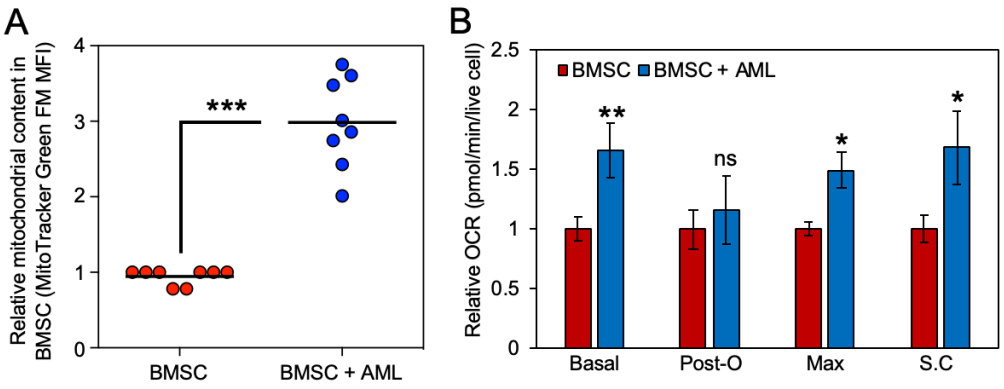

Figure 3.24. AML stimulates BMSC to increase mitochondrial mass and OCR.

Mitochondrial levels in BMSC (n=8) were assessed with and without co-culture with AML blasts, using MitoTracker Green staining (A). (B) OCR in BMSC were determined, with and without AML, using the Seahorse extracellular flux analyser. Relative basal and maximum OCR are presented (along with post oligomycin (Post-O) OCR and spare capacity (S.C)) – all values have non-mitochondrial respiration (after rotenone/antimycin A injection) subtracted.

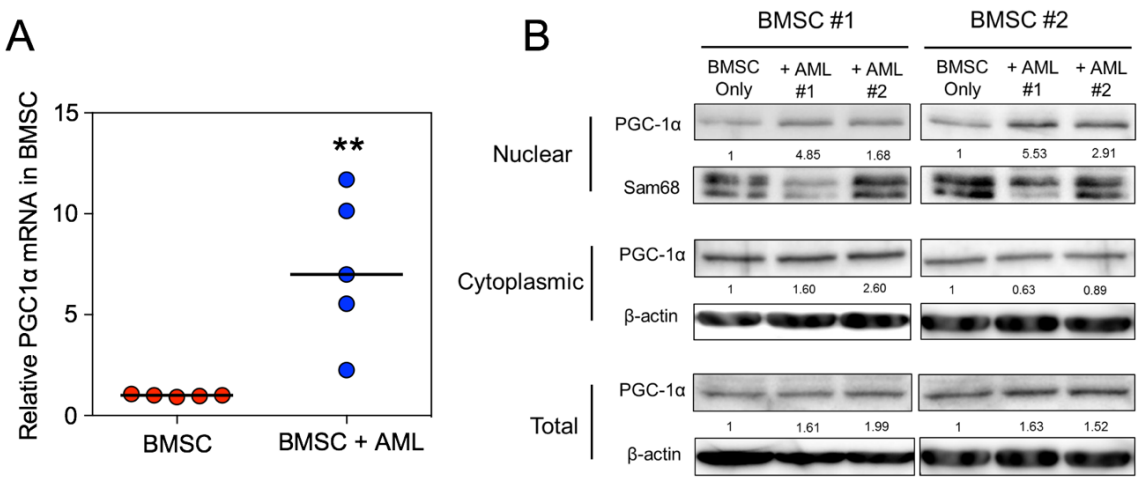

Figure 3.25. PGC-1α is activated in BMSC after co-culture with AML blasts.

PGC-1α mRNA levels were determined in BMSC (n=5) using qPCR with and without culture with AML blasts (A). Nuclear, cytosolic and total PGC-1α protein levels were determined in BMSC (n=2) using Western Blot analysis (B). Densitometries are presented between the Western blots.

Mitochondrial biogenesis is regulated through the transcription factor PGC-1α, which has been shown to be activated by oxidative stress (344). Therefore, I assessed whether PGC-1α is activated in BMSC after culture with AML blasts. PGC-1α mRNA was increased 3-fold in BMSC (n=5) cultured with AML blasts (Figure 3.25A). PGC-1α was activated in BMSC (n=2) cultured with AML blasts, shown through an increased nuclear accumulation of the protein by western blotting (Figure 3.25B). This nuclear accumulation in BMSC (n=2) was reduced upon the addition of NAC (Figure 3.26), which suggests that PGC-1α activation and subsequent mitochondrial biogenesis is through AML-induced oxidative stress.

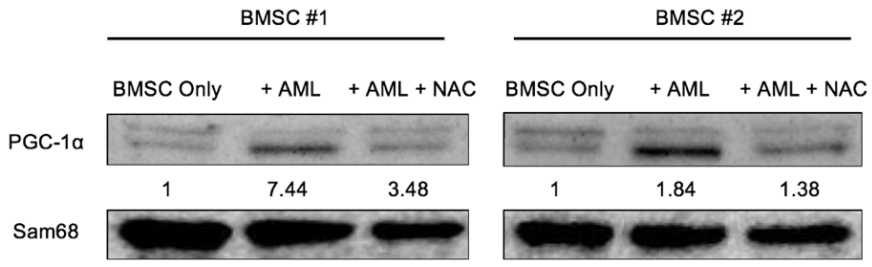

Figure 3.26. Elevated PGC-1α nuclear accumulation in BMSC was reduced by NAC.

Nuclear PGC-1α protein levels in BMSC (n=2) cultured alone and with AML blasts +/- NAC were determined by Western blotting. Densitometries are presented between the Western blots, which were normalised to Sam68 loading control. Experiment carried out with the help of Dr Stuart Rushworth.

3.2.7 Silencing of PGC-1α in BMSC inhibits mitochondrial transfer

In section 3.2.6 I have shown that AML blasts stimulate mitochondrial biogenesis in BMSC through the activation of PGC-1α. I next investigated whether PGC-1α activity in BMSC is essential for mitochondrial transfer to AML blasts. I made a lentivirus encoding shRNA specifically targeted to PGC-1α mRNA, I then transduced BMSC with this virus to knockdown PGC-1α. Figure 3.27A shows that PGC-1α mRNA expression was reduced by around 90% in BMSC transduced with lentivirus targeted to PGC-1α compared to control. Mitochondrial transfer levels were found to be reduced on average by 40% in cultures of PGC-1α KD BMSC and AML blasts – compared with control KD BMSC (Figure 3.27B).

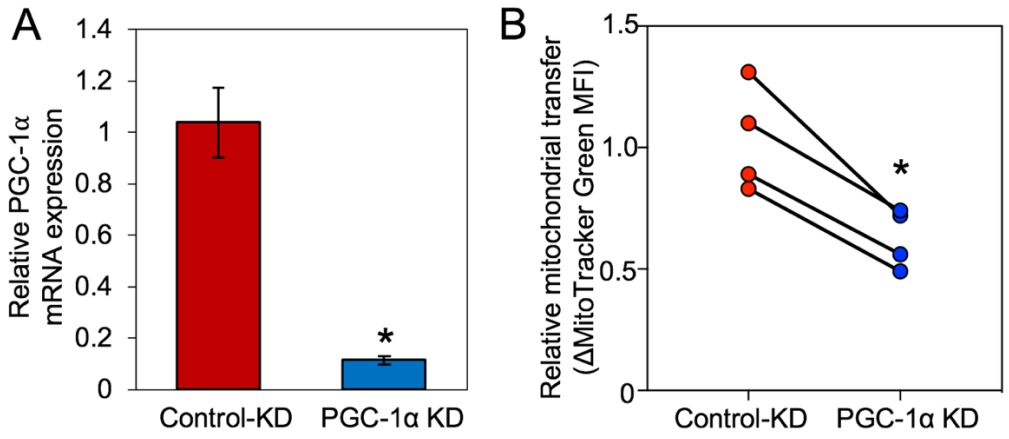

Figure 3.27. Mitochondrial transfer levels to AML are reduced from PGC-1α KD BMSC.

BMSC were transduced with a lentivirus encoding shRNA targeted to PGC-1α, mRNA expression of PGC-1α was analysed using qPCR (A). (B) The MitoTracker based mitochondrial transfer assay was utilised to determine mitochondrial transfer levels between control KD or PGC-1α KD BMSC and AML blasts (n=4). Data is presented as relative ΔMitoTracker Green MFI.

I next determined whether the reduction of mitochondrial transfer (through BMSC PGC-1α KD) impacted on AML disease progression. To do this I utilised a subcutaneous mouse model whereby AML cell lines OCI-AML3 or MV4-11 (containing a luciferase construct) were injected into the hind flank of NSG mice, along with either PGC-1α KD or control KD BMSC. The advantage of this model is that two conditions can be compared in the same animal, as AML was injected with control KD BMSC on the left flank and with PGC-1α KD in the right flank (Figure 3.28A). Live animal imaging showed that AML disease progression was

reduced in the right flank of the animal where AML blasts were injected with PGC-1α KD BMSC, this was the same for both AML cell lines tested (Figure 3.28B). Quantification of bioluminescence highlighted that AML disease progression was reduced with PGC-1α KD BMSC on average by 2.5-fold with OCI-AML3 and 4.5-fold with MV4-11 (Figure 3.28C).

Taken together, the results in this section show that PGC-1α activation in BMSC plays a role in mitochondrial transfer between BMSC and AML blasts.

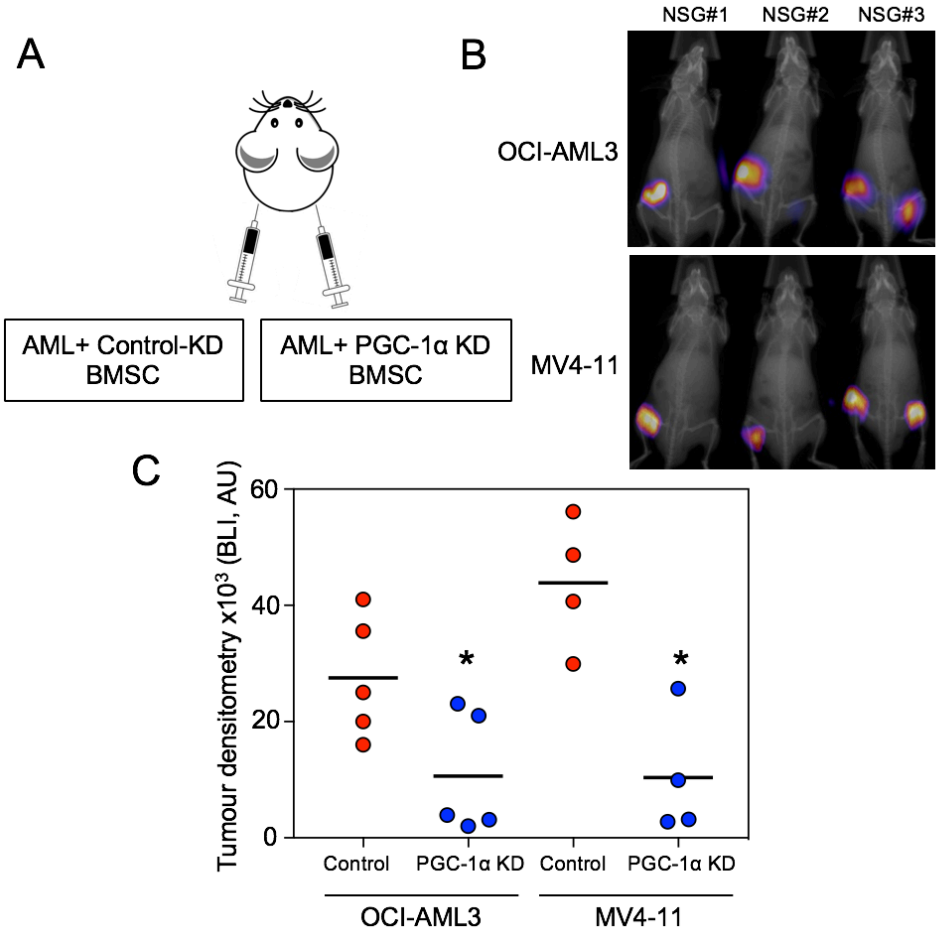

Figure 3.28. AML disease progression is reduced *in vivo* through PGC-1α KD in BMSC.

(A) Schematic representation of the subcutaneous *in vivo* model used to determine AML disease progression when PGC-1α was knocked down in BMSC. (B) Bioluminescent live animal imaging of OCI-AML3/MV4-11 cells containing a luciferase construct, which was enabled by the administration of D-luciferin prior to imaging. (C) Quantification of bioluminescence observed in (B) presented as tumour densitometry x10^3 (Bioluminescence arbitrary unit (BLI AU)).

3.2.8 Pre-clinical *in vivo* model of NOX2 KD in AML disease progression

In section 3.2.5 I described that NOX2 on AML is responsible for stimulating mitochondrial transfer from BMSC - next I aimed to translate this idea *in vivo*. NOX2 was knocked down in the AML cell line OCI-AML3 using a lentivirus targeted to NOX2 mRNA, which reduced NOX2 levels by 75% compared to control KD cells (Figure 3.29A). NSG mice were administered with either control KD or NOX2 KD cells (containing a luciferase construct) and AML disease progression was monitored. It is important to note there was no difference in the growth capacity of control KD and NOX2 KD OCI-AML3 blasts grown *in vitro* prior to injection into mice (Figure 3.29B).

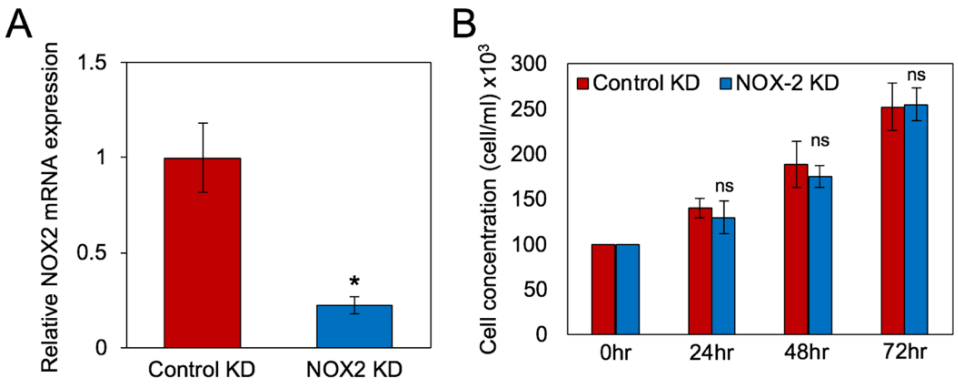

Figure 3.29. The growth capacity of control and NOX2 KD OCI-AML3 cells is un-changed.

OCI-AML3 cells were transduced with a lentivirus encoding shRNA which targeted NOX2 or control. (A) qPCR was used to determine NOX2 mRNA levels in these cells. (B) Growth capacity of control or NOX2 KD OCI-AML3 cells was measured by Trypan blue exclusion cell counts (B).

AML disease progression was measured by live animal bioluminescent imaging over a 5-week period. It was found that AML homed to the bone marrow and progression was reduced in animals injected with NOX2 KD cells (Figure 3.30A). This corresponded with overall animal survival, where mice injected with NOX2 KD OCI-AML3 cells outlived their control KD counterparts (Figure 3.30B).

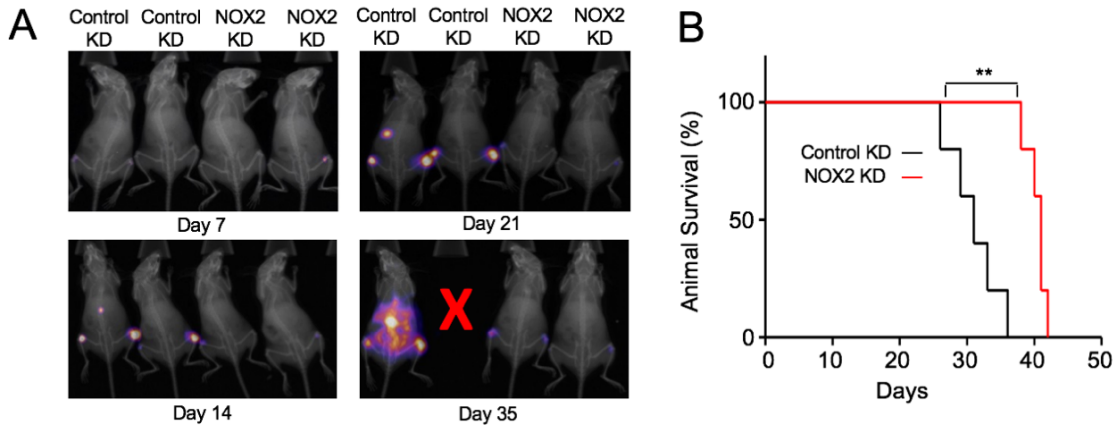

Figure 3.30. AML disease progression is severely reduced upon knockdown of NOX2.

Mice injected with either control or NOX2 KD OCI-AML3 cells were monitored by live animal bioluminescent imaging, through the activation of luciferase construct within AML blasts using D-luciferin (A). Survival of animals in this experiment is presented in a Kaplan-Meier plot (B).

Taking this further, control KD and NOX2 KD OCI-AML3 cells were isolated from mouse bone marrow using MACS with human CD45+ microbeads. Mitochondrial levels in the isolated AML cell population was determined using MitoTracker Green staining and flow cytometry. It was found that NOX2 KD OCI-AML3 cells had approximately half the mitochondrial content than control KD OCI-AML3 cells - there was no change in the mitochondrial content of these cells prior to administration into mice (Figure 3.31). The reduced mitochondrial mass in NOX2 KD cells may therefore be in part due to *in vivo* intercellular mitochondrial transfer, however there still may be a range of other explanations for this observation.

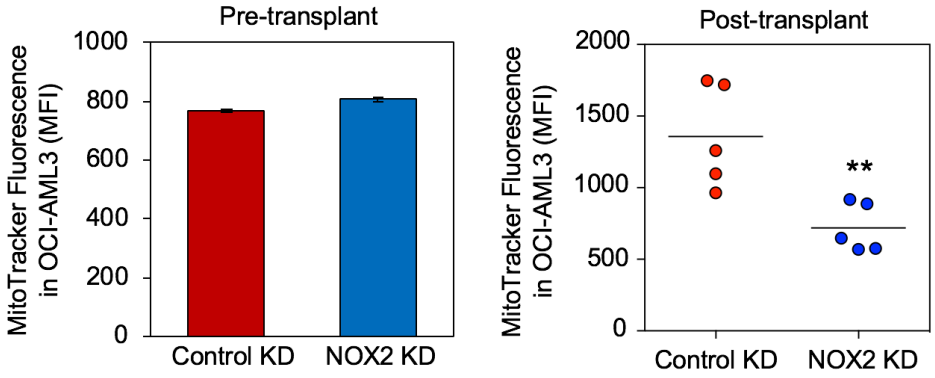

Figure 3.31. Mitochondrial levels are reduced *in vivo* in NOX2 KD OCI-AML3 cells.

Control and NOX2 KD OCI-AML3 cells were isolated from mouse bone marrow by MACS. Mitochondrial levels were measured using MitoTracker Green staining and flow cytometry. Mitochondrial levels are presented as MitoTracker MFI.

Overall this *in vivo* model shows that NOX2 contributes to AML disease progression, in part through the stimulation of mitochondrial transfer in the BMM. Therefore, they may be a therapeutic intervention opportunity whereby NOX2 is targeted on AML blasts.

3.3 Summary

In this chapter of my thesis I have shown that mitochondrial transfer occurred from BMSC to AML blasts, which enhanced OCR. Mitochondria can move through TNTs and is stimulated by NOX2 superoxide, which caused oxidative stress in BMSC. This enhancement of oxidative stress in BMSC promoted PGC-1α driven mitochondrial biogenesis - which facilitated mitochondrial movement to AML blasts. Finally, I have presented NOX2 as a novel therapeutic target in AML. NOX2 reduction on AML blasts increases animal survival. The data presented in this chapter is summarised schematically below (Figure 3.32).

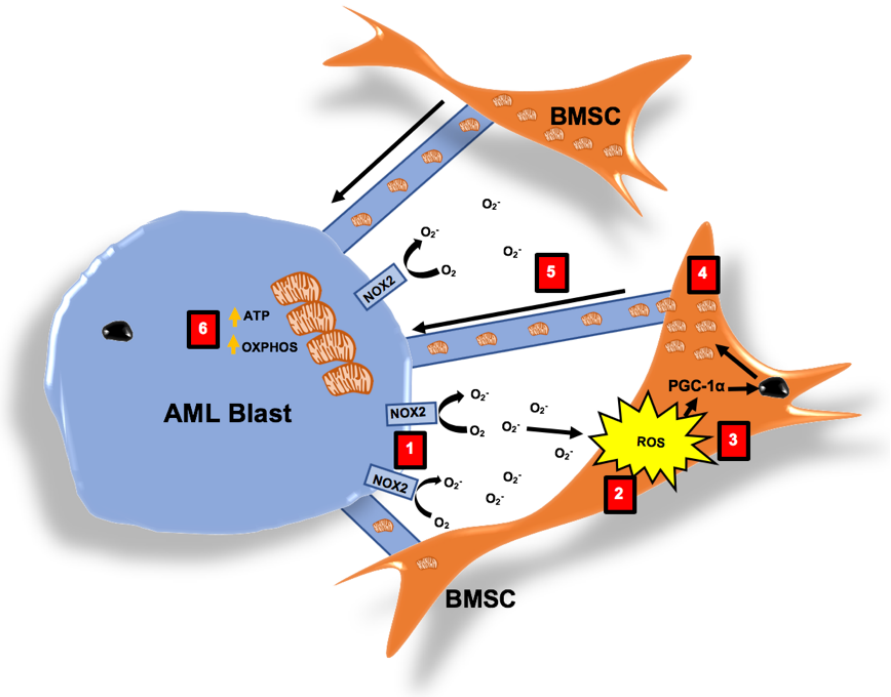

Figure 3.32. Schematic representation of mitochondrial transfer in AML.

(1) NOX2 on AML blasts generate superoxide. (2) NOX2 superoxide causes oxidative stress in BMSC. (3) Oxidative stress in BMSC activates PGC-1α. (4) Activation of PGC-1α stimulates mitochondrial biogenesis. (5) AML acquires mitochondria from BMSC through TNTs. (6) Mitochondrial transfer results in increased mitochondrial levels in AML blasts which increases OCR and ATP generation. This process ultimately leads to AML proliferation and survival.

4 CD38 mediated mitochondrial transfer promotes bio-energetic flexibility in multiple myeloma cells.

4.1 Introduction

It is becoming apparent that not all cancers utilise the Warburg hypothesis to generate ATP required for proliferation and survival. Multiple myeloma has been shown to be a "Warburg Cancer" as MM cells are susceptible to glycolysis inhibitors (316) and have been shown to have a glycolytic gene signature (317). However, these studies were carried out on MM cells alone and didn't take into account the effect of the BMM. In the second chapter of my thesis I will examine the effect the microenvironment has on metabolism within MM cells and if (like AML) intercellular mitochondrial transfer occurs between BMSC and MM cells.

4.2 Results

4.2.1 Multiple myeloma cells enhance mitochondrial respiration in the presence of their BMM.

First, I examined the metabolism within primary MM cells isolated from patients. To achieve this, I used the Seahorse Extracellular flux analyser to determine OCR and glycolysis in patient MM cells immediately after isolation from the bone marrow. Primary MM cells (n=4; from independent patient bone marrow samples) were found to have an increased OCR compared to four MM cell lines (Figure 4.1A and B), in addition to having reduced levels of glycolysis (Figure 4.1C). This shows the BMM of primary MM cells can influence malignant cell metabolism.

To assess how the mouse BMM influences metabolism within MM cell lines, I engrafted the MM cell line MM1S into NSG mice. After 3 weeks I sacrificed the mice and isolated MM1S cells using MACS with human CD45+ microbeads. OCR and glycolysis levels were examined in the isolated MM cells immediately compared to MM1S cells cultured *in vitro*. Increased OCR were found in MM1S cells analysed *ex vivo* (Figure 4.2A and B), with no change observed in glycolysis levels (Figure 4.2C).

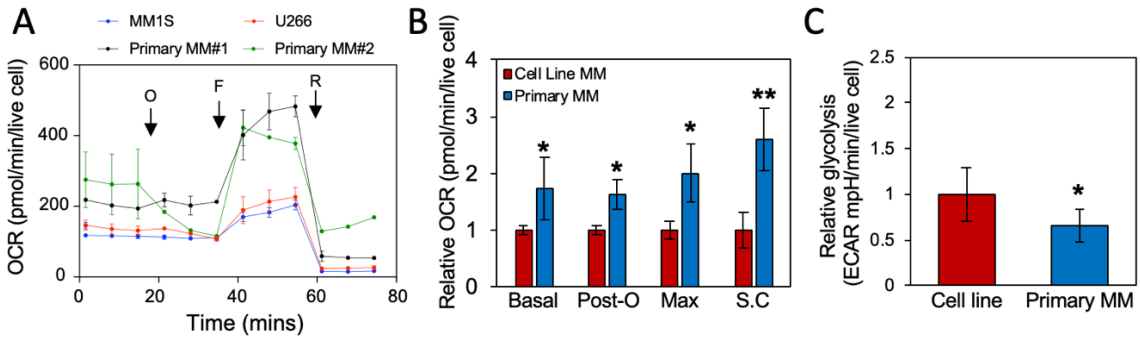

Figure 4.1. Primary MM cells have increased OCR compared to MM cell lines.

Primary MM cells were isolated from four independent patient bone marrows and analysed immediately using the Seahorse extracellular flux analyser compared to four MM cell lines (MM1S, U266, RPMI and H929). (A) Representative OCR plot (with injections of oligomycin, FCCP and rotenone/antimycin A) is shown which contains 2 primary MM and 2 MM cell lines. (B) Relative OCR in 4 primary MM cells and 4 MM cell lines – presenting the basal and maximum OCR along with post oligomycin (Post-O) OCR and spare capacity (S.C). All OCRs have had the non-mitochondrial respiration (after rotenone/antimycin A treatment) subtracted. (C) Relative glycolysis rates in these cells is presented.

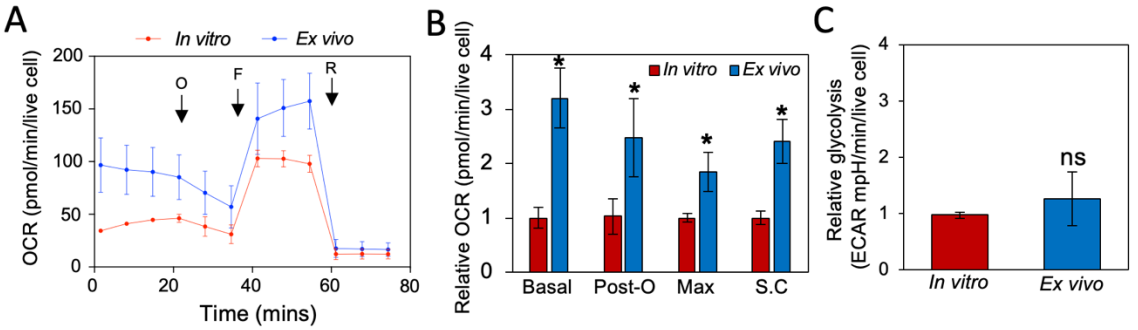

Figure 4.2. MM1S cells isolated from NSG mice have increased OCR.

MM1S cells were injected into the tail vein of NSG mice (n=5), after 3 weeks the mice were sacrificed and MM1S cells were isolated. These cells, along with MM1S cells grown *in vitro*, were immediately analysed using the Seahorse extracellular flux assay. (A) Shows a representative OCR plot with all data accumulated in the bar chart presented in (B). Basal and maximum OCR, along with post oligomycin (Post-O) OCR and spare capacity (S.C), are presented - all values have non-mitochondrial respiration (after rotenone/antimycin A treatment) subtracted. Relative glycolysis levels in the MM1S cells is shown in (C).

Taking this further, I co-cultured three MM cell lines (MM1S, U266 and RPMI) alone and with BMSC for 72 hours. After culture, I analysed OCR and glycolysis using the Seahorse extracellular flux analyser. MM cell lines grown with BMSC were found to have increased OCR (Figure 4.3A and B). A large increase is seen in maximum OCR (after FCCP injection) which suggests an enhancement of the respiratory chain, however this may not be necessarily due to an increase in ATP synthase activity. No change in glycolysis was observed in 2/3 of the cell lines

tested, with a reduction in glycolysis observed in the RPMI cell line (Figure 4.3C). Taken together these results suggest that the microenvironment of MM promotes a more mitochondrial based metabolism, which is contrary to the Warburg hypothesis and previously published literature.

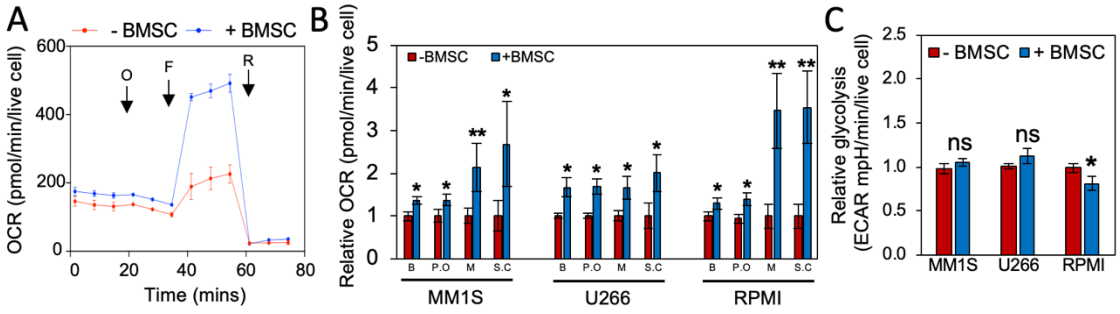

Figure 4.3. MM cell lines have increased OCR after culture with BMSC.

OCR and glycolysis rates were determined in MM cells (MM1S, U266 and RPMI) cultured with and without BMSC. A representative OCR plot is shown in (A). (B) Relative basal (B) and maximum (M) OCR is presented along with post oligomycin (P.O) OCR and spare capacity (S.C) – all OCR values have non-mitochondrial respiration (post rotenone/antimycin A) subtracted. Relative glycolysis rates are presented in (C).

The consequence of increased OCR in MM cell lines was next tested. ATP levels and the growth capacity of MM cell lines after culture with BMSC was assessed, using CellTitre-Glo and Trypan blue cell counts respectively. Increased ATP production and growth capacity was observed in MM cell lines cultured with BMSC compared to when they were cultured alone (Figure 4.4). Therefore, culture with BMSC promotes MM cell growth and proliferation through an enhancement of mitochondrial respiration.

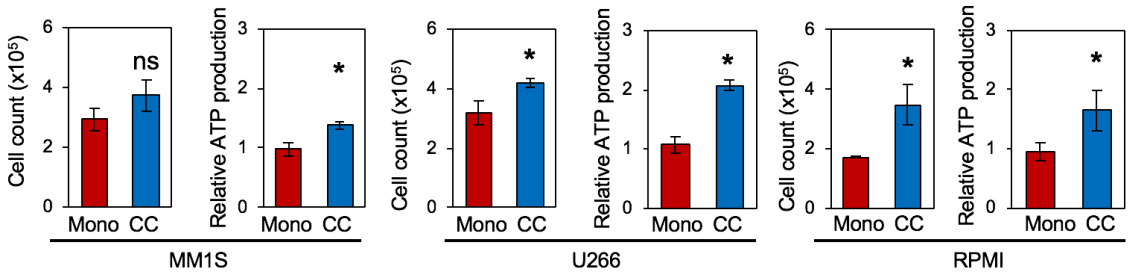

Figure 4.4. MM cells have increased growth and ATP production after BMSC culture.

MM1S, U266 and RPMI cells were grown with BMSC or alone for 72 hours. After culture, the growth capacity and ATP production in MM cells was determined using Trypan blue cell counts and CellTitre-Glo respectively.

4.2.2 Mitochondria are transferred from BMSC to MM cells

To determine the reason why MM cells have increased OCR after co-culture with BMSC, I next examined whether intercellular mitochondrial transfer took place between BMSC and MM cells. I utilised the three methods developed in the AML project to detect mitochondrial transfer. Using the MitoTracker Green based mitochondrial transfer assay, increased MitoTracker MFI was found after co-culture with BMSC in all 10 primary MM cells and in 4/5 MM cell lines tested (Figure 4.5). This showed that MitoTracker labelled mitochondria move from BMSC to MM cells.

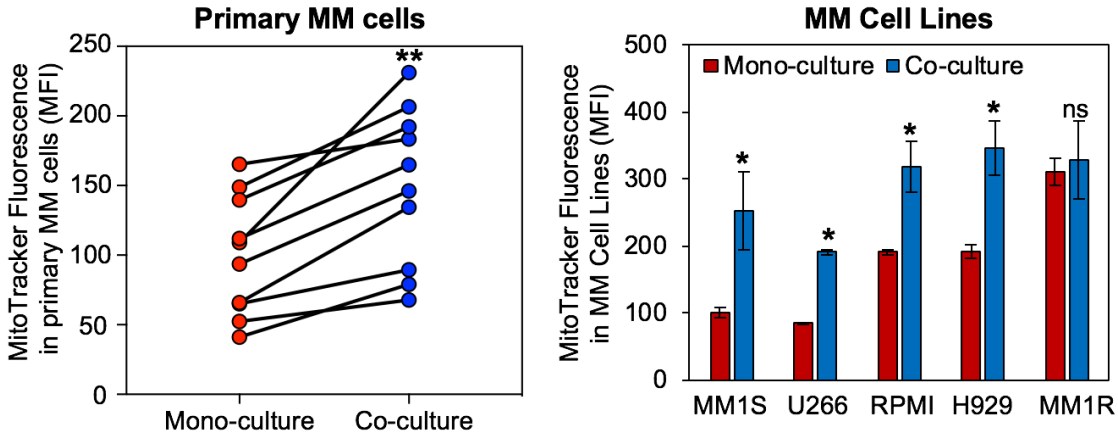

Figure 4.5. Increased MitoTracker MFI is observed in MM cells post co-culture with BMSC.

Primary MM cells (n=10) and MM cell lines (n=5) were stained with 200nM MitoTracker Green and cultured alone or with MitoTracker Green stained BMSC for 24 hours. MitoTracker Green MFI levels were analysed by flow cytometry.

The rLV.EF1.mCherry-Mito-9 lentivirus method was next used. However, the method was optimised to include fixed cell microscopy which was carried out on cells mounted onto cover slips - with mounting solution containing DAPI. The un-labelled MM1S cell line was seen to acquire mCherry fluorescence from rLV.EF1.mCherry-Mito-9 positive BMSC (Figure 4.6). This showed that mCherry labelled mitochondria from BMSC move to the MM1S cells.

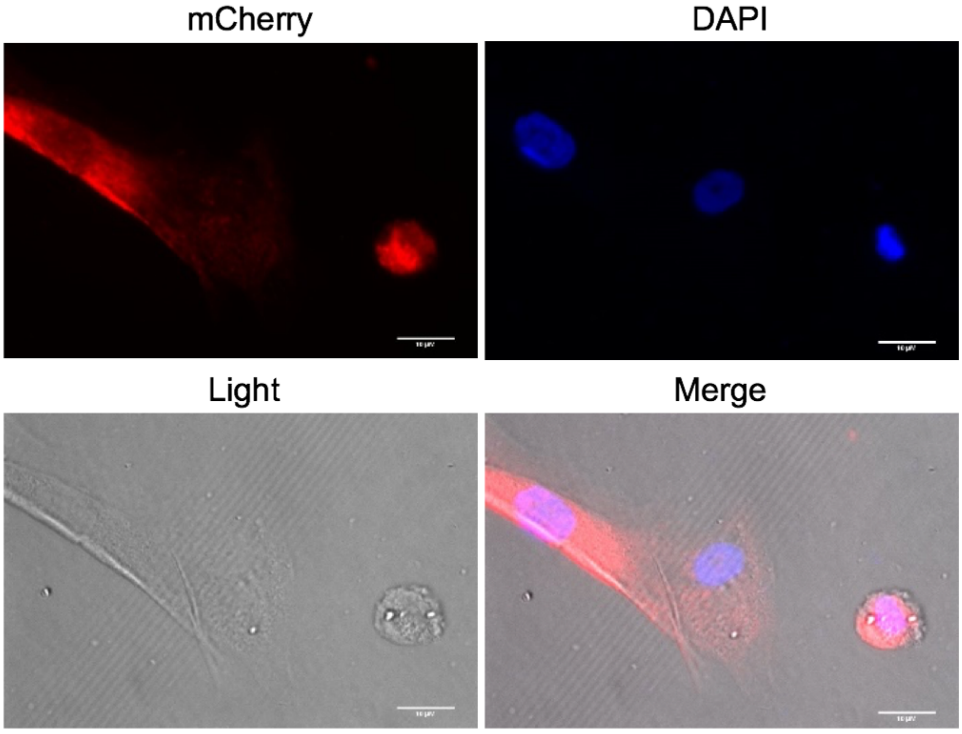

Figure 4.6. mCherry labelled mitochondria move from BMSC to MM cells.

Primary BMSC were transduced with a rLV.EF1.mCherry-Mito-9 lentivirus. These BMSC were cultured with MM1S cells for 72 hours, followed by fixation and mounting on cell culture slides. The slides were imaged using fluorescent microscopy and a representative image is shown in this figure. The scale bar represents a 10μm distance.

The final method utilised to show mitochondrial transfer was the *in vivo* xenograft model. MM1S and U266 MM cell lines were injected into the tail vein of NSG mice. At humane end point animals were sacrificed and human MM cells were then sorted from mouse bone marrow using MACS. qPCR with species specific primers targeted to mtDNA and gDNA was carried out on extracted DNA, PCR products were then visualised using agarose gel electrophoresis. In MM cell lines grown *in vitro* no presence of mouse mtDNA or gDNA was detected, whereas murine mtDNA was detected in MM cell lines isolated from mouse bone marrow - with no gDNA detected (Figure 4.7). This showed that murine mitochondria moved from the mouse BMM to MM cells.

Taken together, these three experiments show that mitochondria moved from BMSC to MM cells which contributed to the increased OCR, ATP production and growth capacity observed in 4.2.1.

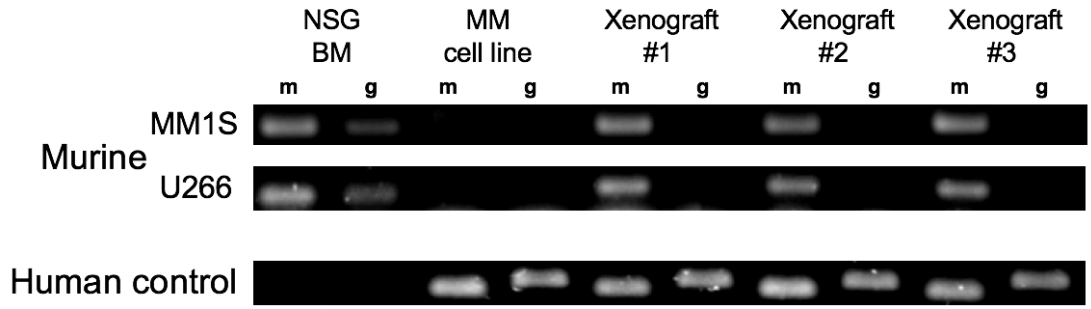

Figure 4.7. Murine mitochondria move to human MM cells *in vivo*.

MM1S and U266 were engrafted into NSG mice. After isolation, DNA from human MM cells was analysed using qPCR with species specific primers targeted to mtDNA and gDNA. PCR products were visualised on an agarose gel and is presented in this figure.

In AML, the chemotherapy agent daunorubicin was seen to increase the level of transfer (Figure 3.13). I next examined whether chemotherapy used in the treatment of MM (Bortezomib) had the same effect in this mitochondrial transfer model. Bortezomib was seen to increase the levels of mitochondrial transfer from BMSC to both primary MM cells (Figure 4.8A) and MM cell lines (Figure 4.8B) by approximately 50%. Therefore, a common theme is emerging whereby current chemotherapeutics increase the level of mitochondrial transfer.

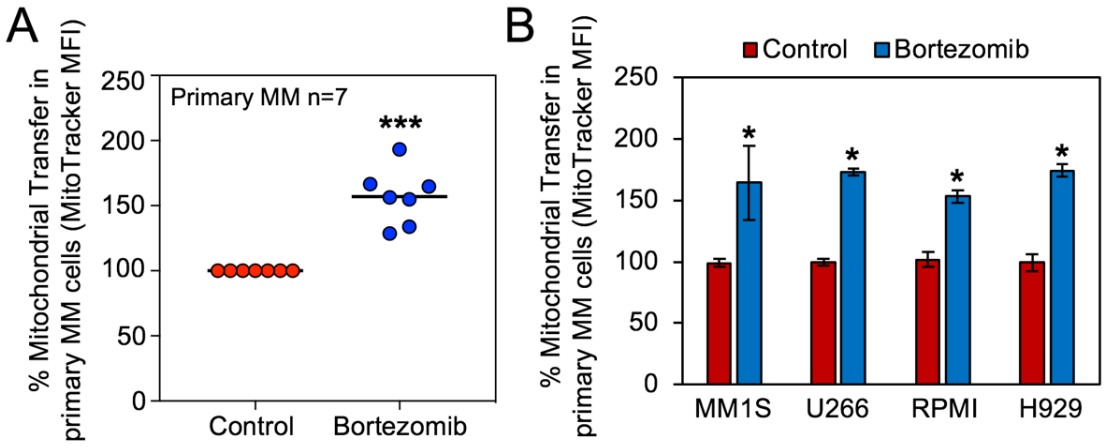

Figure 4.8. Bortezomib increases mitochondrial transfer from BMSC to MM cells.

Mitochondrial levels were analysed between BMSC and primary MM cells (n=7) or MM cell lines (n=4), using the MitoTracker Green based transfer assay upon the addition of 10nM Bortezomib. Mitochondrial transfer levels to primary MM cells (A) and MM cell lines (B) are presented as % mitochondrial transfer compared to DMSO treated control.

4.2.3 Mitochondria are transferred from BMSC to MM cells through TNTs

To examine how mitochondria move from BMSC to MM cells, TNTs were once again analysed to determine whether mitochondrial transfer in MM occurred in a similar way to AML. I used the MitoTracker based mitochondrial transfer assay to quantify the level of transfer between BMSC and MM cells upon the addition of CytoB (TNT inhibitor) and Dansylcadavarine (Endocytosis/Microvesicle inhibitor). Mitochondrial transfer was reduced upon the addition of CytoB by 40%, whereas no change was observed upon the addition of Dansylcadavarine (Figure 4.9).

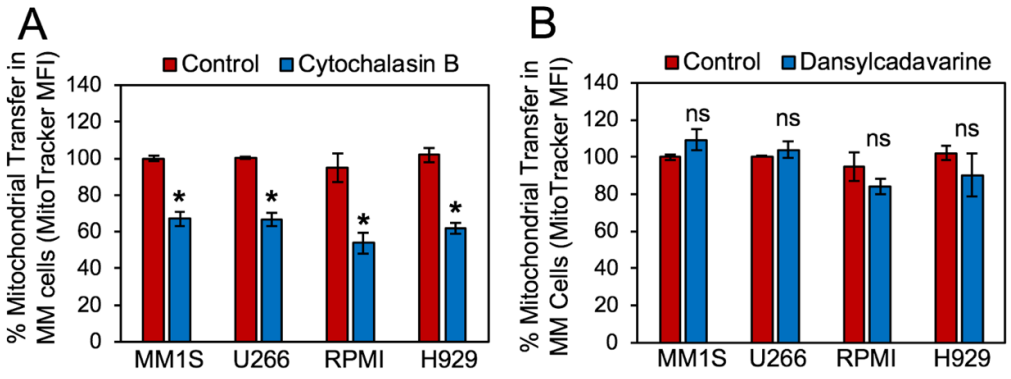

Figure 4.9. CytoB reduces mitochondrial transfer from BMSC to MM cells.

The MitoTracker based transfer assay was used to determine transfer levels upon the addition of CytoB (A) and Dansylcadavarine (B). Mitochondrial transfer levels were determined using the ΔMitoTracker Fluorescence (MFI) between co-cultured and mono-cultured MM cells and are presented as %mitochondrial transfer relative to non-treated controls.

Next, I aimed to visualise TNT formations using the Vybrant DiI staining of MM cells and MitoTracker Green staining of BMSC. After co-culture, fixed cell confocal microscopy was carried out and TNTs were found between MM cells and BMSC (Figure 4.10). These TNTs were formed by the cancer cell and contained mitochondria of BMSC origin. This assay was optimised to enhance the quality of TNT images - the rLV.EF1.AcGFP1-Mem-9 lentivirus was purchased from Clontech which labelled the plasma membrane of MM cells with a GFP fluorophore. These cells were cultured with MitoTracker CMXRos stained BMSC for 24 hours and fixed cell confocal microscopy was carried out. GFP-TNTs were visualised between BMSC and MM cells which contained mitochondria of BMSC origin (Figure 4.10).

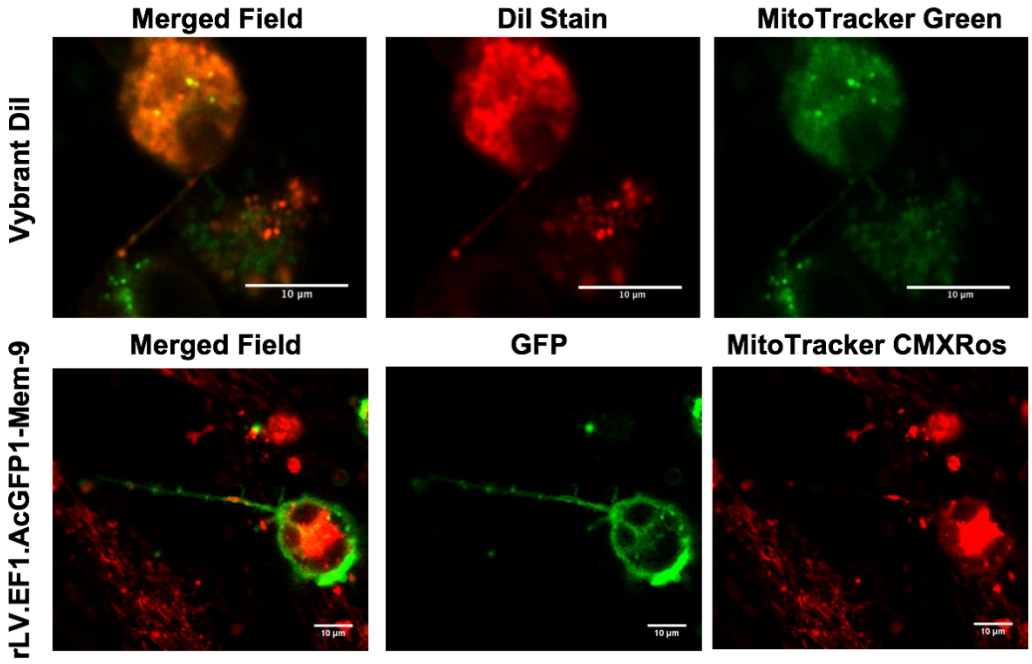

Figure 4.10. TNTs are formed between MM and BMSC which contain BMSC mitochondria.

TNTs were visualised by confocal microscopy using two methods. MM were stained with Vybrant DiI and cultured with MitoTracker Green stained BMSC. Also, MM were transduced with the rLV.EF1.AcGFP1-Mem-9 lentivirus and cultured with MitoTracker CMXRos stained BMSC. Both conditions were visualised by fixed cell confocal microscopy and individual microscope fields are presented, along with the merged field. The scale bar relates to a 10µm diameter.

TAPs are formed on BMSC after co-culture with MM cells stained with Vybrant DiI, these were used again to quantify the number of TNT formations. On average around 250 TAPs are formed per confocal image (Figure 4.11) which is slightly less than the average number of TAPs found on BMSC after AML co-culture.

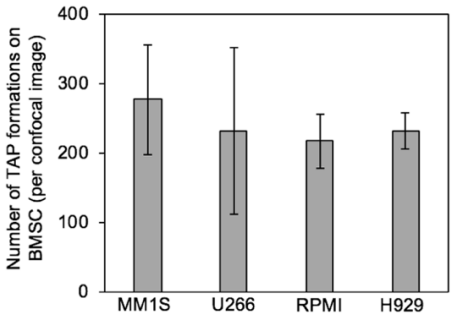

Figure 4.11. TAPs are formed on BMSC after culture with Vybrant DiI labelled MM cells.

Four MM cell lines were stained with Vybrant DiI and cultured with BMSC stained with MitoTracker Green. MM cells were removed and TAPs were quantified and presented as counts per confocal image.

Upon the addition of CytoB the number of TAPs formed on BMSC was reduced by approximately 75% (Figure 4.12). This shows that TAPs are a useful method of quantifying the number of TNT formations that occur during a co-culture of BMSC and MM cells. This will be important in Section 4.2.5.

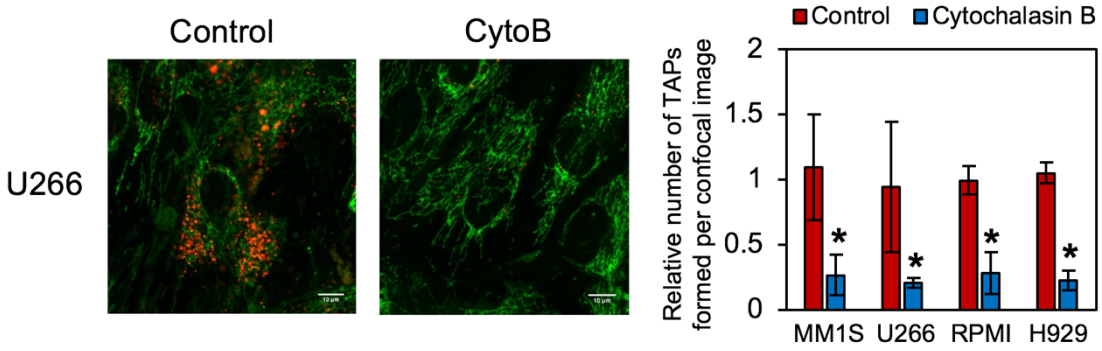

Figure 4.12. The addition of CytoB reduces the number of TAPs formed on BMSC.

Four MM cell lines were stained with Vybrant DiI and cultured with MitoTracker Green stained BMSC (with and without the addition of CytoB). After co-culture MM cells were removed and BMSC were visualised by confocal microscopy, a representative image taken after U266 culture is presented. The number of TAPs per confocal image was determined with and without the addition of CytoB, data is presented as relative TAP formations per confocal image.

The results in this section show that mitochondria can be transferred from BMSC to MM cells via TNTs, which is comparable with the AML mitochondrial transfer mechanism described in Chapter 3.

4.2.4 CD38 on MM cells is crucial for the transfer of mitochondria from BMSC

In the first part of this chapter I have shown that mitochondria are transferred from BMSC to MM cells through TNTs. Next, I wanted to delve deeper into the mechanism which controls mitochondrial transfer in MM. MM cells express high levels of the surface molecule CD38 (244) and this molecule has been recently shown to facilitate mitochondrial transfer from astrocytes to neurons after stroke (331). Therefore, I examined whether CD38 plays a role in mitochondrial transfer observed in MM.

First, I correlated levels of mitochondrial transfer to levels of CD38 on the surface of primary MM cells and MM cell lines. There was a strong positive correlation

(R=0.8727) observed between the levels of CD38 expressed on MM cells and the quantity of mitochondria they acquired from BMSC (Figure 4.13).

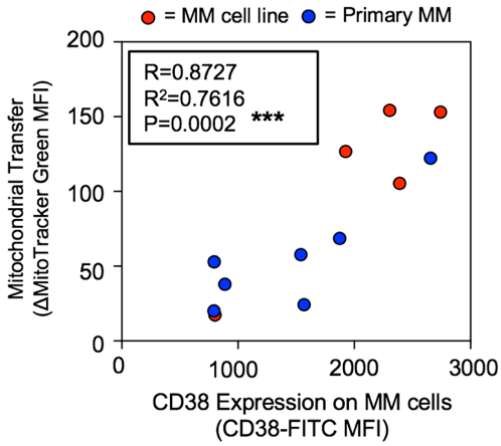

Figure 4.13. CD38 expression on MM cells correlates with mitochondrial transfer levels.

Mitochondrial transfer levels were assessed in primary MM cells (n=7) and MM cell lines (n=5) using the MitoTracker Green based transfer assay. CD38 levels were also measured on MM cells using flow cytometry.

Next, I made a lentivirus encoding shRNA which targets CD38 mRNA. CD38 surface expression was reduced by approximately 80% in MM cell lines transduced with CD38 lentivirus compared to a control virus (Figure 4.14A). The levels of mitochondrial transfer between BMSC and control KD or CD38 KD MM cell lines was next assessed. Mitochondrial transfer was reduced by 40-50% in CD38 KD MM cell lines compared to control KD cells (Figure 4.14B).

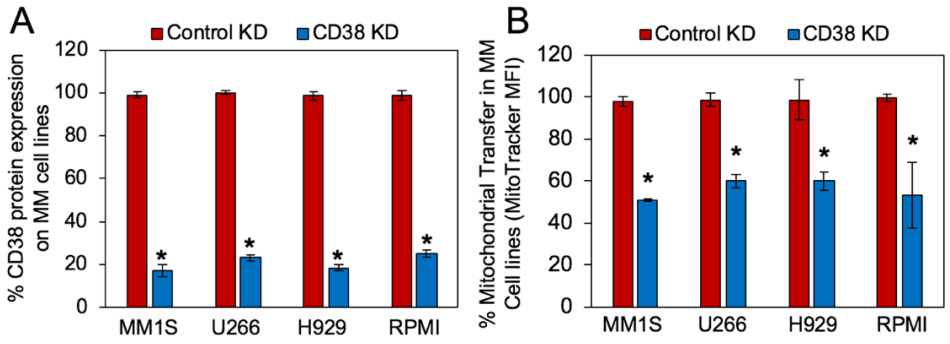

Figure 4.14. CD38 KD MM cells acquire reduced quantities of mitochondria from BMSC.

MM cell lines (MM1S, U266, H929 and RPMI) were transduced with a lentivirus encoding shRNA targeted to CD38 or control. (A) CD38 surface protein levels are presented on control KD or CD38 KD cells. (B) Mitochondrial transfer levels in control KD and CD38 KD cells were assessed using the MitoTracker Green based transfer assay.

To analyse the role of CD38 further, I next overexpressed CD38 on MM cells to assess levels of mitochondrial transfer. All-trans retinoic acid (ATRA) has recently been shown to increase CD38 expression on AML blasts (345), therefore this was utilised in MM cell lines. MM cell lines treated with 1μM ATRA for 16-hours were seen to increase their CD38 mRNA expression (Figure 4.15A) and their CD38 surface protein levels (Figure 4.15B) - compared to DMSO treated controls. Mitochondrial transfer levels were increased from BMSC to MM cell lines treated with ATRA compared to DMSO by between 40 and 70% respectively (Figure 4.15C). Overall, these results provide evidence that CD38 has a role in facilitating mitochondrial transfer between BMSC and MM cells.

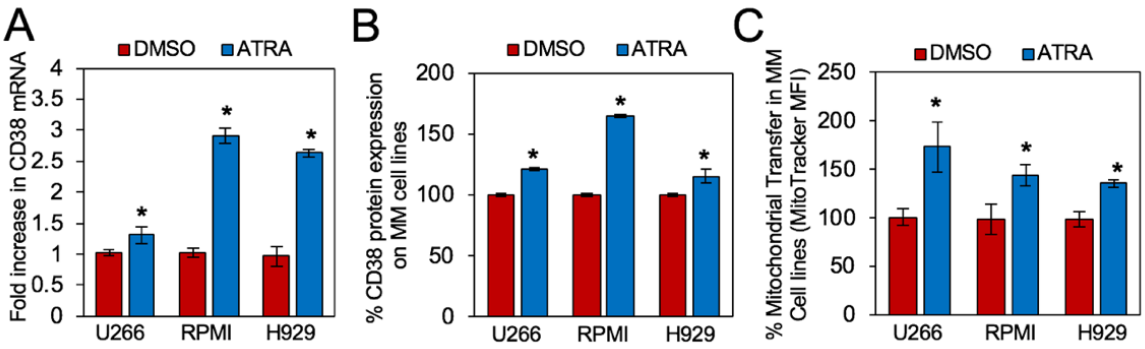

Figure 4.15. CD38 overexpression, using ATRA, causes increased mitochondrial transfer.

Three MM cell lines (U266, RPMI and H929) were treated with 1μM ATRA or DMSO for 16-hours (overnight). CD38 mRNA and protein expression levels were determined using qPCR (A) and flow cytometry (B) respectively. Mitochondrial transfer levels were determined in ATRA/DMSO treated MM cell lines using the MitoTracker Green based transfer assay (C).

4.2.5 CD38 forms the leading edge of a MM tunneling nanotube

Next, I assessed how CD38 controls the transfer of mitochondria from BMSC to MM cells. As CD38 is a cell surface molecule it is likely that it is involved in the extracellular projection (TNT) that facilitates mitochondrial transfer. To examine this hypothesis first, I analysed the number of TAPs (TNT formations) that were present on BMSC after co-culture with ether control KD or CD38 KD MM cell lines. A severe reduction in the number of TAPs formed on BMSC was observed after co-culture with RPMI CD38 KD cells compared to control KD cells (Figure 4.16A). This was also the case with MM1S, U266 and H929 MM cell lines where there

was approximately an 80% reduction in the number of TAPs formed on BMSC after culture with CD38 KD cells (Figure 4.16B). Therefore, the knockdown of CD38 in MM cells reduces the number of TNTs formed between MM cells and BMSC - resulting in reduced levels of mitochondrial transfer.

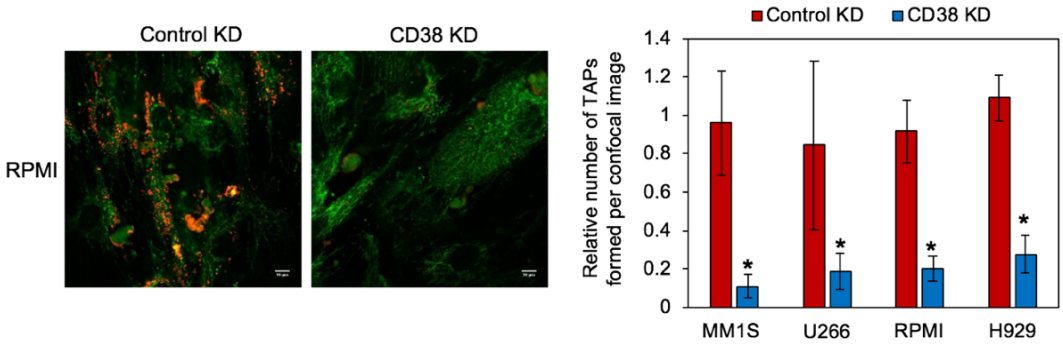

Figure 4.16. CD38 KD MM cell lines form less TNTs with BMSC.

Control KD and CD38 KD MM cell lines (MM1S, U266, RPMI and H929) were stained with Vybrant DiI stain and cultured for 24-hours with MitoTracker Green stained BMSC. TAPs were visualised using fixed cell confocal microscopy and quantified per confocal microscope image.

Next, I analysed in more detail the composition of the TAP and whether CD38 could be present within this formation. First, I examined the expression levels of CD38 on MM cells after co-culture with BMSC. Reduced levels of CD38 were observed on the surface of MM1S and U266 MM cell lines after co-culture with BMSC (Figure 4.17A). BMSC do not express CD38, however after co-culture with MM cell lines they gain CD38 expression - albeit at low levels (Figure 4.17B). This shows that CD38 may be transferred to BMSC during co-culture with MM cells.

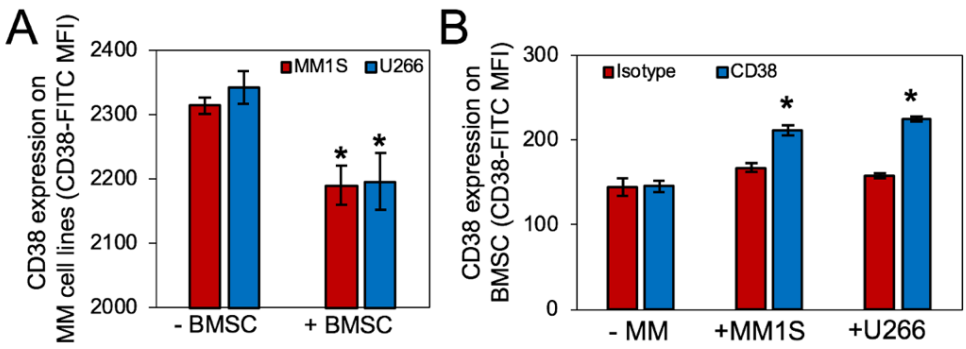

Figure 4.17. CD38 is transferred from MM cells to BMSC during co-culture.

MM1S and U266 cells were cultured with BMSC for 24-hours. CD38 expression on MM1S/U266 cells (A) and BMSC (B) were assessed by flow cytometry.

I next determined the location of CD38 on BMSC that was transferred from MM cells. Using the TAP visualisation method, BMSC were probed with a CD38 antibody conjugated to an Alexa Fluor 647 fluorophore. CD38 was found to be located on BMSC within TAPs formed by TNT contacts (Figure 4.18), therefore CD38 may contribute to the formation of TNTs and resultant TAPs.

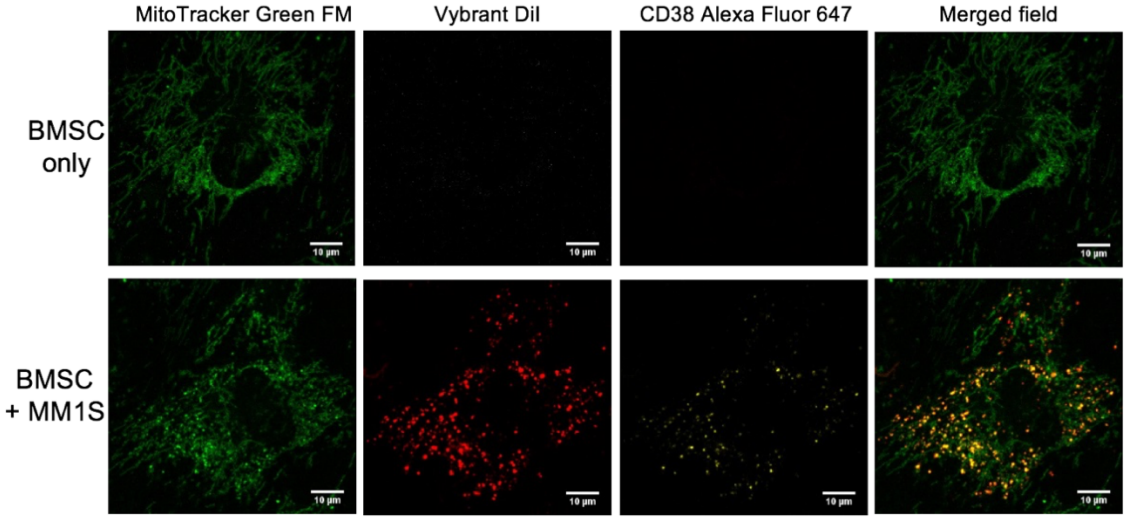

Figure 4.18. MM CD38 is located within the TAP on BMSC after co-culture.

MM1S cells were stained with Vybrant DiI and cultured with BMSC (which were stained with MitoTracker Green) for 24-hours. After culture MM1S cells were removed, BMSC were fixed and probed with CD38 Alexa Fluor 647 antibody before imaging with confocal microscopy. Individual microscope channels are presented along with merged field for BMSC alone and after co-culture with MM1S cells.

Next, I analysed the location of CD38 on TNTs formed by MM cells during co-culture with BMSC. I cultured rLV.EF1.AcGFP1-Mem-9 MM1S cells with MitoTracker CMXRos for 24 hours, the culture was fixed and probed with the CD38 Alexa Fluor 647 antibody. Confocal microscopy highlighted the location of CD38 on a MM cell during TNT formation (Figure 4.19). CD38 was highly clustered at the point of TNT formation and projects down the TNT.

Taken together, these results provide evidence that CD38 may form the leading edge of a TNT projection – which is then deposited on BMSC after dissociation. This mechanism plays a role in the transfer of mitochondria from BMSC to MM cells.

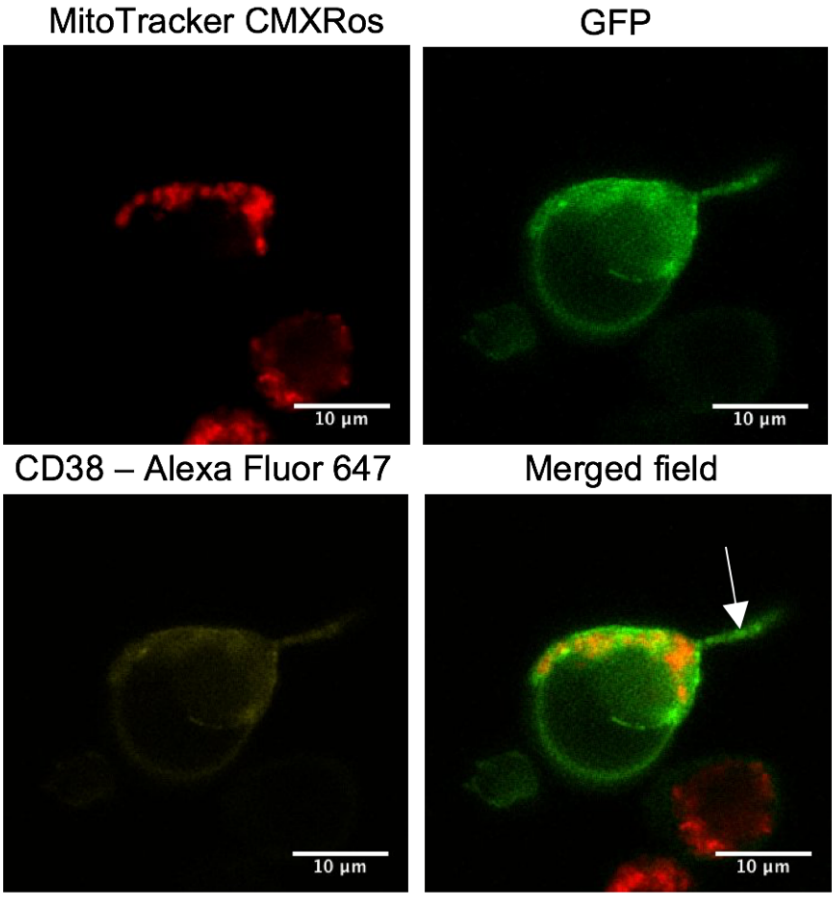

Figure 4.19. CD38 localises of the leading edge of a TNT formation.

MM1S cells were transduced with the rLV.EF1.AcGFP1-Mem-9 lentivirus. These cells were cultured with MitoTracker CMXRos stained BMSC for 24 hours. Co-cultures were then fixed and CD38 was probed using an Alexa Fluor 647 antibody. CD38 location on TNTs was visualised using confocal microscopy, individual microscope channels and merged field are presented.

Next, I tried to determine the binding partner on BMSC which CD38 binds to form a TNT. The only known binding partner of CD38 is CD31 (346), therefore I examined whether CD31 could be this binding molecule on BMSC. As CD31 is a surface receptor I used flow cytometry to first examine whether primary human BMSC expressed CD31. I found that BMSC (n=3) did not express CD31 (Figure 4.20) therefore could not be the molecule that CD38 binds forming a TNT. It is likely there is a novel binding partner to CD38 expressed on BMSC or CD38 could bind un-specifically to BMSC in order to form the TNT. Unfortunately, I was unable to find out anything further during my PhD research and this remains an unanswered question.

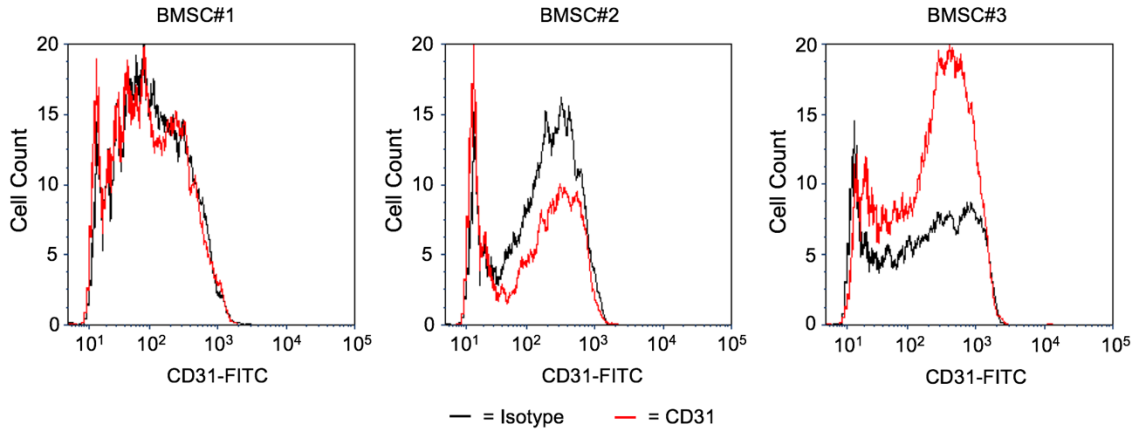

Figure 4.20. BMSC do not express the CD38 binding partner CD31.

Primary human BMSC (n=3) were incubated with a CD31-FITC antibody or isotype control for 15 minutes. CD31 expression on BMSC was analysed using flow cytometry.

4.2.6 Silencing of CD38 *in vivo* reduces MM disease progression.

To determine the effect of CD38 mediated mitochondrial transfer on MM disease progression, I used an *in vivo* xenograft model to monitor the growth of MM. Control KD or CD38 KD MM1S cells (containing a luciferase construct) were injected into the tail vein of NSG mice. There was no difference in the growth capacity of these cells prior to administration into mice (Figure 4.21). MM disease progression in the bone marrow was monitored using live animal bioluminescent imaging, a reduced MM disease burden was found in animals injected with CD38 KD MM cells compared to control KD cells (Figure 4.22A). This resulted in these animals outliving their control KD counterparts (Figure 4.22B).

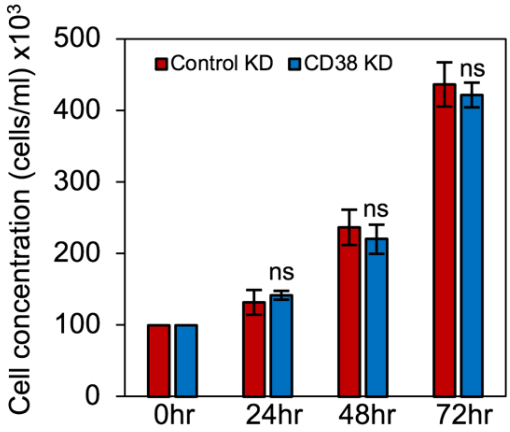

Figure 4.21. Growth capacity is unchanged between control KD and CD38 KD MM1S cells.

Before injection into mice, the growth capacity of control KD and CD38 KD MM1S were analysed using Trypan blue exclusion cell counts.

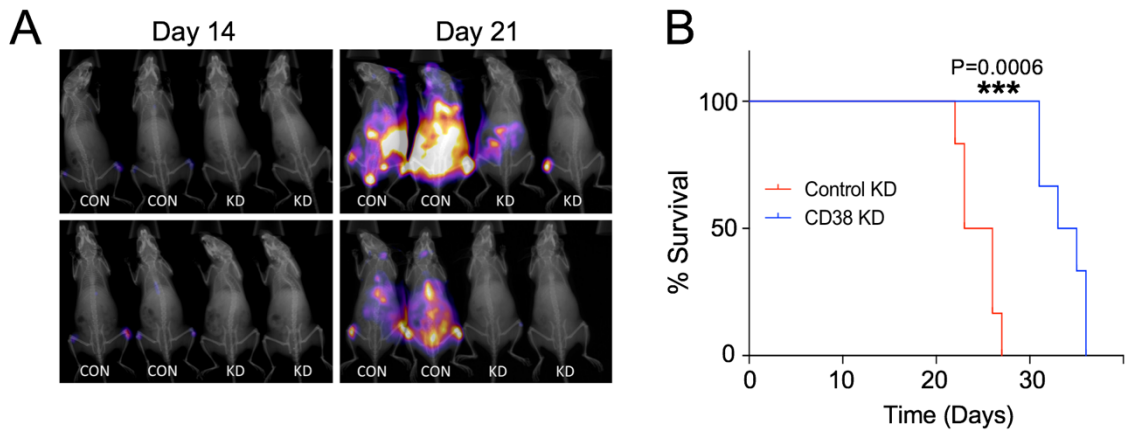

Figure 4.22. MM disease progression is severely reduced upon the knockdown of CD38.

Control KD or CD38 KD MM1S cells (containing luciferase construct) were injected into the tail vein of NSG mice. MM disease progression at day 14 and 21 was analysed using live animal bioluminescent imaging, through activation of the luciferase construct in MM cells using D-luciferin (A). Overall survival of animals in this experiment is presented in a Kaplan-Meier plot (B).

Furthermore, control KD and CD38 KD MM1S cells were isolated from mouse bone marrow and mitochondrial levels were analysed using MitoTracker Green staining. A 2.5-fold decrease in mitochondrial levels was observed in CD38 KD MM1S cells compared to control KD cells (Figure 4.23A). No change in mitochondrial levels was observed in control KD and CD38 KD MM cells pre-transplant into mice (Figure 4.23B). Taking these results together, it suggests that one way that CD38 promotes MM disease progression *in vivo* is through intercellular mitochondrial transfer levels.

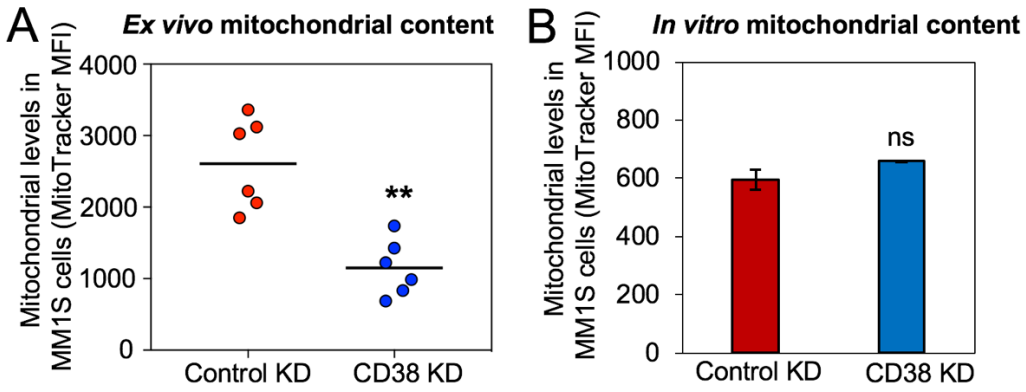

Figure 4.23. *Ex vivo* mitochondrial levels are reduced in CD38 KD MM1S cells.

Mitochondrial content was analysed in control KD and CD38 KD MM1S cells isolated from NSG mice (A) and cultured *in vitro* (B). Mitochondrial levels were determined using MitoTracker Green staining and flow cytometry. Data is presented as MitoTracker Green MFI.

4.3 Summary

In this chapter I have presented data which shows that in the presence of its microenvironment, multiple myeloma utilises a more mitochondrial based metabolism over glycolysis to generate ATP. This is due in part to intercellular mitochondrial transfer from BMSC which can be facilitated through TNTs. Taking this further, I have shown that CD38 expression on the surface of MM cells plays a role in the transfer of mitochondria. CD38 has the ability to form the leading edge of a TNT which docks with BMSC. MM disease progression is reduced *in vivo* through inhibition of CD38 which may be mediated in part by pro-tumoral mitochondrial transfer. Figure 4.24 presents schematically an overview of the results discussed in this chapter.

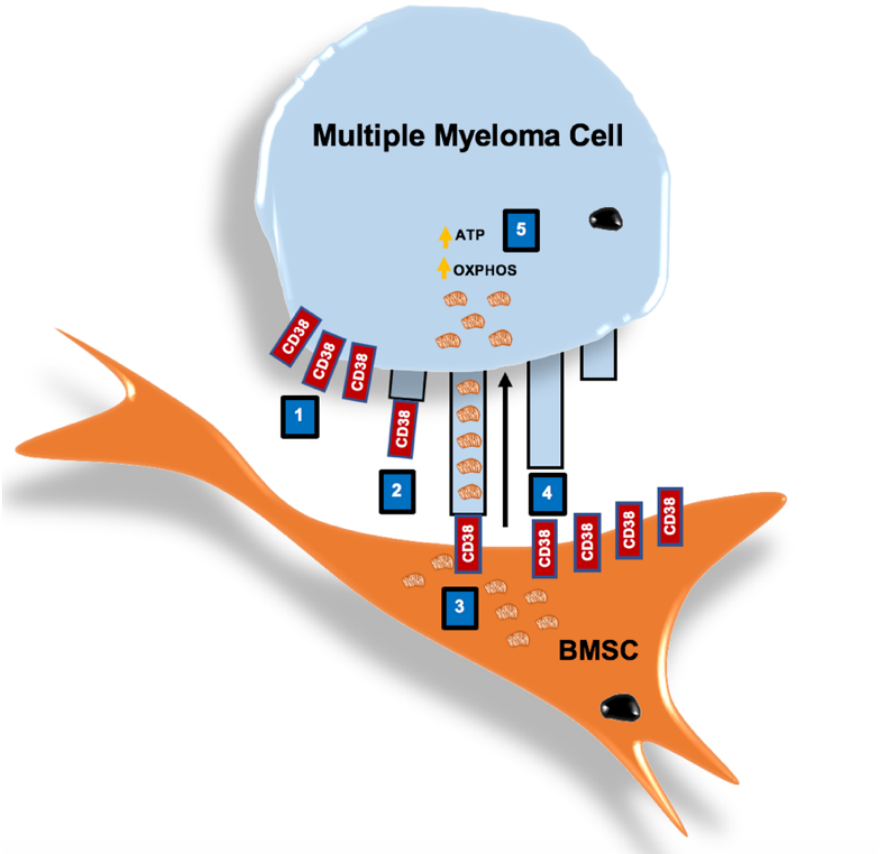

Figure 4.24. Overview of mitochondrial transfer in Multiple Myeloma.

(1) CD38 is highly expressed on the surface of MM cells. (2) CD38 forms the leading edge of a MM derived TNT formation. (3) CD38 binds to BMSC through a currently unknown BMSC molecule and facilitates mitochondrial transfer to MM cells. (4) The TNT dissociates leaving behind MM-CD38 protein on the surface of BMSC - which form TAPs. (5) The consequence of mitochondrial transfer is that MM cells enhance mitochondrial respiration and ATP production.

5 LPS mediated bacterial infection stimulates mitochondrial transfer to haematopoietic stem cells.

5.1 Introduction

In the first two results chapters I have described two haematological malignancies where intercellular mitochondrial transfer aids proliferation and survival. The transfer of mitochondria between cells has previously been shown to also occur in non-malignant systems. In chapter 3 I found under normal circumstances CD34+ cells (HSCs) do not acquire mitochondria from BMSC, however under oxidative stress these cells can be forced to acquire mitochondria. A major stimulus of oxidative stress in the human body is bacterial infection (347), therefore this may stimulate mitochondrial transfer to HSCs in a non-malignant haematological system. LPS is found on the surface of gram negative bacteria and has been shown to stimulate a bacterial-like infection response in mice (16). LPS has also been shown to promote intercellular mitochondrial transfer *in vivo*, where airway instilled BMSC transfer their mitochondria to lung epithelial cells (330). In the final chapter of my thesis I will examine whether mitochondrial transfer occurs from the BMM to HSCs in mouse models simulating bacterial infection. This will determine whether intercellular mitochondrial transfer is a process that AML and MM cells have hijacked to promote their proliferation and survival.

5.2 Results

5.2.1 LPS causes increased mitochondrial content in C57BL/6J ST-HSCs

First, I analysed the effect of LPS on mitochondrial levels in different cell populations within the murine haematopoietic system including ST-HSCs, LT-HSC and MPPs. This was achieved using 7-colour flow cytometry with 6 antibodies targeted to cell surface markers (along with MitoTracker Green). This flow cytometry method was based on a similar method used by Walter and colleagues (16) and included all appropriate colour compensations. The gating

strategy to determine cell populations of interest was defined using FMO controls and is shown in Figure 5.1 Panel A.

C57BL/6J were treated with either 1mg/kg LPS or PBS for 2 hours. This time point was chosen to try and specifically detect changes in mitochondrial levels due to intercellular transfer rather than mitochondrial biogenesis. LPS caused an expansion of haematopoietic cells (Figure 5.1 Panel D) as expected and is comparable to data published by Walter and colleagues (16). As an expansion of the haematopoietic system is a hallmark of the response to bacterial infection, in this experiment I have therefore successfully managed to induce the desired bacterial response in order to analyse mitochondrial levels.

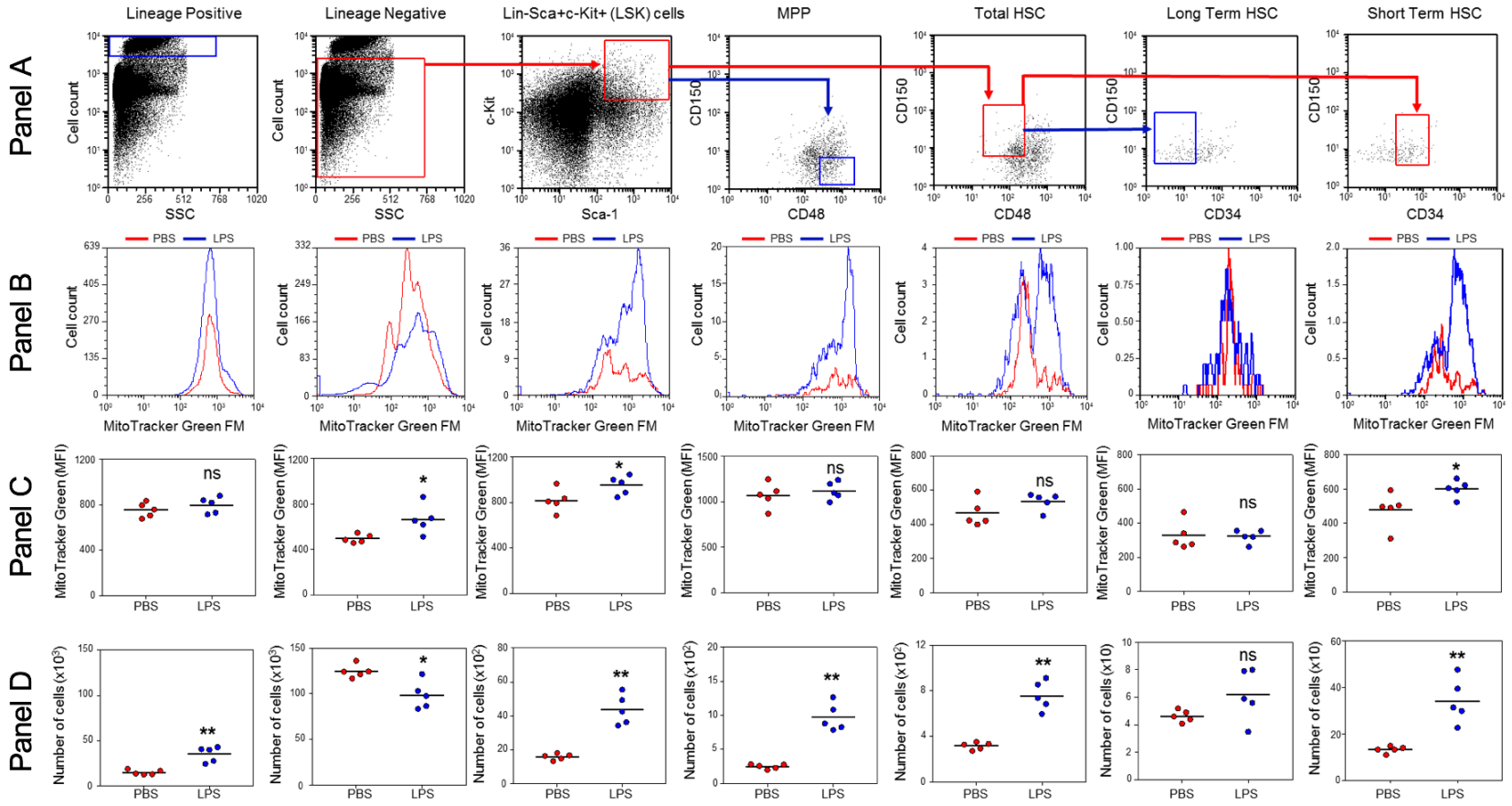

Figure 5.1. LPS induces an expansion of ST-HSCs in C57BL/6J bone marrow and an increase in mitochondrial content.

C57BL/6J mice were treated with either PBS or 1mg/kg LPS for 2 hours, followed by sacrifice and BM isolation. Haematopoietic cell population numbers and mitochondrial content within these populations were analysed using 7-colour flow cytometry. Panel A presents the gating strategy used to specifically analyse haematopoietic cell populations. Panel B shows representative histogram plots of the defined populations presenting MitoTracker Green MFI and cell counts. Panel C presents mitochondrial levels (MitoTracker Green MFI) in specific populations of all animals examined (n=5), with Panel D showing the cell counts.

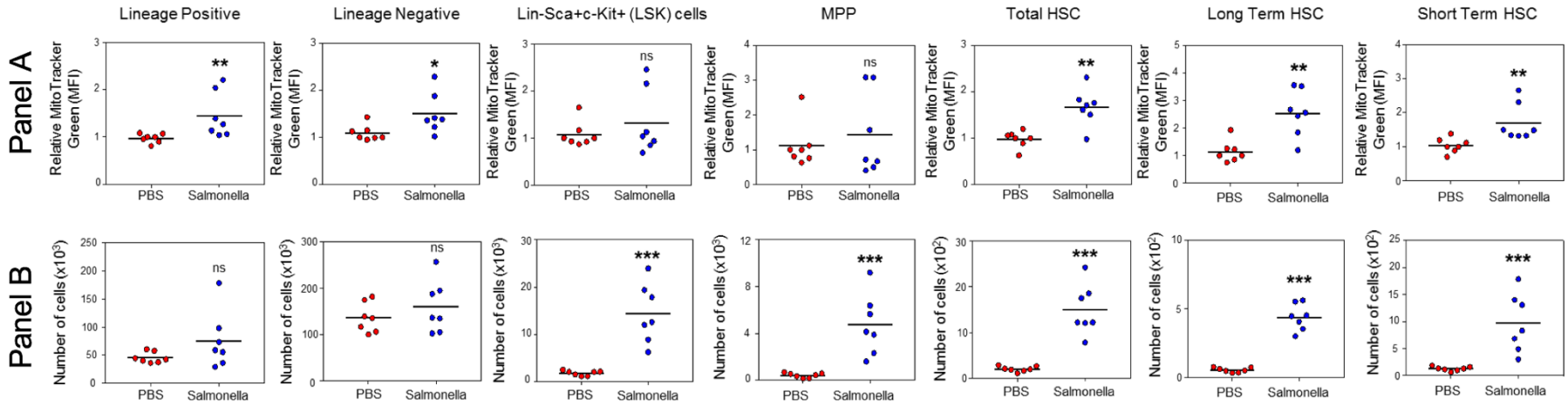

Figure 5.2. *Salmonella enterica* stimulates expansion of the BM haematopetic component through an increase in mitochondria.

Salmonella enterica was administered to C57BL/6J mice, after 72 hours the animals were sacrificed and bone marrow was extracted. Specific haematopoietic cell components were determined using the same gating strategy as Figure 5.1. Panel A presents the mitochondrial content (relative MitoTracker Green MFI). Panel B presents the cell numbers of each specific haematopoietic cell population.

A significant increase in mitochondrial levels were found in the ST-HSC population ($Lin^-Sca^+c\text{-}Kit^+CD150^+CD48^-CD34^+$) but not LT-HSCs ($Lin^-Sca^+c\text{-}Kit^+CD150^+CD48^-CD34^-$) (Figure 5.1 Panel D). Significant increases in mitochondrial levels were also found in Lin^- and $Lin^-Sca^+c\text{-}Kit^+$ (LSK) populations. In the other populations analysed (Lin^+, MPPs and total HSCs) the levels of mitochondria are unchanged.

To determine whether the same effect is observed upon a real bacterial infection, the experiment was repeated with animals administered with live *Salmonella enterica*. This gram-negative bacterium was administered through oral gavage with bacterial infection observed after 72 hours. Therefore, at 72 hours the mice were sacrificed and bone marrow analysis was carried out. As expected, an expansion of the haematopoietic component of the bone marrow was again observed in Salmonella treated mice (Figure 5.2 Panel A). Increased mitochondrial levels were observed again in ST-HSC and LSK cells and additionally in LT-HSC, Total HSCs and MPPs likely due to the increased time point used (72-hour vs 2-hours) compared to the LPS experiment. Taken together, the results from LPS and Salmonella experiments suggest that ST-HSCs increase their mitochondrial levels in order to proliferate and expand the downstream haematopoietic cell component in response to pathogen exposure.

5.2.2 LPS induces intercellular mitochondria transfer to HSCs

Next, I aimed to examine how ST-HSCs increase their mitochondrial levels and whether this could be due to intercellular mitochondrial transfer. To do this I generated “humanised” mice, through the transplantation of umbilical cord blood CD34+ stem and progenitor cells into 3-4-week-old NSG mice. Engraftment was assessed through monthly peripheral blood analysis looking specifically for human CD45+ cells. Figure 5.3 shows that the percentage of human CD45+ cells in the bone marrow rose from around 3% to 40% from month 1 to month 3 - which confirms “humanisation” of the mice.

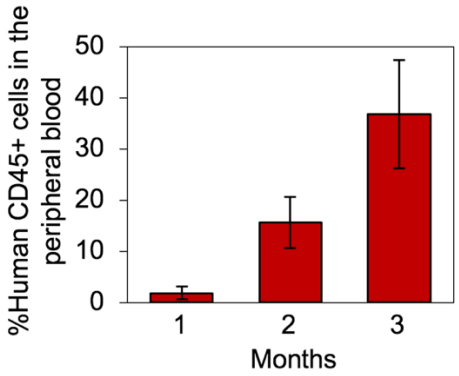

Figure 5.3. Human CD45+ cells are present in the bone marrow of humanised mice.

Cord blood CD34+ stem and progenitor cells were transplanted into 3-4-week-old NSG mice, engraftment was determined through peripheral blood flow cytometry analysis. The percentage of human CD45+ cells is presented over a 3-month time period in 5 humanised NSG mice.

Humanised mice generated were treated with PBS or 1mg/kg LPS for 2 hours, bone marrow was then extracted and haematopoietic cell populations were analysed using flow cytometry. A modified panel of antibodies was used to detect the human HSC population (murineCD45$^-$ humanCD38$^-$CD34$^+$CD45RA$^-$ CD90$^+$CD49f$^+$), MPP (murineCD45$^-$ humanCD38$^-$CD34$^+$CD45RA$^-$CD90$^-$CD49f$^-$), CMP (murineCD45$^-$ humanCD38$^+$CD34$^+$CD45RA$^-$CD90$^-$CD49f$^-$) and GMP (murineCD45$^-$ humanCD38$^+$CD34$^+$CD45RA$^+$CD90$^-$CD49f$^-$). Again, appropriate colour compensations were carried out and gating strategy (Figure 5.4) was determined using FMO controls.

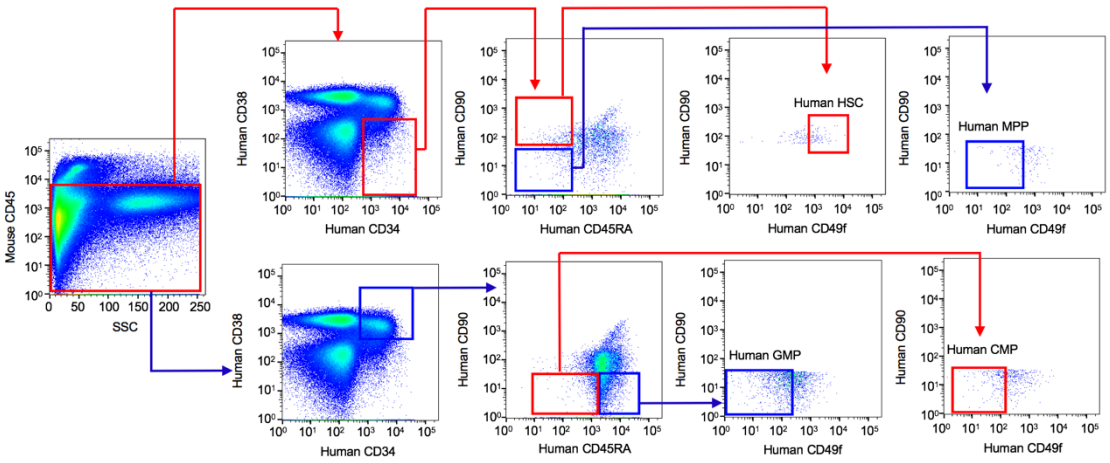

Figure 5.4. Gating strategy of HSC, MPP, CMP and GMP populations in humanised mice.

After sacrifice, humanised NSG BM was isolated and stained with a panel of antibodies to analyse specific HSC, MPP, CMP and GMP populations. The gating strategy is presented.

In addition to the panel of antibodies, humanised mouse BM from PBS/LPS treated mice was stained with MitoTracker Green to determine mitochondrial levels. Increased mitochondrial levels were observed in HSC and MPP populations from LPS treated humanised mice, with no change observed in CMP and GMP populations (Figure 5.5). This result was comparable with results obtained from C57BL/6J mice.

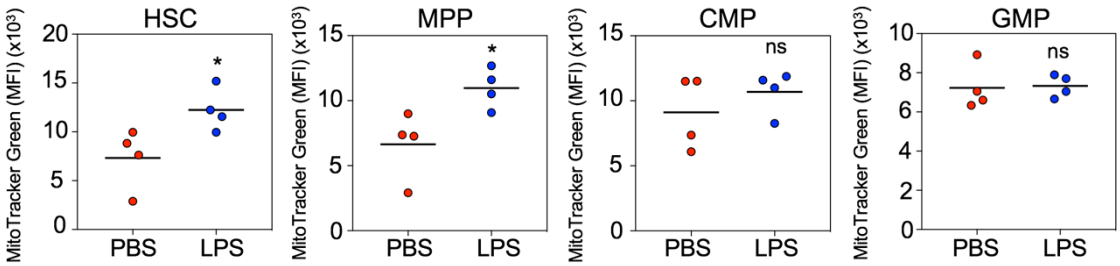

Figure 5.5. LPS increases mitochondria in human HSC and MPP from humanised mice.

Mitochondrial levels were determined in HSC, MPP, CMP and GMP populations isolated from humanised mice after PBS/LPS treatment. These populations were determined using the gating strategy shown in Figure 5.4 and mitochondrial levels were determined using MitoTracker Green staining.

Finally, I determined whether increased mitochondrial levels were in part due to intercellular mitochondrial transfer from the mouse BMM. The humanised NSG mouse model allows the specific analysis of two species mitochondrial transfer. The human HSC population was sorted from the bone marrow of humanised mice after treatment with PBS/LPS, using the gating strategy shown in Figure 5.4. qPCR was directly carried out on HSC cell lysate using duplex Taqman qPCR, with species specific probes targeted to the mitochondrial ND1 gene. A human Tert probe was also used for normalisation of Ct values. The HSC population from PBS treated humanised mice contained no mouse mitochondria. However, on average 3% of the total mitochondria in human HSCs from the LPS treated mice were of mouse origin (Figure 5.6A). There was no difference in the levels of human mitochondria in isolated HSCs, suggesting that mitochondrial biogenesis is not occurring (Figure 5.6B). This presents data which suggests that upon LPS treatment mitochondria are transferred from the BMM to HSCs which allows their expansion and proliferation.

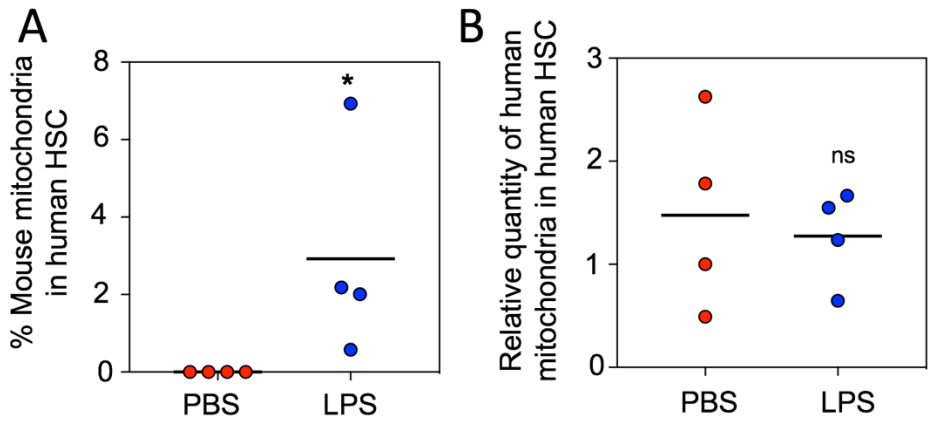

Figure 5.6. Mouse mitochondria move from the BMM to human HSCs upon LPS treatment.

The human HSC population was sorted from the BM of PBS/LPS treated "humanised" mice. qPCR was carried out with species specific Taqman probes targeted to ND1 and Tert. Mouse and human mitochondrial levels were determined using the ΔΔCt normalising the human/mouse mitochondrial Ct to human Tert. (A) The percentage of mouse mitochondria detected in isolated HSC. (B) The relative quantity of human mitochondria in HSCs isolated from PBS/LPS treated mice is presented.

5.3 Summary

In the final results chapter of my thesis I have explored the possibility of intercellular mitochondrial transfer occurring in a non-malignant haematological system. I utilised LPS to simulate bacterial infection in C57BL/6J mice and found that ST-HSCs had increased mitochondrial levels compared to PBS treatment. This result was also observed after the administration of the "real" bacterium *Salmonella enterica*. Through the use of humanised NSG mice, I found that increased mitochondrial levels in HSCs were in part due to intercellular mitochondrial transfer from the BMM. This transfer of mitochondria resulted in the expansion and proliferation of the HSC compartment, which will mount an attack against the foreign pathogen. Results in this chapter show that mitochondrial transfer in the bone marrow is not specific to haematological malignancies and that it's a fundamental process in which AML and MM cells are able to hijack to gain a survival advantage.

6 Discussion and Conclusions

6.1 General Discussion

Acute myeloid leukaemia and multiple myeloma are devastating haematological malignancies which are presently incurable. Current treatments targeting the malignant cell are effective at removing the bulk of the tumour, however disease relapse is very common and ultimately leads to mortality. Small numbers of AML/MM cells remain in bone marrow niches, where they are protected from chemotherapeutics and have the ability to proliferate - leading to the repopulation of the malignancy. It is envisaged that the eradication of the malignant cells which remain within the bone marrow will provide a better prognostic outcome for patients diagnosed with these diseases. One of the ways in which malignant cells are protected is via their interactions with BMSC. A better understanding of the complex biological interactions between these two cell types will ultimately lead to novel therapeutics that will be used in combination with current chemotherapeutic regimens.

In my thesis, I have highlighted the process of intercellular mitochondrial transfer which contributes to AML/MM survival and proliferation. In addition, I have dissected the key mechanisms that underpin this pro-tumoral process. It is hoped these mechanisms can be targeted therapeutically, which may increase the survival and prognostic outcome of patients diagnosed with these currently destructive diseases.

6.2 Key findings

6.2.1 Mitochondrial transfer in the bone marrow niche

In my thesis, I have described two malignancies where intercellular mitochondrial transfer contributes to their survival and proliferation- which will contribute to the literature describing mitochondrial transfer.

AML blasts have previously been shown to be anti-Warburg - relying on mitochondria for ATP production (311) whilst having increased mitochondrial levels (314). I have shown that intercellular mitochondrial transfer from BMSC contributes to the accumulation of mitochondria within AML blasts, resulting in increased ATP production through an enhancement of mitochondrial respiration (Section 3.2.1 – 3.2.3). There may be other factors which contribute to mitochondrial accumulation in AML blasts, one example being defects in the mitochondrial degradation process mitophagy. However, this process has however been shown to be functional in AML stem cells and is required for cellular survival (348). It is therefore unlikely that this process contributes to the observed phenotype. A second study by Moschoi and colleagues also described mitochondrial transfer from BMSC to AML blasts (349). Ergo, the accumulation of mitochondria in AML blasts is most likely due to intercellular mitochondrial transfer.

I have shown that an increase in mitochondrial levels subsequently enhances OCR in AML blasts (Section 3.2.3). The process of FAO is also able to generate ATP from free fatty acids, through OXPHOS (350). AML have been shown to import free fatty acids via the FABP4 transporter protein (273), therefore the increased mitochondria acquired from BMSC may provide extra machinery to metabolise these fatty acids. The combination of OXPHOS and FAO have the ability to provide AML blasts with huge amounts of ATP which can be utilised for rapid proliferation within the bone marrow.

To date, there has been no study comparing mitochondrial levels in MM cells with their non-malignant counterparts. In my thesis, I showed that mitochondrial transfer was also present between MM and BMSC – a highly surprising result (Figure 4.2.2 and 4.2.3). This is because (unlike AML blasts) MM cells have been shown to be a “Warburg Cancer” relying on aerobic glycolysis to generate ATP (316, 317). However, after analysing the effect the MM microenvironment has on metabolism within the malignant cell it becomes apparent why the transfer of

mitochondria occurs. The BMM allows MM cells to switch their metabolism to utilise mitochondria, which contributes to growth capacity and ATP production (Section 4.2.1). Studies showing MM utilised aerobic glycolysis only analysed MM cells in mono-culture and not in the context of their microenvironment. Therefore, it is of paramount importance to study metabolism of malignant cells within their supportive microenvironment as they would be in the human body.

In the final chapter of my thesis I described mitochondrial transfer in a non-malignant haematological system - where HSCs acquire mitochondria from the BMM under LPS induced bacterial infection (Section 5.2). Therefore, I believe mitochondrial transfer is a normal physiological process that malignant haematopoietic cells can hijack to favour their proliferation and survival. Recently HSCs have been shown to transfer mitochondria to BMSC (351). This process occurred through connexin-43 mediated gap junctions and was shown to regulate ROS levels within the HSC. However, only limited conclusions can be drawn as this research was presented as a conference abstract and the full paper has not been published yet. Nevertheless, it can be seen that mitochondrial transfer plays an important role in the regulation of normal haematopoiesis as well as in the malignant bone marrow.

It is becoming ever more apparent that malignant haematopoietic cells can modify their protective microenvironment and utilise normal processes to promote their survival and proliferation (352, 353). My results contribute to the evidence where this is the case; I have shown in my thesis that AML blasts can induce mitochondrial biogenesis in BMSC in order to “steal” these mitochondria to aid its proliferative advantage (Section 3.2.6). The mechanism utilised by AML blasts can not only acquire mitochondria, but also ensures BMSC remain viable to safeguard a constant mitochondrial source. Although not examined in thesis due to time constraints, I believe there will be a similar process exploited in MM to ensure BMSC remain viable. This mechanism will need to be independent of

NOX2 (as MM cells do not express this enzyme) but is likely to be still through PGC-1α activation.

The number of cancers in which intercellular mitochondrial transfer occurs from supporting microenvironment cells is rapidly increasing. These cancers include Breast (326), Lung (323), Ovarian (326) and now AML and MM. It is highly likely that this biological process will also occur in other cancers that are known to have a strong association with their microenvironment such as prostate (354) and colorectal cancer (355). Therefore, I believe that in the not too distance future there will be literature describing mitochondrial transfer in these malignancies.

As mitochondrial transfer appears to be part of the malignant phenotype, it is becoming apparent that the Warburg hypothesis may not be universally applicable. PET scans are a useful tool in diagnosing cancer as malignant cells have increased glucose consumption due to the Warburg hypothesis. Even though MM cells rely on mitochondrial metabolism in their BMM, PET scans are used in the diagnosis of MM and increased glucose consumption is associated with a poor prognosis (356, 357). Warburg stated that cancers generate ATP through glycolysis and this process produces lactate. Recent studies have shown that circulating lactate can feed the TCA cycle in lung cancer (358), which is the case in both human and mouse tumours (359). Therefore, in the context of MM I hypothesise that glucose does feed glycolysis as Warburg hypothesised. However, lactate generated is then fed into the TCA cycle of functional mitochondria (acquired from the BMM) and ATP is generated through OXPHOS. This may be the case for other “Warburg Cancers” where the transfer of mitochondria occurs and may re-define metabolism within tumour cells.

6.2.2 Tunneling nanotubes: The mitochondrial transporter

Mitochondria have been shown to primarily be transferred between cells by TNTs (323, 326, 327, 329) as well as microvesicles (331) and connexion-43 gap

junctions (330). In both AML and MM, I found that mitochondria can be transferred by TNTs which were of malignant cell origin (Section 3.2.2 and 4.2.3). The TNT inhibitor CytoB was found to reduce mitochondrial transfer between BMSC and AML/MM cells. TNTs were visualised using fixed cell confocal microscopy and contained BMSC mitochondria. As the TNTs were of malignant cell origin, this shows that mitochondrial transfer is an active process in which AML/MM cells steal mitochondria from BMSC. As mentioned in section 6.2.1, a second paper has described the transfer of mitochondria from BMSC to AML blasts (349). However, in this paper the authors concluded that mitochondria were transferred via an endocytosis mechanism due to a reduction in mitochondrial transfer observed upon the addition of Dansylcadavarine. The authors didn't assess the effect of CytoB or analyse the formation of TNTs. In my mitochondrial transfer assays, I found Dansylcadavarine had no effect on mitochondrial transfer levels however CytoB caused a reduction in mitochondrial trafficking (Figure 3.8 and 3.10). As a result of these two publications, it suggests that mitochondria move from BMSC to AML blasts by a combination of TNT and endocytosis mechanisms.

Mitochondria are not the only cellular component transported via TNTs. There have been a number of studies describing the movement of endosomes (360), lysosomes (361), autophagosomes (362), endoplasmic reticulum (363), microRNAs (364) and pro-survival cytokines (365). This poses the question - what else is moving between BMSC to AML/MM cells as well as the mitochondria? Malignant haematopoietic cells have the tendency to act as parasites and I believe once they dock with BMSC they will acquire anything that will aid their survival. It is therefore highly important to determine the extent of TNT material transfer between BMSC and AML/MM cells. Unfortunately, this was outside the scope of my PhD thesis but will hopefully be determined in the future.

A recent study also showed that mitochondria can be transferred in the opposite direction from T-ALL (Jurkat) cells to BMSC, which also occurs through TNTs (366). This was shown to reduce ROS levels in the malignant cell, a result that is

in agreement with a study by Golan and colleagues which presented the transfer of mitochondria from HSCs to BMSC (351). This study also showed the transfer of mitochondria from HSCs to BMSC, although in this study the mitochondria were transferred via gap junctions. Mitochondria are a large source of intercellular ROS levels (367) and these levels are increased when mitochondria are dysfunctional (368). Therefore, mitochondria which are transferred to BMSC may be dysfunctional and their transfer may result in reduced ROS levels in the donor cell. It would be interesting to study whether AML/MM cells have the ability to transfer mitochondria to BMSC and whether these mitochondria are dysfunctional. This process may present a dysfunctional mitochondria recycling system which may aid malignant cell survival.

6.2.3 Control mechanisms of mitochondrial transfer in AML/MM

Mitochondrial transfer is becoming a critical part of the malignant phenotype. A full understanding of the mechanisms which underpin this biological phenomenon is therefore very important if this process is to be exploited therapeutically. In my thesis, I have presented controlling mechanisms of intercellular mitochondrial transfer from BMSC to both AML blasts and MM cells.

Firstly, in AML I have shown that NOX2 located on the malignant cell stimulates mitochondrial transfer (Section 3.2.5 and 3.2.6). Superoxide generated by NOX2 can increase oxidative stress in BMSC, causing the activation of PGC-1α and subsequent mitochondrial biogenesis. This process has been shown to be specific to AML cells as oxidative stress is not induced in BMSC cultured with non-malignant CD34+ cells. Mitochondrial transfer was reduced upon the addition of the NOX2 inhibitor DPI (in addition to knocking NOX2 down on AML blasts), which also induced apoptosis in AML blasts. NOX2 is most commonly found on professional phagocytes and is a transmembrane protein that transports electrons across plasma membranes reducing oxygen to superoxide (369). There are six other members of the NOX family (NOX1, 3, 4, 5 and DUOX1 and 2) which

are located on other cell types such as the colon, endothelium, kidney and thyroid cells (370). All seven members have a similar structure based around six transmembrane domains, two haem groups and a NADPH binding site on the COOH terminal (seen Figure 6.1). The crystal structure was only recently determined in 2017 (371) and is very similar to the long accepted predicted structure (369). Although the involvement of NOX2 in malignant mitochondrial transfer is most likely confined to AML (or CML if it occurs), other members of the NOX family could contribute to other mitochondrial transfer systems. For example NOX1 is highly expressed on colon cells (372) and colon cancers are known to have a high association with their microenvironment (355). This highlights a potential role for NOX1 in any intercellular mitochondrial transfer that may occur in this malignancy.

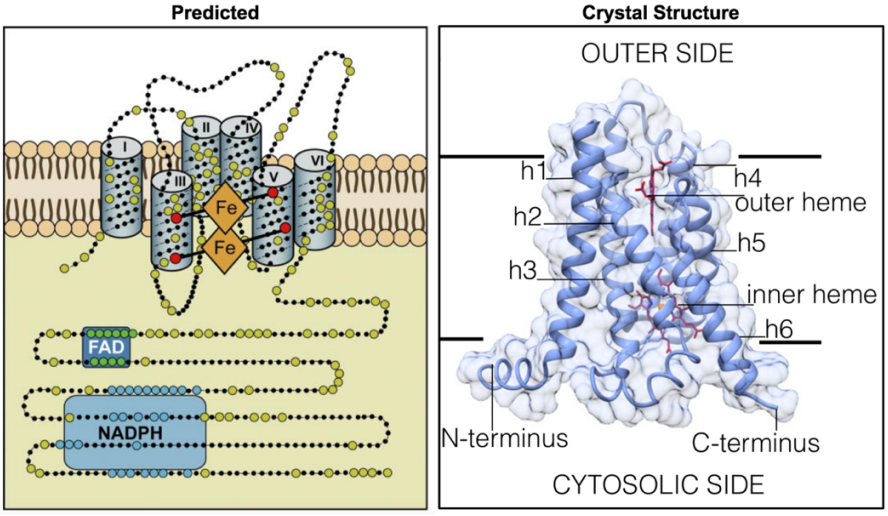

Figure 6.1. The structure of NADPH oxidase family of enzymes.

The predicted (left) (369) and the X-ray crystal structure (right) (371) of the NOX family of enzymes. The two structures are very similar with 6 transmembrane domains 2 haem groups. Electrons pass from NADPH to the haem groups (through FAD) and then reduce oxygen to superoxide.

NOX2 may also play a role in the mechanism behind mitochondrial transfer from the BMM to HSCs under bacterial infection. NOX2 on monocytes/macrophages is crucial in the defence from bacterial infections and inactivity of this enzyme can lead to chronic granulomatous disease (CGD) (373). Superoxide generated by NOX2 monocytes/macrophages may also induce oxidative stress and mitochondrial biogenesis in BMSC. This may result in the trafficking of

mitochondria to HSCs, inducing cycling and the expansion of blood cells needed to fight the pathogen. However, this is still very much a hypothesis which requires further work.

In addition to elucidating the mechanism behind mitochondrial transfer in AML, I have also determined the mechanism which can cause the transfer of mitochondria to MM cells. I have shown that CD38 located on the surface of MM cells form TNTs which dock with BMSC facilitating the movement of mitochondria (Section 4.2.4 and 4.2.5). CD38 is left behind on BMSC after the dissociation of the TNT and CD38 knockdown reduces the number of TNTs formed. CD38 has two known functions firstly, as an ectozyme catalysing the metabolism of the calcium messengers cyclic ADP-ribose and nicotinic acid adenine dinucleotide phosphate (374). Secondly CD38 functions as a cell surface receptor – the likely mechanism utilised in mitochondrial transfer. The X-ray crystallography structure of CD38 (375) is shown in Figure 6.2.

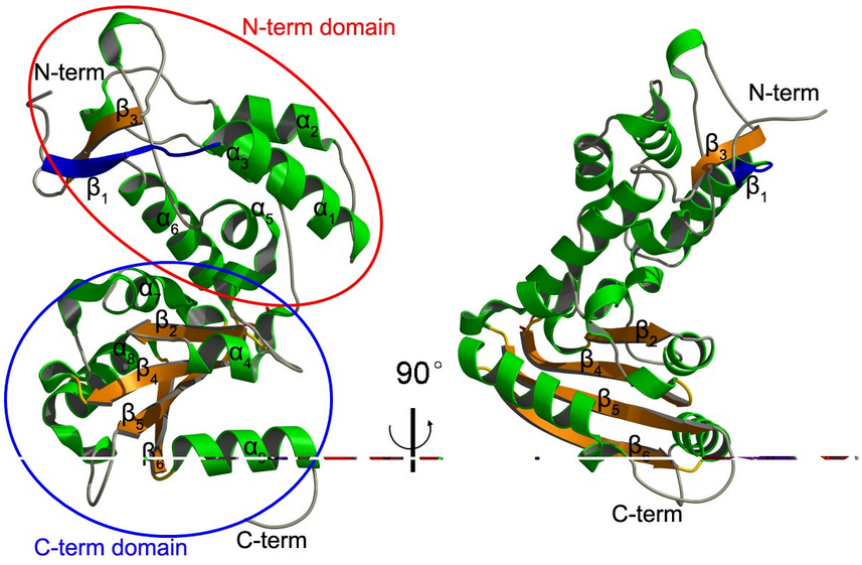

Figure 6.2. X-Ray Crystallography structure of CD38.

The structure of CD38 was determined in 2005 (375) and is presented in this figure. The left and red images are a 90˚ rotation of each other in the vertical axis. CD38 is made up of 8 alpha helices and 6 beta sheets. The C-terminal binds to the plasma membrane anchoring the protein.

As CD38 is found on the leading edge of the TNT and is deposited on the surface of BMSC after TNT dissociation, I believe that its role in mitochondrial transfer is as a receptor. However, in my thesis I was unable to determine the binding partner of CD38 on the surface of BMSC. CD38 has one known binding partner CD31 (346), however CD31 is not expressed on BMSC (Figure 4.20) and is a known negative marker in the characterisation of BMSC (376). Therefore, there may be an unknown binding partner of CD38 present on the surface of BMSC. BMSC do express CD157 which is a homologue of CD38 (377), therefore there may be an association of CD38 with CD157 leading to TNT docking. Unfortunately, there was no time to assess CD157 and other possible factors as part of my thesis.

The discovery of the role of CD38 in the MM mitochondrial transfer mechanism has highlighted an unknown role of this molecule. CD38 was initially thought to be only expressed on haematopoietic cells (378), however CD38 is known today to be expressed on a range of different tissues like brain, prostate, pancreas and kidney (377). This opens up the possibility that CD38 may be involved in other mitochondrial transfer systems in other malignancies as well as non-malignant systems. CD38 has already been shown to mediate mitochondrial transfer from astrocytes to neurons after stroke (331). AML blasts have been shown to express CD38, albeit at lower levels than MM (379). It would be very interesting to test whether CD38 plays a role in the TNT formation shown between AML blasts and BMSC. If this were the case, it may pave the way for the use of the CD38 monoclonal antibody Daratumumab to treat patients with AML.

A common observation between the two malignant mitochondrial transfer systems described in my thesis is that chemotherapy drugs increase the level of mitochondrial transfer. Daunorubicin and Bortezomib, used in the treatment of AML and MM respectively, were shown to increase the level of mitochondrial transfer from BMSC by on average 2-fold (Figure 3.13 and 4.8). This presents a system where malignant cells can adapt to treatments they encounter in order to survive. This is extremely interesting in the context of minimal residual disease,

where mitochondrial transfer may contribute to the survival of a small number of AML/MM cells in close proximity to BMSC within the bone marrow. This mechanism may lead to the patient relapse which is currently responsible for the current poor survival rates of AML and MM. Chemotherapeutics have been shown to induce oxidative stress in the bone marrow (380), which suggests that this stimulates mitochondrial transfer as per NOX2. In my results, I did not analyse the effect of oxidative stress in the mitochondrial transfer to MM cells. The effect of Bortezomib suggests that oxidative stress is also involved in this mechanism, albeit in an independent process to NOX2.

Taken together, these malignant mitochondrial transfer mechanisms describe biological molecules that may be therapeutically targetable in the context of AML and MM. In addition, the mechanisms described may provide a molecular basis for the elucidation of other transfer systems where the trafficking of mitochondria has already been or will be described in the future.

6.2.4 Therapeutically targeting mitochondrial transfer

The overall aim of any cancer research project is to determine key biological processes and molecules which can be targeted therapeutically for the benefit of the patient. In my thesis, I have shown that in both AML and MM intercellular mitochondrial transfer from the BMM is a process that contributes to the survival and proliferation of these malignancies. Furthermore, I have highlighted the biological role of NOX2, PGC-1α and CD38 in the mitochondrial transfer process and present these as novel biological targets in the treatment of AML and MM - which may stop the flow of mitochondria. I have shown that current chemotherapy treatments increase the level of mitochondrial transfer (Figure 3.13 and 4.8), it is therefore apparent that treatments targeting mitochondrial transfer could be used in conjunction with lower doses of the current chemotherapy regimens to provide a more effective therapy.

In the AML mitochondrial transfer system, I have highlighted NOX2 and PGC-1α as molecules that contribute to the trafficking of mitochondria from BMSC (Section 3.2.5 and 3.2.6). There may be a novel opportunity to target these therapeutically to treat AML and hopefully increase patient survival. In my thesis, I have used the commercially available DPI to inhibit NOX2 on the surface of AML and shown that induction of apoptosis is specific to malignant cells over non-malignant cells (Figure 3.18). However, DPI and the other commercially available inhibitor Apocymin are not isoform specific as they also inhibit NOX1, 3, 4 and 5 (381). Therefore, these compounds would be unsuitable to be used in the clinic. The only known NOX2 specific inhibitor is the small peptide NOX2-ds-tat, which has an IC_{50} for NOX2 inhibition of 0.74μM (382). However currently there are no clinical trials which use this compound in any disease, the only NOX inhibitor in clinical trials is the NOX1/4 inhibitor GKT137831 used to the treat primary biliary cholangitis (NCT03226067) and type 2 diabetes (NCT02010242). It would be very interestingly to test NOX2-ds-tat in *in vitro* and *in vivo* models of AML, specifically focussing on mitochondrial transfer.

The second molecule that could be targeted in the AML mitochondrial transfer system is PGC-1α in BMSC. In my thesis, I specifically inhibited PGC-1α using shRNA (Section 3.2.7) however there is a chemical inhibitor of PGC-1α (SR-18292) which was not tested (383). The clinical efficacy of this drug has not been examined and SR-18292 has currently not been used in any clinical trials to date. As PGC-1α is crucial to normal bodily homeostasis (through mitochondrial biogenesis) any treatments targeting PGC-1α in BMSC must be specific to avoid any of target effects. In addition, PGC-1α inhibition in BMSC may interfere and alter normal haematopoiesis disrupting the bone marrow further. For these reasons, I believe that NOX2 is the more favourable target in AML to inhibit the transfer of mitochondria from the BMM.

Elucidation of the mitochondrial transfer system in MM highlighted the role of CD38 in the formation of the TNT (Section 4.2.4 – 4.2.6). Targeting CD38 may

reduce the levels of mitochondrial transfer, which could potentially lead to increased patient survival. Contrary to treating AML with NOX2 inhibitors, a specific CD38 antibody Daratumumab has been shown to induce MM apoptosis in the presence of the protective BMM (249). Early clinical trials using Daratumumab targeting CD38 have been shown to be well tolerated and clinically efficacious in early phase studies of the treatment of relapsed refractory MM (251). In addition, phase 3 clinical trials of anti-CD38 antibodies in MM therapy have demonstrated improvements in overall response rates and progression free survival when combined with chemotherapy (384). Further to this, Daratumumab has been FDA approved for the treatment of refractory MM in combination with bortezomib and lenalidomide (252). Although I didn't use Daratumumab, my thesis results provide a further insight into potential mechanisms of action of CD38 antibodies in the treatment of MM - where pro-tumoral mitochondrial transfer is also inhibited. Therefore, the data I have presented here shows that CD38 inhibition in MM (using Daratumumab) also has the ability to inhibit mitochondrial transfer for clinical benefit.

I have shown in my third results chapter that mitochondrial transfer can occur to non-malignant HSCs under stress stimuli (Section 5.2). It is therefore very important to consider this process when designing treatments targeting malignant mitochondrial transfer. Although I have not determined the control mechanisms in non-malignant transfer, there are likely to be similarities between the processes. Therefore, targeting specific mechanisms such as the NOX2 oxidative stress mechanism may also impair non-malignant mitochondrial transfer to HSCs which could make patients more susceptible to bacterial infections.

6.3 Limitations of the Study and Further Work

Despite the results obtained, as with any study there are limitations which should be considered. The number of primary patient samples in some experiments is limited, this is due to sample availability and sharing samples around a highly

active research group. However, I believe experiments using small numbers of primary cells outweighs equivalent experiments using cell lines. Likewise, in animal experimentation increased numbers of mice would give more statistically significant results. However, I chose to refine animal experimentations to use the minimum number of mice to generate a statistically significant result.

Ideally, the isolation of primary BMSC could have been more specific. I cultured and expanded all adherent cells from the mononuclear cell fraction and characterised them as CD73, CD90 and CD105 positive BMSC - this population was therefore very heterogeneous. Different cells within the BMSC population could have transferred varying levels of mitochondria to malignant AML/MM cells. Enhanced characterisation of stromal cells within the bone marrow has led to the discovery of specific subtypes like CAR and Nestin GFP+ cells (discussed in my introduction section 1.2.3). It would be of interest to isolate these cells specifically and analyse mitochondrial transfer levels from these to malignant AML/MM cells.

In the MM mitochondrial transfer system, I have shown that CD38 is crucial for the process and CD38 KD in MM xenograft models increases animal survival (Section 4.2.6). As discussed in section 6.2.4, the CD38 monoclonal antibody Daratumumab has been FDA approved for the treatment of refractory MM. Unfortunately, I was unable to obtain Daratumumab from Janssen during my PhD and was therefore unable to test the role of this drug in mitochondrial transfer. If in the future my research group could obtain Daratumumab, I would suggest further work should examine the effect of Daratumumab on the intercellular mitochondrial transfer which occurs in MM. In addition, I would examine whether CD38 is involved in the AML mitochondrial transfer system to determine whether Daratumumab could be a viable therapeutic to treat AML.

Although I have elucidated parts of the mitochondrial transfer mechanisms in MM, there is still further work needed to fully understand this system. I was unable to determine the molecule on BMSC which CD38 binds to anchor the TNT formation.

The obvious candidate was CD31, however this is not expressed on the surface of BMSC. Therefore, there is either a novel binding partner of CD38 on the surface on BMSC or CD38 binds un-specifically with BMSC to facilitate the transfer of mitochondria. Further work is needed to address this issue.

Finally, I have shown that LPS induced bacterial infections stimulates mitochondrial transfer from the BMM to non-malignant HSCs. Due to time constraints, I was unable to determine the mechanism behind this but hypothesise that NOX2 may play a part due to its essential role to bacterial infection. Hopefully, future work will determine if NOX2 is involved in the non-malignant mitochondrial transfer mechanism which I have shown to occur between the BMM and HSCs under bacterial infection.

6.4 Concluding remarks

Overall in my thesis I have shown that intercellular mitochondrial transfer occurs from BMSC to both AML and MM cells and this transfer can occur via TNTs. AML NOX2 superoxide stimulates PGC-1α in BMSC, which results in increased mitochondrial biogenesis and contributes to the pro-tumoral trafficking of mitochondria. In MM, CD38 on the surface of the malignant cell has the ability to form TNTs which dock with BMSC and allows the transfer of mitochondria. Inhibition of both these processes has been shown to induce apoptosis and increase the survival of mice which have been injected with AML/MM cells. In addition, I have shown that mitochondrial transfer is an already established process that can be hijacked by malignant haematopoietic cells. My work highlights the nature of mitochondrial transfer in the progression and survival of AML and MM. My thesis presents novel biological molecules which underpin pro-tumoral mitochondrial transfer, which could be targeted therapeutically in the clinic to improve the survival of patients who are affected by AML and MM.

7 References

1. Ogawa M, Porter PN, Nakahata T. Renewal and commitment to differentiation of hemopoietic stem cells (an interpretive review). Blood. 1983;61(5):823-9.
2. Ogawa M. Differentiation and proliferation of hematopoietic stem cells. Blood. 1993;81(11):2844-53.
3. Orkin SH, Zon LI. Hematopoiesis: an evolving paradigm for stem cell biology. Cell. 2008;132(4):631-44.
4. Doulatov S, Notta F, Laurenti E, Dick JE. Hematopoiesis: a human perspective. Cell Stem Cell. 2012;10(2):120-36.
5. McCulloch EA, Till JE. The radiation sensitivity of normal mouse bone marrow cells, determined by quantitative marrow transplantation into irradiated mice. Radiat Res. 1960;13:115-25.
6. Weissman IL. Clonal origins of the hematopoietic system: the single most elegant experiment. J Immunol. 2014;192(11):4943-4.
7. Becker AJ, Mc CE, Till JE. Cytological demonstration of the clonal nature of spleen colonies derived from transplanted mouse marrow cells. Nature. 1963;197:452-4.
8. Ng AP, Alexander WS. Haematopoietic stem cells: past, present and future. Cell Death Discov. 2017;3:17002.
9. Seita J, Weissman IL. Hematopoietic stem cell: self-renewal versus differentiation. Wiley Interdiscip Rev Syst Biol Med. 2010;2(6):640-53.
10. Till JE, Mc CE. A direct measurement of the radiation sensitivity of normal mouse bone marrow cells. Radiat Res. 1961;14:213-22.
11. Rossi DJ, Seita J, Czechowicz A, Bhattacharya D, Bryder D, Weissman IL. Hematopoietic stem cell quiescence attenuates DNA damage response and permits DNA damage accumulation during aging. Cell Cycle. 2007;6(19):2371-6.
12. Muller-Sieburg CE, Whitlock CA, Weissman IL. Isolation of two early B lymphocyte progenitors from mouse marrow: a committed pre-pre-B cell and a clonogenic Thy-1-lo hematopoietic stem cell. Cell. 1986;44(4):653-62.
13. Spangrude GJ, Heimfeld S, Weissman IL. Purification and characterization of mouse hematopoietic stem cells. Science. 1988;241(4861):58-62.
14. Uchida N, Weissman IL. Searching for hematopoietic stem cells: evidence that Thy-1.1lo Lin- Sca-1+ cells are the only stem cells in C57BL/Ka-Thy-1.1 bone marrow. J Exp Med. 1992;175(1):175-84.
15. Morrison SJ, Weissman IL. The long-term repopulating subset of hematopoietic stem cells is deterministic and isolatable by phenotype. Immunity. 1994;1(8):661-73.
16. Walter D, Lier A, Geiselhart A, Thalheimer FB, Huntscha S, Sobotta MC, et al. Exit from dormancy provokes DNA-damage-induced attrition in haematopoietic stem cells. Nature. 2015;520(7548):549-52.
17. Challen GA, Boles N, Lin KK, Goodell MA. Mouse hematopoietic stem cell identification and analysis. Cytometry A. 2009;75(1):14-24.
18. Marlein CR, Rushworth SA. Bone Marrow. eLS: John Wiley & Sons, Ltd: Chichester.; 2018.

19. Fulop GM, Phillips RA. The scid mutation in mice causes a general defect in DNA repair. Nature. 1990;347(6292):479-82.
20. Mosier DE, Gulizia RJ, Baird SM, Wilson DB. Transfer of a functional human immune system to mice with severe combined immunodeficiency. Nature. 1988;335(6187):256-9.
21. Ishikawa F. Modeling normal and malignant human hematopoiesis in vivo through newborn NSG xenotransplantation. Int J Hematol. 2013;98(6):634-40.
22. Audige A, Rochat MA, Li D, Ivic S, Fahrny A, Muller CKS, et al. Long-term leukocyte reconstitution in NSG mice transplanted with human cord blood hematopoietic stem and progenitor cells. BMC Immunol. 2017;18(1):28.
23. Jagannathan-Bogdan M, Zon LI. Hematopoiesis. Development. 2013;140(12):2463-7.
24. Kondo M. Lymphoid and myeloid lineage commitment in multipotent hematopoietic progenitors. Immunol Rev. 2010;238(1):37-46.
25. Wolff L, Humeniuk R. Concise review: erythroid versus myeloid lineage commitment: regulating the master regulators. Stem Cells. 2013;31(7):1237-44.
26. Adolfsson J, Mansson R, Buza-Vidas N, Hultquist A, Liuba K, Jensen CT, et al. Identification of Flt3+ lympho-myeloid stem cells lacking erythro-megakaryocytic potential a revised road map for adult blood lineage commitment. Cell. 2005;121(2):295-306.
27. Suh HC, Gooya J, Renn K, Friedman AD, Johnson PF, Keller JR. C/EBPalpha determines hematopoietic cell fate in multipotential progenitor cells by inhibiting erythroid differentiation and inducing myeloid differentiation. Blood. 2006;107(11):4308-16.
28. Xie H, Ye M, Feng R, Graf T. Stepwise reprogramming of B cells into macrophages. Cell. 2004;117(5):663-76.
29. Zhang P, Iwasaki-Arai J, Iwasaki H, Fenyus ML, Dayaram T, Owens BM, et al. Enhancement of hematopoietic stem cell repopulating capacity and self-renewal in the absence of the transcription factor C/EBP alpha. Immunity. 2004;21(6):853-63.
30. Kuhl C, Atzberger A, Iborra F, Nieswandt B, Porcher C, Vyas P. GATA1-mediated megakaryocyte differentiation and growth control can be uncoupled and mapped to different domains in GATA1. Mol Cell Biol. 2005;25(19):8592-606.
31. Pevny L, Simon MC, Robertson E, Klein WH, Tsai SF, D'Agati V, et al. Erythroid differentiation in chimaeric mice blocked by a targeted mutation in the gene for transcription factor GATA-1. Nature. 1991;349(6306):257-60.
32. Lai AY, Kondo M. T and B lymphocyte differentiation from hematopoietic stem cell. Semin Immunol. 2008;20(4):207-12.
33. von Andrian UH, Mackay CR. T-cell function and migration. Two sides of the same coin. N Engl J Med. 2000;343(14):1020-34.
34. LeBien TW, Tedder TF. B lymphocytes: how they develop and function. Blood. 2008;112(5):1570-80.
35. Caligiuri MA. Human natural killer cells. Blood. 2008;112(3):461-9.
36. Eason DD, Cannon JP, Haire RN, Rast JP, Ostrov DA, Litman GW. Mechanisms of antigen receptor evolution. Semin Immunol. 2004;16(4):215-26.

37. Kondo M, Weissman IL, Akashi K. Identification of clonogenic common lymphoid progenitors in mouse bone marrow. Cell. 1997;91(5):661-72.
38. Ramirez J, Lukin K, Hagman J. From hematopoietic progenitors to B cells: mechanisms of lineage restriction and commitment. Curr Opin Immunol. 2010;22(2):177-84.
39. Bain G, Maandag EC, Izon DJ, Amsen D, Kruisbeek AM, Weintraub BC, et al. E2A proteins are required for proper B cell development and initiation of immunoglobulin gene rearrangements. Cell. 1994;79(5):885-92.
40. Lin H, Grosschedl R. Failure of B-cell differentiation in mice lacking the transcription factor EBF. Nature. 1995;376(6537):263-7.
41. Hoffman W, Lakkis FG, Chalasani G. B Cells, Antibodies, and More. Clin J Am Soc Nephrol. 2016;11(1):137-54.
42. Hardy RR, Kincade PW, Dorshkind K. The protean nature of cells in the B lymphocyte lineage. Immunity. 2007;26(6):703-14.
43. Novobrantseva TI, Martin VM, Pelanda R, Muller W, Rajewsky K, Ehlich A. Rearrangement and expression of immunoglobulin light chain genes can precede heavy chain expression during normal B cell development in mice. J Exp Med. 1999;189(1):75-88.
44. Sandel PC, Monroe JG. Negative selection of immature B cells by receptor editing or deletion is determined by site of antigen encounter. Immunity. 1999;10(3):289-99.
45. Cambier JC, Getahun A. B cell activation versus anergy; the antigen receptor as a molecular switch. Immunol Lett. 2010;128(1):6-7.
46. Weinreich MA, Hogquist KA. Thymic emigration: when and how T cells leave home. J Immunol. 2008;181(4):2265-70.
47. Krueger A, Zietara N, Lyszkiewicz M. T Cell Development by the Numbers. Trends Immunol. 2017;38(2):128-39.
48. Schwarz BA, Bhandoola A. Circulating hematopoietic progenitors with T lineage potential. Nat Immunol. 2004;5(9):953-60.
49. Kisielow P, von Boehmer H. Negative and positive selection of immature thymocytes: timing and the role of the ligand for alpha beta T cell receptor. Semin Immunol. 1990;2(1):35-44.
50. Vrisekoop N, Monteiro JP, Mandl JN, Germain RN. Revisiting thymic positive selection and the mature T cell repertoire for antigen. Immunity. 2014;41(2):181-90.
51. Davis MM, Boniface JJ, Reich Z, Lyons D, Hampl J, Arden B, et al. Ligand recognition by alpha beta T cell receptors. Annu Rev Immunol. 1998;16:523-44.
52. Klein L, Kyewski B, Allen PM, Hogquist KA. Positive and negative selection of the T cell repertoire: what thymocytes see (and don't see). Nat Rev Immunol. 2014;14(6):377-91.
53. Schebesta M, Heavey B, Busslinger M. Transcriptional control of B-cell development. Curr Opin Immunol. 2002;14(2):216-23.
54. Pui JC, Allman D, Xu L, DeRocco S, Karnell FG, Bakkour S, et al. Notch1 expression in early lymphopoiesis influences B versus T lineage determination. Immunity. 1999;11(3):299-308.

55. Bozzano F, Marras F, De Maria A. Natural Killer Cell Development and Maturation Revisited: Possible Implications of a Novel Distinct Lin(-)CD34(+)DNAM-1(bright)CXCR4(+) Cell Progenitor. Front Immunol. 2017;8:268.
56. Fathman JW, Bhattacharya D, Inlay MA, Seita J, Karsunky H, Weissman IL. Identification of the earliest natural killer cell-committed progenitor in murine bone marrow. Blood. 2011;118(20):5439-47.
57. Romagnani C, Juelke K, Falco M, Morandi B, D'Agostino A, Costa R, et al. CD56brightCD16- killer Ig-like receptor- NK cells display longer telomeres and acquire features of CD56dim NK cells upon activation. J Immunol. 2007;178(8):4947-55.
58. Jenne CN, Enders A, Rivera R, Watson SR, Bankovich AJ, Pereira JP, et al. T-bet-dependent S1P5 expression in NK cells promotes egress from lymph nodes and bone marrow. J Exp Med. 2009;206(11):2469-81.
59. Zhao E, Xu H, Wang L, Kryczek I, Wu K, Hu Y, et al. Bone marrow and the control of immunity. Cell Mol Immunol. 2012;9(1):11-9.
60. Brandi ML. Microarchitecture, the key to bone quality. Rheumatology (Oxford). 2009;48 Suppl 4:iv3-8.
61. Islam A, Glomski C, Henderson ES. Bone lining (endosteal) cells and hematopoiesis: a light microscopic study of normal and pathologic human bone marrow in plastic-embedded sections. Anat Rec. 1990;227(3):300-6.
62. Morrison SJ, Scadden DT. The bone marrow niche for haematopoietic stem cells. Nature. 2014;505(7483):327-34.
63. Scheiermann C, Frenette PS, Hidalgo A. Regulation of leucocyte homeostasis in the circulation. Cardiovasc Res. 2015;107(3):340-51.
64. Tavassoli M, Crosby WH. Bone marrow histogenesis: a comparison of fatty and red marrow. Science. 1970;169(3942):291-3.
65. Gurevitch O, Slavin S, Feldman AG. Conversion of red bone marrow into yellow - Cause and mechanisms. Med Hypotheses. 2007;69(3):531-6.
66. Pino AM, Miranda M, Figueroa C, Rodriguez JP, Rosen CJ. Qualitative Aspects of Bone Marrow Adiposity in Osteoporosis. Front Endocrinol (Lausanne). 2016;7:139.
67. Lo Celso C, Fleming HE, Wu JW, Zhao CX, Miake-Lye S, Fujisaki J, et al. Live-animal tracking of individual haematopoietic stem/progenitor cells in their niche. Nature. 2009;457(7225):92-6.
68. Pittenger MF, Mackay AM, Beck SC, Jaiswal RK, Douglas R, Mosca JD, et al. Multilineage potential of adult human mesenchymal stem cells. Science. 1999;284(5411):143-7.
69. Ferrari G, Cusella-De Angelis G, Coletta M, Paolucci E, Stornaiuolo A, Cossu G, et al. Muscle regeneration by bone marrow-derived myogenic progenitors. Science. 1998;279(5356):1528-30.
70. Dominici M, Le Blanc K, Mueller I, Slaper-Cortenbach I, Marini F, Krause D, et al. Minimal criteria for defining multipotent mesenchymal stromal cells. The International Society for Cellular Therapy position statement. Cytotherapy. 2006;8(4):315-7.

71. Lindner U, Kramer J, Rohwedel J, Schlenke P. Mesenchymal Stem or Stromal Cells: Toward a Better Understanding of Their Biology? Transfus Med Hemother. 2010;37(2):75-83.
72. Winkler IG, Barbier V, Wadley R, Zannettino AC, Williams S, Levesque JP. Positioning of bone marrow hematopoietic and stromal cells relative to blood flow in vivo: serially reconstituting hematopoietic stem cells reside in distinct nonperfused niches. Blood. 2010;116(3):375-85.
73. Schajnovitz A, Itkin T, D'Uva G, Kalinkovich A, Golan K, Ludin A, et al. CXCL12 secretion by bone marrow stromal cells is dependent on cell contact and mediated by connexin-43 and connexin-45 gap junctions. Nat Immunol. 2011;12(5):391-8.
74. Greenbaum A, Hsu YM, Day RB, Schuettpelz LG, Christopher MJ, Borgerding JN, et al. CXCL12 in early mesenchymal progenitors is required for haematopoietic stem-cell maintenance. Nature. 2013;495(7440):227-30.
75. Sugiyama T, Kohara H, Noda M, Nagasawa T. Maintenance of the hematopoietic stem cell pool by CXCL12-CXCR4 chemokine signaling in bone marrow stromal cell niches. Immunity. 2006;25(6):977-88.
76. Mendez-Ferrer S, Lucas D, Battista M, Frenette PS. Haematopoietic stem cell release is regulated by circadian oscillations. Nature. 2008;452(7186):442-7.
77. Anthony BA, Link DC. Regulation of hematopoietic stem cells by bone marrow stromal cells. Trends Immunol. 2014;35(1):32-7.
78. Langley KE, Bennett LG, Wypych J, Yancik SA, Liu XD, Westcott KR, et al. Soluble stem cell factor in human serum. Blood. 1993;81(3):656-60.
79. Pesce M, Di Carlo A, De Felici M. The c-kit receptor is involved in the adhesion of mouse primordial germ cells to somatic cells in culture. Mech Dev. 1997;68(1-2):37-44.
80. Barker JE. Sl/Sld hematopoietic progenitors are deficient in situ. Exp Hematol. 1994;22(2):174-7.
81. Tokoyoda K, Egawa T, Sugiyama T, Choi BI, Nagasawa T. Cellular niches controlling B lymphocyte behavior within bone marrow during development. Immunity. 2004;20(6):707-18.
82. Mendez-Ferrer S, Michurina TV, Ferraro F, Mazloom AR, Macarthur BD, Lira SA, et al. Mesenchymal and haematopoietic stem cells form a unique bone marrow niche. Nature. 2010;466(7308):829-34.
83. Ding L, Saunders TL, Enikolopov G, Morrison SJ. Endothelial and perivascular cells maintain haematopoietic stem cells. Nature. 2012;481(7382):457-62.
84. Omatsu Y, Sugiyama T, Kohara H, Kondoh G, Fujii N, Kohno K, et al. The essential functions of adipo-osteogenic progenitors as the hematopoietic stem and progenitor cell niche. Immunity. 2010;33(3):387-99.
85. Canalis E. Notch signaling in osteoblasts. Sci Signal. 2008;1(17):pe17.
86. Stein GS, Lian JB, van Wijnen AJ, Stein JL, Montecino M, Javed A, et al. Runx2 control of organization, assembly and activity of the regulatory machinery for skeletal gene expression. Oncogene. 2004;23(24):4315-29.

87. Komori T, Yagi H, Nomura S, Yamaguchi A, Sasaki K, Deguchi K, et al. Targeted disruption of Cbfa1 results in a complete lack of bone formation owing to maturational arrest of osteoblasts. Cell. 1997;89(5):755-64.
88. Rutkovskiy A, Stenslokken KO, Vaage IJ. Osteoblast Differentiation at a Glance. Med Sci Monit Basic Res. 2016;22:95-106.
89. Xie Y, Yin T, Wiegraebe W, He XC, Miller D, Stark D, et al. Detection of functional haematopoietic stem cell niche using real-time imaging. Nature. 2009;457(7225):97-101.
90. Visnjic D, Kalajzic I, Gronowicz G, Aguila HL, Clark SH, Lichtler AC, et al. Conditional ablation of the osteoblast lineage in Col2.3deltatk transgenic mice. J Bone Miner Res. 2001;16(12):2222-31.
91. Visnjic D, Kalajzic Z, Rowe DW, Katavic V, Lorenzo J, Aguila HL. Hematopoiesis is severely altered in mice with an induced osteoblast deficiency. Blood. 2004;103(9):3258-64.
92. Calvi LM, Adams GB, Weibrecht KW, Weber JM, Olson DP, Knight MC, et al. Osteoblastic cells regulate the haematopoietic stem cell niche. Nature. 2003;425(6960):841-6.
93. Ding L, Morrison SJ. Haematopoietic stem cells and early lymphoid progenitors occupy distinct bone marrow niches. Nature. 2013;495(7440):231-5.
94. Oswald J, Boxberger S, Jorgensen B, Feldmann S, Ehninger G, Bornhauser M, et al. Mesenchymal stem cells can be differentiated into endothelial cells in vitro. Stem Cells. 2004;22(3):377-84.
95. Yao L, Yokota T, Xia L, Kincade PW, McEver RP. Bone marrow dysfunction in mice lacking the cytokine receptor gp130 in endothelial cells. Blood. 2005;106(13):4093-101.
96. Ponomaryov T, Peled A, Petit I, Taichman RS, Habler L, Sandbank J, et al. Induction of the chemokine stromal-derived factor-1 following DNA damage improves human stem cell function. J Clin Invest. 2000;106(11):1331-9.
97. Rafii S, Shapiro F, Pettengell R, Ferris B, Nachman RL, Moore MA, et al. Human bone marrow microvascular endothelial cells support long-term proliferation and differentiation of myeloid and megakaryocytic progenitors. Blood. 1995;86(9):3353-63.
98. Ulyanova T, Scott LM, Priestley GV, Jiang Y, Nakamoto B, Koni PA, et al. VCAM-1 expression in adult hematopoietic and nonhematopoietic cells is controlled by tissue-inductive signals and reflects their developmental origin. Blood. 2005;106(1):86-94.
99. Horowitz MC, Berry R, Holtrup B, Sebo Z, Nelson T, Fretz JA, et al. Bone marrow adipocytes. Adipocyte. 2017;6(3):193-204.
100. Meunier P, Aaron J, Edouard C, Vignon G. Osteoporosis and the replacement of cell populations of the marrow by adipose tissue. A quantitative study of 84 iliac bone biopsies. Clin Orthop Relat Res. 1971;80:147-54.
101. Rosen ED, Sarraf P, Troy AE, Bradwin G, Moore K, Milstone DS, et al. PPAR gamma is required for the differentiation of adipose tissue in vivo and in vitro. Mol Cell. 1999;4(4):611-7.

102. Barak Y, Nelson MC, Ong ES, Jones YZ, Ruiz-Lozano P, Chien KR, et al. PPAR gamma is required for placental, cardiac, and adipose tissue development. Mol Cell. 1999;4(4):585-95.
103. Wang ND, Finegold MJ, Bradley A, Ou CN, Abdelsayed SV, Wilde MD, et al. Impaired energy homeostasis in C/EBP alpha knockout mice. Science. 1995;269(5227):1108-12.
104. Zhou BO, Yu H, Yue R, Zhao Z, Rios JJ, Naveiras O, et al. Bone marrow adipocytes promote the regeneration of stem cells and haematopoiesis by secreting SCF. Nat Cell Biol. 2017;19(8):891-903.
105. Mattiucci D, Maurizi G, Izzi V, Cenci L, Ciarlantini M, Mancini S, et al. Bone marrow adipocytes support hematopoietic stem cell survival. J Cell Physiol. 2018;233(2):1500-11.
106. Goldring MB, Tsuchimochi K, Ijiri K. The control of chondrogenesis. J Cell Biochem. 2006;97(1):33-44.
107. Bi W, Deng JM, Zhang Z, Behringer RR, de Crombrugghe B. Sox9 is required for cartilage formation. Nat Genet. 1999;22(1):85-9.
108. Bentzinger CF, Wang YX, Rudnicki MA. Building muscle: molecular regulation of myogenesis. Cold Spring Harb Perspect Biol. 2012;4(2).
109. Miyamoto T, Suda T. Differentiation and function of osteoclasts. Keio J Med. 2003;52(1):1-7.
110. Boyle WJ, Simonet WS, Lacey DL. Osteoclast differentiation and activation. Nature. 2003;423(6937):337-42.
111. Yasuda H, Shima N, Nakagawa N, Yamaguchi K, Kinosaki M, Mochizuki S, et al. Osteoclast differentiation factor is a ligand for osteoprotegerin/osteoclastogenesis-inhibitory factor and is identical to TRANCE/RANKL. Proc Natl Acad Sci U S A. 1998;95(7):3597-602.
112. Mansour A, Abou-Ezzi G, Sitnicka E, Jacobsen SE, Wakkach A, Blin-Wakkach C. Osteoclasts promote the formation of hematopoietic stem cell niches in the bone marrow. J Exp Med. 2012;209(3):537-49.
113. Liu K, Kaffes AJ. Iron deficiency anaemia: a review of diagnosis, investigation and management. Eur J Gastroenterol Hepatol. 2012;24(2):109-16.
114. Johnson-Wimbley TD, Graham DY. Diagnosis and management of iron deficiency anemia in the 21st century. Therap Adv Gastroenterol. 2011;4(3):177-84.
115. Brodsky RA, Jones RJ. Aplastic anaemia. Lancet. 2005;365(9471):1647-56.
116. Tefferi A, Vardiman JW. Myelodysplastic syndromes. N Engl J Med. 2009;361(19):1872-85.
117. Allart-Vorelli P, Porro B, Baguet F, Michel A, Cousson-Gelie F. Haematological cancer and quality of life: a systematic literature review. Blood Cancer J. 2015;5:e305.
118. Ramanarayanan J, Dunford LM, Baer MR, Sait SN, Lawrence W, McCarthy PL. Chronic myeloid leukemia after treatment of lymphoid malignancies: response to imatinib mesylate and favorable outcomes in three patients. Leuk Res. 2006;30(6):701-5.

119. Rajkumar SV, Kumar S. Multiple Myeloma: Diagnosis and Treatment. Mayo Clin Proc. 2016;91(1):101-19.
120. Kuppers R. The biology of Hodgkin's lymphoma. Nat Rev Cancer. 2009;9(1):15-27.
121. Estey E, Dohner H. Acute myeloid leukaemia. Lancet. 2006;368(9550):1894-907.
122. Lane SW, Scadden DT, Gilliland DG. The leukemic stem cell niche: current concepts and therapeutic opportunities. Blood. 2009;114(6):1150-7.
123. Kumar CC. Genetic abnormalities and challenges in the treatment of acute myeloid leukemia. Genes Cancer. 2011;2(2):95-107.
124. Juliusson G, Lazarevic V, Horstedt AS, Hagberg O, Hoglund M, Swedish Acute Leukemia Registry G. Acute myeloid leukemia in the real world: why population-based registries are needed. Blood. 2012;119(17):3890-9.
125. SEER Statistics: National Cancer Institute; [Available from: https://seer.cancer.gov/statfacts/.
126. Shysh AC, Nguyen LT, Guo M, Vaska M, Naugler C, Rashid-Kolvear F. The incidence of acute myeloid leukemia in Calgary, Alberta, Canada: a retrospective cohort study. BMC Public Health. 2017;18(1):94.
127. Cancer Research UK Statistics 2018 [Available from: https://www.cancerresearchuk.org/health-professional/cancer-statistics/statistics-by-cancer-type/leukaemia-aml - heading-Zero.
128. Tomaszewski EL, Fickley CE, Maddux L, Krupnick R, Bahceci E, Paty J, et al. The Patient Perspective on Living with Acute Myeloid Leukemia. Oncol Ther. 2016;4(2):225-38.
129. NHS Choices: Diagnosis of Acute Myeloid Leukaemia.
130. Dohner H, Estey EH, Amadori S, Appelbaum FR, Buchner T, Burnett AK, et al. Diagnosis and management of acute myeloid leukemia in adults: recommendations from an international expert panel, on behalf of the European LeukemiaNet. Blood. 2010;115(3):453-74.
131. Lowenberg B, Downing JR, Burnett A. Acute myeloid leukemia. N Engl J Med. 1999;341(14):1051-62.
132. Harris NL, Jaffe ES, Diebold J, Flandrin G, Muller-Hermelink HK, Vardiman J, et al. World Health Organization classification of neoplastic diseases of the hematopoietic and lymphoid tissues: report of the Clinical Advisory Committee meeting-Airlie House, Virginia, November 1997. J Clin Oncol. 1999;17(12):3835-49.
133. Stone RM, O'Donnell MR, Sekeres MA. Acute myeloid leukemia. Hematology Am Soc Hematol Educ Program. 2004:98-117.
134. Dombret H, Gardin C. An update of current treatments for adult acute myeloid leukemia. Blood. 2016;127(1):53-61.
135. Koreth J, Schlenk R, Kopecky KJ, Honda S, Sierra J, Djulbegovic BJ, et al. Allogeneic stem cell transplantation for acute myeloid leukemia in first complete remission: systematic review and meta-analysis of prospective clinical trials. JAMA. 2009;301(22):2349-61.

136. van Besien K. Allogeneic transplantation for AML and MDS: GVL versus GVHD and disease recurrence. Hematology Am Soc Hematol Educ Program. 2013;2013:56-62.
137. Bennett JM, Catovsky D, Daniel MT, Flandrin G, Galton DA, Gralnick HR, et al. Proposals for the classification of the acute leukaemias. French-American-British (FAB) co-operative group. Br J Haematol. 1976;33(4):451-8.
138. Bloomfield CD, Brunning RD. FAB M7: acute megakaryoblastic leukemia--beyond morphology. Ann Intern Med. 1985;103(3):450-2.
139. Lee EJ, Pollak A, Leavitt RD, Testa JR, Schiffer CA. Minimally differentiated acute nonlymphocytic leukemia: a distinct entity. Blood. 1987;70(5):1400-6.
140. Duchayne E, Demur C, Rubie H, Robert A, Dastugue N. Diagnosis of acute basophilic leukemia. Leuk Lymphoma. 1999;32(3-4):269-78.
141. Acute Myeloid Leukemia Staging 2011 [Available from: https://emedicine.medscape.com/article/2006750-overview.
142. Vardiman JW, Harris NL, Brunning RD. The World Health Organization (WHO) classification of the myeloid neoplasms. Blood. 2002;100(7):2292-302.
143. Vardiman JW, Thiele J, Arber DA, Brunning RD, Borowitz MJ, Porwit A, et al. The 2008 revision of the World Health Organization (WHO) classification of myeloid neoplasms and acute leukemia: rationale and important changes. Blood. 2009;114(5):937-51.
144. Byrd JC, Mrozek K, Dodge RK, Carroll AJ, Edwards CG, Arthur DC, et al. Pretreatment cytogenetic abnormalities are predictive of induction success, cumulative incidence of relapse, and overall survival in adult patients with de novo acute myeloid leukemia: results from Cancer and Leukemia Group B (CALGB 8461). Blood. 2002;100(13):4325-36.
145. Rowley JD. Identificaton of a translocation with quinacrine fluorescence in a patient with acute leukemia. Ann Genet. 1973;16(2):109-12.
146. Linggi B, Muller-Tidow C, van de Locht L, Hu M, Nip J, Serve H, et al. The t(8;21) fusion protein, AML1 ETO, specifically represses the transcription of the p14(ARF) tumor suppressor in acute myeloid leukemia. Nat Med. 2002;8(7):743-50.
147. Liu P, Tarle SA, Hajra A, Claxton DF, Marlton P, Freedman M, et al. Fusion between transcription factor CBF beta/PEBP2 beta and a myosin heavy chain in acute myeloid leukemia. Science. 1993;261(5124):1041-4.
148. Kogan SC, Lagasse E, Atwater S, Bae SC, Weissman I, Ito Y, et al. The PEBP2betaMYH11 fusion created by Inv(16)(p13;q22) in myeloid leukemia impairs neutrophil maturation and contributes to granulocytic dysplasia. Proc Natl Acad Sci U S A. 1998;95(20):11863-8.
149. Dohner H, Weisdorf DJ, Bloomfield CD. Acute Myeloid Leukemia. N Engl J Med. 2015;373(12):1136-52.
150. Prange KHM, Mandoli A, Kuznetsova T, Wang SY, Sotoca AM, Marneth AE, et al. MLL-AF9 and MLL-AF4 oncofusion proteins bind a distinct enhancer repertoire and target the RUNX1 program in 11q23 acute myeloid leukemia. Oncogene. 2017;36(23):3346-56.

151. Gaidzik V, Dohner K. Prognostic implications of gene mutations in acute myeloid leukemia with normal cytogenetics. Semin Oncol. 2008;35(4):346-55.
152. Cancer Genome Atlas Research N, Ley TJ, Miller C, Ding L, Raphael BJ, Mungall AJ, et al. Genomic and epigenomic landscapes of adult de novo acute myeloid leukemia. N Engl J Med. 2013;368(22):2059-74.
153. Schnittger S, Schoch C, Kern W, Mecucci C, Tschulik C, Martelli MF, et al. Nucleophosmin gene mutations are predictors of favorable prognosis in acute myelogenous leukemia with a normal karyotype. Blood. 2005;106(12):3733-9.
154. Falini B, Nicoletti I, Martelli MF, Mecucci C. Acute myeloid leukemia carrying cytoplasmic/mutated nucleophosmin (NPMc+ AML): biologic and clinical features. Blood. 2007;109(3):874-85.
155. Dohner K, Schlenk RF, Habdank M, Scholl C, Rucker FG, Corbacioglu A, et al. Mutant nucleophosmin (NPM1) predicts favorable prognosis in younger adults with acute myeloid leukemia and normal cytogenetics: interaction with other gene mutations. Blood. 2005;106(12):3740-6.
156. Marcucci G, Haferlach T, Dohner H. Molecular genetics of adult acute myeloid leukemia: prognostic and therapeutic implications. J Clin Oncol. 2011;29(5):475-86.
157. Marcucci G, Metzeler KH, Schwind S, Becker H, Maharry K, Mrozek K, et al. Age-related prognostic impact of different types of DNMT3A mutations in adults with primary cytogenetically normal acute myeloid leukemia. J Clin Oncol. 2012;30(7):742-50.
158. Shlush LI, Zandi S, Mitchell A, Chen WC, Brandwein JM, Gupta V, et al. Identification of pre-leukaemic haematopoietic stem cells in acute leukaemia. Nature. 2014;506(7488):328-33.
159. Maroc N, Rottapel R, Rosnet O, Marchetto S, Lavezzi C, Mannoni P, et al. Biochemical characterization and analysis of the transforming potential of the FLT3/FLK2 receptor tyrosine kinase. Oncogene. 1993;8(4):909-18.
160. Kelly LM, Liu Q, Kutok JL, Williams IR, Boulton CL, Gilliland DG. FLT3 internal tandem duplication mutations associated with human acute myeloid leukemias induce myeloproliferative disease in a murine bone marrow transplant model. Blood. 2002;99(1):310-8.
161. Gale RE, Green C, Allen C, Mead AJ, Burnett AK, Hills RK, et al. The impact of FLT3 internal tandem duplication mutant level, number, size, and interaction with NPM1 mutations in a large cohort of young adult patients with acute myeloid leukemia. Blood. 2008;111(5):2776-84.
162. Marcucci G, Maharry K, Wu YZ, Radmacher MD, Mrozek K, Margeson D, et al. IDH1 and IDH2 gene mutations identify novel molecular subsets within de novo cytogenetically normal acute myeloid leukemia: a Cancer and Leukemia Group B study. J Clin Oncol. 2010;28(14):2348-55.
163. Paschka P, Schlenk RF, Gaidzik VI, Habdank M, Kronke J, Bullinger L, et al. IDH1 and IDH2 mutations are frequent genetic alterations in acute myeloid leukemia and confer adverse prognosis in cytogenetically normal acute myeloid leukemia with NPM1 mutation without FLT3 internal tandem duplication. J Clin Oncol. 2010;28(22):3636-43.

164. Chou WC, Chou SC, Liu CY, Chen CY, Hou HA, Kuo YY, et al. TET2 mutation is an unfavorable prognostic factor in acute myeloid leukemia patients with intermediate-risk cytogenetics. Blood. 2011;118(14):3803-10.
165. Saultz JN, Garzon R. Acute Myeloid Leukemia: A Concise Review. J Clin Med. 2016;5(3).
166. Meyers S, Downing JR, Hiebert SW. Identification of AML-1 and the (8;21) translocation protein (AML-1/ETO) as sequence-specific DNA-binding proteins: the runt homology domain is required for DNA binding and protein-protein interactions. Mol Cell Biol. 1993;13(10):6336-45.
167. Mendler JH, Maharry K, Radmacher MD, Mrozek K, Becker H, Metzeler KH, et al. RUNX1 mutations are associated with poor outcome in younger and older patients with cytogenetically normal acute myeloid leukemia and with distinct gene and MicroRNA expression signatures. J Clin Oncol. 2012;30(25):3109-18.
168. Meshinchi S, Stirewalt DL, Alonzo TA, Zhang Q, Sweetser DA, Woods WG, et al. Activating mutations of RTK/ras signal transduction pathway in pediatric acute myeloid leukemia. Blood. 2003;102(4):1474-9.
169. Kiyoi H, Towatari M, Yokota S, Hamaguchi M, Ohno R, Saito H, et al. Internal tandem duplication of the FLT3 gene is a novel modality of elongation mutation which causes constitutive activation of the product. Leukemia. 1998;12(9):1333-7.
170. Ning ZQ, Li J, Arceci RJ. Signal transducer and activator of transcription 3 activation is required for Asp(816) mutant c-Kit-mediated cytokine-independent survival and proliferation in human leukemia cells. Blood. 2001;97(11):3559-67.
171. Longley BJ, Jr., Metcalfe DD, Tharp M, Wang X, Tyrrell L, Lu SZ, et al. Activating and dominant inactivating c-KIT catalytic domain mutations in distinct clinical forms of human mastocytosis. Proc Natl Acad Sci U S A. 1999;96(4):1609-14.
172. Rushworth SA, Murray MY, Zaitseva L, Bowles KM, MacEwan DJ. Identification of Bruton's tyrosine kinase as a therapeutic target in acute myeloid leukemia. Blood. 2014;123(8):1229-38.
173. Lewis TS, Shapiro PS, Ahn NG. Signal transduction through MAP kinase cascades. Adv Cancer Res. 1998;74:49-139.
174. Kim SC, Hahn JS, Min YH, Yoo NC, Ko YW, Lee WJ. Constitutive activation of extracellular signal-regulated kinase in human acute leukemias: combined role of activation of MEK, hyperexpression of extracellular signal-regulated kinase, and downregulation of a phosphatase, PAC1. Blood. 1999;93(11):3893-9.
175. Hayakawa F, Towatari M, Kiyoi H, Tanimoto M, Kitamura T, Saito H, et al. Tandem-duplicated Flt3 constitutively activates STAT5 and MAP kinase and introduces autonomous cell growth in IL-3-dependent cell lines. Oncogene. 2000;19(5):624-31.
176. Milella M, Kornblau SM, Estrov Z, Carter BZ, Lapillonne H, Harris D, et al. Therapeutic targeting of the MEK/MAPK signal transduction module in acute myeloid leukemia. J Clin Invest. 2001;108(6):851-9.

177. Porta C, Paglino C, Mosca A. Targeting PI3K/Akt/mTOR Signaling in Cancer. Front Oncol. 2014;4:64.
178. Fruman DA, Meyers RE, Cantley LC. Phosphoinositide kinases. Annu Rev Biochem. 1998;67:481-507.
179. Fresno Vara JA, Casado E, de Castro J, Cejas P, Belda-Iniesta C, Gonzalez-Baron M. PI3K/Akt signalling pathway and cancer. Cancer Treat Rev. 2004;30(2):193-204.
180. Park S, Chapuis N, Tamburini J, Bardet V, Cornillet-Lefebvre P, Willems L, et al. Role of the PI3K/AKT and mTOR signaling pathways in acute myeloid leukemia. Haematologica. 2010;95(5):819-28.
181. Ward AC, Touw I, Yoshimura A. The Jak-Stat pathway in normal and perturbed hematopoiesis. Blood. 2000;95(1):19-29.
182. Carter-Su C, Smit LS. Signaling via JAK tyrosine kinases: growth hormone receptor as a model system. Recent Prog Horm Res. 1998;53:61-82; discussion -3.
183. Valentino L, Pierre J. JAK/STAT signal transduction: regulators and implication in hematological malignancies. Biochem Pharmacol. 2006;71(6):713-21.
184. Spiekermann K, Biethahn S, Wilde S, Hiddemann W, Alves F. Constitutive activation of STAT transcription factors in acute myelogenous leukemia. Eur J Haematol. 2001;67(2):63-71.
185. Faderl S, Ferrajoli A, Harris D, Van Q, Kantarjian HM, Estrov Z. Atiprimod blocks phosphorylation of JAK-STAT and inhibits proliferation of acute myeloid leukemia (AML) cells. Leuk Res. 2007;31(1):91-5.
186. Valencia A, Roman-Gomez J, Cervera J, Such E, Barragan E, Bolufer P, et al. Wnt signaling pathway is epigenetically regulated by methylation of Wnt antagonists in acute myeloid leukemia. Leukemia. 2009;23(9):1658-66.
187. Guzman ML, Neering SJ, Upchurch D, Grimes B, Howard DS, Rizzieri DA, et al. Nuclear factor-kappaB is constitutively activated in primitive human acute myelogenous leukemia cells. Blood. 2001;98(8):2301-7.
188. DiNardo CD, Pratz KW, Letai A, Jonas BA, Wei AH, Thirman M, et al. Safety and preliminary efficacy of venetoclax with decitabine or azacitidine in elderly patients with previously untreated acute myeloid leukaemia: a non-randomised, open-label, phase 1b study. Lancet Oncol. 2018;19(2):216-28.
189. DiNardo C, Pratz KW, Potluri J, Pullarkat VA, Jonas BA, Wei AH, et al. Durable response with venetoclax in combination with decitabine or azacitadine in elderly patients with acute myeloid leukemia (AML). American Society of Clinical Oncology 2018.
190. Saygin C, Carraway HE. Emerging therapies for acute myeloid leukemia. J Hematol Oncol. 2017;10(1):93.
191. Palumbo A, Anderson K. Multiple myeloma. N Engl J Med. 2011;364(11):1046-60.
192. Rajkumar SV, Dimopoulos MA, Palumbo A, Blade J, Merlini G, Mateos MV, et al. International Myeloma Working Group updated criteria for the diagnosis of multiple myeloma. Lancet Oncol. 2014;15(12):e538-48.

193. Durie BG, Salmon SE. A clinical staging system for multiple myeloma. Correlation of measured myeloma cell mass with presenting clinical features, response to treatment, and survival. Cancer. 1975;36(3):842-54.
194. Kyle RA, Gertz MA, Witzig TE, Lust JA, Lacy MQ, Dispenzieri A, et al. Review of 1027 patients with newly diagnosed multiple myeloma. Mayo Clin Proc. 2003;78(1):21-33.
195. Ferlay J, Soerjomataram I, Dikshit R, Eser S, Mathers C, Rebelo M, et al. Cancer incidence and mortality worldwide: sources, methods and major patterns in GLOBOCAN 2012. Int J Cancer. 2015;136(5):E359-86.
196. Landgren O, Gridley G, Turesson I, Caporaso NE, Goldin LR, Baris D, et al. Risk of monoclonal gammopathy of undetermined significance (MGUS) and subsequent multiple myeloma among African American and white veterans in the United States. Blood. 2006;107(3):904-6.
197. Waxman AJ, Mink PJ, Devesa SS, Anderson WF, Weiss BM, Kristinsson SY, et al. Racial disparities in incidence and outcome in multiple myeloma: a population-based study. Blood. 2010;116(25):5501-6.
198. Smith A, Howell D, Patmore R, Jack A, Roman E. Incidence of haematological malignancy by sub-type: a report from the Haematological Malignancy Research Network. Br J Cancer. 2011;105(11):1684-92.
199. Kazandjian D. Multiple myeloma epidemiology and survival: A unique malignancy. Semin Oncol. 2016;43(6):676-81.
200. Landgren O, Kyle RA, Pfeiffer RM, Katzmann JA, Caporaso NE, Hayes RB, et al. Monoclonal gammopathy of undetermined significance (MGUS) consistently precedes multiple myeloma: a prospective study. Blood. 2009;113(22):5412-7.
201. Kyle RA, Therneau TM, Rajkumar SV, Larson DR, Plevak MF, Melton LJ, 3rd. Long-term follow-up of 241 patients with monoclonal gammopathy of undetermined significance: the original Mayo Clinic series 25 years later. Mayo Clin Proc. 2004;79(7):859-66.
202. Waldenstrom J. Studies on conditions associated with disturbed gamma globulin formation (gammopathies). Harvey Lect. 1960;56:211-31.
203. Rajkumar SV, Kyle RA, Buadi FK. Advances in the diagnosis, classification, risk stratification, and management of monoclonal gammopathy of undetermined significance: implications for recategorizing disease entities in the presence of evolving scientific evidence. Mayo Clin Proc. 2010;85(10):945-8.
204. International Myeloma Working G. Criteria for the classification of monoclonal gammopathies, multiple myeloma and related disorders: a report of the International Myeloma Working Group. Br J Haematol. 2003;121(5):749-57.
205. Kyle RA, Durie BG, Rajkumar SV, Landgren O, Blade J, Merlini G, et al. Monoclonal gammopathy of undetermined significance (MGUS) and smoldering (asymptomatic) multiple myeloma: IMWG consensus perspectives risk factors for progression and guidelines for monitoring and management. Leukemia. 2010;24(6):1121-7.
206. Gregersen H, Mellemkjaer L, Ibsen JS, Dahlerup JF, Thomassen L, Sorensen HT. The impact of M-component type and immunoglobulin

concentration on the risk of malignant transformation in patients with monoclonal gammopathy of undetermined significance. Haematologica. 2001;86(11):1172-9.
207. Rajkumar SV, Landgren O, Mateos MV. Smoldering multiple myeloma. Blood. 2015;125(20):3069-75.
208. Kyle RA, Remstein ED, Therneau TM, Dispenzieri A, Kurtin PJ, Hodnefield JM, et al. Clinical course and prognosis of smoldering (asymptomatic) multiple myeloma. N Engl J Med. 2007;356(25):2582-90.
209. Rajkumar SV. Preventive strategies in monoclonal gammopathy of undetermined significance and smoldering multiple myeloma. Am J Hematol. 2012;87(5):453-4.
210. Mateos MV, Hernandez MT, Giraldo P, de la Rubia J, de Arriba F, Lopez Corral L, et al. Lenalidomide plus dexamethasone for high-risk smoldering multiple myeloma. N Engl J Med. 2013;369(5):438-47.
211. Nakaya A, Fujita S, Satake A, Nakanishi T, Azuma Y, Tsubokura Y, et al. Impact of CRAB Symptoms in Survival of Patients with Symptomatic Myeloma in Novel Agent Era. Hematol Rep. 2017;9(1):6887.
212. Fernandez de Larrea C, Kyle RA, Durie BG, Ludwig H, Usmani S, Vesole DH, et al. Plasma cell leukemia: consensus statement on diagnostic requirements, response criteria and treatment recommendations by the International Myeloma Working Group. Leukemia. 2013;27(4):780-91.
213. Noel P, Kyle RA. Plasma cell leukemia: an evaluation of response to therapy. Am J Med. 1987;83(6):1062-8.
214. Coleman RE. Skeletal complications of malignancy. Cancer. 1997;80(8 Suppl):1588-94.
215. Giuliani N, Colla S, Morandi F, Lazzaretti M, Sala R, Bonomini S, et al. Myeloma cells block RUNX2/CBFA1 activity in human bone marrow osteoblast progenitors and inhibit osteoblast formation and differentiation. Blood. 2005;106(7):2472-83.
216. Knudsen LM, Hippe E, Hjorth M, Holmberg E, Westin J. Renal function in newly diagnosed multiple myeloma--a demographic study of 1353 patients. The Nordic Myeloma Study Group. Eur J Haematol. 1994;53(4):207-12.
217. Katzmann JA, Dispenzieri A, Kyle RA, Snyder MR, Plevak MF, Larson DR, et al. Elimination of the need for urine studies in the screening algorithm for monoclonal gammopathies by using serum immunofixation and free light chain assays. Mayo Clin Proc. 2006;81(12):1575-8.
218. Chawla SS, Kumar SK, Dispenzieri A, Greenberg AJ, Larson DR, Kyle RA, et al. Clinical Course and Prognosis of Non-Secretory Multiple Myeloma. Eur J Haematol. 2015.
219. Hillengass J, Fechtner K, Weber MA, Bauerle T, Ayyaz S, Heiss C, et al. Prognostic significance of focal lesions in whole-body magnetic resonance imaging in patients with asymptomatic multiple myeloma. J Clin Oncol. 2010;28(9):1606-10.
220. Solly S. Remarks on the pathology of mollities ossium; with cases. Med Chir Trans. 1844;27:435-98 8.

221. Blokhin N, Larionov L, Perevodchikova N, Chebotareva L, Merkulova N. [Clinical experiences with sarcolysin in neoplastic diseases]. Ann N Y Acad Sci. 1958;68(3):1128-32.
222. Mass RE. A comparison of the effect of prednisone and a placebo in the treatment of multiple myeloma. Cancer Chemother Rep. 1962;16:257-9.
223. Singhal S, Mehta J, Desikan R, Ayers D, Roberson P, Eddlemon P, et al. Antitumor activity of thalidomide in refractory multiple myeloma. N Engl J Med. 1999;341(21):1565-71.
224. Richardson PG, Barlogie B, Berenson J, Singhal S, Jagannath S, Irwin D, et al. A phase 2 study of bortezomib in relapsed, refractory myeloma. N Engl J Med. 2003;348(26):2609-17.
225. San Miguel JF, Schlag R, Khuageva NK, Dimopoulos MA, Shpilberg O, Kropff M, et al. Bortezomib plus melphalan and prednisone for initial treatment of multiple myeloma. N Engl J Med. 2008;359(9):906-17.
226. Jiwani S, Bornhost J, Alapat D. Biphenotypic plasma cell myeloma: two cases of plasma cell neoplasm with a coexpression of kappa and lambda light chains. Int J Clin Exp Pathol. 2015;8(7):8536-44.
227. Schroeder HW, Jr., Cavacini L. Structure and function of immunoglobulins. J Allergy Clin Immunol. 2010;125(2 Suppl 2):S41-52.
228. Blade J, Lust JA, Kyle RA. Immunoglobulin D multiple myeloma: presenting features, response to therapy, and survival in a series of 53 cases. J Clin Oncol. 1994;12(11):2398-404.
229. Kumar S, Fonseca R, Ketterling RP, Dispenzieri A, Lacy MQ, Gertz MA, et al. Trisomies in multiple myeloma: impact on survival in patients with high-risk cytogenetics. Blood. 2012;119(9):2100-5.
230. Kuehl WM, Bergsagel PL. Multiple myeloma: evolving genetic events and host interactions. Nat Rev Cancer. 2002;2(3):175-87.
231. Bergsagel PL, Kuehl WM. Chromosome translocations in multiple myeloma. Oncogene. 2001;20(40):5611-22.
232. Lohr JG, Stojanov P, Carter SL, Cruz-Gordillo P, Lawrence MS, Auclair D, et al. Widespread genetic heterogeneity in multiple myeloma: implications for targeted therapy. Cancer Cell. 2014;25(1):91-101.
233. Bazzi M, Badros A. Multiple myeloma: Implementing signaling pathways and molecular biology in clinical trials. Cancer Biol Ther. 2010;10(9):830-8.
234. Mitsiades CS, Mitsiades N, Munshi NC, Anderson KC. Focus on multiple myeloma. Cancer Cell. 2004;6(5):439-44.
235. Han K, Xu X, Chen G, Zeng Y, Zhu J, Du X, et al. Identification of a promising PI3K inhibitor for the treatment of multiple myeloma through the structural optimization. J Hematol Oncol. 2014;7:9.
236. de Oliveira MB, Fook-Alves VL, Eugenio AIP, Fernando RC, Sanson LFG, de Carvalho MF, et al. Anti-myeloma effects of ruxolitinib combined with bortezomib and lenalidomide: A rationale for JAK/STAT pathway inhibition in myeloma patients. Cancer Lett. 2017;403:206-15.
237. Hideshima T, Akiyama M, Hayashi T, Richardson P, Schlossman R, Chauhan D, et al. Targeting p38 MAPK inhibits multiple myeloma cell growth in the bone marrow milieu. Blood. 2003;101(2):703-5.

238. Pomerantz JL, Baltimore D. Two pathways to NF-kappaB. Mol Cell. 2002;10(4):693-5.
239. Moreaux J, Veyrune JL, De Vos J, Klein B. APRIL is overexpressed in cancer: link with tumor progression. BMC Cancer. 2009;9:83.
240. Neri P, Kumar S, Fulciniti MT, Vallet S, Chhetri S, Mukherjee S, et al. Neutralizing B-cell activating factor antibody improves survival and inhibits osteoclastogenesis in a severe combined immunodeficient human multiple myeloma model. Clin Cancer Res. 2007;13(19):5903-9.
241. Hayden MS, Ghosh S. Shared principles in NF-kappaB signaling. Cell. 2008;132(3):344-62.
242. Demchenko YN, Kuehl WM. A critical role for the NFkB pathway in multiple myeloma. Oncotarget. 2010;1(1):59-68.
243. Beg AA, Baltimore D. An essential role for NF-kappaB in preventing TNF-alpha-induced cell death. Science. 1996;274(5288):782-4.
244. van de Donk N, Richardson PG, Malavasi F. CD38 antibodies in multiple myeloma: back to the future. Blood. 2018;131(1):13-29.
245. Reinherz EL, Kung PC, Goldstein G, Levey RH, Schlossman SF. Discrete stages of human intrathymic differentiation: analysis of normal thymocytes and leukemic lymphoblasts of T-cell lineage. Proc Natl Acad Sci U S A. 1980;77(3):1588-92.
246. Funaro A, Reinis M, Trubiani O, Santi S, Di Primio R, Malavasi F. CD38 functions are regulated through an internalization step. J Immunol. 1998;160(5):2238-47.
247. Ferrero E, Malavasi F. Human CD38, a leukocyte receptor and ectoenzyme, is a member of a novel eukaryotic gene family of nicotinamide adenine dinucleotide+-converting enzymes: extensive structural homology with the genes for murine bone marrow stromal cell antigen 1 and aplysian ADP-ribosyl cyclase. J Immunol. 1997;159(8):3858-65.
248. Deaglio S, Morra M, Mallone R, Ausiello CM, Prager E, Garbarino G, et al. Human CD38 (ADP-ribosyl cyclase) is a counter-receptor of CD31, an Ig superfamily member. J Immunol. 1998;160(1):395-402.
249. Lokhorst HM, Plesner T, Laubach JP, Nahi H, Gimsing P, Hansson M, et al. Targeting CD38 with Daratumumab Monotherapy in Multiple Myeloma. N Engl J Med. 2015;373(13):1207-19.
250. de Weers M, Tai YT, van der Veer MS, Bakker JM, Vink T, Jacobs DC, et al. Daratumumab, a novel therapeutic human CD38 monoclonal antibody, induces killing of multiple myeloma and other hematological tumors. J Immunol. 2011;186(3):1840-8.
251. Lonial S, Weiss BM, Usmani SZ, Singhal S, Chari A, Bahlis NJ, et al. Daratumumab monotherapy in patients with treatment-refractory multiple myeloma (SIRIUS): an open-label, randomised, phase 2 trial. Lancet. 2016;387(10027):1551-60.
252. Bhatnagar V, Gormley NJ, Luo L, Shen YL, Sridhara R, Subramaniam S, et al. FDA Approval Summary: Daratumumab for Treatment of Multiple Myeloma After One Prior Therapy. Oncologist. 2017;22(11):1347-53.

253. Paget S. The distribution of secondary growths in cancer of the breast. 1889. Cancer Metastasis Rev. 1989;8(2):98-101.
254. Fidler IJ. The pathogenesis of cancer metastasis: the 'seed and soil' hypothesis revisited. Nat Rev Cancer. 2003;3(6):453-8.
255. Bissell MJ, Radisky D. Putting tumours in context. Nat Rev Cancer. 2001;1(1):46-54.
256. Senthebane DA, Rowe A, Thomford NE, Shipanga H, Munro D, Mazeedi M, et al. The Role of Tumor Microenvironment in Chemoresistance: To Survive, Keep Your Enemies Closer. Int J Mol Sci. 2017;18(7).
257. Shafat MS, Gnaneswaran B, Bowles KM, Rushworth SA. The bone marrow microenvironment - Home of the leukemic blasts. Blood Rev. 2017;31(5):277-86.
258. Bendall LJ, Daniel A, Kortlepel K, Gottlieb DJ. Bone marrow adherent layers inhibit apoptosis of acute myeloid leukemia cells. Exp Hematol. 1994;22(13):1252-60.
259. Garrido SM, Appelbaum FR, Willman CL, Banker DE. Acute myeloid leukemia cells are protected from spontaneous and drug-induced apoptosis by direct contact with a human bone marrow stromal cell line (HS-5). Exp Hematol. 2001;29(4):448-57.
260. Pezeshkian B, Donnelly C, Tamburo K, Geddes T, Madlambayan GJ. Leukemia Mediated Endothelial Cell Activation Modulates Leukemia Cell Susceptibility to Chemotherapy through a Positive Feedback Loop Mechanism. PLoS One. 2013;8(4):e60823.
261. Ryningen A, Wergeland L, Glenjen N, Gjertsen BT, Bruserud O. In vitro crosstalk between fibroblasts and native human acute myelogenous leukemia (AML) blasts via local cytokine networks results in increased proliferation and decreased apoptosis of AML cells as well as increased levels of proangiogenic Interleukin 8. Leuk Res. 2005;29(2):185-96.
262. Burger JA, Peled A. CXCR4 antagonists: targeting the microenvironment in leukemia and other cancers. Leukemia. 2009;23(1):43-52.
263. Tavor S, Petit I. Can inhibition of the SDF-1/CXCR4 axis eradicate acute leukemia? Semin Cancer Biol. 2010;20(3):178-85.
264. Xia B, Tian C, Guo S, Zhang L, Zhao D, Qu F, et al. c-Myc plays part in drug resistance mediated by bone marrow stromal cells in acute myeloid leukemia. Leuk Res. 2015;39(1):92-9.
265. Sansone P, Bromberg J. Targeting the interleukin-6/Jak/stat pathway in human malignancies. J Clin Oncol. 2012;30(9):1005-14.
266. Abdul-Aziz AM, Shafat MS, Mehta TK, Di Palma F, Lawes MJ, Rushworth SA, et al. MIF-Induced Stromal PKCbeta/IL8 Is Essential in Human Acute Myeloid Leukemia. Cancer Res. 2017;77(2):303-11.
267. Waugh DJ, Wilson C. The interleukin-8 pathway in cancer. Clin Cancer Res. 2008;14(21):6735-41.
268. Becker PS. Dependence of acute myeloid leukemia on adhesion within the bone marrow microenvironment. ScientificWorldJournal. 2012;2012:856467.

269. Sier CF, Zuidwijk K, Zijlmans HJ, Hanemaaijer R, Mulder-Stapel AA, Prins FA, et al. EMMPRIN-induced MMP-2 activation cascade in human cervical squamous cell carcinoma. Int J Cancer. 2006;118(12):2991-8.
270. Zhou J, Zhu P, Jiang JL, Zhang Q, Wu ZB, Yao XY, et al. Involvement of CD147 in overexpression of MMP-2 and MMP-9 and enhancement of invasive potential of PMA-differentiated THP-1. BMC Cell Biol. 2005;6(1):25.
271. Zhang S, Wang X, Li G, Chong Y, Zhang J, Guo X, et al. Osteoclast regulation of osteoblasts via RANKRANKL reverse signal transduction in vitro. Mol Med Rep. 2017;16(4):3994-4000.
272. Schmiedel BJ, Nuebling T, Steinbacher J, Malinovska A, Wende CM, Azuma M, et al. Receptor activator for NF-kappaB ligand in acute myeloid leukemia: expression, function, and modulation of NK cell immunosurveillance. J Immunol. 2013;190(2):821-31.
273. Shafat MS, Oellerich T, Mohr S, Robinson SD, Edwards DR, Marlein CR, et al. Leukemic blasts program bone marrow adipocytes to generate a protumoral microenvironment. Blood. 2017;129(10):1320-32.
274. Ye H, Adane B, Khan N, Sullivan T, Minhajuddin M, Gasparetto M, et al. Leukemic Stem Cells Evade Chemotherapy by Metabolic Adaptation to an Adipose Tissue Niche. Cell Stem Cell. 2016;19(1):23-37.
275. Lee EA, Angka L, Rota SG, Hanlon T, Mitchell A, Hurren R, et al. Targeting Mitochondria with Avocatin B Induces Selective Leukemia Cell Death. Cancer Res. 2015;75(12):2478-88.
276. Rashidi A, Uy GL. Targeting the microenvironment in acute myeloid leukemia. Curr Hematol Malig Rep. 2015;10(2):126-31.
277. Konopleva MY, Jordan CT. Leukemia stem cells and microenvironment: biology and therapeutic targeting. J Clin Oncol. 2011;29(5):591-9.
278. Hole PS, Zabkiewicz J, Munje C, Newton Z, Pearn L, White P, et al. Overproduction of NOX-derived ROS in AML promotes proliferation and is associated with defective oxidative stress signaling. Blood. 2013;122(19):3322-30.
279. Rada B, Leto TL. Oxidative innate immune defenses by Nox/Duox family NADPH oxidases. Contrib Microbiol. 2008;15:164-87.
280. Nefedova Y, Landowski TH, Dalton WS. Bone marrow stromal-derived soluble factors and direct cell contact contribute to de novo drug resistance of myeloma cells by distinct mechanisms. Leukemia. 2003;17(6):1175-82.
281. Alsayed Y, Ngo H, Runnels J, Leleu X, Singha UK, Pitsillides CM, et al. Mechanisms of regulation of CXCR4/SDF-1 (CXCL12)-dependent migration and homing in multiple myeloma. Blood. 2007;109(7):2708-17.
282. Manier S, Sacco A, Leleu X, Ghobrial IM, Roccaro AM. Bone marrow microenvironment in multiple myeloma progression. J Biomed Biotechnol. 2012;2012:157496.
283. Nefedova Y, Cheng P, Alsina M, Dalton WS, Gabrilovich DI. Involvement of Notch-1 signaling in bone marrow stroma-mediated de novo drug resistance of myeloma and other malignant lymphoid cell lines. Blood. 2004;103(9):3503-10.

284. Kumar S, Witzig TE, Timm M, Haug J, Wellik L, Fonseca R, et al. Expression of VEGF and its receptors by myeloma cells. Leukemia. 2003;17(10):2025-31.
285. Roccaro AM, Sacco A, Maiso P, Azab AK, Tai YT, Reagan M, et al. BM mesenchymal stromal cell-derived exosomes facilitate multiple myeloma progression. J Clin Invest. 2013;123(4):1542-55.
286. Dinarello CA. Interleukin-1 in the pathogenesis and treatment of inflammatory diseases. Blood. 2011;117(14):3720-32.
287. Piddock RE, Marlein CR, Abdul-Aziz A, Shafat MS, Auger MJ, Bowles KM, et al. Myeloma-derived macrophage inhibitory factor regulates bone marrow stromal cell-derived IL-6 via c-MYC. J Hematol Oncol. 2018;11(1):66.
288. Hideshima T, Mitsiades C, Tonon G, Richardson PG, Anderson KC. Understanding multiple myeloma pathogenesis in the bone marrow to identify new therapeutic targets. Nat Rev Cancer. 2007;7(8):585-98.
289. Lust JA, Lacy MQ, Zeldenrust SR, Dispenzieri A, Gertz MA, Witzig TE, et al. Induction of a chronic disease state in patients with smoldering or indolent multiple myeloma by targeting interleukin 1{beta}-induced interleukin 6 production and the myeloma proliferative component. Mayo Clin Proc. 2009;84(2):114-22.
290. Yaccoby S, Pearse RN, Johnson CL, Barlogie B, Choi Y, Epstein J. Myeloma interacts with the bone marrow microenvironment to induce osteoclastogenesis and is dependent on osteoclast activity. Br J Haematol. 2002;116(2):278-90.
291. Tanaka Y, Abe M, Hiasa M, Oda A, Amou H, Nakano A, et al. Myeloma cell-osteoclast interaction enhances angiogenesis together with bone resorption: a role for vascular endothelial cell growth factor and osteopontin. Clin Cancer Res. 2007;13(3):816-23.
292. Urbaniak-Kujda D, Kapelko-Slowik K, Prajs I, Dybko J, Wolowiec D, Biernat M, et al. Increased expression of metalloproteinase-2 and -9 (MMP-2, MMP-9), tissue inhibitor of metalloproteinase-1 and -2 (TIMP-1, TIMP-2), and EMMPRIN (CD147) in multiple myeloma. Hematology. 2016;21(1):26-33.
293. Arendt BK, Walters DK, Wu X, Tschumper RC, Jelinek DF. Multiple myeloma dell-derived microvesicles are enriched in CD147 expression and enhance tumor cell proliferation. Oncotarget. 2014;5(14):5686-99.
294. Karadag A, Oyajobi BO, Apperley JF, Russell RG, Croucher PI. Human myeloma cells promote the production of interleukin 6 by primary human osteoblasts. Br J Haematol. 2000;108(2):383-90.
295. Tian E, Zhan F, Walker R, Rasmussen E, Ma Y, Barlogie B, et al. The role of the Wnt-signaling antagonist DKK1 in the development of osteolytic lesions in multiple myeloma. N Engl J Med. 2003;349(26):2483-94.
296. DeBerardinis RJ, Thompson CB. Cellular metabolism and disease: what do metabolic outliers teach us? Cell. 2012;148(6):1132-44.
297. Bonora M, Patergnani S, Rimessi A, De Marchi E, Suski JM, Bononi A, et al. ATP synthesis and storage. Purinergic Signal. 2012;8(3):343-57.
298. Kennedy EP, Lehninger AL. Oxidation of fatty acids and tricarboxylic acid cycle intermediates by isolated rat liver mitochondria. J Biol Chem. 1949;179(2):957-72.

299. Lenaz G, Genova ML. Structure and organization of mitochondrial respiratory complexes: a new understanding of an old subject. Antioxid Redox Signal. 2010;12(8):961-1008.
300. Walker JE. The regulation of catalysis in ATP synthase. Curr Opin Struct Biol. 1994;4(6):912-8.
301. Ferguson SJ. ATP synthase: from sequence to ring size to the P/O ratio. Proc Natl Acad Sci U S A. 2010;107(39):16755-6.
302. Wallace DC. A mitochondrial paradigm of metabolic and degenerative diseases, aging, and cancer: a dawn for evolutionary medicine. Annu Rev Genet. 2005;39:359-407.
303. Sato M, Sato K. Maternal inheritance of mitochondrial DNA by diverse mechanisms to eliminate paternal mitochondrial DNA. Biochim Biophys Acta. 2013;1833(8):1979-84.
304. Chan DC. Mitochondria: dynamic organelles in disease, aging, and development. Cell. 2006;125(7):1241-52.
305. Scarpulla RC. Metabolic control of mitochondrial biogenesis through the PGC-1 family regulatory network. Biochim Biophys Acta. 2011;1813(7):1269-78.
306. Warburg O. On the origin of cancer cells. Science. 1956;123(3191):309-14.
307. Hsu PP, Sabatini DM. Cancer cell metabolism: Warburg and beyond. Cell. 2008;134(5):703-7.
308. Fantin VR, St-Pierre J, Leder P. Attenuation of LDH-A expression uncovers a link between glycolysis, mitochondrial physiology, and tumor maintenance. Cancer Cell. 2006;9(6):425-34.
309. Rodriguez-Enriquez S, Carreno-Fuentes L, Gallardo-Perez JC, Saavedra E, Quezada H, Vega A, et al. Oxidative phosphorylation is impaired by prolonged hypoxia in breast and possibly in cervix carcinoma. Int J Biochem Cell Biol. 2010;42(10):1744-51.
310. Duvel K, Yecies JL, Menon S, Raman P, Lipovsky AI, Souza AL, et al. Activation of a metabolic gene regulatory network downstream of mTOR complex 1. Mol Cell. 2010;39(2):171-83.
311. Suganuma K, Miwa H, Imai N, Shikami M, Gotou M, Goto M, et al. Energy metabolism of leukemia cells: glycolysis versus oxidative phosphorylation. Leuk Lymphoma. 2010;51(11):2112-9.
312. Farge T, Saland E, de Toni F, Aroua N, Hosseini M, Perry R, et al. Chemotherapy-Resistant Human Acute Myeloid Leukemia Cells Are Not Enriched for Leukemic Stem Cells but Require Oxidative Metabolism. Cancer Discov. 2017;7(7):716-35.
313. Khan AUH, Rathore MG, Allende-Vega N, Vo DN, Belkhala S, Orecchioni S, et al. Human Leukemic Cells performing Oxidative Phosphorylation (OXPHOS) Generate an Antioxidant Response Independently of Reactive Oxygen species (ROS) Production. EBioMedicine. 2016;3:43-53.
314. Boultwood J, Fidler C, Mills KI, Frodsham PM, Kusec R, Gaiger A, et al. Amplification of mitochondrial DNA in acute myeloid leukaemia. Br J Haematol. 1996;95(2):426-31.

315. Skrtic M, Sriskanthadevan S, Jhas B, Gebbia M, Wang X, Wang Z, et al. Inhibition of mitochondrial translation as a therapeutic strategy for human acute myeloid leukemia. Cancer Cell. 2011;20(5):674-88.
316. Sanchez WY, McGee SL, Connor T, Mottram B, Wilkinson A, Whitehead JP, et al. Dichloroacetate inhibits aerobic glycolysis in multiple myeloma cells and increases sensitivity to bortezomib. Br J Cancer. 2013;108(8):1624-33.
317. Fujiwara S, Kawano Y, Yuki H, Okuno Y, Nosaka K, Mitsuya H, et al. PDK1 inhibition is a novel therapeutic target in multiple myeloma. Br J Cancer. 2013;108(1):170-8.
318. Dalva-Aydemir S, Bajpai R, Martinez M, Adekola KU, Kandela I, Wei C, et al. Targeting the metabolic plasticity of multiple myeloma with FDA-approved ritonavir and metformin. Clin Cancer Res. 2015;21(5):1161-71.
319. Borsi E, Perrone G, Terragna C, Martello M, Dico AF, Solaini G, et al. Hypoxia inducible factor-1 alpha as a therapeutic target in multiple myeloma. Oncotarget. 2014;5(7):1779-92.
320. Chen H, Chan DC. Mitochondrial dynamics--fusion, fission, movement, and mitophagy--in neurodegenerative diseases. Hum Mol Genet. 2009;18(R2):R169-76.
321. Rustom A, Saffrich R, Markovic I, Walther P, Gerdes HH. Nanotubular highways for intercellular organelle transport. Science. 2004;303(5660):1007-10.
322. Kukat A, Kukat C, Brocher J, Schafer I, Krohne G, Trounce IA, et al. Generation of rho0 cells utilizing a mitochondrially targeted restriction endonuclease and comparative analyses. Nucleic Acids Res. 2008;36(7):e44.
323. Spees JL, Olson SD, Whitney MJ, Prockop DJ. Mitochondrial transfer between cells can rescue aerobic respiration. Proc Natl Acad Sci U S A. 2006;103(5):1283-8.
324. Cho YM, Kim JH, Kim M, Park SJ, Koh SH, Ahn HS, et al. Mesenchymal stem cells transfer mitochondria to the cells with virtually no mitochondrial function but not with pathogenic mtDNA mutations. PLoS One. 2012;7(3):e32778.
325. Tan AS, Baty JW, Dong LF, Bezawork-Geleta A, Endaya B, Goodwin J, et al. Mitochondrial genome acquisition restores respiratory function and tumorigenic potential of cancer cells without mitochondrial DNA. Cell Metab. 2015;21(1):81-94.
326. Pasquier J, Guerrouahen BS, Al Thawadi H, Ghiabi P, Maleki M, Abu-Kaoud N, et al. Preferential transfer of mitochondria from endothelial to cancer cells through tunneling nanotubes modulates chemoresistance. J Transl Med. 2013;11:94.
327. Lou E, Fujisawa S, Morozov A, Barlas A, Romin Y, Dogan Y, et al. Tunneling nanotubes provide a unique conduit for intercellular transfer of cellular contents in human malignant pleural mesothelioma. PLoS One. 2012;7(3):e33093.
328. Antanaviciute I, Rysevaite K, Liutkevicius V, Marandykina A, Rimkute L, Sveikatiene R, et al. Long-distance communication between laryngeal carcinoma cells. PLoS One. 2014;9(6):e99196.

329. Lu J, Zheng X, Li F, Yu Y, Chen Z, Liu Z, et al. Tunneling nanotubes promote intercellular mitochondria transfer followed by increased invasiveness in bladder cancer cells. Oncotarget. 2017;8(9):15539-52.
330. Islam MN, Das SR, Emin MT, Wei M, Sun L, Westphalen K, et al. Mitochondrial transfer from bone-marrow-derived stromal cells to pulmonary alveoli protects against acute lung injury. Nat Med. 2012;18(5):759-65.
331. Hayakawa K, Esposito E, Wang X, Terasaki Y, Liu Y, Xing C, et al. Transfer of mitochondria from astrocytes to neurons after stroke. Nature. 2016;535(7613):551-5.
332. Berridge MV, McConnell MJ, Grasso C, Bajzikova M, Kovarova J, Neuzil J. Horizontal transfer of mitochondria between mammalian cells: beyond co-culture approaches. Curr Opin Genet Dev. 2016;38:75-82.
333. Wang X, Gerdes HH. Transfer of mitochondria via tunneling nanotubes rescues apoptotic PC12 cells. Cell Death Differ. 2015;22(7):1181-91.
334. Dong LF, Kovarova J, Bajzikova M, Bezawork-Geleta A, Svec D, Endaya B, et al. Horizontal transfer of whole mitochondria restores tumorigenic potential in mitochondrial DNA-deficient cancer cells. Elife. 2017;6.
335. Murray MY, Zaitseva L, Auger MJ, Craig JI, MacEwan DJ, Rushworth SA, et al. Ibrutinib inhibits BTK-driven NF-kappaB p65 activity to overcome bortezomib-resistance in multiple myeloma. Cell Cycle. 2015;14(14):2367-75.
336. Zaitseva L, Cherepanov P, Leyens L, Wilson SJ, Rasaiyaah J, Fassati A. HIV-1 exploits importin 7 to maximize nuclear import of its DNA genome. Retrovirology. 2009;6:11.
337. Hogan CJ, Shpall EJ, McNulty O, McNiece I, Dick JE, Shultz LD, et al. Engraftment and development of human CD34(+)-enriched cells from umbilical cord blood in NOD/LtSz-scid/scid mice. Blood. 1997;90(1):85-96.
338. Piddock RE, Loughran N, Marlein CR, Robinson SD, Edwards DR, Yu S, et al. PI3Kdelta and PI3Kgamma isoforms have distinct functions in regulating pro-tumoural signalling in the multiple myeloma microenvironment. Blood Cancer J. 2017;7(3):e539.
339. Abdul-Aziz AM, Shafat MS, Sun Y, Marlein CR, Piddock RE, Robinson SD, et al. HIF1alpha drives chemokine factor pro-tumoral signaling pathways in acute myeloid leukemia. Oncogene. 2018;37(20):2676-86.
340. Zaitseva L, Myers R, Fassati A. tRNAs promote nuclear import of HIV-1 intracellular reverse transcription complexes. PLoS Biol. 2006;4(10):e332.
341. Lew WY, Bayna E, Molle ED, Dalton ND, Lai NC, Bhargava V, et al. Recurrent exposure to subclinical lipopolysaccharide increases mortality and induces cardiac fibrosis in mice. PLoS One. 2013;8(4):e61057.
342. Vick B, Rothenberg M, Sandhofer N, Carlet M, Finkenzeller C, Krupka C, et al. An advanced preclinical mouse model for acute myeloid leukemia using patients' cells of various genetic subgroups and in vivo bioluminescence imaging. PLoS One. 2015;10(3):e0120925.
343. Ma Y, Gao M, Liu D. N-acetylcysteine Protects Mice from High Fat Diet-induced Metabolic Disorders. Pharm Res. 2016;33(8):2033-42.

344. Valle I, Alvarez-Barrientos A, Arza E, Lamas S, Monsalve M. PGC-1alpha regulates the mitochondrial antioxidant defense system in vascular endothelial cells. Cardiovasc Res. 2005;66(3):562-73.
345. Buteyn NJ, Fatehchand K, Santhanam R, Fang H, Dettorre GM, Gautam S, et al. Anti-leukemic effects of all-trans retinoic acid in combination with Daratumumab in acute myeloid leukemia. Int Immunol. 2018;30(8):375-83.
346. Deaglio S, Aydin S, Grand MM, Vaisitti T, Bergui L, D'Arena G, et al. CD38/CD31 interactions activate genetic pathways leading to proliferation and migration in chronic lymphocytic leukemia cells. Mol Med. 2010;16(3-4):87-91.
347. Ivanov AV, Bartosch B, Isaguliants MG. Oxidative Stress in Infection and Consequent Disease. Oxid Med Cell Longev. 2017;2017:3496043.
348. Pei S, Minhajuddin M, Adane B, Khan N, Stevens BM, Mack SC, et al. AMPK/FIS1-Mediated Mitophagy Is Required for Self-Renewal of Human AML Stem Cells. Cell Stem Cell. 2018;23(1):86-100 e6.
349. Moschoi R, Imbert V, Nebout M, Chiche J, Mary D, Prebet T, et al. Protective mitochondrial transfer from bone marrow stromal cells to acute myeloid leukemic cells during chemotherapy. Blood. 2016;128(2):253-64.
350. Houten SM, Wanders RJ. A general introduction to the biochemistry of mitochondrial fatty acid beta-oxidation. J Inherit Metab Dis. 2010;33(5):469-77.
351. Golan K, Wellendorf A, Takihara Y, Kumari A, Khatib-Massalha E, Kollit O, et al. Mitochondria Transfer from Hematopoietic Stem and Progenitor Cells to Pdgfrα+/Sca-1-/CD48dim BM Stromal Cells Via CX43 Gap Junctions and AMPK Signaling Inversely Regulate ROS Generation in Both Cell Populations. Blood. 2016;128(22):5.
352. Kumar B, Garcia M, Weng L, Jung X, Murakami JL, Hu X, et al. Acute myeloid leukemia transforms the bone marrow niche into a leukemia-permissive microenvironment through exosome secretion. Leukemia. 2018;32(3):575-87.
353. Battula V, L., Le P, M., Sun J, Mu H, McQueen T, Shpall E, J., et al. Acute Myeloid Leukemia (AML) Cells Alter the Bone Marrow Microenvironment By Inducing Osteogenic and Suppressing Adipogenic Differentiation of MSCs through BMP-RUNX2-CTGF Mediated Mechanisms. Blood. 2015;126(23):2403.
354. Corn PG. The tumor microenvironment in prostate cancer: elucidating molecular pathways for therapy development. Cancer Manag Res. 2012;4:183-93.
355. Roodhart JM, Daenen LG, Stigter EC, Prins HJ, Gerrits J, Houthuijzen JM, et al. Mesenchymal stem cells induce resistance to chemotherapy through the release of platinum-induced fatty acids. Cancer Cell. 2011;20(3):370-83.
356. Dammacco F, Rubini G, Ferrari C, Vacca A, Racanelli V. (1)(8)F-FDG PET/CT: a review of diagnostic and prognostic features in multiple myeloma and related disorders. Clin Exp Med. 2015;15(1):1-18.
357. Cavo M, Terpos E, Nanni C, Moreau P, Lentzsch S, Zweegman S, et al. Role of (18)F-FDG PET/CT in the diagnosis and management of multiple myeloma and other plasma cell disorders: a consensus statement by the International Myeloma Working Group. Lancet Oncol. 2017;18(4):e206-e17.

358. Hui S, Ghergurovich JM, Morscher RJ, Jang C, Teng X, Lu W, et al. Glucose feeds the TCA cycle via circulating lactate. Nature. 2017;551(7678):115-8.
359. Hensley CT, Faubert B, Yuan Q, Lev-Cohain N, Jin E, Kim J, et al. Metabolic Heterogeneity in Human Lung Tumors. Cell. 2016;164(4):681-94.
360. Onfelt B, Nedvetzki S, Benninger RK, Purbhoo MA, Sowinski S, Hume AN, et al. Structurally distinct membrane nanotubes between human macrophages support long-distance vesicular traffic or surfing of bacteria. J Immunol. 2006;177(12):8476-83.
361. Yasuda K, Khandare A, Burianovskyy L, Maruyama S, Zhang F, Nasjletti A, et al. Tunneling nanotubes mediate rescue of prematurely senescent endothelial cells by endothelial progenitors: exchange of lysosomal pool. Aging (Albany NY). 2011;3(6):597-608.
362. de Rooij B, Polak R, Stalpers F, Pieters R, den Boer ML. Tunneling nanotubes facilitate autophagosome transfer in the leukemic niche. Leukemia. 2017;31(7):1651-4.
363. Wang Y, Cui J, Sun X, Zhang Y. Tunneling-nanotube development in astrocytes depends on p53 activation. Cell Death Differ. 2011;18(4):732-42.
364. Thayanithy V, Dickson EL, Steer C, Subramanian S, Lou E. Tumor-stromal cross talk: direct cell-to-cell transfer of oncogenic microRNAs via tunneling nanotubes. Transl Res. 2014;164(5):359-65.
365. Polak R, de Rooij B, Pieters R, den Boer ML. B-cell precursor acute lymphoblastic leukemia cells use tunneling nanotubes to orchestrate their microenvironment. Blood. 2015;126(21):2404-14.
366. Wang J, Liu X, Qiu Y, Shi Y, Cai J, Wang B, et al. Cell adhesion-mediated mitochondria transfer contributes to mesenchymal stem cell-induced chemoresistance on T cell acute lymphoblastic leukemia cells. J Hematol Oncol. 2018;11(1):11.
367. Lenaz G. The mitochondrial production of reactive oxygen species: mechanisms and implications in human pathology. IUBMB Life. 2001;52(3-5):159-64.
368. Sun Q, Zhong W, Zhang W, Zhou Z. Defect of mitochondrial respiratory chain is a mechanism of ROS overproduction in a rat model of alcoholic liver disease: role of zinc deficiency. Am J Physiol Gastrointest Liver Physiol. 2016;310(3):G205-14.
369. Bedard K, Krause KH. The NOX family of ROS-generating NADPH oxidases: physiology and pathophysiology. Physiol Rev. 2007;87(1):245-313.
370. Lambeth JD. NOX enzymes and the biology of reactive oxygen. Nat Rev Immunol. 2004;4(3):181-9.
371. Magnani F, Nenci S, Millana Fananas E, Ceccon M, Romero E, Fraaije MW, et al. Crystal structures and atomic model of NADPH oxidase. Proc Natl Acad Sci U S A. 2017;114(26):6764-9.
372. Szanto I, Rubbia-Brandt L, Kiss P, Steger K, Banfi B, Kovari E, et al. Expression of NOX1, a superoxide-generating NADPH oxidase, in colon cancer and inflammatory bowel disease. J Pathol. 2005;207(2):164-76.

373. Pizzolla A, Hultqvist M, Nilson B, Grimm MJ, Eneljung T, Jonsson IM, et al. Reactive oxygen species produced by the NADPH oxidase 2 complex in monocytes protect mice from bacterial infections. J Immunol. 2012;188(10):5003-11.
374. Lee HC. Structure and enzymatic functions of human CD38. Mol Med. 2006;12(11-12):317-23.
375. Liu Q, Kriksunov IA, Graeff R, Munshi C, Lee HC, Hao Q. Crystal structure of human CD38 extracellular domain. Structure. 2005;13(9):1331-9.
376. Bohrnsen F, Schliephake H. Supportive angiogenic and osteogenic differentiation of mesenchymal stromal cells and endothelial cells in monolayer and co-cultures. Int J Oral Sci. 2016;8(4):223-30.
377. Quarona V, Zaccarello G, Chillemi A, Brunetti E, Singh VK, Ferrero E, et al. CD38 and CD157: a long journey from activation markers to multifunctional molecules. Cytometry B Clin Cytom. 2013;84(4):207-17.
378. Bhan AK, Reinherz EL, Poppema S, McCluskey RT, Schlossman SF. Location of T cell and major histocompatibility complex antigens in the human thymus. J Exp Med. 1980;152(4):771-82.
379. Keyhani A, Huh YO, Jendiroba D, Pagliaro L, Cortez J, Pierce S, et al. Increased CD38 expression is associated with favorable prognosis in adult acute leukemia. Leuk Res. 2000;24(2):153-9.
380. Conklin KA. Chemotherapy-associated oxidative stress: impact on chemotherapeutic effectiveness. Integr Cancer Ther. 2004;3(4):294-300.
381. Altenhofer S, Radermacher KA, Kleikers PW, Wingler K, Schmidt HH. Evolution of NADPH Oxidase Inhibitors: Selectivity and Mechanisms for Target Engagement. Antioxid Redox Signal. 2015;23(5):406-27.
382. Csanyi G, Cifuentes-Pagano E, Al Ghouleh I, Ranayhossaini DJ, Egana L, Lopes LR, et al. Nox2 B-loop peptide, Nox2ds, specifically inhibits the NADPH oxidase Nox2. Free Radic Biol Med. 2011;51(6):1116-25.
383. Sharabi K, Lin H, Tavares CDJ, Dominy JE, Camporez JP, Perry RJ, et al. Selective Chemical Inhibition of PGC-1alpha Gluconeogenic Activity Ameliorates Type 2 Diabetes. Cell. 2017;169(1):148-60 e15.
384. Dimopoulos MA, Oriol A, Nahi H, San-Miguel J, Bahlis NJ, Usmani SZ, et al. Daratumumab, Lenalidomide, and Dexamethasone for Multiple Myeloma. N Engl J Med. 2016;375(14):1319-31.